CERN/ECFA/72/4 Vol. II
January 1973

E C F A

European Committee for Future Accelerators

300 GeV Working Group

[Reports.]

Volume II

Proceedings of the Second Tirrenia Study Week

Tirrenia, Italy, 20-29 September 1972

ORGANISATION EUROPÉENNE POUR LA RECHERCHE NUCLÉAIRE
CERN EUROPEAN ORGANIZATION FOR NUCLEAR RESEARCH

Tirrenia 1972

EUROPEAN ORGANIZATION FOR NUCLEAR RESEARCH

ERRATUM TO CERN/ECFA/72/4, Volume II

(Proceedings of the Second Tirrenia Study Week
Tirrenia, Italy, 20-29 September 1972)

This figure should replace Fig. 10, on p. 160 of this volume.

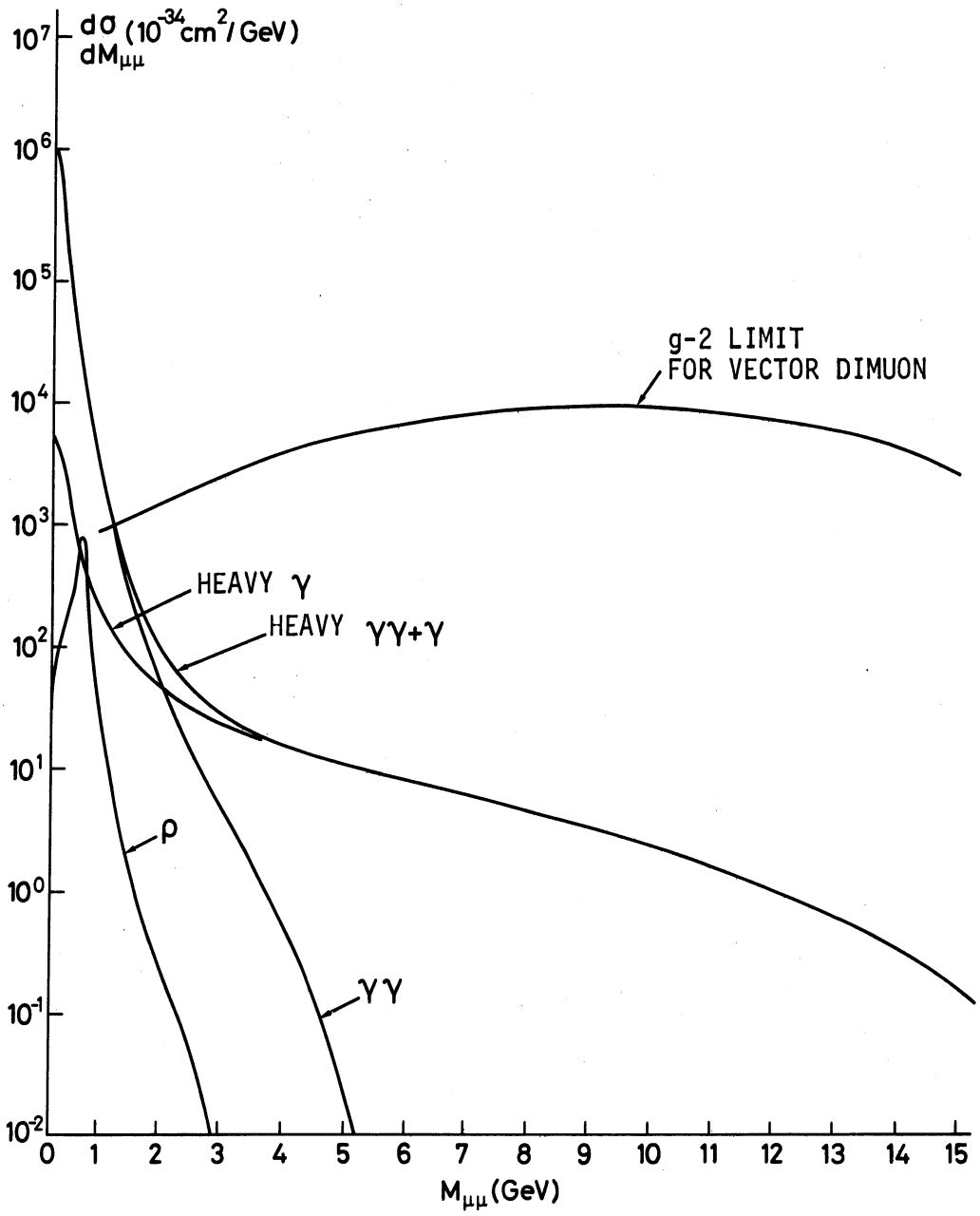

CONTENTS

CHAPTER I

INTRODUCTION

THE SECOND TIRRENIA STUDY WEEK

P. Falk-Vairant
DPhPE, Saclay, France

The second Tirrenia study week was mainly devoted to the presentation and discussion of the status reports of the nine ECFA Working Parties concerning the first experimental facilities for the 300 GeV CERN accelerator. These status reports have been published in CERN/ECFA/72/4, Vol. I.

In addition to these reports, talks were given by invited speakers on specific topics related to this project. The programme of the meeting is given on the next page.

Among the 150 participants, about 100 were representatives of the Working Parties.

This volume contains the comments and discussions which followed the presentation of the Working Parties' Reports, most of the invited talks (sometimes with a summary of the discussion that followed), and some of the contributed papers which, for various reasons, were omitted from the Status Report of the Working Parties (Vol. I of CERN/ECFA/72/4).

Chapters I to IV are each devoted to a session. Chapter V contains the sessions concerning the techniques to be used for experiments at the SPS. Chapter VI is the reproduction of the GESSS report and Chapter VII is devoted to the session on colliding beams.

Brief commentaries on a few questions which arose in the course of the meeting were prepared by the session secretaries. They wish to apologize to the speakers for any misinterpretation or omission of certain remarks.

The ECFA Working Group Executive Committee would like to thank all the members of the Istituto di Fisica dell'Università, Pisa, who contributed to the excellent organization of this meeting.

ECFA/SW/72-17 20.10.72

THE ECFA STUDY WEEK ON THE 300 GeV ACCELERATOR

Tirrenia (Italy) - September 20-29, 1972

P R O G R A M M E

	Subjects and Speakers		Subjects and Speakers	
	8.30 - 10.30 hrs	11.00 - 12.30 hrs	16.00 - 17.30 hrs	18.00 - 19.30 hrs
Wednesday 20th Sept.	THE 300 GeV ACCELERATOR *H.O. Wüster*		PRIMARY BEAMS FROM THE 300 GeV ACCELERATOR *E. Wilson*	POSSIBLE UTILIZATION OF THE WEST HALL *J.V. Allaby*
Thursday 21st Sept.	BEBC W.P. REPORT *J. Meyer, A. Grant and D. Miller*	GARGAMELLE W.P. REPORT *F. Jacquet*	SPECIAL TOPICS CONCERNING THE BUBBLE CHAMBER WORKING PARTIES	
Friday 22nd Sept.	NEUTRINO W.P. REPORT *H. Wachsmuth*	NEUTRINO PHYSICS *C.H. Llewellyn-Smith*	NEW FACILITIES IN VISUAL DEVICES W.P. REPORT *H. Meyer and C. Fisher*	SPECIAL TOPICS ON ν AND ν-μ
Saturday 23rd Sept.	SPECTROMETERS AND OMEGA W.P. REPORT *J. Dowell and W. Koch*	STRONG INTERACTIONS *M. Jacob*	SPECIAL TOPICS ON SPECTROMETERS AND OMEGA	SPECIAL TOPICS ON INSTRUMENTATION SPECIAL TOPICS ON ν AND ν-μ
Monday 25th Sept.	HADRONIC BEAMS W.P. REPORT *M. Steuer*	POSSIBILITIES IN ELECTRON AND PHOTON BEAMS IN THE WORLD AROUND 1977 *B.H. Wiik*	PHYSICS PROGRAMME AT NAL *D. Reeder*	SPECIAL TOPICS CONCERNING HADRONIC BEAMS
Tuesday 26th Sept.	CHARGED LEPTON AND PHOTON BEAMS W.P. REPORT *F.W. Brasse and G. Barbiellini*	PRESENT CHARACTERISTICS AND FUTURE DEVELOPMENT AT NAL *R.R. Wilson*	ELECTRON VERSUS MUON PHYSICS *E. Picasso*	SPECIAL TOPICS CONCERNING e, μ AND γ
Wednesday 27th Sept.	COLLIDING BEAM PHYSICS AND DEVICES *C. Rubbia and K. Johnsen*	PARTICLE IDENTIFICATION W.P. REPORT *P. Murphy*	SPECIAL TOPICS IN EXPERIMENTAL AREAS AND SUPERCONDUCTING DEVICES	
Thursday 28th Sept.	GESSS REPORT *W. Heinz*	NORTH EXPERIMENTAL AREA PROBLEMS AND IDEAS *G. Brianti*	DECISIONS ON THE 300 GeV PROGRAMME *J.B. Adams*	THE PHYSICS PROGRAMME AT CERN AND ITS ORGANIZATION & FINANCING *W. Jentschke*
Friday 29th Sept.	PANEL DISCUSSIONS ON THE WORKING PARTIES' RESULTS	CONCLUSIONS OF THE STUDY WEEK *G. Salvini*		

THE PHYSICS PROGRAMME AT CERN AND ITS ORGANIZATION AND FINANCING

W. Jentschke
CERN, Geneva, Switzerland

1. PHYSICS PROGRAMME

The facilities at CERN have grown impressively over the last years. The Intersecting Storage Rings (ISR) have come into operation, and in five intersection regions, experiments have been installed in 1972. The big split-field spectrometer is being assembled and will considerably increase the experimental capacity at the ISR from 1973 on. The heavy-liquid bubble chamber, Gargamelle, became fully operative in 1972. The big European hydrogen bubble chamber, BEBC, and the large magnetic Omega spectrometer, equipped with spark chambers, underwent their first tests this year and will be ready for physics runs in 1973. The booster of the PS also started operation in 1972, and an improvement programme for the SC is under way.

Last but not least the preparations for 300 GeV physics have already started and will require an increasing fraction of the total effort.

In view of the financial and man-power limitations it is quite obvious that the complete programme with all its parts cannot be continued at full speed everywhere, and it will be necessary to set priorities and to reduce or even stop some parts of the programme even if they are scientifically justified and technically feasible.

Indeed, two reductions of the programme have already been decided upon:

i) the PS booster will essentially not be used for experiments before the start-up of the 300 GeV accelerator; and

ii) the West Hall will not be opened up for 25 GeV physics except for the Omega spectrometer.

Other decisions will have to be made at different times. They would have to be reconsidered in the light of one of the 300 GeV machine construction schedules discussed by J.B. Adams at this meeting, i.e. to install all iron magnets in order to achieve 400 GeV at an early date. This would have the effect that the physics in the West Area would start a few months later, probably towards the end of 1976, but making available 18 to 21 months for physics until February 1979 instead of 14 as foreseen in the previous time-schedule. In addition, the new time-schedule would permit the North Area to be opened up earlier.

Let me mention a few questions that will have to be considered in the future with the aim of optimizing the physics programme.

i) For the neutrino beam in the West Area, should one choose the underground (tunnel) or surface solution? Since civil engineering has to start early, this decision must be taken in October 1972.

ii) Should the neutrino target and beam in the West Area be laid out for 200 GeV only, and a 400 GeV beam foreseen early in the North Area? or should one have also 400 GeV in the West Area?

iii) Neutrino physics with bubble chambers: should Gargamelle be moved behind BEBC? or should BEBC be filled with neon in addition to deuterium? or does one need both?

iv) Shall BEBC be equipped with a muon identifier, a downstream spectrometer and/or a Track Sensitive Target (TST).

v) Is it reasonable to plan counter neutrino experiments in the West Area? or should they wait until the North Area is opened?

vi) Should a muon beam (combined or separate from a neutrino beam) be installed in the North Area?

vii) How many electron and photon beams will be necessary? and when, where and at what energies?

viii) Should the Omega spectrometer be improved (optical chambers replaced by wire chambers)? and how much effort should go into the development of specialized spectrometers.

A difficult decision will concern the fractions of the total effort that should go into the investigation of weak, strong, and electromagnetic interactions. Since the physics in the 300 GeV range has been discussed extensively by the ECFA Working Group I do not want to repeat the arguments here. However, it seems to me that everybody agrees that the most exciting results might be obtained from the weak interaction. The unitarity limit indicates that something is bound to happen in the hundred GeV region. Therefore, weak interaction experiments should have a high priority. On the other hand, we learned that the SPS will also provide high-energy electron and photon beams which cannot be obtained with electron accelerators.

With respect to strong interactions, more detailed information on the dynamical behaviour is needed. ISR experiments at high centre-of-mass energies, and SPS experiments at lower energies but much higher luminosities, will contribute to this information.

It seems to me to be very important that we keep our programme flexible enough so that we can adjust it according to the results that will be found.

In the coming years we shall not only have to balance the various parts of the SPS programme, but the SPS physics will also have to be confronted with the other activities carried out at CERN.

2. ISR PHYSICS PROGRAMME

For many years to come the ISR will provide by far the highest centre-of-mass energies, although only for pp interactions.

One of the most exciting parts of the programme, the search for exotic particles, has already yielded rather low limits for the production of quarks. Similar good limits are hoped for in the near future for intermediate bosons and magnetic monopoles. If no exotic particles are found, this activity will probably come to an end in two or three years.

The investigation of two-body processes has given interesting results. The total cross-section is approximately constant. The slope of elastic pp scattering was found to have a more complicated behaviour than was expected, and at large t-values the cross-section seems to drop faster than an extrapolation from low-energy data would have suggested. The

accuracy of these data should be improved since, for example, a possible logarithmic rise of σ_{tot} cannot yet be excluded. An extension of two-body processes to quasi-two-body reactions has already started (e.g. $p + p \to P + N^*$) and these kinds of measurements will continue for several years.

An impressive amount of data has already been collected on multiparticle reactions. Some results on multiplicities have been obtained, and several experiments investigated the scaling behaviour for single-particle inclusive spectra. The results indicate that for most types of produced particles, the scaling limit is reached at ISR energies. It is quite remarkable that the scaling seems to hold also in the central region ($\approx 90°$). However, these data have to be completed since the whole admissible kinematic range has not yet been covered, some particle have not yet been measured, and all the errors should be reduced.

The results obtained thus far have revealed some gross features of multiparticle reactions. The features can be explained in terms of various models. In order to distinguish between different models and to get a better understanding of the dynamical details, more refined measurements are necessary. They include different kinds of correlations and the selection of specific types of events. From such measurements one might expect surprises, and indeed a surprisingly large number of events with high momentum transfers have already been observed in two experiments. At any rate, the study of the detailed dynamical behaviour of multiparticle events is barely starting and will have to continue for many years. The split-field spectrometer becoming available for physics in 1973 will provide an excellent facility for such investigations. From this one concludes that the second generation of ISR experiments starting in 1973 will continue for several years.

For the short-term programme one has to answer the following questions:

i) How much effort should go into an increase of luminosity (low beta section)? Should a second large magnet spectrometer be built in particular to investigate large momentum events around 90°?

ii) For the long-term development the impact of the SPS on the ISR programme has to be assessed. A major conversion of the ISR may then have to be considered.

3. 25 GeV PHYSICS PROGRAMME

In a superficial way one could argue that at a time when the SPS and the ISR will be fully exploited the interest would shift almost completely from 25 GeV physics to high energies. This would be a wrong conclusion, however. For the strong interaction, the asymptotic behaviour at very high energies will certainly be of fundamental importance, but the whole richness of the strong interaction lies in the resonance region where many important problems remain to be solved. But even for the weak interaction where qualitatively new information can be expected at high energies, the investigation of rare processes at low energies will contribute essentially to our understanding. Hence it seems premature and superficial to expect that the new fundamental discoveries will be made exclusively at very high energies. To put this statement on a firmer ground, let me give you some examples.

The two most successful and complementary schemes for classifying elementary particles are SU(3) multiplets and Regge trajectories. Quite a number of complete SU(3) multiplets are known by now, and it would be desirable to fill a few more and to discover possible discrepancies. The question of Regge trajectories is not yet settled, however. For bosons, in particular, the situation is deplorable, as is shown in Fig. 1.

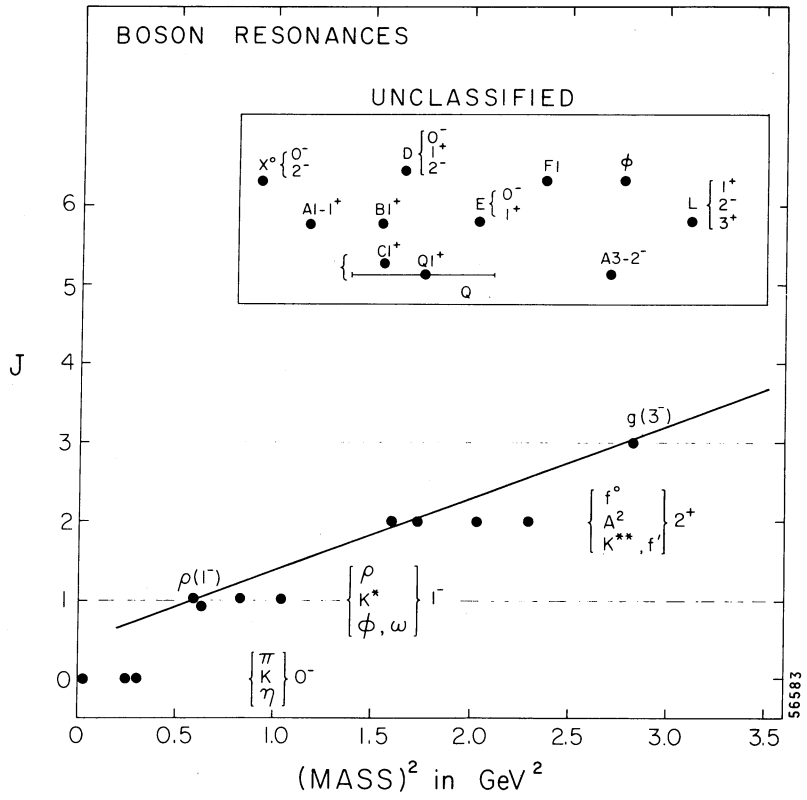

Fig. 1

For the three multiplets (with 0^-, 1^-, and 2^+) which are completely known, only one recurrence has been found, the g meson which is the recurrence of the ρ meson. There are about a dozen well-established resonances which, however, cannot be associated with trajectories since their spin-parities are not yet well established. Besides these, there is a large group of resonances whose existence is not yet certain. Because of this lack of information, several fundamental questions cannot be answered. For example, the validity of exchange degeneracy relies mainly on the fact that the 2^+ multiplet lies on the respective trajectories of the 1^- multiplet. Nothing is known about the trajectory of the 0^- multiplet (pion trajectory).

An obvious way to improve on the present experimental situation is by improving the statistics. Some of the doubtful candidates come from experiments with a statistical accuracy of about 4 to 6 events/μb obtained from about 100,000 bubble chamber pictures with 15 particles per picture. Counter experiments could sometimes help, as in the case of the g meson, but the restricted acceptance poses problems especially for decays into more than two particles.

The experimental situation for baryon resonances is somewhat better than for bosons. The main reason is that bosons can be found only in production experiments, whereas baryons can be detected also in formation experiments where a long experience in phase-shift analysis exists. The richer information manifests itself in several known trajectories. Figure 2 shows, as an example, the trajectories of the SU(3) decuplet. The five resonances on the Δ trajectory are quite impressive, but they immediately raise the question, How far do the

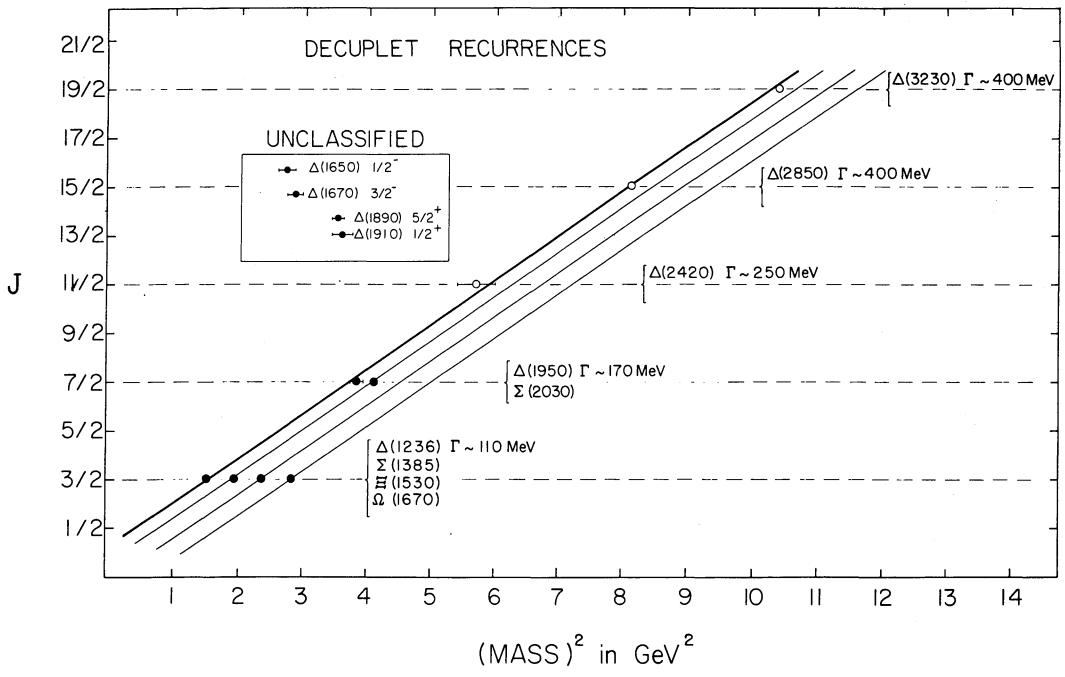

Fig. 2

trajectories continue to rise linearly? One of the difficulties of extending the measurements to higher masses comes from the fact that higher partial waves enter into the phase-shift analysis. The development of polarized targets has made it possible to measure the polarization P, which helps to unravel some ambiguities. In future, however, it will become necessary to measure also the R and A parameters. Hence a long programme of sophisticated precision experiments seems necessary to clarify some of the fundamental problems of the Regge classification.

But also some problems concerning *reaction mechanism* can best be studied at low energies, and a few examples will be mentioned. The Regge model with the exchange of moving poles was quite successful in explaining many two-body reactions qualitatively. In a second approximation, however, Regge cuts are needed. They correspond to corrections in low partial waves, i.e. corrections for central collisions. The situation is particularly unclear for unnatural parity exchanges (π, K, B), where even very little is known about the leading pole. Pion exchange can be investigated in np charge exchange, $\pi^- p \to n p^0$ or $\pi^+ p \to \Delta^{++} \rho^0$. Since the cross-sections for these reactions drop fast with energy, they can best be studied with high accuracy at lower energies.

The typical structure length in Regge theory is about $\Delta\alpha(t) \approx 2$, and hence one needs measurements up to $t = 2$ GeV^2. Many results are only for $t \approx 0.4$ GeV^2. Of course, cross-sections are low at large t-values and the measurements are accordingly difficult.

Another field of great theoretical interest is that of reactions with exotic exchanges since they will throw some light on higher-order effects, e.g. the exchange of two Regge poles. The $K^- p$ backward scattering is an example for exotic baryon exchange, while $\pi^- p \to K^+ \Sigma^-$ proceeds through exotic meson exchange. Since the cross-sections for such reactions fall with a high power (> 4) of the incident momentum, they cannot be investigated at high energies.

Also for the study of *weak interactions* the 25 GeV domain will preserve its attraction. The interest will centre on rare decays of kaons and hyperons. From such investigations one will get information on the validity of various selection rules (e.g. $\Delta Q = 0$, $\Delta Q = \Delta S$) or on the Cabbibo hypothesis. Most of the selection rules are not required by a known fundamental theory, and therefore it seems interesting to test how exact those rules are. In the past most of the rare decays have been measured up to the level of about 10^{-5}. With higher intensities available after the commissioning of the booster or even the SPS, these limits could be pushed into the 10^{-6} to 10^{-10} range.

In conclusion one can state that the 25 GeV physics programme will have considerable scientific value for many years to come. However, the examples of experiments mentioned above will all require a considerable technical and financial effort in order to be able to obtain the needed precision, to measure extremely small cross-sections, or to determine the polarization parameter. This will require strong groups with complex and elaborate equipment. Hence it will be important to concentrate the man-power and the financial means.

From the above deliberations it seems safe to draw the conclusion that the South and East Halls cannot both be closed at the same time during the coming years, and that the 2 m hydrogen chamber will continue to operate. However, the following possibilities will have to be looked into:

i) Can secondary beams derived from 200 GeV protons improve the 25 GeV programme qualitatively?

ii) Should the South Hall be closed? The implications are: no internal targets, number of counter beams reduced to about half the present number.

iii) The necessity of 25 GeV test beams for the preparation of 300 GeV physics should be studied.

iv) Can one close the PS North Hall after the hyperon bubble chamber (HYBUC) has finished its operation?

v) Should the South-East Hall be made available to 25 GeV or intermediate-energy physics?

4. NUCLEAR STRUCTURE AND ATOMIC PHYSICS

European intermediate-energy nuclear physics has been given strong incentives by CERN and a long tradition has been established there. The SC was the central facility which permitted this field to develop and to thrive. It may be useful to mention some of the major achievements of the past.

The SC is an excellent source of muons. The investigation of muonic atoms yielded results on nuclear sizes and shapes of ground and excited states, on the distribution of the nuclear magnetization, and on higher-order QED effects. From measurements on muonium, one of the best values of the fine structure constant could be deduced. Muon capture in nuclei gave information on the induced pseudoscalar coupling and played a major role in the development of PCAC. The investigation of pionic atoms gives precise values for the pion mass and information on the πN interaction.

Pion-nuclear scattering has provided valuable information on the validity of isospin invariance, it has shown that the 3,3 resonance survives in nuclei, and it has helped to test dispersion relations.

The results of quite a number of scattering experiments were the basis of an understanding of multiple scattering effects in all its various aspects (Glauber theory).

The isotope separation facility ISOLDE made it possible to study many new isotopes far away from the stability line. As examples of interesting results, one might mention the sudden change of nuclear volume as a function of the neutron number, or the systematic determination of β-decay strength functions.

Many important questions remain open. One cannot pretend to understand the nucleus until one knows the behaviour of all the particles it contains. The classical picture of an assembly of protons and neutrons is too simplified. Mesons and excited nucleon states play a role. Presumably the nuclear meson field is modified by the other nucleons, and hence the pion field is probably coupled collectively to the nucleus. Quasi-elastic knock-out of mesons or radiative π capture could shed some light on these problems. There have also been suggestions that the pion can interact coherently with the entire nucleus in such a way as to produce "size resonances" in the nucleus. While this is known for nucleons in nuclei, the pion case is very different since it is a field quantum. The question of the existence of hard-core correlations in nuclei is also not settled.

Hence I have no doubt that nuclear structure and atomic physics will have to be continued at CERN for quite some time to come. However, this could be done in many different ways, and the following points arise:

i) The time schedule for the delayed improvement programme of the SC poses some problems, and how much longer the users are prepared to wait has to be clarified very soon.

ii) The improved SC seems to be competitive with other meson factories for a certain period, but most people agree that as far as the long-term programme is concerned, the CERN Synchro-cyclotron might become an obsolete machine.

iii) Another question is, How much should the PS be made available to this kind of physics? Especially after the start-up of the booster, the PS will be a unique facility in Europe for the production of low-energy kaons. Two low-energy kaon beams exist already at the PS and the interest will probably increase.

Internal targets will probably not be permissible after the commissioning of the booster, and low-energy kaon beams have to be set up at 0° production angle at external targets. Hence there will be a considerable interference with high-energy physics experiments, and the question of how many low-energy K beams can be installed at the PS requires very careful study.

iv) One must also consider very seriously the danger of overloading the PS by using it as an injector both for the SPS and the ISR and also for a heavy physics research programme.

5. NUMBER OF HIGH-ENERGY PHYSICISTS

When setting up a long-term programme one must consider the physics interest and the financial limitations, but certainly the physicists cannot be neglected. Although it is extremely difficult to guess how the various interest will develop, some statistical considerations seem appropriate. Of course, one should be very careful not to draw too definite conclusions from the numbers given below, but they should at least indicate the over-all situation in 1976.

Since 1966 ECFA has made a census of the total number of high-energy physicists in Europe every two years, and the main result is shown in Table 1 for the end of the years 1966, 1968, and 1970. As one notices, not only has the total number of physicists increased, but also the percentage of physicists depending on CERN is rising. Extrapolating these figures from 1970 to 1976, it seems reasonable to assume that there will be a slight further growth of the high-energy physics community. This is based on the assumption that the present rate of increase will not drop suddenly but will change only slowly because of a certain inertia. The estimated figures for 1976 as shown in the table also take into account that the actual number of physicists using CERN is already considerably higher than the 1970 figure. However, it can be expected that the total number of high-energy physicists is approaching a constant level. Nevertheless, since some of the national programmes will be reduced, it seems likely that more physicists will have to depend on CERN. Hence the estimate that about 900 physicists will be involved in electronics experiments at CERN and about 750 physicists will analyse bubble chamber pictures taken at CERN does not appear to be exaggerated. Of course, it does not imply that all these counter physicists will have to work all the time at CERN. Since the data analysis is requiring an increasing effort in counter experiments, many of these physicists will only spend very short periods at CERN.

Table 1

Total number of high-energy physicists in Europe

	End 1966		End 1968		End 1970		1976 (estimate)	
	Total	Using CERN	Total	Using CERN (estimate)	Total	Using *) CERN (estimate)	Total	Using CERN
SC + EM (electronics experiments + emulsion)	718	271 ≃ 38%	929	460 ≃ 50%	1012	630 ≃ 62%	1200 ± 100	900 ≃ 75%
BC (bubble chamber)	607	474 ≃ 78%	694		708	600 ≃ 85%	900 ± 100	750 ≃ 83%
	1325	745	1623		1720	1229	2100	1650
Nuclear structure		111		118		167		

*) Including physicists preparing experiments for CERN, e.g. for the ISR.

Another question is, How many experimental groups will be present at CERN? Over the last ten years the number of experimental groups has linearly increased with about 2.4 new groups/year and there is still no sign of saturation (see Fig. 3). Indeed, when the ISR came into operation some groups moved from the PS to the ISR. But their places were filled by new groups. On the other hand, the number of groups increases less than the number of physicists using CERN. The average number of physicists per group increased from about 12 in 1966 to 23 in 1970, and one might guess that it will be around 25 to 30 in 1976 (see Table 2).

On the basis of these figures one may try to estimate how many physicists will be engaged in various activities in 1976. This is shown in Table 3. It has been assumed that 12 groups will work in the West Area, half of them with the Omega spectrometer. All these

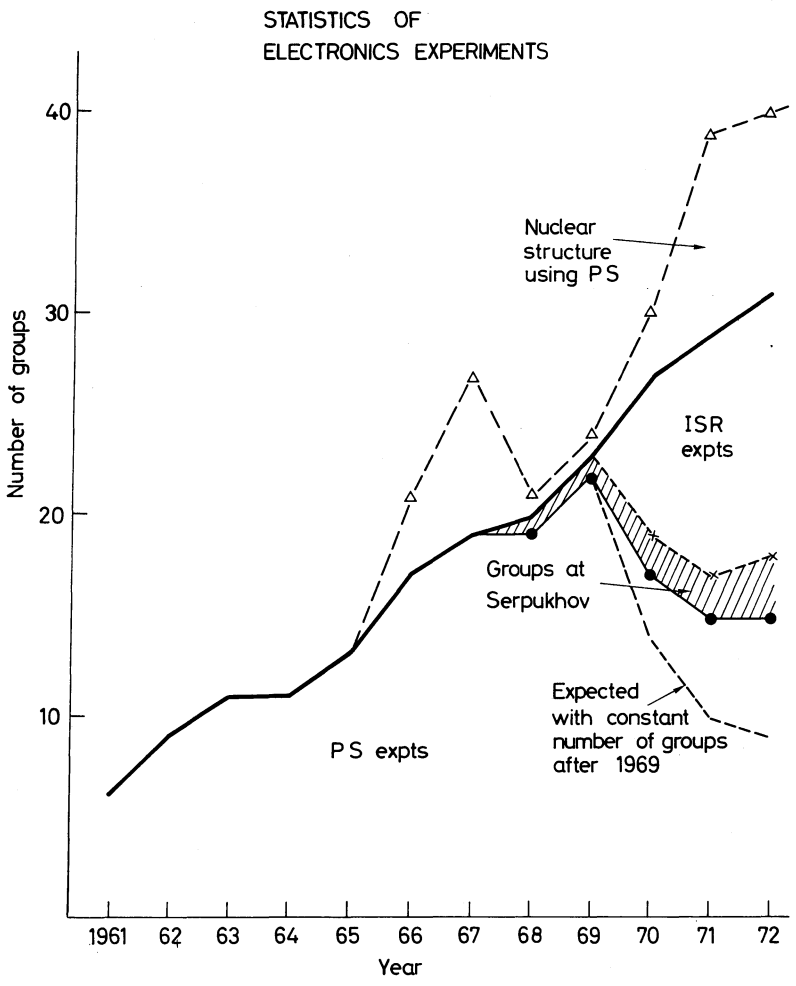

Fig. 3

Table 2

Evolution of the number of physicists per group
in electronics experiments

	1966	1968	1970	1976 estimate
Number of physicists in electronics experiments	271	460	630	900
Number of groups with electronics experiments	17	20	27	30-36
Physicists/Group	16	23	23	25-30

(excluding nuclear structure physics)

Table 3

Number of physicists involved in various activities

	End 1971	1976
Electronics experiments		
- 25 GeV physics at PS	630	370
- ISR	130	200
- 200 GeV West Area	-	300
- 200 GeV North Area	-	30
	760	900
Bubble chamber experiments		
- 2 m chamber	450	300
- Gargamelle	150	150
- BEBC	-	200
- Mirabelle	-	100
	600	750

(excluding nuclear structure physics)

groups will not, however, be present at CERN at the same time, and indeed some of the physicists will appear at CERN only very rarely since, like bubble chamber physicists, they will mainly be involved in data analysis. It has also been assumed that some physicists will be busy with preparations for the North Hall. When the North Hall comes into full operation, about the same number of electronics physicists as those working in the East Hall might be accommodated. This implies that after 1978 about 500 to 600 of the total of 900 electronics physicists will be engaged in 300 GeV physics. As a consequence, about a third of them will still be interested in ISR and 25 GeV physics.

6. THE 300 GeV PREPARATORY EXPERIMENTS COMMITTEE

On 31 May, 1972, the NPRC decided to set up a Committee which should take over from the ECFA Working Group the preparation of 300 GeV physics and, in particular, call for proposals at the proper time. The terms of reference of this Committee are as follows:

i) The 300 GeV Preparatory Experiments Committee will have the task of advising the NPRC on all matters and decisions concerning the preparation of the 300 GeV experimental programme. The results of the present ECFA working group will provide a basis from which to start.

ii) Since the preparations for bubble chamber and electronics experiments will need very good co-ordination, not only from the technical but also from the financial point of view, the Committee will be concerned with all kinds of experiments.

iii) The Committee must make sure that all necessary consultation is held between potential users and CERN Laboratory I and Laboratory II (SPS). This includes informing the future users of the technical and operational possibilities of the new facilities on the one hand, and conveying to the responsible staff of CERN the needs and desires of future users on the other hand. For this purpose open meetings will be organized.

iv) The Committee will call for proposals for 300 GeV experiments, which will then be presented in open meetings. It will help to form collaborations, taking into account physics, technical, and financial conditions.

v) The Committee is also expected to make recommendations to the NPRC concerning general experimental facilities, e.g. beams, big spectrometers, special fillings, or modifications for bubble chambers.

vi) As its first task, the Committee should submit to the NPRC a consistent programme for a first generation of experiments. After this the NPRC will reconsider the function of all Experiments Committees.

7. FINANCIAL PROBLEMS

Let me say a few words on the budget and its implication in the physics programme, and in particular in the 300 GeV physics preparation.

In 1969 we had set up a programme for Laboratory I for the years 1971 to 1978 in which a good exploitation of the facilities was planned.

As a consequence of building the 300 GeV accelerator at CERN we agreed to reduce the total cost over these years by 210 MSF. In 1972 prices this lead to the following yearly budget figures:

Laboratory I

	71	72	73	74	75	76	77	78	79
MSF	391	371	360	345	345	357	357	357	

Laboratory II

MSF	30.9	95.0	176.6	200	194	183	183	183	30

In addition to the reduction of 210 MSF, Laboratory I has to cover additional items which will be needed for the 300 GeV programme:

a) equipment for the West Area (beams and experiments) for 300 GeV physics;

b) improvement of the PS, and additions to make it a reliable injector for the SPS.

Beams for the North Area will be covered by the Laboratory II budget, but there still remain the detectors to be provided for.

In order to be able to provide the necessary funds for the items mentioned under (a) and (b), several steps have been taken. A Budget Analysis Committee, with the help of many working groups, studied the cost and man-power required for the various CERN activities. On the basis of the material provided by this Committee, various options for the ISR, PS, and SC programmes were examined and evaluated by a Programme Evaluation Committee composed of the Board of Directors and the Chairmen of the Experimental Committees.

Apart from many small measures which I shall not discuss here (which, however, led to non-negligible savings), the following decisions were taken:

i) The number of electronics experiments at the PS should not be increased. Except for the Omega, no other 25 GeV physics beams for electronics experiments should be set up in the West Area.

ii) Bubble chamber pictures should be limited to about 8 million per year.

iii) The growth of computer capacity should be restricted.

iv) The booster should, for the next few years, be operated only at intermediate intensity, for which no additional equipment would be required in the PS; of course, the full intensity should be available for experiments with the SPS.

v) No neutrino physics should be done in BEBC at 25 GeV.

vi) To stop all development work which is not connected with the ISR and the 300 GeV programme.

vii) To keep the staff numbers well below the ceiling authorized by the Council.

viii) To get all Group and Division Leaders to be economy-minded.

Very rough estimates, which are based on the programme as it is known at present, have shown that Laboratory I will have the following expenditure:

1. About 100 MSF on the first generation of experiments in the West Area including an RF-separated beam for BEBC, a neutrino facility, a superconducting RF-separated beam for Omega, and several beams for counter experiments.

   Half of this sum is required for beams and buildings, and the other half, i.e. about 50 MSF, will be split approximately between electronics and bubble chamber physics experiments. At present various options are still open, but they require further study and discussion before a final decision can be made.

2. 30 MSF on equipment for further development of the experimental areas. At the moment it is not possible to specify in more detail how this money will be used.

In summary, a total sum of about 130 MSF of capital expenses will be necessary to start the 300 GeV physics programme. In addition, funds for operating the beams and experiments in the West Area and to cover staff expenses will have to be found.

With the economy measures I have mentioned above it has already become possible to save considerable amounts of money. At present it seems that about 40 MSF will still have to be found until 1976, which I am afraid will make necessary some further cuts in the programme.

If the physicists would want a 400 GeV neutrino beam in the West Area, this will require additional shielding. Furthermore, if muon and/or neutrino facilities are wanted at an earlier date in the North Area, some additional expenses will arise.

In conclusion I can say that even with the economy measures which have been already established it will not be possible to carry out the full programme. We shall have to establish priorities and make choices.

300 GeV PROGRAMME: MACHINE CONSTRUCTION SCHEDULES

J.B. Adams
CERN, Geneva, Switzerland

INTRODUCTION

1. The basic document defining the 300 GeV Programme, on which the CERN Council reached its decision to start the Programme on 19 February 1971, is CERN/958/Rev. This document makes the following statements concerning the utilization of the accelerator during the Programme:

   a) The existing West Hall will be used as the initial experimental area (Section III, para 3).

   b) Research can start at the 300 GeV energy level or at an intermediate-energy level in the existing West Hall experimental area during the sixth year of the Programme (Section III, para 4).

   c) The Programme will be completed by the construction of a new experimental area, called the North Area, on the new site, which will become operational at the 300 GeV energy level eight years after the start of the Programme (Section III, para 5).

2. CERN/958/Rev. also lays down the financial provisions for the 300 GeV Programme in two ways. Firstly, the expenditure during the Programme must not exceed 1150 MSF at 1970 costs and constant prices (Section IV, para 1). Secondly, the annual expenditures during the course of the Programme, which add up over the eight years to 1150 MSF, are specified year by year (Section IV, para 3).

3. A machine construction schedule applicable to iron-cored magnets, which would satisfy both the utilization requirements and the financial provisions mentioned above, is described in report CERN/1050. This schedule assumed two energy stages, namely 200 GeV and 300 GeV. It proposed operation of the West Area at 200 GeV energy during the sixth year of the Programme, and operation of the North Area at 300 GeV energy at the end of the eighth year of the Programme. An alternative schedule proposed operation of the West Area at 300 GeV energy towards the end of the sixth year of the Programme and operation of the North Area also at 300 GeV energy at the end of the eighth year of the Programme.

4. Yet another construction schedule is mentioned in CERN/1050, involving superconducting magnets. This schedule considers operation of the West Area at 200 GeV energy using iron-cored magnets during the sixth year of the Programme, and the installation of a half-set of superconducting bending magnets for the second energy stage which would give about 400 GeV energy, which could then be used for beams to the North Area. Whether such a schedule could be completed by the end of the Programme and within its financial provisions was not clear when the Programme started, and is still not clear today. It was therefore proposed to start by ordering iron-cored bending magnets to give 200 GeV energy, and then to take a decision towards the end of the third year of the Programme whether to order a second set of iron-cored magnets to give 300 GeV energy or a set of superconducting magnets to give about 400 GeV energy. The decision would depend on the

state of technological development of superconducting magnets and their estimated costs at the time.

5. This note discusses the machine construction schedules mentioned above, in the light of the developments which have taken place since the start of the Programme on 19 February 1971.

CONSTRUCTION SCHEDULE A (see Fig. 1)

6. This schedule follows the one mentioned in CERN/1050 which results in the operation of the West Area at 200 GeV energy level during the sixth year of the Programme.

7. In this schedule, the production of the first set of bending magnets for 200 GeV energy begins in the second half of 1973 and is completed towards the end of 1974. Installation of these magnets is completed in the middle of 1975, and magnet system testing is completed at the end of 1975. Final machine commissioning then starts, and experiments in the West Area at 200 GeV energy could begin early in September 1976 (i.e. about the middle of the sixth year of the Programme). In order to synchronize with this schedule, the beam lines, detectors, and other experimental equipment in the West Area should be installed and tested-out early in 1976.

8. Towards the end of 1973 the decision on superconducting magnets is taken, and it is assumed in this schedule that it is decided to go ahead with iron-cored magnets. It is further assumed that the financial provisions of the Programme and the annual budgets will allow a second set of iron-cored magnets to be ordered so that 400 GeV could be reached as the second energy stage. Therefore a second order for iron-cored bending magnets is placed towards the end of 1973 such that their production in industry follows

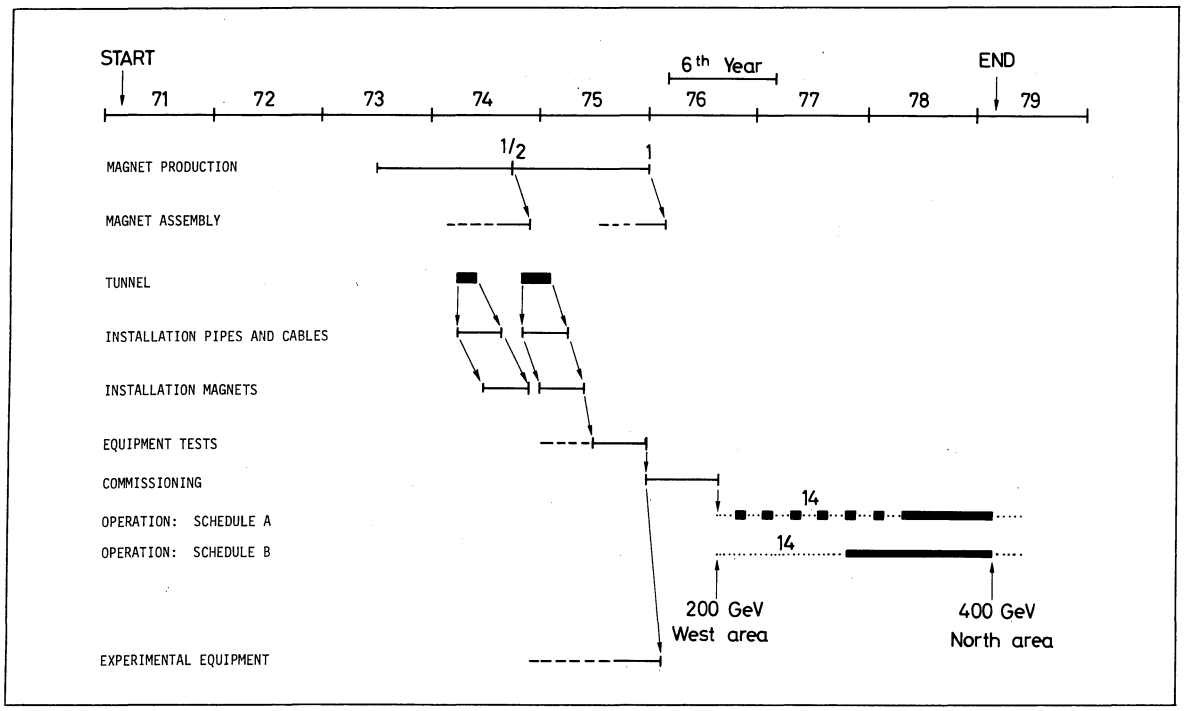

Fig. 1

on the production of the first set and at the same rate of production. The production of the second set is completed by the beginning of 1976, at about the same time as the accelerator is being commissioned at the 200 GeV energy level. The second set of bending magnets are stored on site in the Assembly Hall and the problem is how to get them into the accelerator.

9. Schedule A proposes that these magnets are installed in the machine tunnel during shut-downs of the machine in the following 20 months. It is imagined that the machine runs at 200 GeV energy, feeding the West Area experiments for periods of 2 months duration, and after each run there is a shut-down of 1 month during which time the bending magnets are brought into the machine tunnel. Thus during the 20 months, 6 months are allocated to installing bending magnets and 14 months to machine operation. Owing to the remanent fields of the bending magnets it seems inadvisable to install them in the machine itself, but rather to mount them above the vacuum chamber in the machine tunnel.

10. In the spring of 1978 when the second set of bending magnets are all in the machine tunnel, there is a long shut-down of 10 months during which time the second set of bending magnets are installed in the machine, the machine is realigned, the magnet system is tested with all its magnets in place, and the machine is commissioned at the 400 GeV energy level.

11. In this schedule the beam extraction system for the West Area is installed and commissioned together with the beam transfer lines so that beams are available in the West Area by the middle of 1976. The beam extraction system for the North Area is installed and commissioned during the long shut-down at the end of the Programme.

12. Schedule A as just described would give 14 months of machine operation at 200 GeV energy during the Programme starting in September 1976, and 400 GeV energy operation in the North Area at the end of the Programme, starting in February 1979.

13. From the financial point of view Schedule A has two consequences. Firstly, it requires more expenditure on the accelerator during the Programme, since bending magnets for 400 GeV energy are ordered in place of bending magnets for 300 GeV energy. Secondly, this extra expenditure, which occurs in 1975 and 1976, increases the annual budgets during these years. Since the total Programme cost is fixed, this extra expenditure, which amounts to about 20 MSF, could be recuperated from whatever contingency remains after 1976 or, if all the contingency is used up at that time, it could be recuperated from the sum set aside for the North Area.

14. Recent re-estimating of the 300 GeV Programme suggests that Schedule A could probably be carried out within the financial provisions of the Programme.

CONSTRUCTION SCHEDULE B (see Fig. 1)

15. An alternative construction schedule which follows closely Schedule A but avoids the continuous interruption of machine operation at 200 GeV energy for installing the second set of bending magnets, is simply to store these bending magnets in the Assembly Hall until towards the end of 1977 and then, during a shut-down of 16 months, to install them in the machine, realign the machine, test the magnet system, and commission the accelerator at 400 GeV energy altogether at the end of the Programme. This schedule also gives

14 months of machine operation at 200 GeV energy during the Programme and has the same financial implications as Schedule A. However, it may possibly be preferred from the experimental point of view.

DISCUSSION OF SCHEDULES A AND B

16. Both Schedules A and B satisfy the 300 GeV Programme as defined in CERN/958/Rev. and described in CERN/1050. In addition they make available 400 GeV instead of 300 GeV at the end of the Programme, which is more than was originally promised. They make available 200 GeV in the middle of 1976 so that experiments can start in the West Area as soon as possible during the Programme. After the end of the Programme the maximum beam energy of ejection to the West Area could be increased up to 400 GeV should this be required by the experimental programme at that time.

17. From the experimental point of view the limitation of Schedules A and B is that the energy available from the machine is 200 GeV until 1979, and only the West Area is available for experiments up to that time.

18. The main problems of both schedules from the machine construction point of view are firstly that the accelerator is commissioned twice during the Programme, once at 200 GeV and later at 400 GeV, and secondly that the machine groups responsible for the magnet system and the extraction systems must be maintained at nearly full strength during the entire eight years of the Programme.

19. It has always been realized that installing the second set of bending magnets in the machine once it has started operation at the 200 GeV energy level may not be the best solution either from the point of view of the experimental programme or from the point of view of machine construction. From both points of view it might be better, as foreseen in CERN/958/Rev., to install all the bending magnets in one operation as they become available from the manufacturers. In this case there would only be one machine-commissioning period during the Programme, and once the machine is operating there would only be normal shut-downs for maintenance and modifications rather than six longer shut-downs during which the second set of bending magnets are brought into the machine tunnel. Furthermore, it might be possible to open up the North Area earlier than 1979. Such a construction programme is described below and is called Schedule C.

CONSTRUCTION SCHEDULE C (see Fig. 2)

20. Schedule C follows Schedules A and B until towards the end of 1973 when the decision must be taken concerning superconducting magnets. Again it is assumed that a second set of iron-cored magnets is ordered so as to reach 400 GeV energy. However, in Schedule C the firms manufacturing the bending magnets are asked to increase their rate of production over the rate at which they are then producing the first set of bending magnets. In this way all the bending magnets for 400 GeV energy might be made available by mid 1975; and allowing the same times as in Schedules A and B for assembly, alignment, testing and machine commissioning, a proton beam could be made available in the West Area at the end of 1976, i.e. only four months later than proposed in Schedules A and B.

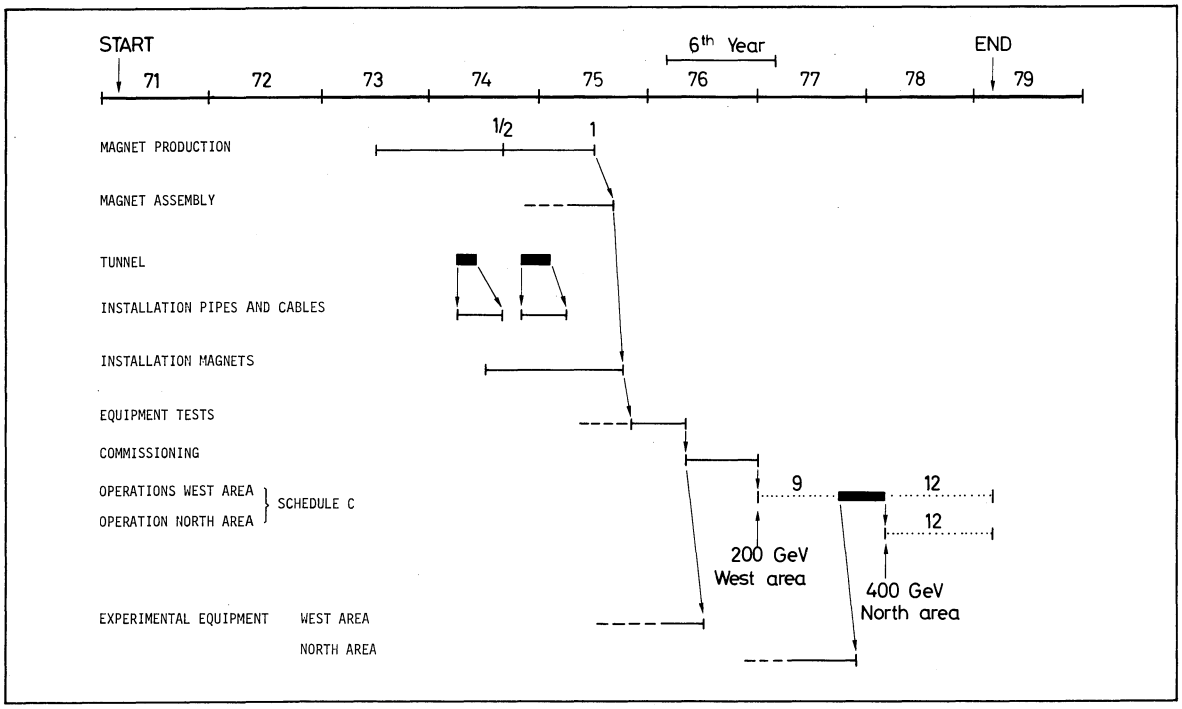

Fig. 2

21. From the beginning of 1977 to the end of the Programme in February 1979 the machine is operated with normal shut-downs and one long shut-down of a few months in order to complete and commission the extraction system for the North Area. Thus in Schedule C experimentation starts a few months later than in Schedules A and B, but machine operation time during the Programme is 18-21 months instead of 14 months, i.e. 4 to 7 months longer.

22. Clearly, Schedule C also raises the possibility of an energy higher than 200 GeV to feed the underground neutrino target in the West Area during the Programme, and 400 GeV earlier than at the end of the Programme in the North Area. Both these possibilities arise from the machine being commissioned at the end of 1976 complete with all its bending magnets.

DISCUSSION OF SCHEDULE C

23. As in Schedules A and B the bending magnet cost during the Programme is increased over what was foreseen, since bending magnets for 400 GeV energy would be ordered rather than for 300 GeV. In Schedules A and B this extra cost falls in the year 1975, but in Schedule C it falls in 1974 and 1975 which is more difficult since the annual budgets up to the end of 1975 are very tight indeed. The total sum available according to the Programme up to the end of 1975 is 634 MSF, of which 201 MSF are allocated for the equipment for the accelerator, including the magnet system. If all the bending magnets for 400 GeV energy are produced and paid for by the end of 1975 -- which follows from Schedule C -- then an extra 40 MSF is required, which is 20% more expenditure on machine equipment than was foreseen up to the end of 1975.

24. A similar problem arises with the possibility of supplying more than 200 GeV energy to the West Area. In the estimates for the Programme given in CERN/1050, an extraction system for 200 GeV energy was foreseen for the West Area together with a beam transport system to the neutrino target also for 200 GeV. According to Schedule C the production and payment of this equipment must also take place before the end of 1975 if it is to be ready in 1976, and the extra cost for a 400 GeV extraction system together with a 400 GeV beam transport system to the underground neutrino target, compared with the cost of a 200 GeV system, is about 10 MSF.

25. Furthermore, considerably more expenditure is required to set up a 400 GeV neutrino facility in the West Area than is needed for a 200 GeV neutrino facility -- a cost which does not fall on the 300 GeV Programme but on the budgets of Laboratory I.

26. Another possibility with Schedule C is to open up the North Area at 400 GeV energy before the end of the Programme, i.e. before February 1979.

27. Considerations of staff availability and the technical possibilities of the 300 GeV Construction Programme suggest that the North Area might be opened up for some experimentation about a year earlier than is now foreseen, i.e. about February 1978. However, financial limitations then arise in two ways. Firstly, as much as possible of the North Area extraction system should be installed before the machine is first brought into operation towards the end of 1976. This would both shorten the installation and commissioning time for this system after 1976, and allow a continuous development, construction, and commissioning programme to be established for the group responsible for this equipment and the industry involved in its manufacture. Some of this expenditure will fall before the end of 1975 and hence add to the financial problems already mentioned above. Secondly, in the Programme now foreseen, the development of the North Area is scheduled such that its expenditure falls in the three years 1976, 1977, and 1978, so that if the North Area is made ready for limited experimentation earlier than February 1979, some expenditure, mainly for civil engineering and for the staff of the group carrying out this work, will fall in 1975 and further add to the financial problems of the first five years of the Programme. The extra money required in 1975 is estimated to be about 15 MSF, which would have to be recuperated from the budgets of the remaining years of the Programme.

28. From this brief discussion of Schedule C it is clear that although the technical problems it presents could probably be overcome, the financial problems it presents are serious. It will be recalled that the Council, in agreeing to the 300 GeV Programme, decided to restrict the annual budgets and to spread the costs of the Programme over an eight-year period. This financial restriction on the annual budgets came about because of the difficulties experienced in the Member States in increasing their annual budgets for the high-energy physics in the years following the start of the 300 GeV Programme. In some Member States the decision to go ahead with the 300 GeV Programme was coupled with a decision either to hold constant the annual budgets for the national laboratories and the universities in this field of research or in some cases to reduce them. It seems only prudent at this stage, therefore, to plan the machine construction schedule on the basis of the annual budgets which are now agreed by Council.

29. The extra costs of Schedule C over the original estimates made for the 300 GeV Programme can be summarized as follows (see Table 1):

a) As with Schedules A and B there is the extra cost for 400 GeV bending magnets rather than 300 GeV bending magnets which were originally foreseen. This amounts to an additional 20 MSF on the total Programme cost, and since the latter is fixed this 20 MSF must be recovered from the contingency or, in the last resort, from the North Area expenditure. Also, a 400 GeV West Area extraction system and beam transport to the neutrino target adds a further 10 MSF to the total Programme cost.

b) In addition, Schedule C requires a shift of expenditure from the latter years of the Programme to the years 1974 and 1975, which increases the annual budgets of those years over that which is available. The shift of expenditure arises from three requirements:

- Firstly, all the bending magnets are ordered, delivered, and must be paid for by the end of 1975 instead of only half the bending magnets. As a result, about 40 MSF is added to the annual budgets of 1974 and 1975.
- Secondly, if 400 GeV protons are fed to the neutrino target in the West Area instead of 200 GeV protons, about 10 MSF must be added to the annual budgets of 1974 and 1975 (in addition there will be considerably more expenditure incurred by Laboratory I if a 400 GeV neutrino facility is set up in the West Area in place of a 200 GeV facility).
- Thirdly, if the North Area is opened up early in 1978 rather than early in 1979, about 15 MSF must be shifted from the last three years of the Programme into 1975, mainly to pay for civil engineering installations. In addition, the North Area extraction system should be completed earlier than now foreseen, which adds a further 20 MSF to the cost of the Programme in 1974 and 1975.

Table 1

	Additional project cost (in MSF)	Additional cost 1974-1975 (in MSF)
400 GeV instead of 300 GeV	20	-
400 GeV magnets by mid 1975	-	40
400 GeV protons to ν target, West Area	10	10
North Area 1 year earlier	-	15
North Area extraction system by 1976	-	20
Totals	30	85

30. If all the possibilities of Schedule C were taken up, the 300 GeV Programme cost would be increased by 30 MSF, and since the total budget is fixed by Council this amount would have to be recuperated from whatever contingency remains towards the end of the Programme, or as a last resort from the sum put aside for the development of the North Area (143 MSF). The most serious financial problem is the extra expenditure incurred up to the end of 1975, which amounts to 80 to 90 MSF and is comparable with the total sum put aside as a contingency up to that time. This contingency sum is 82 MSF and is intended to cover any unforeseen expenditure for machine components, civil engineering and site installations, and personnel costs.

31. Clearly, it is far too early at this stage of the Programme to allocate all the contingency to the machine components alone, and in any case the decision on which machine construction to follow will not have to be taken until the second part of 1973. Nevertheless, it seems possible that some of the features offered by Schedule C might be carried out, and it is important to know from the experimenters which of those listed above are the most interesting and most important from their point of view.

32. In this respect the following list of questions to experimenters may help the discussion:

a) Schedules A, B, and C compared with original schedule

Is 400 GeV rather than 300 GeV worth the extra expenditure during the Programme, remembering that the extra cost is only 20 MSF?

b) Schedule C versus A or B

Which is more attractive? to start experiments in the West Area in the middle of 1976 and have available about 14 months of machine operating time up to February 1979? or to start experiments in the West Area at the end of 1976 and have available 18-21 months of machine operating time up to February 1979 plus the possibility of opening up the North Area in 1978 rather than in 1979?

c) Choice of possibilities of Schedule C

Is it more important to feed the underground neutrino target in the West Area with 400 GeV protons rather than 200 GeV protons at the earliest possible date, or to open up the North Area at 400 GeV energy early in 1978 rather than early in 1979?

33. It is important to note that all the schedules mentioned above refer to what could be done during the 300 GeV Construction Programme and do not affect what might be done after the end of the Programme. For example, if it is decided to limit the energy to the neutrino target in the West Area to 200 GeV during the Programme, it is always possible to raise this energy to 400 GeV should this be required after the construction programme is finished.

MACHINE CONSTRUCTION SCHEDULE D (see Fig. 3)

34. Schedules A, B, and C all assume that a decision is taken towards the end of 1973 to complete the machine with iron-cored bending magnets. Schedule D, on the other hand, assumes that it is decided at that time to install superconducting rather than iron-cored bending magnets. The time-scales mentioned below are taken from the most recent GESSS estimates (GESSS-1, May 1972).

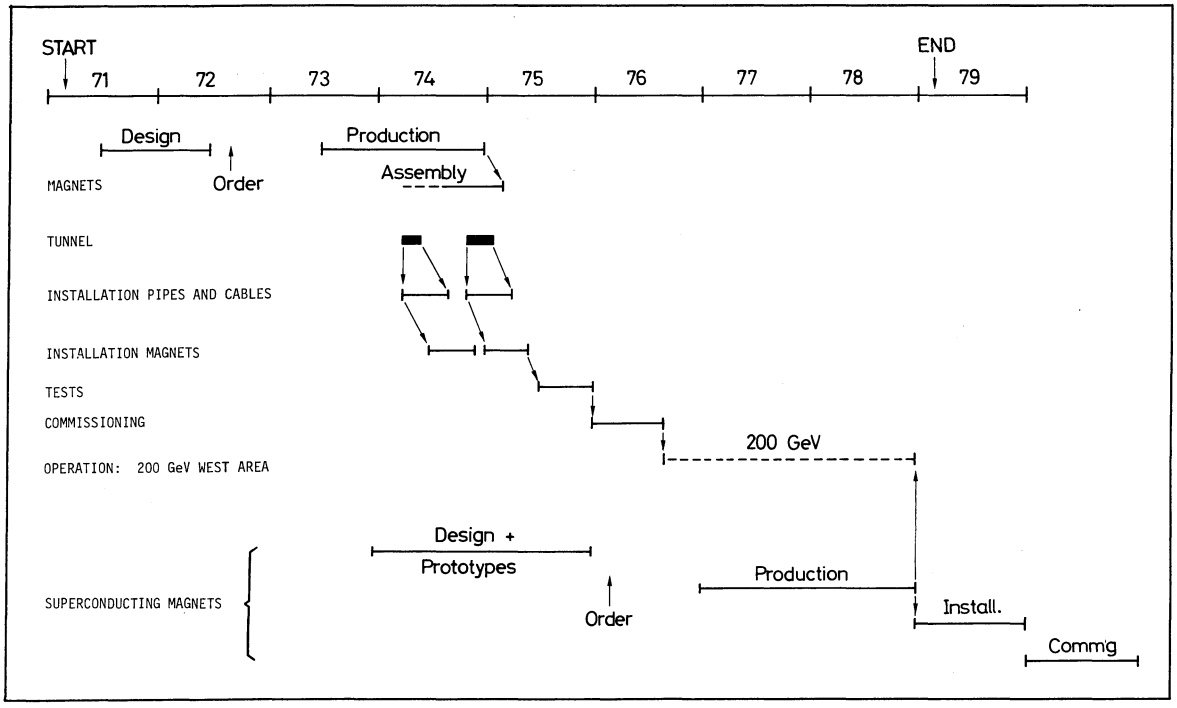

Fig. 3

35. If, towards the end of 1973, a decision is taken in favour of superconducting bending magnets, it is clear that the design and production of these magnets will take longer than simply ordering another set of iron-cored bending magnets which are already in production. Schedule D might then go as follows. Detail design on the superconducting magnets starts at the beginning of 1974 and is completed, including prototypes, by the end of 1975. Offers for tenders are sent out at the beginning of 1976; production starts early in 1977 and is completed by the end of 1978. Installation of the magnets then starts early in 1979, and the accelerator is running at 400-500 GeV energy by the end of 1980 after a commissioning period of one year.

36. From mid 1976, when 200 GeV is available in the West Area, until the end of 1978, experimentation is limited to 200 GeV energy, and no higher energy than this would be available until the end of 1980 at the earliest.

37. The North Area could be opened up at the end of the Programme and possibly earlier, but only at 200 GeV energy.

DISCUSSION OF SCHEDULE D

38. Since Schedule D extends outside the eight years of the 300 GeV Programme, it does not conform with the Programme requirement that at least 300 GeV energy should be reached by the end of the Programme. Therefore a modified Programme would have to be presented to the Council and could only be adopted by a new decision taken by Council.

39. The cost of a set of superconducting magnets for 400-500 GeV energy is still not known. However, it should be noted that the cost to go from 200 GeV to 400 GeV using iron-cored magnets is 40 MSF, and it seems very unlikely that superconducting magnets for 400-500 GeV energy could be manufactured, together with their cryogenic system, for 40 MSF. Whatever extra cost is involved could either be recuperated from the sum of money put aside for the North Area development, or the Council could be asked for additional money for the 300 GeV Programme with superconducting magnets for its second energy stage. Again the CERN Council and the Member States would be presented with a new decision.

40. Schedule D, from the point of view of experimenters, offers about the same energy (400-500 GeV) as Schedules A, B, and C; it delays experimentation at 400 GeV energy by at least two years; and it may delay the North Area for financial reasons in order to recuperate the extra expense incurred by the superconducting magnets. It does not therefore look very attractive from the experimental point of view, and it would only be interesting if it offered something more to experimenters than the other schedules offer. This something more is the possibility later on, after the 300 GeV Programme is completed, of raising the machine energy to 1000 GeV. It must therefore be considered whether Schedule D is the best way of achieving this goal.

41. An alternative way to that of Schedule D of reaching 1000 GeV is to complete Schedules A, B, or C, and then to build a new accelerator with superconducting magnets either inside the machine tunnel then existing or in another tunnel alongside it, using the existing machine as the injector into the superconducting magnet machine. By using 200 or 400 GeV as the injection energy, considerable reductions can be made in the apertures of the superconducting magnets and hence in their costs, and these savings might compensate the extra costs involved in building a complete accelerator with superconducting magnets.

42. Machine design studies for such a superconducting magnet accelerator are being carried out by the GESSS Collaboration in conjunction with CERN Laboratory II, and will form an important element in the decision to be taken towards the end of 1973.

43. Clearly a new accelerator using superconducting magnets will constitute a new Programme for CERN; it cannot be considered as part of the present 300 GeV Construction Programme. It will therefore be compared with any other new Programme proposed at that time (about 1980), such as electron-proton or proton-proton intersecting rings.

CONCLUSION

44. This note has compared the main features of several machine construction schedules with the aim of stimulating discussion amongst experimenters on the interest and importance they would attach to the particular features offered by the different schedules.

45. The principal limitation on all schedules is financial, both in respect of the extra expenditure they impose on the total Programme cost and, particularly, on the annual budgets up to the end of 1975.

46. Technical and man-power limitations also arise, but these can probably be overcome, again at some extra cost.

47. It is important in planning the 300 GeV Programme that experimenters establish priorities amongst the various possibilities offered by the different schedules. From the point of view of the 300 GeV Programme itself, the important decisions must be taken in the second half of 1973. Until then, all the possibilities can be maintained by including options in the machine component contracts which are placed in 1972 and 1973.

48. The views and opinions of experimenters will help us to make the decisions on the Programme as they arise in the next year, so that what is finally built will best suit the needs of the European nuclear particle physicists.

CHAPTER II

EXPERIMENTAL AREAS

OUTPUT BEAMS FROM THE SPS

E.J.N. Wilson
CERN, Geneva, Switzerland

1. GENERAL

In an earlier session, H.O. Wüster explained to you some of the limitations to the performance of an accelerator such as the SPS. In this talk I would like to give you a summary of the parameters of the proton beam which we expect to emerge from the SPS, and to indicate which of the performance limitations he mentioned come into play.

In Table 1 I have listed the parameters of the output beam. Some of them, such as the energy or duty cycle, one can predict with some precision. For others, for instance intensity or ripple amplitude, one can only define a range in which we expect the machine's performance to lie.

Table 1

Energy and repetition rate
Intensity and extraction efficiency
Beam emittance and momentum spread
Flat top and slow spill ripple structure

I would like you to have a clear understanding of the level of confidence we attach to each end of the range and to have no illusions. To give you a feeling for this, let us imagine that the machine is being commissioned and we have got past the initial stage of just getting systems to work at the same time. Then there will be a period of trying to get the machine working in a respectable way for high-energy physics. We will feel this task is nearing its end when we reach the performance figures which we term "design parameters": the numbers we quote in CERN/1050. The range of possible performance extends upwards from these design parameters. Given the incentive, certain parameters, such as intensity and extraction efficiency, will of course be improved during the life of the machine. They will in some cases and with varying success approach the upper end of the range -- the upper end of the range (the "design aim", if you like) being the theoretical estimate of performance which can only be reached with ideal conditions and after an infinite amount of machine development.

2. ENERGY AND REPETITION RATE

Figure 1 shows a typical acceleration cycle. Let us look at the lower figure (400 GeV). We see, after a short pause for injection, a constant rate of rise in current (the solid line). Particle energy and magnetic field of course follow the same curve. The magnet behaves just like an inductance, and this rise rate is just proportional to the voltage applied. The voltage, or more precisely the peak power, is the maximum we can persuade the Electricité de France (EdF) to let us take from their super-grid. Altogether it comes to about 110 MW. The RF system is designed to just provide this acceleration rate. So the maximum rise (and fall) rates are fixed, and a lower energy cycle inevitably gives a shorter rise and a quicker repetition rate. In Table 2 I have given the maximum rise-times for 200 and 400 GeV and the total cycle time. The first two lines are for the nominal 0.7 sec flat top, and the last shows the effect of a 2 sec flat top which, if you remember, we included in our plans following your request at Tirrenia last year.

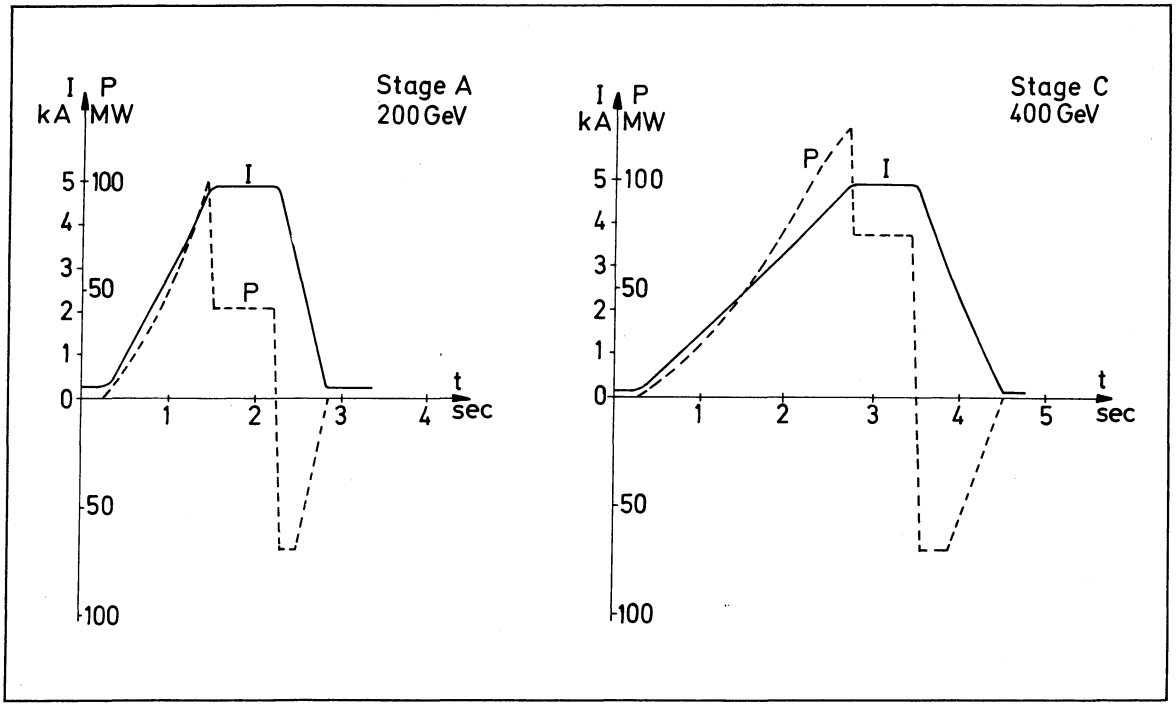

Fig. 1 Pulse profiles

The last line, incidentally, corresponds almost exactly to the "Future 400 GeV cycle" given in the NAL design report. I would like to emphasize, however, that none of these cycles exceeds the mean and peak power limits already agreed with the EdF, and cooling water sufficient to operate these cycles will be available from the start.

Table 2

Energy (GeV)	Flat top (sec)	Rise-time (sec)	Cycle time (sec)	Duty cycle (%)
200	0.7	1.11	3.33	21
400	0.7	2.42	5.6	12.5
400	2.0	2.42	8.6	23.2

3. INTENSITY AND EXTRACTION EFFICIENCY

Intensity, I have said, can only be estimated within a range, and one's estimate must depend on how rapidly the machine commissioning progresses.

The space charge limit at injection of the CPS, without the PS Booster, was clearly reached a few years ago in the CPS at 2×10^{12}. Putting in more protons at 50 MeV only led to more losses and the CPS was obviously saturated. This, you may remember, was what led to the PS Booster (PSB) being built, since the only way of pushing more protons in the CPS

was to raise the injection energy so that space charge forces become less important. The PS Booster is designed to inject at 800 MeV. Its design intensity is 10^{13} ppp, and success with the running in of the PSB gives us considerable confidence that it will be reached.

Even supposing the 10^{13} protons then pass through the CPS without difficulty, the SPS will not immediately be able to digest them.

First of all we shall start setting up with a pencil beam of less than 10^{11} protons -- this we expect to have very quickly once all systems are working together. We then plan to measure the shape of the closed orbit. We expect, because we have cut the machine aperture to the minimum, that the wiggles in the closed orbit will then be almost as big as the vacuum chamber, and computed correction currents will have to be fed to small dipoles to straighten the orbit at injection. Then we will start to work the machine energy up to, say, 200 GeV to allow us to find out how much of the wiggle remains. This residual component will be that due to misalignments of magnets, and will be directly compensated by moving a few sensitive magnets.

Even if this procedure works easily and we have enough room for a fat beam from the CPS, there will remain much hard work to be done before we can allow an intense beam anywhere near the SPS. The self-destructive capacity of the machine is impressive. For example, if the full intensity beam is allowed to drift into the vacuum chamber or any other component, it will raise its temperature to about 3000°C. Only 3×10^{11} particles, i.e. 3% of the 10^{13} intensity, can be allowed to be lost on a regular basis if components like the extraction septum are to be accessible for removal, let alone maintenance.

There are many opportunities for beam loss. After injection we must capture the beam in the RF bucket. Then we must pass through transition where strong correcting sextupoles will be needed to keep the edges of the energy spread from hitting the net of resonance lines in the Q diagram. The beam must also be coaxed through $\sqrt{3}\ \gamma_{tr}$, where the bucket area is smallest compared to the beam. Finally, the complicated extraction system has to be tuned up to be efficient to at least 97%, and we must be confident that on bad pulses the beam does not strike anything. People keep asking how long this will take. Well, the intensity laid down in the programme definition is 10^{12} protons per second corresponding to a few times 10^{12} protons per pulse. We hope that if everything goes smoothly in the commissioning, this design parameter will be reached between six months and a year of establishing the first turn. However, this assumes that no new and unforeseeable difficulty emerges. Nasty surprises can happen. Look at the instabilities in storage rings or the injection losses NAL are worried about, neither of which were predicted. Should anything like this arise, of course, we will all just have to be patient.

If we have 10^{12} protons per second as the design parameter, what about the design aim? Obviously we will try eventually to take the full 10^{13} per pulse that the CPS offers.

We have, of course, our own SPS limits to intensity. Interaction between the beam and the high-impedance RF cavities will become important as we approach 10^{13} ppp. This could prevent RF capture. Transverse instabilities, which grow as the retarded image forces become strong between the resistive walls of the vacuum chambers and the beam, will become important at about the same intensity level. To combat these effects and to reach 10^{13}, certain measures can be taken. Momentum spread helps and damps rebunching; so does adding a "pinch

of non-linear field". However, these remedies make it more difficult to steer the beam through the net of resonance lines. In short, it will be a long, hard job to reach 10^{13}, the upper limit of the intensity range; and although one might one day dream of pumping in more than one PS load, we cannot say yet whether more than 10^{13} protons will ever be accelerated. What is clear is that NAL and ourselves are in a very similar situation as far as these intensity limits are concerned. This is perhaps the best answer to those who wish to compare these two machines.

4. BEAM EMITTANCE AND MOMENTUM SPREAD

Table 3 is just reproduced from CERN/1050. Emittances before extraction have been estimated assuming that the SPS aperture is full at injection, as is indeed likely to be the case for the bunch-by-bunch transfer mode from the CPS. In theory, emittance then shrinks as $1/\beta\gamma$ during acceleration, but experience in the CPS suggests that the final emittance may be twice as large as one might calculate in this way. This factor of 2 inflation has been included in the values given in Table 3. The continuous transfer scheme will, it is hoped, inject a smaller beam into the SPS, and the horizontal emittance may well be as small as the figure given for the vertical emittance. So much for the beam in the machine.

Fast extraction does not affect the emittance; but slow extraction, because it peels the beam, reduces the horizontal emittance. On the other hand, slow extraction over a long spill must be with a debunched (large momentum spread) beam.

Table 3

	Stage A	Stage B	Stage C
Fast spill			
Energy (GeV)	200	300	400
Horizontal emittance (π mm mrad)	0.7	0.5	0.4
Vertical emittance (π mm mrad)	0.35	0.25	0.2
Momentum spread (‰)	±0.5	±0.4	±0.3
Slow spill			
Horizontal emittance (π mm mrad)	< 0.4	< 0.3	< 0.3
Vertical emittance (π mm mrad)	< 0.4	< 0.3	< 0.2
Momentum spread (‰)	±1.5	±1.2	±1.0

These emittances can be focused down to a few millimetres without much difficulty.

5. SLOW EXTRACTION AND FLAT TOPS

Slow extraction is not an easy concept and I will spend a minute or so reminding you of some of its features.

Slow extraction is the more delicate of the two extraction modes. Normally, during acceleration, protons oscillate about the centre of the vacuum chamber performing linear betatron motion. In horizontal phase space (x,x') their motion follows an ellipse (Fig. 2).

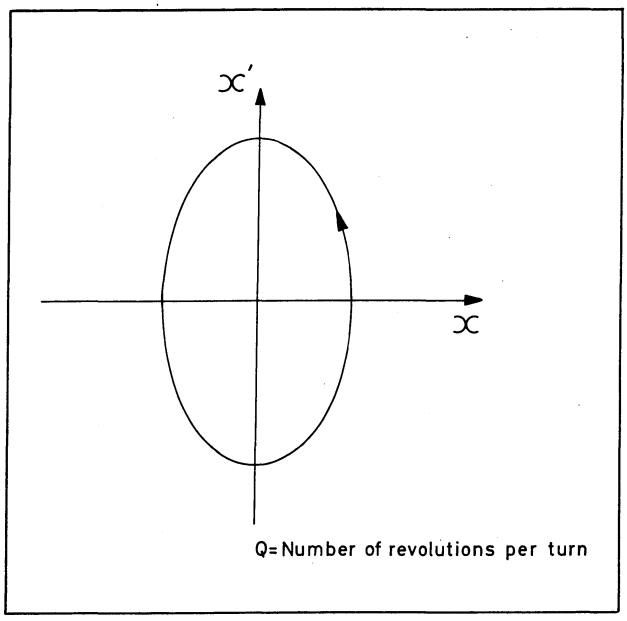

Fig. 2 Betatron motion

The frequency of their motion around the ellipse is Q per turn of the machine. If Q is a whole number of an integer divided by 2 or 3, resonances of growing amplitude can build up since imperfections in field are seen in the same phase every third turn. In the slow extraction process the machine is deliberately tuned, by increasing the quadrupole strength, until Q = 83/3. The proton amplitude then grows until it "jumps" the extraction septum and flies out of the machine down the extraction channel.

To make the jump grow rapidly so that few particles actually hit the septum, non-linear sextupole fields are switched on. This has the effect that above a certain amplitude threshold the resonant motion becomes unstable and the proton gets out of the machine in a few tens of turns (Fig. 3). In phase space terms, we say there is a separatrix between stable and unstable motion, the "cliff edge" if you like.

As the Q of the machine is tuned towards the 83/3 value, this separatrix shrinks, gradually squeezing all protons out into resonance.

What is really happening is that the Q is amplitude-dependent, and at the separatrix becomes exactly equal to 83/3. Nearer the centre of the triangle the Q is further away from resonance. If we sweep the Q of the machine slowly towards 83/3, first the large-amplitude particles become resonant, then those of smaller amplitude. The stable triangle shrinks, squeezing out protons in a steady stream. This, of course, is just what we need to give a long spill for counters.

Figure 4 shows how Q is gradually tuned by increasing the machine quadrupole strength until the whole Q-spread in the beam (ΔQ) from small to large amplitudes is brought into resonance. If τ is the spill time, the gradient dQ/dt is just $\Delta Q/\tau$.

The gradient of this change in Q, dQ/dt, is very shallow indeed, and any small ripple component in the quadrupole or dipole magnet current, both of

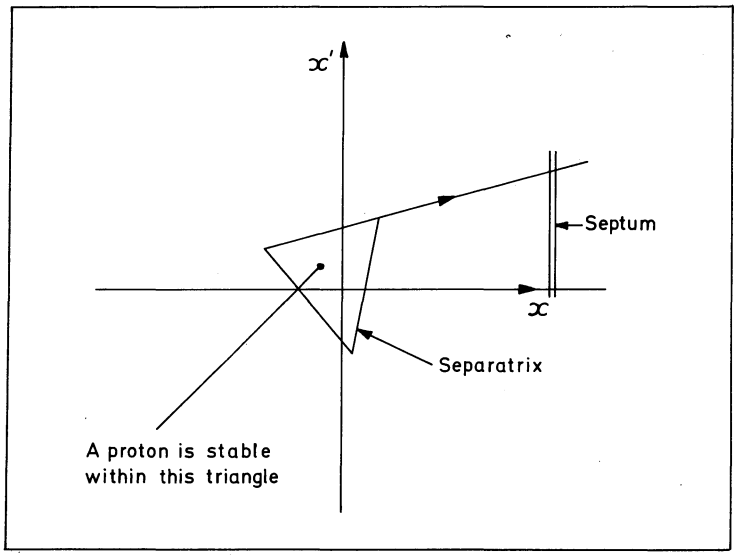

Fig. 3 Extraction at 1/3 integer

which affect Q, can upset the smooth sweep through the Q-spread in the beam and modulate the rate of spill. Figure 5a shows how, if the time derivative dQ/dt and that of the ripple are comparable, the approach to the resonance can momentarily be halted and the rate of spill be modulated with 100% amplitude (Fig. 5b). Figure 5b is in fact the differential of Fig. 5a.

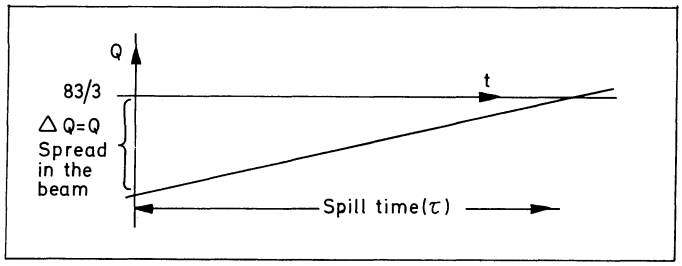

Fig. 4 Ideal slow spill

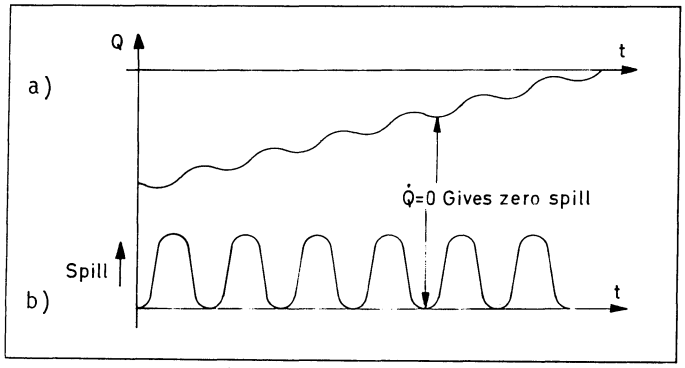

Fig. 5 Spill modulated 100% owing to ripple

If we ask for spill over a long time (say 2 sec instead of 0.7 sec), or if we wish to extract only a fraction γ of the beam (say 20%) before fast-ejecting the major part to, say, a neutrino target, then dQ/dt becomes proportionally shallower and the modulation gets worse. However, there is one thing which helps and which makes the ripple problems just tolerable.

I have simplified this explanation of the effect of ripple by ignoring the dependence of Q on momentum, the refractive index of the machine. This makes the Q-spread in the beam large, and can help to make dQ/dt larger and the sensitivity to ripple better.

It is important to blow up the $\Delta p/p$ in the beam to the maximum which the RF can hold before slow extraction to help with the ripple situation.

But even with this to aid us it would be impossible to keep ripple structure down to tolerable limits were it not for one of the features peculiar to the 1/3 integer scheme.

Protons take longer to get out of the machine with 1/3 integer scheme than with the integer. This is a considerable help. You must first realize that because of the dependence of Q upon momentum, different combinations of amplitude and momentum are extracted at the same time. Protons of smaller amplitude take more turns and therefore a longer time to get to the septum than those of a larger amplitude and lower momentum, though they may start together. If these differences in exit time are comparable with the ripple period, the effect of ripple is smeared out. The exit time for 1/3 integer ejection is just long enough for this smearing to blot out all but the lowest frequencies of ripple which we expect from the power supply waveform ($\sim$ 100 Hz). This is why we must use the 1/3 integer scheme for slow spill.

When all this is put together we find we can guarantee as a design parameter that, given 1/3 integer ejection and provided $\Delta p/p$ is blown up, the modulation of the spill rate

$\Delta R/R$ will be less than 50% for a 0.7 sec spill[1]. We will try to improve on this, of course. Our design aim is to give you only 80% modulation even in the extreme case of extracting 20% of the beam over 2 sec. On paper this is possible if we ignore one thing -- the transmission line modes of ripple which propagate around the ring. How rapidly we ascend the range from parameters to aim will depend on how serious these modes are -- they are almost impossible to calculate.

These spill modulations seem large, but remember that as far as accidental rates and dead-times are concerned, 100% ripple reduces the duty cycle by 36%. We cannot, like the PS, correct this by servo spill -- the exit time is too long and the phase lag too big.

There is a very big IF in all this. We must increase $\Delta p/p$ by switching off the RF and letting the beam smear-out. This means that in an intermediate flat top (Fig. 6) where such gymnastics are prohibited because the beam must be kept within the bucket ready for acceleration up to 400 GeV, ripple will be a problem. Add to this the need to slow extract only a fraction of the beam to leave some for 400 GeV and the situation becomes even worse. In fact we cannot guarantee a slow spill on an intermediate flat top as long as 100 milliseconds.

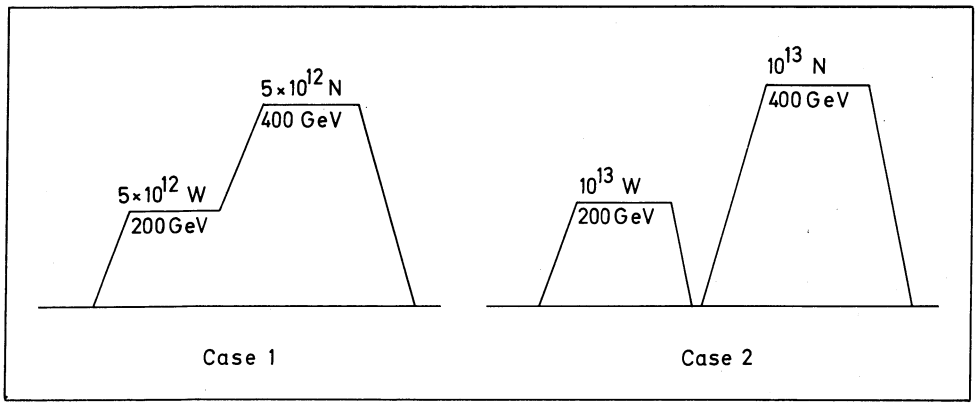

Fig. 6 Alternative sharing modes

Fortunately there is a solution which has other attractions (Fig. 6). If we make alternate 200 and 400 GeV pulses we can give ripple-free spill to each area[2]. Of course the double pulse is longer (Table 4).

Table 4

	Case 1	Case 2
West flat top	0.7 sec	0.7 sec
North flat top	0.7 sec	0.7 sec
Cycle time	5.5 sec	7.7 sec
Protons/second	1.8×10^{12}	2.6×10^{12}
Spill modulation in West	84%	7%

But imagine you are sitting in a counting room in the West Hall. You see one pulse every 7.7 sec but it contains twice as many protons. Not only that, but the ripple modulation is about 10 times better, so there is no question that you cannot handle the increased intensity; in fact you may find you can ask for 50% of the beam instead of only 10% if with the intermediate flat top you were rate-limited. This request makes ripple even better.

Even fast spill experiments and users who are not rate-limited will perhaps find the double cycle an advantage. It gives 50% more protons per second and the ability to have long slow spills at 200 GeV will make it easier to schedule BEBC in the double pulse mode.

The comparison becomes even more favourable when long (2.0 sec) flat tops are demanded. Then the fact that the repetition rate is limited by heating of the magnet rather than rise rate makes the two repetition rates almost the same (8.6 and 9.0 sec).

This is because there is quite a lot of dead-time in the 8.6 sec cycle to let the magnet cool. The extra 200 GeV cycle which does not heat the magnet much can be largely substituted for this dead-time.

5. FAST-SLOW EJECTION

I have said that extraction of a particle (the exit time) is longer for 1/3 integer ejection than for integer ejection, and this is essential if we are to have good slow spill. Add to this that 1/3 integer extraction can be made less sensitive to bending magnet ripple by putting the driving sextupoles 180° apart and opposite in polarity, and one sees that we must start by setting up 1/3 integer extraction.

However, the long exit time means that if we try to extract over less than 5 msec, the stable area, which re-forms as Q passes through the resonance to the other side, traps the majority of particles which have had no time to get out.

Once we have solved the problem of slow spill with the 1/3 integer, we might try to make spills as short as 1 msec with an integer scheme; but apart from the many months (perhaps longer) involved in getting this to work at high efficiency, one would never be able to switch from one scheme to the other within a pulse. Any fast-slow spill user would therefore monopolize the beam, which could not be shared with counters wanting a really long spill. So I am afraid that we cannot assume a fast-slow spill of less than 5 msec. There is therefore a big gap between it and the fast extraction (35 μsec).

6. FAST EXTRACTION

Ideally, fast extraction would be a 100% efficient process. A fast rise-time kicker would deflect the beam across the septum and down the spout. The rise would be within the time interval between bunches. Such a system was designed for the CPS, but there, because there is a long gap between bunches, the rise-time can be as slow as a hundred nsec. In our case, not only would the kicker have to be many times as powerful (because of the energy of the SPS), but 20 times as fast because of the bunch spacing. It is just not possible for the SPS. Fortunately there is another way of doing it. A pair of bumpers rising within a turn (23 μsec) can sweep the beam across the septum over 30 μsec (the rise-time plus one turn). Smaller fractions can be extracted for just a few microseconds if needed for RF beams. This kind of "beam shaving" extraction is very flexible.

7. SEQUENCES OF EXTRACTION

Experience with the CPS has shown that the sequence of fast and slow spills can become quite complicated, especially when more than one experimental area is being fed. The principles of extraction in the SPS are similar to those employed on the CPS, and there is no fundamental reason why the SPS should not be scheduled in the same way with fast and slow spills following each other, taking different fractions of the beam and with extraction at different energies on the same alternate cycles. In many ways the natural separation of the energies of the West and North Areas will simplify the sequencing, as will (at least initially) the absence of a need for fast spill in the North. One of the apparently difficult sharing problems in the SPS is to give simultaneous slow beam to two extraction channels. This seems to be ruled out by the numerology and symmetry of a machine designed to avoid rather than stimulate resonances. Fortunately, we have a hope of dedicating each area to a different energy range, so that sequential rather than simultaneous spill will be a more natural request. Life will certainly be easier if we can keep it that way.

Figure 7 is an illustration of what one might do.

a) A slow spill to the West of 20% to 100% of the beam. This would then be split in the West Hall to feed a number of counter experiments simultaneously.

b) A fast spill, perhaps 1% in 5 μsec, to the RF target. This could be followed by another such 1% burst at the end of the flat top, followed even by a further one during the rise of the second pulse, giving altogether three bursts to BEBC. It must be said that the second of these would be better placed before the slow spill, since to fast-eject 1% of an already depleted beam is difficult, and one must not forget that its momentum would have been blown up for slow spill.

c) Slow spill to the North Area at 400 GeV.

Clearly there are many variations on this theme which can be scheduled on a day-to-day basis. More detailed information is to be found in the references below.

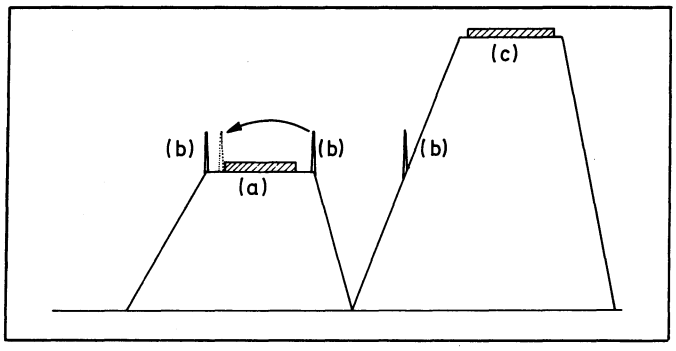

Fig. 7 A possible sequence

REFERENCES

1) G. von Holtey, Ripple requirements for the slow extracted beam, Lab. II-DI-PA/Int. 72-13 (1972).

2) G. von Holtey, Comparison of acceleration cycles for the SPS, Lab. II-DI-PA/Int. 72-9 (1972).

* * *

POINTS ARISING IN THE DISCUSSION AFTER E. WILSON'S TALK

1. PULSE DURATION FOR THE WEST AREA UNDERGROUND NEUTRINO FACILITY

The question was asked whether it would be possible to increase the pulse duration from $\sim$ 30 μsec to $\sim$ 1 msec. The motivation would be not so much the requirements of the EMI for BEBC, but the installation of a neutrino counter experiment behind BEBC.

To achieve this, one would have either to substantially increase the fast burst duration (extraction on many turns) or operate the slow extraction on a fast mode.

The following comments concerning these two alternative methods can be made:

1.1 Slow-fast extraction

The main limitation comes from the losses (and consequent heating) of the thin electrostatic septum. It is not possible to prolong the pulse duration at full intensity; this can only be done by substantially reducing the beam intensity (and density).

1.2 Fast-slow extraction

Of the two resonant extraction modes, the best for slow extraction is the 1/3 integer, because it is essential if the long spill is to be reasonably free of ripple, and it should be the most stable. Unfortunately it is also an intrinsically slow process and, if driven fast, a substantial number of particles would not be extracted and would be lost in the machine. From the point of view of fast-slow extraction, the situation would be better with an integer resonant mode, but this implies operating the machine on a less favourable working point (close to an integer stop-band). Moreover, it cannot be shared on the same machine pulse with a 1/3 integer extraction used for counters.

On the whole, it is not possible to promise anything intermediate between normal fast extraction (< 30 μsec) and slow 1/3 integer extraction (> 5 msec) at substantial intensity before considerable operational experience is gained.

2. SHARING OF PROTONS BETWEEN THE WEST AREA AND THE NORTH AREA ON THE SAME MACHINE PULSE

2.1 Slow extraction in both areas

With the two Areas operating at different energies (e.g. West at 200 GeV and North at 400 GeV), the West Area slow extraction can be done on an intermediate flat top of a combined 200-400 GeV cycle (Case 1 of Fig. 6) or on a separate 200 GeV cycle (Case 2). Examples of these two cycles are given below:

Comparison of Case 1 and Case 2
(updated figures for two RF cavities)

τ_W (sec)	τ_N (sec)	T (sec)		T_2/T_1	Dissipation limited		Protons per hour
		1	2		1	2	N_2/N_1
0.7	0.7	6.6	9.4	1.42	no	no	1.41
0.7	2.0	9.1	10.7	1.18	yes	no	1.69
2.0	2.0	9.8	12.0	1.23	yes	no	1.63

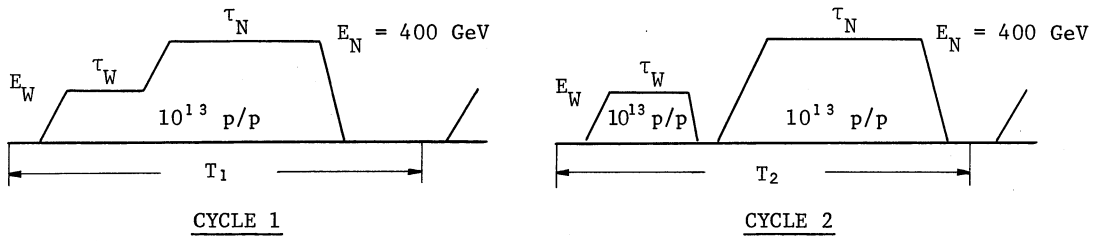

Case 2 presents no problems, whereas in Case 1 the 200 GeV extraction must be done with the RF on and a bunched beam if one wants to reaccelerate the remaining beam to 400 GeV/c.

From the machine point of view, a spill with RF on implies tolerances on both the magnetic field ripple and the RF stability which cannot be guaranteed at this stage. The reason is that these tolerances strongly depend on the beam emittance and could, for small emittances, be extremely difficult to meet.

Even if these difficulties for Case 1 could be overcome, a separate 200 GeV cycle has still several advantages. In Case 2 the slow extraction to both the North and West Areas can be done with a debunched beam, and in this case the modulation of the extracted beam current by magnetic field ripple will be several times smaller than in Case 1*). Moreover, the number of protons accelerated per hour is larger in Case 2, as shown in the above table. This is obviously to the advantage of the experiments at 200 GeV, but in general it is also true for experiments at 400 GeV since they do not suffer from a reduction in the accelerated beam current owing to the removal of part of the protons by slow extraction during the intermediate flat top.

The conclusion is that the separate cycles look more attractive.

*) A detailed study of this effect is available from G. von Holtey (CERN Lab. II).

2.2 Fast extraction in the West Area and slow extraction in the North Area

No special problems exist if the two operations are done at the same energy [e.g. fast extraction (FE) for the WA neutrino target at 400 GeV and slow extraction (SE) for the NA counter targets also at 400 GeV].

If the two operations are required at different energies, the situation is as follows:

- FE at low intensity at 200 GeV (e.g. RF-separated beam to BEBC) followed by SE at 400 GeV: possible.
- Same but FE at high intensity: may result in a subsequent slow spill with strong ripple structure.

3. FAST EXTRACTION FOR THE NORTH AREA (RAPID-CYCLING BUBBLE CHAMBER)

So far only the slow extraction is planned for the North Area, but the design of the EPB is compatible with both slow and fast extraction.

Concerning the rapid-cycling bubble chamber, the number of particles that it can accept per burst suggests that it may operate in a secondary beam fed by slow extraction. Two problems exist; namely the supply of secondary particles to the chamber only during the sensitive time, and the particle separation. The former may be solved by a special pulsed magnet at the end of a secondary beam, while the latter seems to imply the use of a long-pulse separated beam.

POSSIBLE UTILIZATION OF THE WEST HALL

J.V. Allaby
CERN, Geneva, Switzerland

1. INTRODUCTION

Before entering into details of a possible way of using the West Hall at the new high-energy level which will become available in 1976, let me first review briefly just what is meant by "the West Hall". It is in fact not one hall but a complex of several adjoining halls and two wide approach tunnels. Figure 1 shows a sketch of the West Area showing the dimensions and nomenclature of the various parts of the complex.

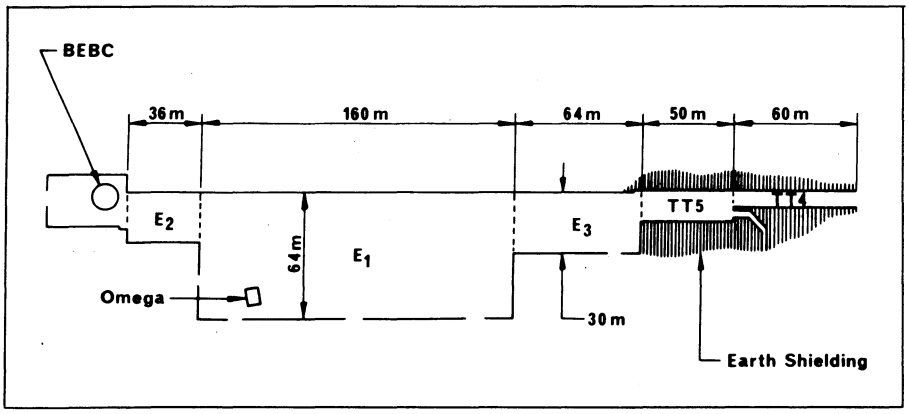

Fig. 1 Diagram of the West Area showing the dimensions of the halls

Crudely we can say that starting from the right with TT4, which is approximately 8 m wide, each successive area is double the width of its predecessor until we arrive at the main hall E_1, which is 64 m wide. The hall E_2, which is 25 m wide, links the main hall with the BEBC building. All the halls except TT4 are equipped with overhead cranes. The approach tunnels TT4 and TT5 have external earth shielding which makes them especially suitable for a target region.

Figure 2 shows the location of the West Area with respect to the 300 GeV accelerator. The link between the accelerator and the area is fairly straightforward in the horizontal or plan view, and involves no major bending of the ejected proton beam (EPB). However, in the vertical view or elevation, it is clear that because of the depth of the accelerator the EPB must be bent quite strongly in order to transport it to the surface. The choice of the form of this vertical bending is very constrained owing to the presence of the road RN 84 under which the EPB must pass at a safe depth. It is this constraint which makes it impractical to put the counter target zone further upstream than TT5. The special case of the target for the RF beam to BEBC will be discussed later, but the reason it is possible to place this target inside the transfer tunnel itself (which is only 4 m diameter) is because the intensities needed for this target are always less than 10^{11} protons per pulse. Such low intensities are not very interesting for counter beams.

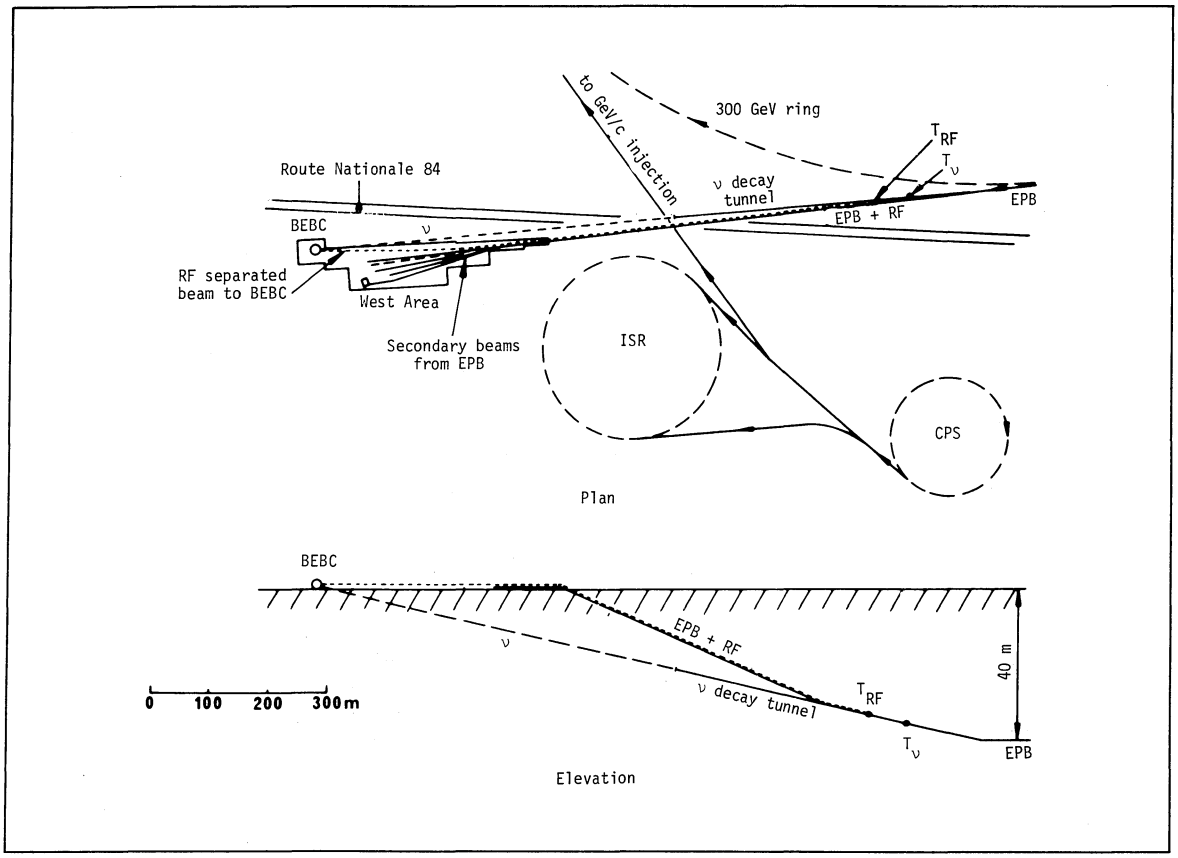

Fig. 2 Diagram showing the link between the SPS and the West Area

Thus a first point to recognize about the West Area is that there are definite limitations in length. Assuming that primary targets are located in TT5, then there are about 250 m to the end of hall E_1 and about 285 m to the end of hall E_2 in which to accommodate secondary beams and experiments. In addition, there is behind E_1 about 250 m of space before the boundary of the CERN site is reached, and this could eventually be used if needed in the future.

The West Area contains two important assets which play a significant role in the plans for its utilization. These are the large (3.5 m) hydrogen bubble chamber BEBC, and the large magnet and spark chamber facility called the Omega. Both of these have already been constructed. BEBC is in the testing stage, and Omega has already had some preliminary runs with beam.

2. BASIC ASSUMPTIONS

Before discussing the details of possible ways of utilizing the West Area, it is perhaps useful to review the basic assumptions we have had in mind throughout the whole planning stage.

a) The West Area is not the only experimental area to be available, but merely the first to become operational, because it exists already. The North Area, which has far less constraints on length, energy, or intensity of beams, should be utilized for those facilities which would be much inferior if located in the West Area.

b) The 3.5 m hydrogen bubble chamber BEBC is a facility which is assumed to be fixed. Although in principle, it could be moved, the cost in both time and money would be prohibitively high. Thus the bubble chamber programme is naturally centred around the West Area.

c) The Omega spectrometer, although not as immobile as BEBC, is already working in the West Area with beams provided by 24 GeV protons from the CPS. It is attractive to consider this -- at least initially -- as a West Area facility which should be operational with good beams at the earliest opportunity.

d) The limited length of the West Area leads to the conclusion that the area is most suited to secondary beams of momentum $\lesssim$ 150 GeV/c. This is clearly a limitation. However, the fact that the beams are above ground and contained in halls serviced by cranes makes for great flexibility in the possible utilization. Beam layouts can and will be changed quite often to suit the demands of individual experiments, as is the case now at the CPS.

e) The fact that the counter beams are produced above the surface means that massive quantities of shielding material are needed. Because of the space limitations of the West Area and the proximity of RN 84, this leads to a natural limit of $\sim$ 200 GeV for the energy of protons entering the West Hall itself. This limit is in fact not serious given the limitation of secondary beams to $\lesssim$ 150 GeV/c and the availability of the North Area for higher energy beams.

3. PARTICLE PRODUCTION AT HIGH ENERGIES

Let us now look at possible ways of utilizing the slow ejected proton beam to produce secondary beams for counter physics. The important feature of particle production at high energies is the strong forward collimation of secondaries because of the natural limitation in transverse momentum. This can be represented algebraically by

$$\frac{d\sigma}{dp_T} = A\, p_T\, e^{-Bp_T} , \tag{1}$$

where $p_T = p \sin\theta$ is the transverse momentum, and A and B are independent of p_T.

If we consider a beam of secondaries of momentum p produced at 0° with an acceptance of $\pm\Delta\theta$ in both planes, then all secondaries with momentum transfer less than $p_T' = p\Delta\theta$ will be collected by the beam. This number can be obtained by integrating Eq. (1):

$$\int_0^{p_T'} \left(\frac{d\sigma}{dp_T}\right) dp_T = \frac{A}{B^2} \int_0^{p_T'} B^2 p_T\, e^{-Bp_T}\, dp_T = \frac{A}{B^2}\left[1 - (1 + Bp_T')\, e^{-Bp_T'}\right] .$$

Hence we can define a geometrical efficiency ε for a 0° beam by

$$\varepsilon(\theta = 0) = \frac{\int_0^{p_T'} (d\sigma/dp_T)\, dp_T}{\int_0^{\infty} (d\sigma/dp_T)\, dp_T} = 1 - (1 + Bp_T')\, e^{-Bp_T'} . \tag{2}$$

In an analogous manner we can derive the yield of secondaries for a beam produced at an angle θ. All particles produced at momentum transfers between $p_T'' = p(\theta - \Delta\theta)$ and

$p_T' = p(\theta + \Delta\theta)$ will be distributed over an annulus of which approximately the fraction $\Delta\theta/\pi\theta$ will be accepted by the beam. Thus in this case the efficiency will be

$$\varepsilon(\theta \neq 0) = \frac{\int_{p_T''}^{p_T'} (d\sigma/dp_T)\, dp_T \cdot \Delta\theta/\pi\theta}{\int_0^{\infty} (d\sigma/dp_T)\, dp_T}$$

$$= \frac{\Delta\theta}{\pi\theta}\left[(1 + Bp_T'')\, e^{-Bp_T''} - (1 + Bp_T')\, e^{-Bp_T'}\right] . \qquad (3)$$

Figure 3 shows the geometrical efficiency for hypothetical beams of acceptance ±2 mrad in each plane (i.e. $\Delta\Omega = 4\pi \times 10^{-6}$ sr) evaluated from Eqs. (2) and (3) using the value $B = 6$ GeV/c^{-1}. It can immediately be seen that the efficiency falls rapidly as the production angle is increased, especially at higher momenta. The efficiency of 0° secondary beams clearly increases for a fixed solid angle, as the momenta increases. Figure 4 shows the geometrical efficiency of the above hypothetical beam at 0° as a function of secondary momentum. The efficiency rises rapidly as a function of momentum up to about 200 GeV/c and then rises more slowly, asymptotically approaching unity. Finally one can ask what solid

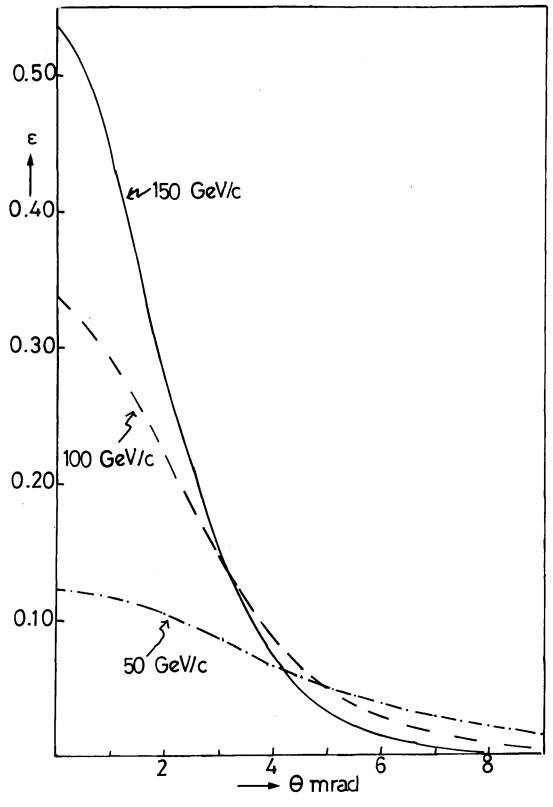

Fig. 3 Geometrical efficiency of a charged particle beam, with $\Delta\Omega = 4\pi \times 10^{-6}$ sr, as a function of the production angle θ, for three secondary momenta

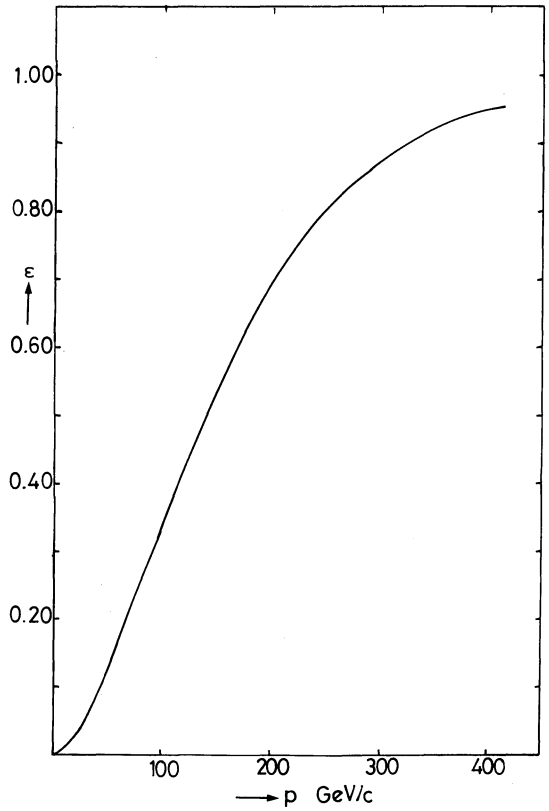

Fig. 4 Geometrical efficiency of a charged particle beam, with $\Delta\Omega = 4\pi \times 10^{-6}$ sr and at $\theta = 0$ mrad, as a function of secondary momentum

angle should be used to obtain an efficiency of, say, $\varepsilon = 0.6$. This is shown as a function of secondary momentum for 0° beams in Fig. 5. Clearly the solid angle needed at 300 GeV/c is much smaller than that needed at 150 GeV/c, which is helpful for beam designers.

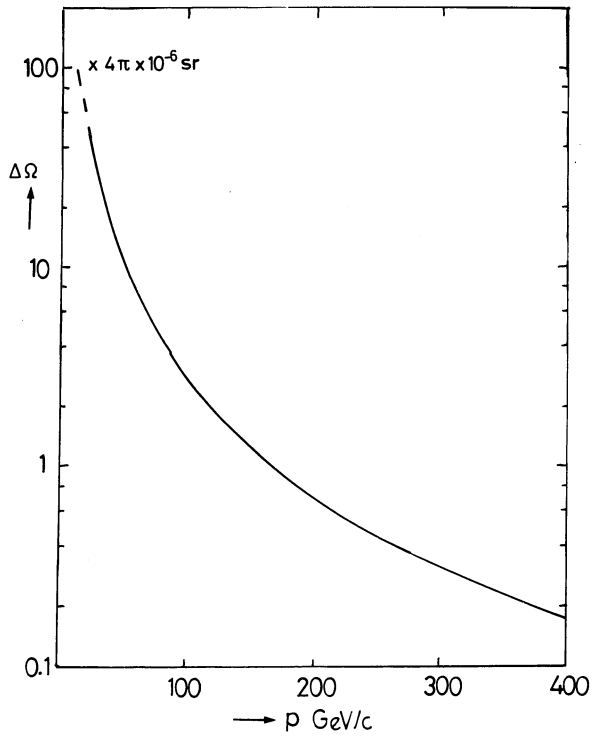

Thus it is extremely important to produce beams at very small angles and preferably at 0°. It is not easy to produce more than one charged beam at 0° from a target, which leads to the possibility of having to consider several targets, each of which can be fed by some fraction of the EPB. To do this one must split the EPB.

Fig. 5
Solid angle of a charged particle beam needed to maintain a geometrical efficiency of $\varepsilon = 0.60$, as a function of momentum

Figure 6 shows a scheme to split the EPB into three separate beams. This is based on the familiar iron septum magnets used at present in the East Hall at the CPS. Using this method, it is possible to design secondary beams from three separate targets, thus allowing one to approach the ideal situation in which beams are produced very close to the forward direction. The three targets T_1, T_2, and T_3, can be located in the shielded tunnel TT5, as shown in Fig. 7.

Before dicussing possible beams it is perhaps useful to look at the spectra of secondary particles one can obtain from 200 GeV protons. Figure 8 shows a comparison of the yield of π^- in a 1 μsr beam into 1% $\Delta p/p$ for 10^{12} interacting protons, from 200 GeV incident protons and from 24 GeV incident protons. This comparison is interesting in that it demonstrates the extremely high flux of secondaries which will become available in the West Area from 200 GeV protons. Not only will there be higher energy particles, but they will be sufficient in number to enable really precise measurements to be carried out on reactions with quite small cross-sections. If one reflects that for the past 13 years good physics has been done with the spectrum of secondaries available from 24 GeV protons, it is exciting to view the enormous increase in potentiality to be provided by 200 GeV protons. It is often said that 200 GeV, being only eight times the CPS energy and thus an increase of only less than three times the centre-of-mass energy now available, is not very exciting. Figure 8 shows that this statement is not correct from the point of view of secondary beam production. Figure 8 also shows that the yield of π^- from 200 GeV protons is very healthy up to 150 GeV/c, supporting the earlier statement that for secondary counter beams in the West Area a limitation to 200 GeV incident proton energy is not serious.

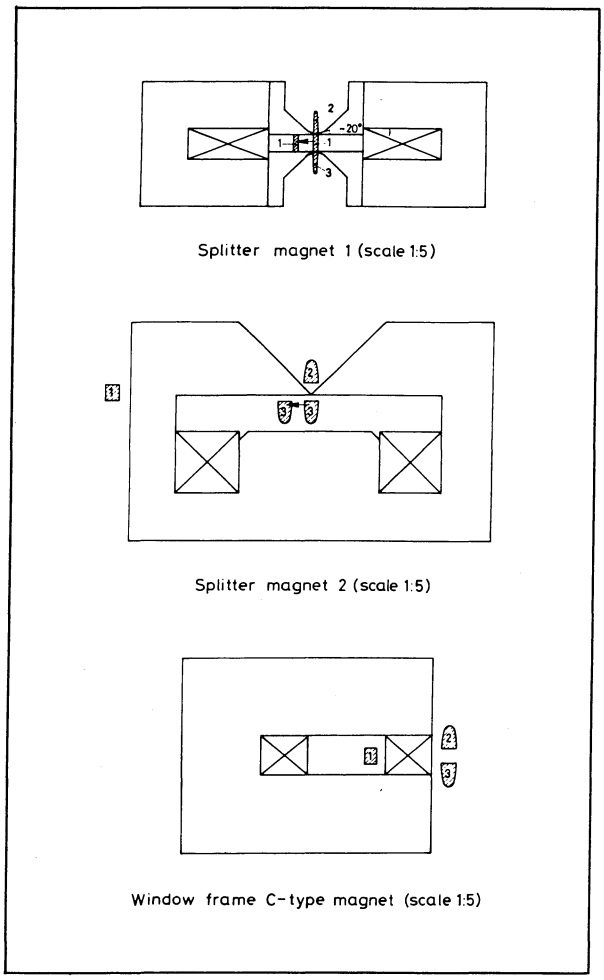

Fig. 6
Diagram of magnets for three-way beam split

Fig. 7
Plan of possible beam split in the West Area

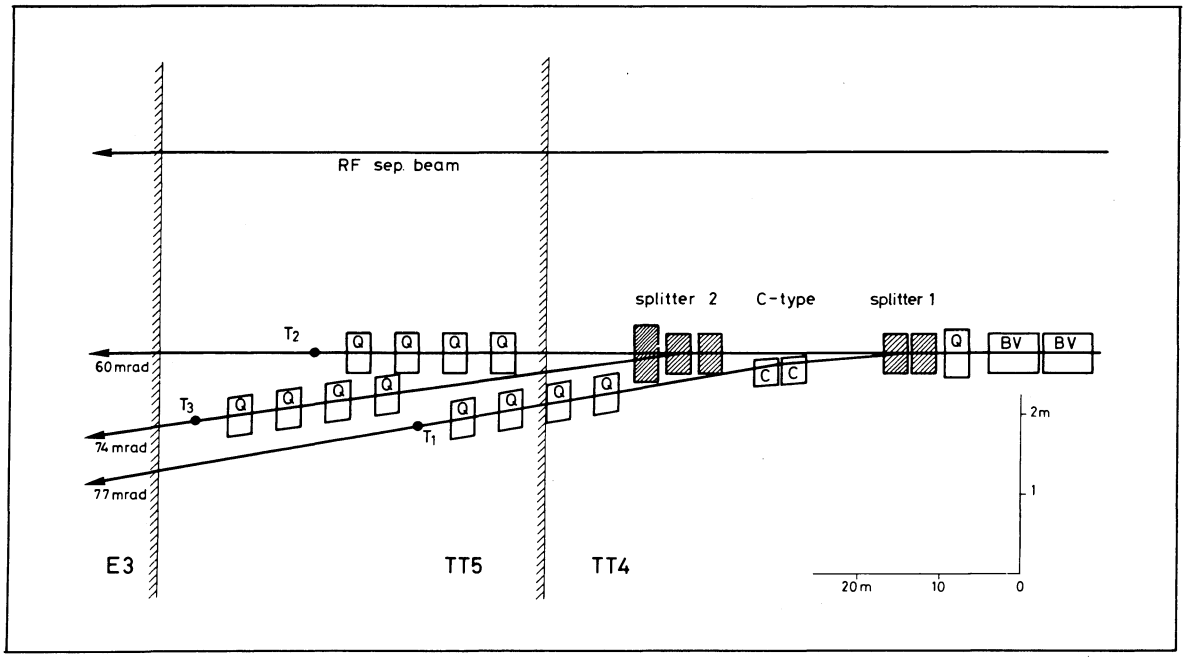

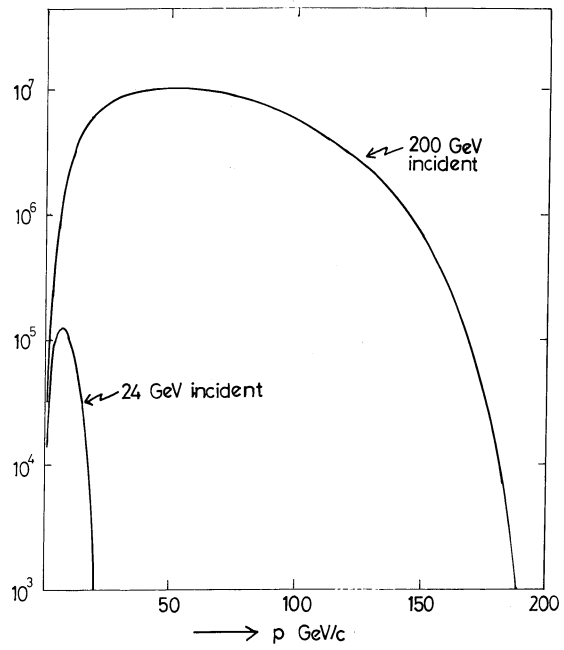

Fig. 8
Comparison of the π^- yield from 24 GeV and 200 GeV protons

Figure 9a shows the spectra of positive particles which will be produced by 200 GeV protons. Notice the extremely rich yield of K^+, although at momenta above 100 GeV/c the huge flux of protons will be an embarrassing contamination to handle. Figure 9b shows the spectra of negative particles. Here one does not have protons, but for high statistics experiments with K^- or $\bar{p}$ using a device such as the Omega spectrometer, the high yield of π^- would severely limit the data acquisition rate. This can be overcome by using superconducting RF separation techniques, which will be mentioned later.

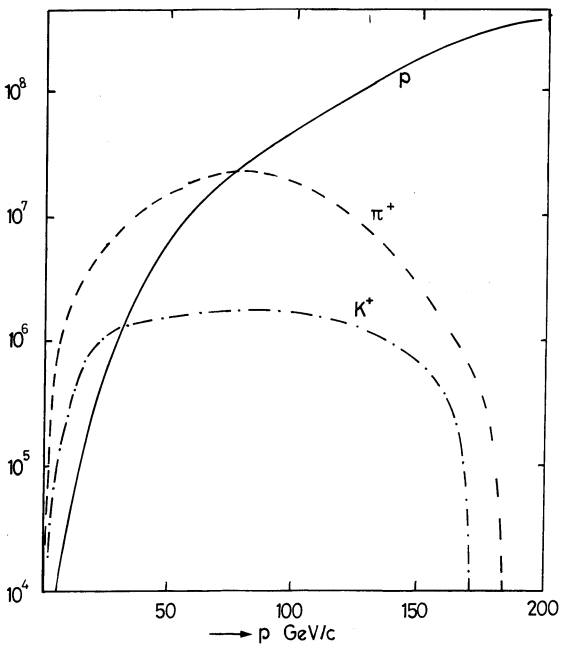

Fig. 9a Positive particle yields, in 1 μsr and with $\Delta p/p$ = 1%, for 10^{12} interacting protons and 0 mrad production angle

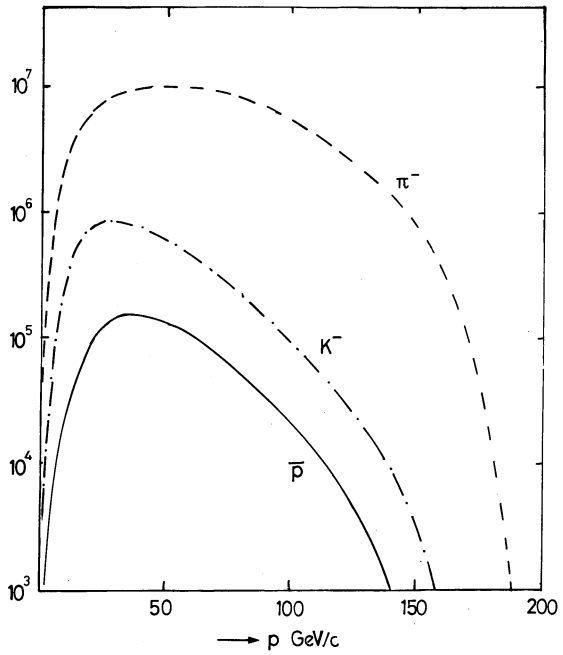

Fig. 9b Negative particle yields, in 1 μsr and with $\Delta p/p$ = 1%, for 10^{12} interacting protons and 0 mrad production angle

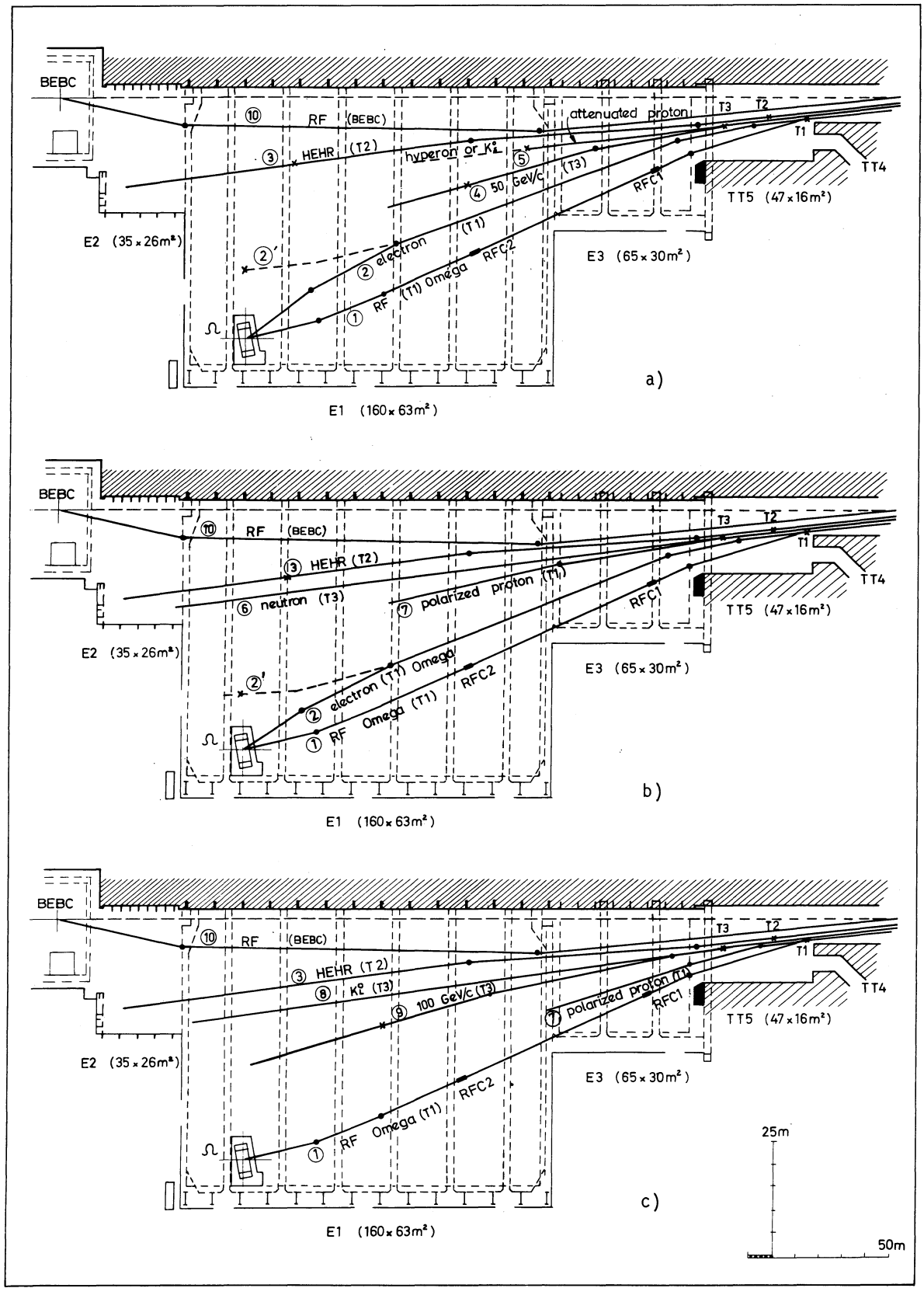

Fig. 10 Possible beam layouts in the West Area [for discussion of the differences between (a), (b), and (c), see text]

4. POSSIBLE COUNTER BEAM LAYOUT

A great deal of work has been done within the ECFA Working Parties on the question of what counter beams should be envisaged for the West Area at 200 GeV. Detailed discussions can be found in Volume I of the ECFA Working Group report, and in the presentations during this meeting. Figures 10a, 10b, and 10c show three examples of how some of the beams discussed in the Working Parties could be combined into a West Area layout. Common to all three layouts are:

i) an RF separated beam to BEBC -- to be discussed later;

ii) an RF separated beam to Omega;

iii) a high-energy high-resolution conventional charged beam.

These might be considered as the basic beams in the West Hall.

The use of superconducting RF separators for producing high-energy counter beams enriched in rare particles has been discussed for some years. Such beams are advantageous when the experimental apparatus is saturated by the total flux of charged particles of an unseparated beam, and one wishes to obtain the maximum number of events produced by a rare constituent of the beam, for example $K^{\pm}$ or $\bar{p}$. The Omega spectrometer would be saturated by a typical unseparated beam produced by 200 GeV protons, and thus the rate of accumulating events produced by $K^{\pm}$ or $\bar{p}$ would be severely limited. The use of superconducting RF cavities allows the construction of an RF separated beam which would enhance the data rate on these rare particles by at least an order of magnitude. The use of S-band cavities limits the separation up to between 30 and 40 GeV/c (depending on the quality of the separator) for a beam which could be accommodated in the space available between target T_1 and Omega. Since the separated beam is rather complex and costly in magnetic elements, the beam (1) is limited to 40 GeV/c and is thus specifically designed for use with RF separators. More details regarding this beam and the physics experiments that can be carried out with it are given in the report of the Working Party on the use of Omega (CERN/ECFA/72/4, Vol. I, Chapter 8).

Since the West Area will be the first experimental area in operation at the SPS, it is felt to be important that one beam should be available which will allow experiments up to reasonably high energies, with good momentum resolution. Such a beam is shown as beam (3) in Figs. 10, and is produced at 0° from target T_2. The maximum momentum is 150 GeV/c and the acceptance is about 10 μsr. The beam has been located so that the experiments can extend into hall E_2, thus giving an extra 35 m of space. Nevertheless it is true that the length is a limiting factor, and only about 80 m are available after the experimental target. This is why the momentum has been chosen to be a maximum of 150 GeV/c, rather than 200 GeV/c.

A lot of interest has emerged during the past year on the use of high-energy electrons or photons for experiments either with the Omega spectrometer or with specialized detector systems. Beam (2) of Fig. 10 shows how an electron beam of maximum momentum 100 GeV/c and acceptance of 20 μsr can be produced by conversion of the γ-rays produced in target T_1. Electrons of this beam could be used directly in Omega or used to produce a tagged photon beam for Omega. A simple modification of the downstream end of this beam would allow the electrons or tagged photons to be used by an independent experiment simultaneously with the operation of beam (1) for Omega. This modification is shown as 2′ in Fig. 10a, b. Finally, beam (2) could, if desired, be used without major modification to produce an unseparated charged hadron beam up to 100 GeV/c for the Omega spectrometer.

The target T_3 can be used to produce many different kinds of beams depending on the demands of the experimental programme. In Fig. 10a it is used to derive a 50 GeV/c unseparated beam (4) of high intensity produced at 0°, which might be used, for example, to study processes with rapidly falling cross-sections utilizing the very high fluxes of secondaries available below 50 GeV/c. In addition, one can utilize the protons in the T_3 branch, suitably attenuated in intensity, to produce a special short-lived beam such as a hyperon beam or a K^0_S beam, as is shown schematically in Fig. 10a as beam (5).

In Fig. 10b, target T_3 is used to produce a neutron beam (6), and a polarized proton beam from Λ^0 decay (7). Both the neutrons and the Λ^0 are produced at 0°. The polarized proton beam (7) could alternatively be derived from target T_1, as shown in Fig. 10c. A final possible combination of beams from T_3 is shown in Fig. 10c, where a K^0_L beam (8) produced at about 6 mrad, is combined with an unseparated beam of maximum momentum 100 GeV/c (9), produced at 0°.

The conclusion of this section is that the West Area can be used to provide a wide selection of secondary beams for physics experiments using 200 GeV/c protons. All the beams discussed are produced at 0°, with the exception of the K^0_L beam, where there is some advantage in moving away from the forward direction in order to reduce the neutron background. Thus one has tried to make the most efficient use possible of the protons coming from the SPS. Although the shielding will be designed in such a way that each target can accept up to 3×10^{12} protons, it is quite clear that many experiments will not need such intensities all the time. This is important in view of the desire to utilize a good fraction of the accelerated protons to produce a neutrino beam; this will be discussed later. An important beam for counter physics which does not appear in Figs. 10 is a muon beam. This point will also be taken up later.

5. AN RF SEPARATED BEAM FOR BEBC

The need for RF separation of particles in a beam for a bubble chamber is even more apparent than is the case of an electronic detector. Not only is a bubble chamber saturated by the beam intensities available, but it completely lacks any time resolution. Although tagging schemes have been proposed which would enable the particles entering a bubble chamber to be labelled, only the interactions of the dominant particle in the charged particle spectrum could be studied with high statistics. Thus the statistics of experiments with $K^{\pm}$ or $\bar{p}$ would be extremely limited.

Fortunately, a bubble chamber does not need -- and indeed cannot use -- a long-spill beam. Thus the RF cavities do not need to be superconducting but can be pulsed at room temperature. Such cavities have already been in use at CERN for many years, and the technique is well developed.

The maximum momentum at which separation of particles can be achieved depends on the square root of the frequency of the RF cavities multiplied by the distance between the separators.

Separation of $K^{\pm}$ has been achieved at the CPS up to 16 GeV/c, with a length between cavities of 50 m and using S-band cavities of frequencies of 2856 MHz. Thus an attempt can be made to achieve separation at higher momenta by increasing the intercavity distance and by increasing the frequency. It is technically feasible to use a frequency of $\sim$ 6000 MHz

(C-band), and components for such separators exist at the right power levels and are readily available. The higher frequency offered by X-band cavities, operating at $\sim$ 9000 MHz, is less attractive since the components do not all exist in industry, and furthermore the aperture of X-band cavities is very small, limiting their usefulness in a beam.

Assuming the use of C-band cavities, the next step is to consider what length is available for intercavity separation. If an RF beam for BEBC were produced from a target located in TT5, then only about 100 m would be available for the intercavity separation, remembering that there must be sufficient bending before the first cavity to momentum-select the beam, and sufficient space after the last cavity for the beam-stopper and final beam optics. Thus there would be a gain of only a factor of two in maximum momentum compared to the present 16 GeV/c separated beam at the CPS. Since there already exists a 32 GeV/c separated $K^{\pm}$ beam at Serpukhov, this would not be so exciting for the SPS in 1976.

Thus one was led to explore the possibility of moving the target for the BEBC RF beam much further upstream in order to provide a greater intercavity separation. It was found possible to locate a target inside the EPB transfer tunnel at a total distance of 905 m from BEBC, thus allowing a beam to be designed with an intercavity separation of 504 m. Using C-band cavities, full separation of $K^{\pm}$ can be thus achieved up to 73 GeV/c, and separation of K^- from π^- only up to about 100 GeV/c.

The schematic diagram of this beam is shown in Fig. 11. A fast-ejected beam, of intensity < 10^{11} protons per pulse in a 5 μsec pulse, will travel along the EPB line to a beam switch which will direct these protons onto the RF target. Charged particles produced at 0° are collected by the RF beam and momentum-selected in the vertical plane. Separation is achieved by RF modulation in the transverse plane. Three cavities would enable the separator system to cover the momentum range smoothly from about 20 GeV/c up to the maximum. The magnetic elements would operate up to a beam momentum of 150 GeV/c.

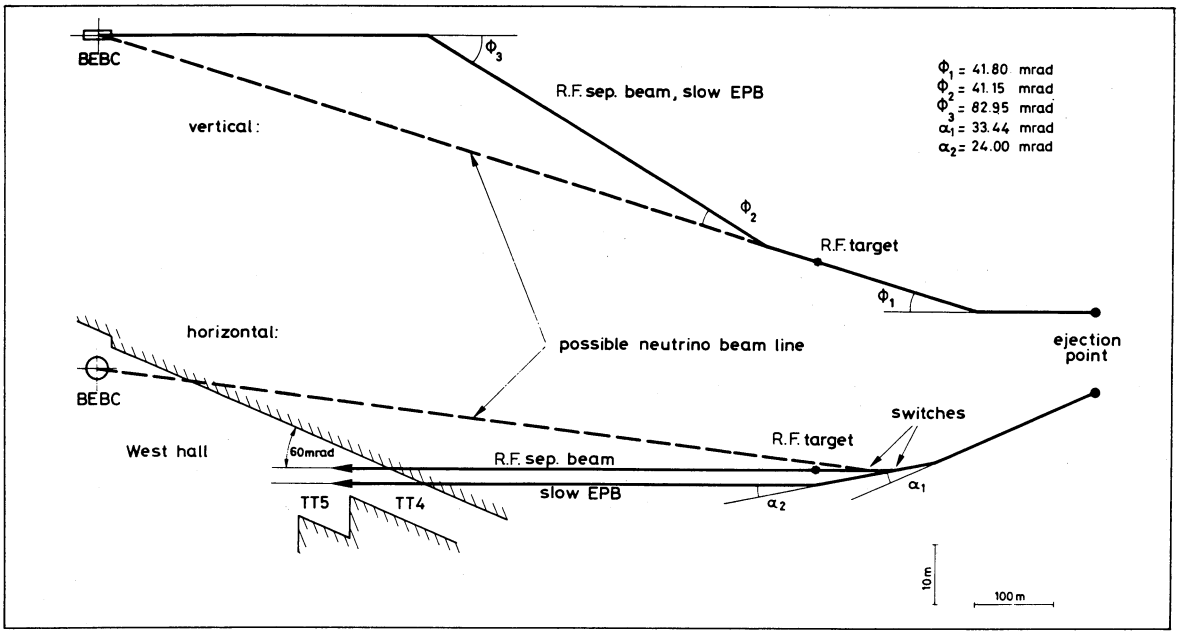

Fig. 11 Schematic diagram showing initial part of the proposed RF separated beam to BEBC

Notice that the momentum analysis is provided by those vertical bending magnets needed to bring the beam to the surface in the West Hall. It must be stressed that this target can only be located in the transfer tunnel, because the intensities to be used are always less than 10^{11} protons per pulse.

Details of this beam and of its use for hadronic physics with BEBC are presented in the BEBC Working Party report in Vol. I, and will be discussed later in this meeting. I will merely draw the sweeping conclusion that BEBC seems capable of providing a wide range of interesting experiments up to about 100 GeV/c momentum, and thus the provision of an RF separated beam of the kind described seems well justified.

6. A NEUTRINO FACILITY IN THE WEST AREA

All the beams that have been discussed so far have been basically beams for the study of hadronic reactions either by direct hadron-hadron interactions or, in the case of the electron or γ-beams, by using an electromagnetic probe to study the hadronic structure of particles. The field of weak interactions has been explored in the past either by the study of decay of particles -- which does not always necessitate high energies -- or by the study of neutrino interactions.

Although probably the most significant individual experiment using neutrino beams was carried out by Steinberger and collaborators using spark chambers, the major effort in neutrino physics over the last ten years has been undertaken using the bubble chamber technique and, until recently, using heavy-liquid chambers. European physicists have played an important role in this work, and it is natural that there is great interest in a neutrino facility at the SPS. The construction of massive liquid-hydrogen bubble chambers in recent years has opened up the possibility of study neutrino interactions on pure hydrogen and deuterium, and the first experiments of this kind, using low-energy neutrinos, have already been carried out at Argonne. BEBC was constructed originally with the intention of using it for neutrino physics, so it is also natural to see if one can provide an interesting neutrino beam for BEBC in the West Area.

The major problem in neutrino physics at high energies lies in the detector and its shielding. Because the neutrino has such a small cross-section, the detector must be massive. However, since neutrinos are identified by the appearance of a muon in the detector, one must take great care to limit the background of muons passing through the detector. Since muons are produced in the beam along with the neutrinos, from the decay of pions and kaons, one has a difficult shielding problem to solve, because muons are difficult to stop. Thus although a bubble chamber has some ideal qualities in the detection of rare events such as neutrino interactions, great care must be taken to eliminate the muons coming from the beam, and the only realistic solution seems to be to stop them in material by their ionization and electromagnetic energy-loss. At high energies the shield necessary to stop the muons becomes very massive and takes up a lot of space, thus limiting the solid angle acceptance of the detector.

A neutrino beam consists of a target, which must be irradiated by an intense beam of protons to produce the maximum possible number of secondaries, a focusing device to make the beam of π and K as parallel as possible, and a decay region in which the π and K can decay to produce the desired neutrinos.

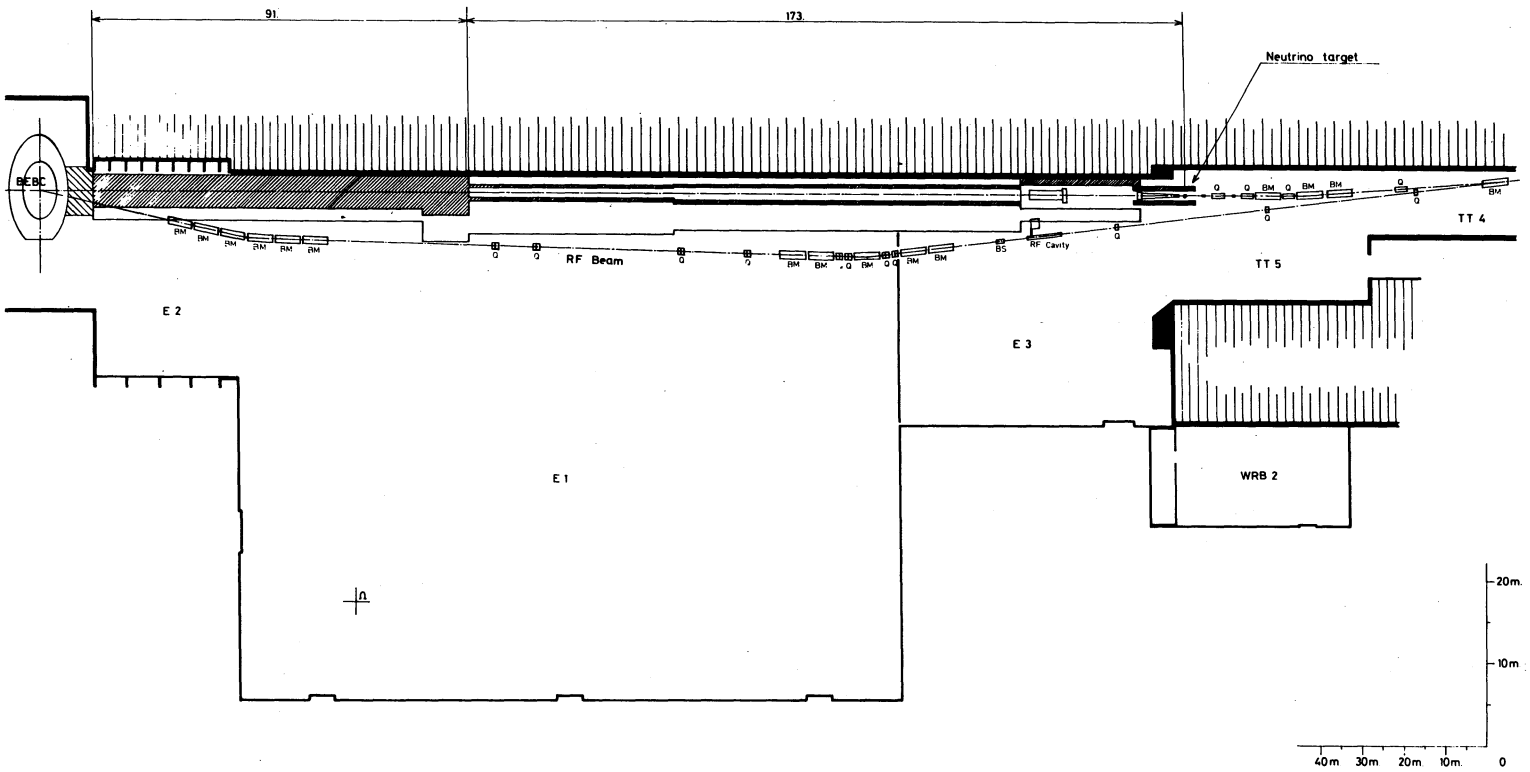

Fig. 12 Neutrino "surface" solution and RF beam in the West Area

If one considers a wide-band neutrino beam produced from a target located in TT5 in the West Area, one has a total distance of 283 m up to BEBC. A good neutrino beam could be constructed for incident protons of up to 150 GeV/c momentum. At the highest momentum, this would have a decay region 170 m long and a steel muon shield plus some inevitable dead space of 113 m length. Beams optimized at lower proton momentum could have a thinner steel shield and more decay length. Above 150 GeV/c incident proton momentum, the muon shield becomes even thicker, and the space left for the decay region is inadequate so that there is a loss of neutrino flux compared with the flux obtained at 150 GeV/c. The layout of such a beam, usually called the "surface solution", is shown in Fig. 12. Notice that in addition to the steel for the muon shield, a large amount of steel must be used to shield the decay region.

Another possibility which has been considered is to produce the neutrino beam from a special neutrino target located underground and fed with 200 GeV protons by a special beam switch located as close as possible to the point at which the beam emerges from the accelerator. A schematic diagram of this underground beam switch is shown in Fig. 13. Here one sees that the first part of the beam switch is provided by the magnets necessary for the RF beam to BEBC. By adding more switching magnets, the proton beam could be deflected even further into a special tunnel for the neutrino beam. This so-called "tunnel" solution was already discussed in concept at the first Tirrenia meeting last year, and as a result the EPB tunnel connecting the accelerator and the West Area will have a widened section to allow these beam switches to be accommodated if needed. The decision to do this was taken by John Adams last year in order to keep open the possibility of having the long RF beam to BEBC and the "tunnel" neutrino beam.

After the beam switch, the proton beam must be focused onto the target. When sufficient space is left for this a solution is arrived at which gives a distance between neutrino target and BEBC of 830 m. In this solution, the decay region would be a simple 2 m diameter tunnel bored in the rock, preceded of course by a wider region to accommodate the focusing device, which for a wide-band beam would be the familiar "horn". Figure 14 shows the details of such an underground neutrino facility optimized for 200 GeV incident protons. The muon shield is provided by 50 m of steel followed by 230 m of rock, earth, and concrete. This leaves a decay region 550 m long.

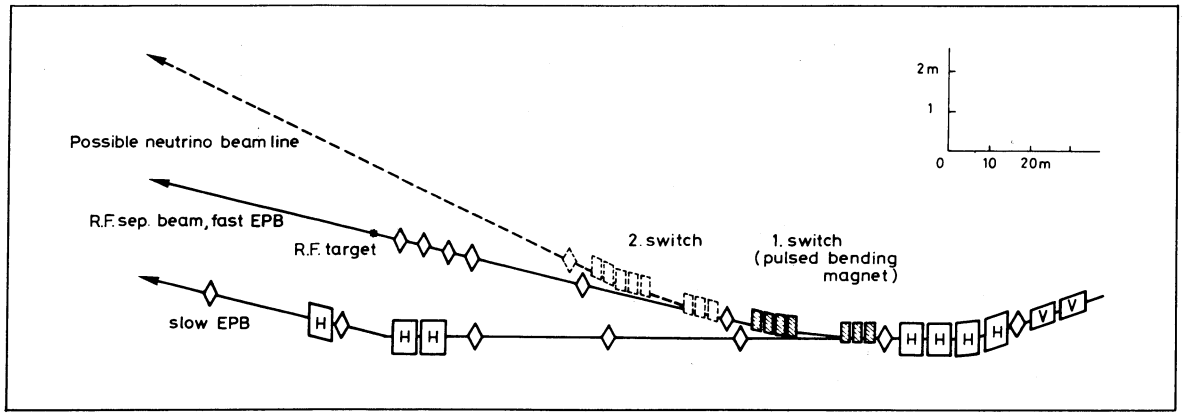

Fig. 13 Schematic diagram of underground beam switch to feed the RF target, and the "tunnel" solution neutrino target

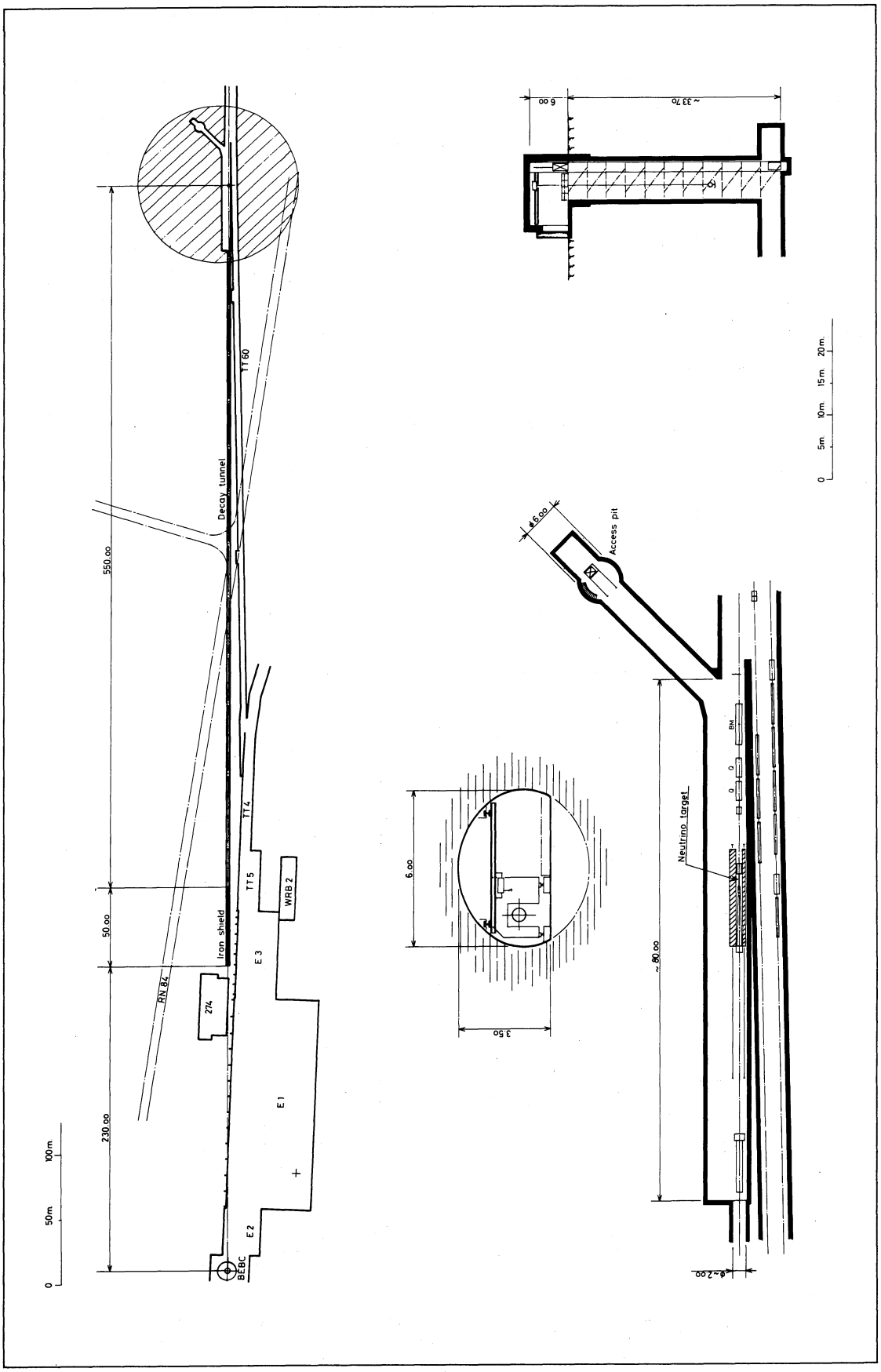

Fig. 14 Neutrino "tunnel" solution

One advantage of the "tunnel" solution is that if at a later date a beam using 400 GeV protons is required, it is possible to achieve this by, for example, adding a further 120 m of steel at the end of the decay tunnel to stop the higher energy muons; but it is hoped that a better solution can be found.

What are the physics possibilities offered by these two solutions? Figures 15 and 16 are linear graphs showing the event spectra and integrated event spectra, respectively, for the "surface" solution and the "tunnel" solution at 200 GeV.

It can readily be seen from Figs. 15 and 16 that both solutions give respectable event spectra leading to total event rates which are only marginally different. The difference lies in the shape of the two spectra. At neutrino energies of < 10 GeV, the surface solution yields more events. For $15 < E_\nu < 40$ GeV, the tunnel solution gives better yields. Finally, for $40 < E_\nu < 80$ GeV the two solutions have identical yields, within the errors of the calculations. Clearly, before trying to decide which solution will yield the most physics, it would be valuable to know how efficiently BEBC will operate as a function of E_ν.

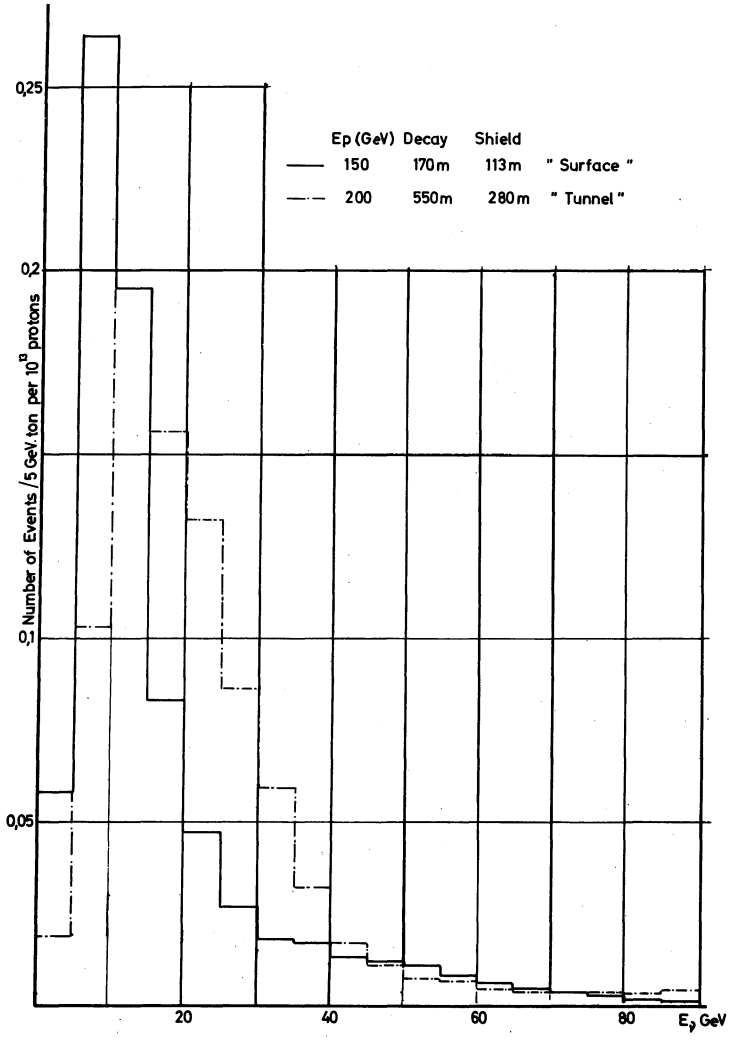

Fig. 15 Comparison between neutrino event spectra (in BEBC) for "tunnel" and "surface" solutions. (Assumptions: ideal focusing; $\sigma_{tot} = 0.8\ E_{GeV} \times 10^{-38}\ cm^2$.)

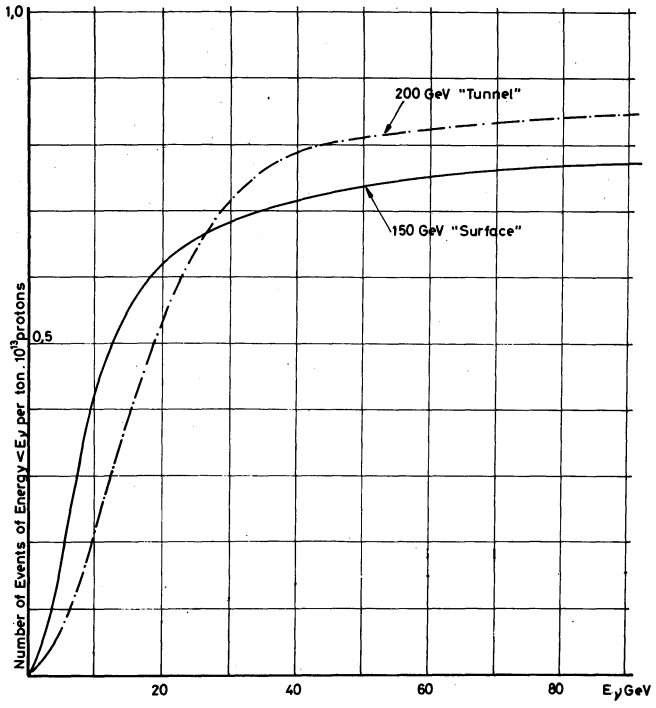

Fig. 16
Integral event spectra for "tunnel" and "surface" solutions

Figure 17 shows the yield of neutrino events for the tunnel solution at 400 GeV. Note that the horizontal (E_ν) scale has been doubled, reflecting the higher neutrino energies available. The integrated number of events for 10^{13} protons is almost twice that for the solutions at lower energy but this will be completely compensated by the increased cycle time at 400 GeV, so that the number of events/hour will stay the same. The interest of increasing the energy to 400 GeV lies again in the effect which this has on the spectrum. Figure 18 shows a comparison of the event spectra for the two "tunnel" solutions (200 GeV and 400 GeV). Even bearing in mind the loss in cycle time at 400 GeV, it is clear that above 40 GeV a considerable gain in neutrino events will be obtained by going to higher energy incident protons.

The decision whether to build the "tunnel" neutrino beam or not must be taken very soon, if such a facility is to be available when the accelerator begins to operate. The detailed dicussions of the advantages and disadvantages of the "tunnel" versus the "surface" solution will take place during and following the report of the neutrino Working Party, later in this meeting.

The neutrino beams described so far have been optimized from the point of view of BEBC as detector. However, one must not lose sight of the relevance of other neutrino detectors which might be available. One obvious example is the large heavy-liquid chamber, Gargamelle. This could, if desired, be moved into a location behind BEBC and thus benefit from the neutrino facilities described. The physics possibilities of Gargamelle located behind BEBC will be discussed in the Gargamelle Working Party report at this meeting, and are contained in Chapter 3 of the Working Group Report, CERN/ECFA/72/4, Vol. I.

The SPS can also be considered for neutrino experiments using electronic detectors. Clearly such an experiment could also be located behind BEBC. However, an electronic neutrino experiment usually involves a massive target of some hundreds of tons and is thus

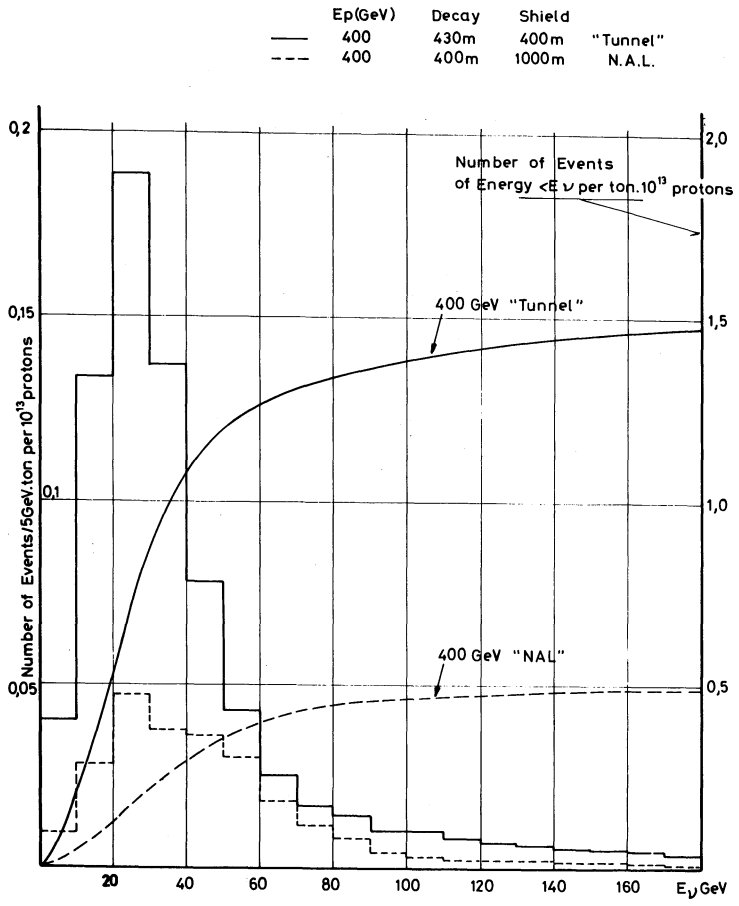

Fig. 17 Neutrino event spectra (in BEBC) for the "tunnel" solution at 400 GeV, compared with those for the NAL facility at the same energy. (Assumptions: ideal focusing; $\sigma_{tot} = 0.8\ E_{GeV} \times 10^{-38}\ cm^2$.)

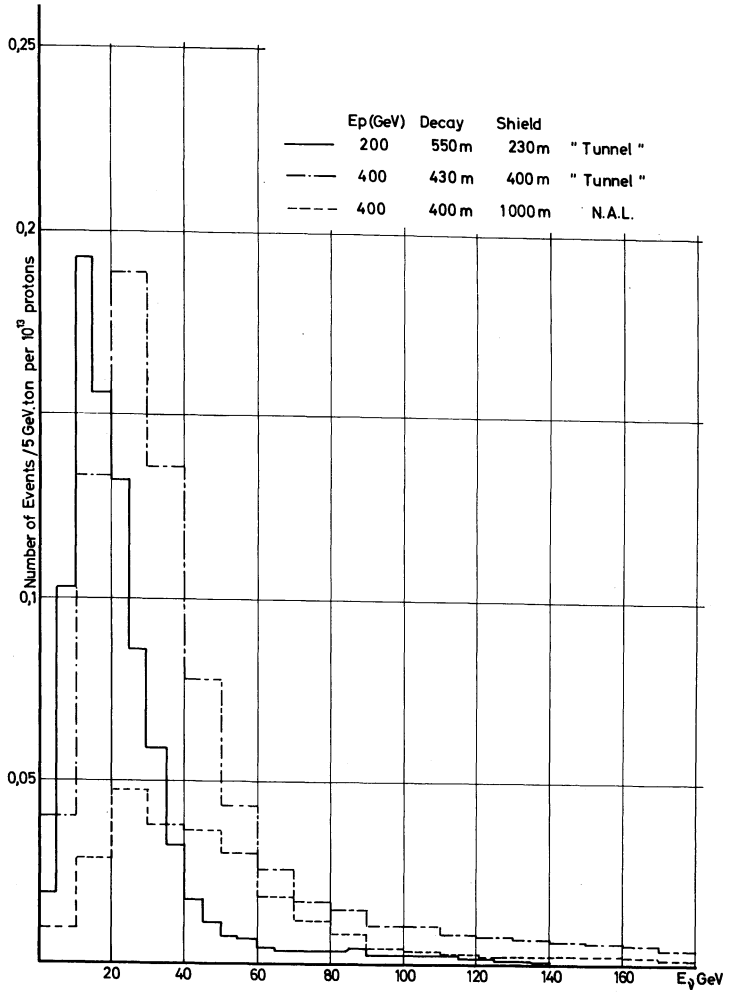

Fig. 18 Comparison between neutrino event spectra of the "tunnel" solution, at 200 GeV and at 400 GeV, and those of the NAL facility. (Assumptions: ideal focusing; $\sigma_{tot} = 0.8\ E_{GeV} \times 10^{-38}\ cm^2$.)

more specifically powerful in the highest momentum region of the neutrino spectrum where the statistics and energy-measuring capability of bubble chambers are limited. Furthermore, the neutrino beams described are fed implicitly by the fast ejection from the SPS, since the slow ejection mode cannot be made to operate for a time shorter than 5 msec, which is too long for a bubble chamber. The longest spill from fast ejection is about 30 μsec, which is very short for an electronic experiment. Thus if an electronic experiment were located behind BEBC, it would have to either accept a 30 μsec spill and run simultaneously with BEBC (and possibly also with Gargamelle), or it would have slow ejection and have to be the sole user of the accelerator, since a slow-ejected beam cannot be split in the space available in the EPB tunnel. The tunnel neutrino facility could operate together with slow ejection to the counter targets in the West Hall provided it operates on fast ejection. An additional complication for a counter neutrino experiment behind BEBC is that if a wide-band neutrino beam is desired with ejection longer than $\sim$ 30 μsec, a special long-pulse neutrino horn would have to be constructed.

Perhaps by far the best solution for neutrino physics with electronic experiments would be to combine, in one facility which would be located in the North Area, both a long-spill neutrino beam and a high-energy muon beam. Studies of this possibility have taken place within the Working Parties this year, and look extremely attractive.

It is impossible to construct a good high-energy muon beam in the West Hall itself because of the limitations in length and also in proton energy. It is also very unattractive to try to obtain a muon beam from the decay region of either the "tunnel" or the "surface" neutrino solutions discussed above, since the muon beam needs slow ejection and a d.c. focusing system distributed along the whole length of the decay tunnel, whereas the bubble chamber neutrino beam needs fast ejection and a horn focusing system followed by an evacuated decay tunnel. Furthermore, the muon beam which could be derived from either the "tunnel" or "surface" solutions would be not well located for experimental use, being essentially outside the West Hall proper.

The advantages of the North Area for a combined muon-neutrino facility are many. The proton beam energy would be 400 GeV. There is adequate space to build a well-optimized facility. The cost should not be too high, since the decay region would be only about 10 m below the surface. Details of a possible facility of this kind will be given by Brianti in his talk on the North Area.

7. CONCLUSIONS

A possible way of utilizing the West Area to provide a wide range of beams for physics in the early period of operation of the SPS has been described. The limitations of the West Area in the beam length, and the muon shielding problems, suggest that it will be a valid area for secondary beams of momenta less than 150 GeV/c and using incident protons up to 200 GeV. These limitations, together with the desire for a good muon-neutrino facility for counter experiments -- which is difficult to realize in the West Area -- make it imperative for us to operate the North Area as soon as possible.

Facilities outlined for BEBC include an RF separated beam giving separated K^- and π^+ up to 100 GeV/c, and two possible alternative wide-band neutrino facilities, one of which can be extended to operate at the highest energies expected from the SPS.

POINTS ARISING IN THE DISCUSSION AFTER J.V. ALLABY'S TALK

The question of the height of the beam in the West Area was raised. The present plans assume that the beam height will be 2 m above the floor of hall E_1, just as it is now with the beams produced from the CPS.

Questions were raised concerning the possibility of deflecting the superconducting RF separated beam envisaged for Omega so that it might be used for other experiments, in particular a rapid-cycling bubble chamber. The answer is, in principle, it is possible, but there is little space in which good use could be made of such a beam. On one side, the wall of the Hall E_1 would impede the installation of all but the simplest experimental equipment. If the electron beam (2) were in place, the other side would also be completely blocked.

The logic of putting only one beam derived from target T_2 was questioned. The reason why only one beam has been indicated so far is that until a decision is reached on the neutrino facility (surface or tunnel solution) it is necessary to leave space to accommodate the surface solution in the Hall. If the tunnel solution is chosen, there would possibly be enough space to derive a second beam from T_2 in addition to the high-energy high-resolution beam (3). A further question concerned the possibility of extending outside the walls of the West Hall complex in order to place light equipment such as Čerenkov counters after the high-energy beam. It is certainly possible to consider this since the walls at that place are light and not an integral part of the roof support.

Questions were also raised concerning the possibility of constructing other hadron beams for BEBC, such as a polarized proton beam or lower energy, separated K^+ beams, since the proposed long RF separated beam has a lower limit in K momentum of about 30 GeV/c owing to decay. Lower energy K beams or any other special short beam for BEBC could be obtained by using the RF beam to transport 150 GeV/c protons to a special target close to the chamber. Such an arrangement would conflict in space requirements with the proposed counter beams and so could not be maintained as a permanent facility but could be installed if needed for a special experiment.

A final question concerned how much money is really available to cover the many expensive beams and options discussed. The answer to this question is contained in the talk presented by Professor Jentschke.

LAYOUT OF THE 300 GeV NORTH EXPERIMENTAL AREA: A Summary of Problems and Present Ideas

H. Atherton, G. Brianti and N. Doble
CERN, Geneva, Switzerland

Abstract

This is a revised and more complete version of our contribution to this meeting[1]. It summarizes the studies carried out to date with a view to determining the layout of the North Experimental Area, starting from an external proton beam at the end of tunnel TT20. A tentative layout is presented. Some elements, such as production of secondary particles, target stations, and basic features of a high-energy secondary beam, are considered in more detail.

* * *

The design of the North Area (NA) is still in a very preliminary stage. We present, however, a list of problems and present ideas on possible solutions, merely to stimulate discussion and arrive at a reasonable compromise between potential requests by experimenters and over-all technical and financial limitations.

When considering the NA, one should bear in mind that the West Area (WA), with its specific features and facilities, will contribute substantially to the physics programme at the same time. Moreover, the WA will be fed by its own extraction system and external proton beam, so that both Areas will be completely independent (operationally) from each other.

Therefore, the ideas presented in this report are based on the following assumptions:

i) The NA should be considered, at least for a first period, as complementary to the WA, namely reserved for facilities which, because of their nature, cannot or will not be constructed in the WA. In this way the best use can be made of the limited funds available.

ii) It is not necessary to plan for the mutual independence of the various facilities to be installed in the first part of the NA.

1. GENERAL CONSIDERATIONS

A 400 GeV experimental area, by its size and nature, presents problems which cannot be solved simply by extrapolation of the "comprehensive experimental hall" philosophy, adopted so far at energies up to 25-30 GeV. This philosophy envisages primary target, secondary beam, and experiment laid down on a common floor (and mostly under the same roof), served by its extracted beam, and then surrounded by the necessary quantity of mobile shielding (concrete or iron blocks). Within limits, the position of the target and the layout of the secondary beams can then be changed rather freely. However, the price of such a flexibility becomes excessive, and one can hardly envisage this solution at the highest energy of the accelerator.

The extension to 400 GeV would lead to a very large and expensive experimental floor, most of which would be permanently buried under shielding whose very quantity would reduce

flexibility in the sense that a layout, once installed, would necessitate a rather long shut-down period to introduce major modifications.

The ideas outlined here do not remove the rigidity but attempt to reduce the cost of a 400 GeV beam layout by suppressing most of the so-called mobile shielding. It has to be remembered that the cost of a given effective shielding thickness varies in the proportions 1/10/100 depending on whether it is realized with earth/concrete blocks/iron blocks.

It therefore seems attractive and almost compelling to locate primary target, secondary beam, and experiment in different and specialized building enclosures, better adapted to the particular needs of each part.

Of course such an approach makes it necessary to understand in detail the main parts of the layout before attempting to recombine them into a coherent solution.

To date, a first round of studies to present a tentative layout has been completed. Even if such a layout were acceptable for physics, more work would be necessary to assess feasibility and to elaborate detailed technical solutions.

The following sections enter into more detail on some features and problems of the various parts of the layout.

2. EXTERNAL PROTON BEAM (EPB) AND ITS BRANCHES

The EPB is completely designed as a slow extracted beam with classical iron magnets for 400 GeV/c, to allow the construction of the tunnel TT20 which has started. The beam is pulsed to follow the machine cycle, thus providing the possibility of performing experiments at different energies on successive pulses. The end point of the EPB ($\sim$ 470 m from the machine tunnel and $\sim$ 590 m from the ejection point) is assumed to be the origin O of the area (see Section 5).

It is envisaged to divide the EPB after the point O into branches so as to allow some kind of multiple use of the area. The sub-division may be obtained by switches (protons only in one branch at a time), by splitters (protons simultaneously in all branches), or by a suitable combination of both.

Since a split provides the highest degree of multiple use of the area and is also the most demanding in terms of longitudinal space, we consider a three-way split similar to the one described in CERN/1050 (page 166 - Section 13.3.6). The distance needed for the splitting section is about 150 m. A further 50-100 m are needed to separate the branches by 1 or 2 m and to focus the beams onto the targets.

It is important to stress that all targets for the layout presented below will be included in one common radiation zone to which there will be no access whenever one target operates.

Although this limitation may give rise to some inconvenience, it is practically impossible to eliminate it, since only a further considerable lateral separation ($\sim$ 10 m) of the EPB branches would make the independence possible. This separation would require a distance of $\sim$ 200-300 m, thus limiting even more the space before the river available to experiments and would cost a considerable amount of money ($\sim$ 3 MSF per branch).

3. PRODUCTION OF SECONDARY PARTICLES

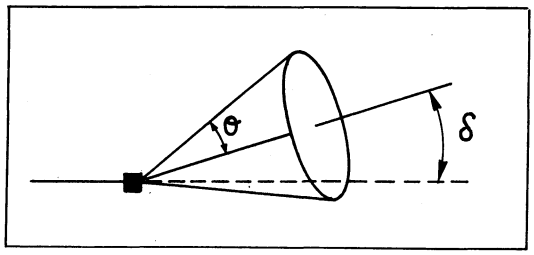

Two main parameters are of interest for the design of secondary beams:

i) the production angle δ;

ii) the angular semi-aperture of the acceptance cone θ.

In fact, normally with quadrupole focusing the acceptance cone has an elliptical rather than a circular cross-section, with an acceptance defined by

$$\Omega = \pi\, \theta_x\, \theta_y = \pi\, \theta^2 \ ,$$

where

$$\theta = \sqrt{\theta_x\, \theta_y} \quad (x,y \text{ are the two transverse coordinates}).$$

Calculations have been carried out, following the Hagedorn-Ranft thermodynamical model[2], by means of the CERN computer library program SPUKJ for a hydrogen target. For heavier-element targets, the flux will be less by a factor 1 to 2, depending on the element.

A first set of curves (Fig. 1) illustrates the well-known forward-peaked characteristics of the production, which implies that with $\delta \neq 0$ the beam intensity is considerably

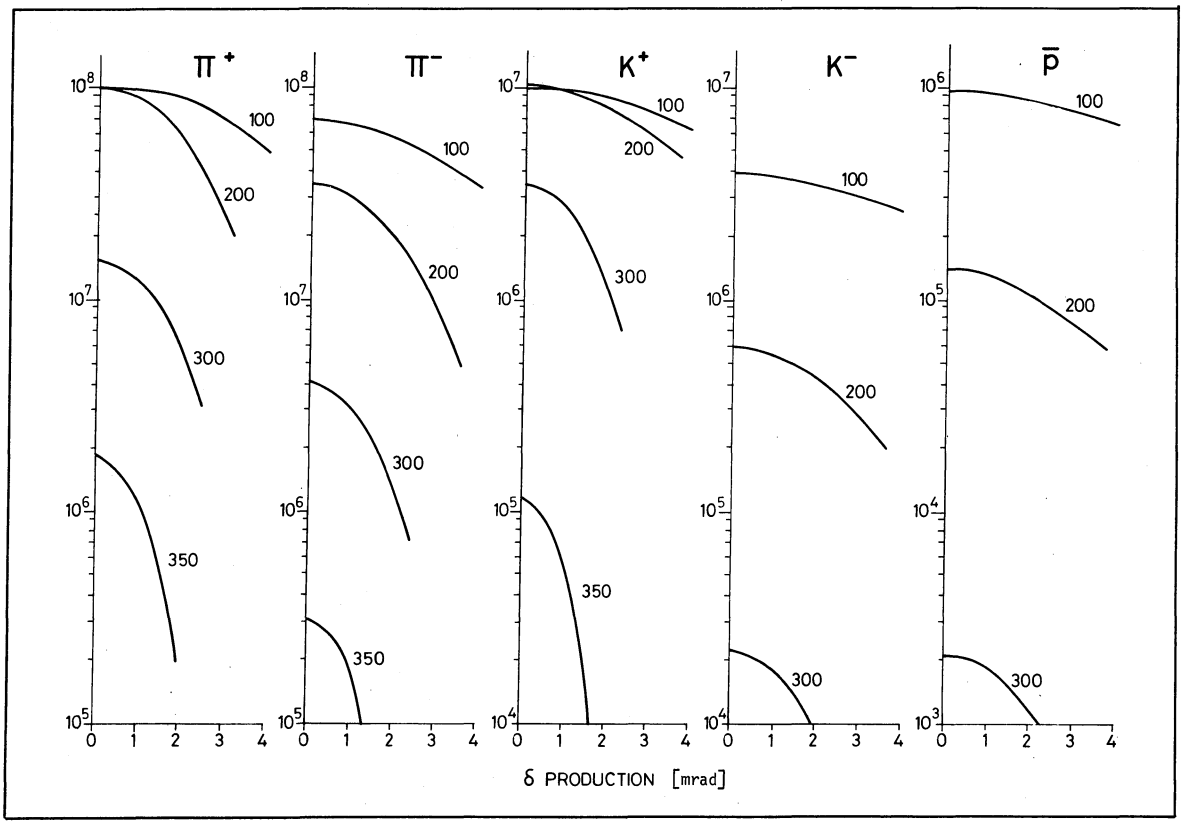

Fig. 1 Production characteristics of secondary particles (p_{EPB} = 400 GeV/c; 10^{12} interacting protons; $\Delta p/p$ = 1%; total acceptance ellipse: 1 mrad × 1/2 mrad)

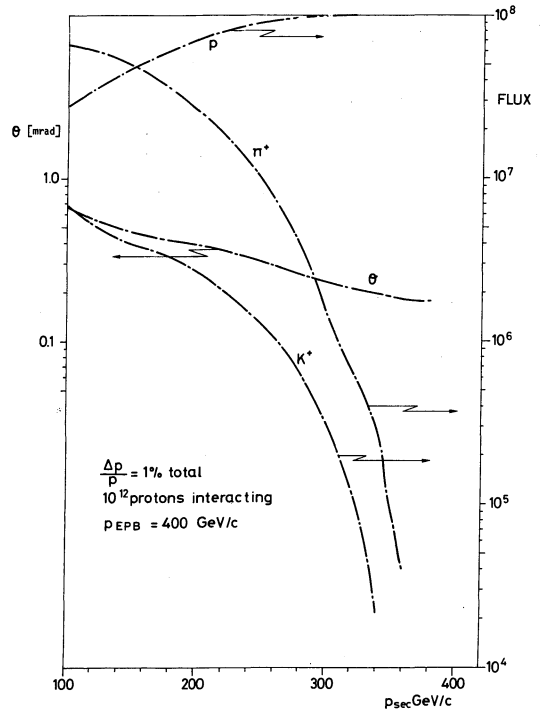

Fig. 2 Positive particle fluxes (right-hand scale) and acceptance angle (left-hand scale) required for total flux limited to 10^8

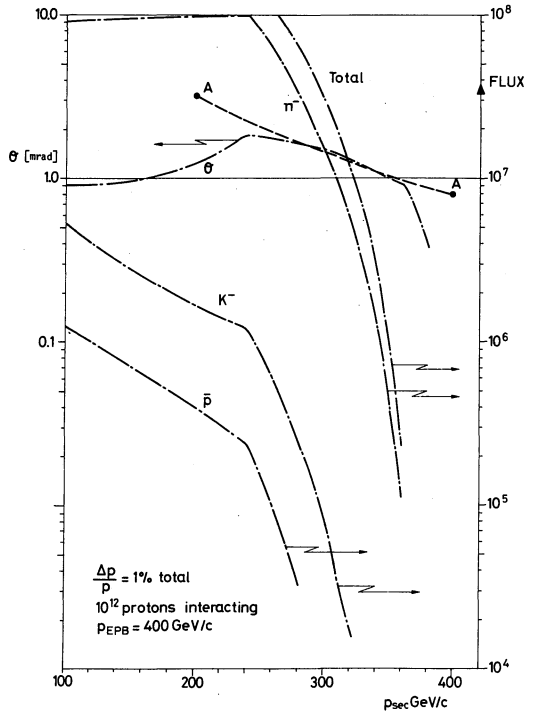

Fig. 3 Negative particle fluxes (right-hand scale) and acceptance angle (left-hand scale) required for total flux limited to 10^8 (or to 50% of total flux possible if this is < 10^8)

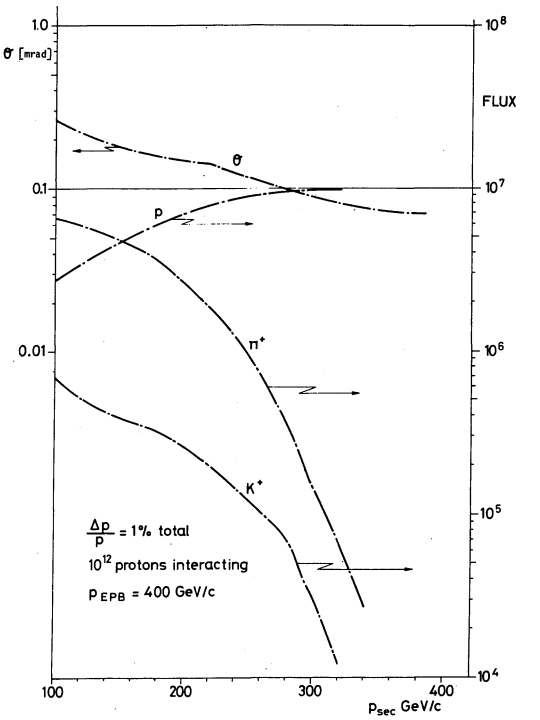

Fig. 4 Positive particle fluxes (right-hand scale) and acceptance angle (left-hand scale) required for total flux limited to 10^7

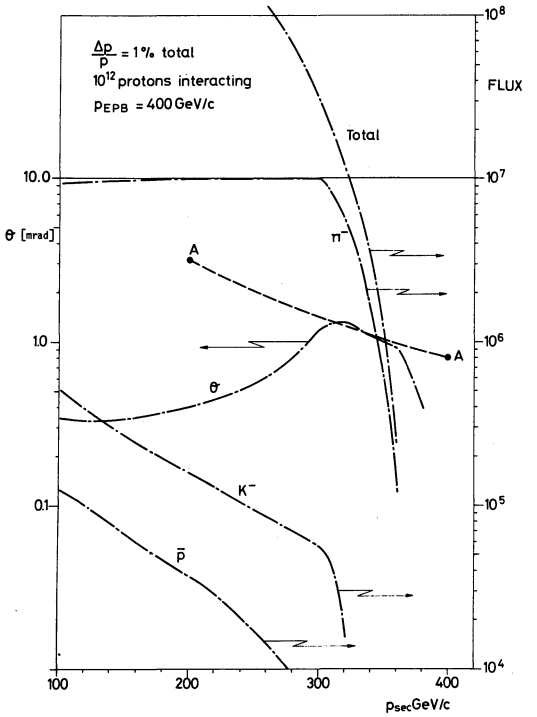

Fig. 5 Negative particle fluxes (right-hand scale) and acceptance angle (left-hand scale) required for total flux limited to 10^7 (or to 50% of total flux possible if this is < 10^7)

reduced, especially at high energy. Only for an energy of the secondaries not exceeding one-half of the primary energy, is a small δ ($\lesssim$ 3 mrad) still acceptable. It should be noted that the characteristics assumed in Fig. 1 (number of interacting protons, $\Delta p/p$, and acceptance) correspond to those of a realistic beam reaching the highest energy available.

Concerning the second parameter θ, clearly the larger it is the more flux one gets (up to a certain value). Since limitations are, however, imposed on θ, both by the configuration of the target stations and, above all, by financial considerations, it is important to assess values of θ which may realize the best compromise between the various requirements in each particular case. Moreover, many experiments will be intensity-limited so that it is legitimate to ask, What is the minimum θ necessary to collect a given flux of particles?

Figures 2, 3, 4, and 5 attempt to answer this question. The flux of all particles of a given sign has been limited to 10^8 or 10^7. One should underline that for negative particles above a certain energy a flux of 10^8 particles (or even 10^7) is not obtained whatever the angle θ, and therefore the total flux (smaller and varying with energy) is indicated. The angle θ necessary to obtain 10^8 or 10^7 total is shown where it is possible to obtain this intensity, and where it is not possible we show the angle that is necessary to obtain 50% of the total flux possible. The flux of individual particles under these conditions is also shown. In Figs. 2 and 4 one should note the preponderance of protons, while in Figs. 3 and 5 the line A-A corresponds to the limiting divergence (referred back to a target of ± 1 mm) accepted by a DISC counter of 8 cm aperture with an angular divergence tolerance of 0.02 mrad.

The general conclusions which can be drawn are as follows:

i) In principle, all beams should be designed for $\delta = 0$ over the widest possible momentum range. This allows the most efficient use of protons.
However, to be able in some cases to vary the flux of secondary particles at "low" and "medium" energies and to obtain positive secondaries at the highest energy, the range $0 \leq \delta < 4$ mrad should be available.

ii) $\theta \lesssim 1$ mrad seems to be adequate for $p_{sec} \gtrsim 100$ GeV, even if a total flux of 10^8 ppp is required.

iii) A beam of a given acceptance produced at $\delta = 0$ collects considerably more particles at high momentum than several beams arranged to receive roughly equal shares of flux at $\delta \neq 0$.

4. TARGET STATIONS

Various schemes for deriving charged secondary beams from targets placed in branches of the EPB are being studied with the aim of providing the following conditions:

i) zero production angle δ for the secondary particles, but range $0 \leq \delta < 4$ mrad available (see conclusions of Section 3);

ii) fixed beam lines, independent of the sign of the charge and the momentum of the secondary particles selected.

In an attempt to show how these requirements might be met, we consider schematically two different types of target station and discuss briefly some of their basic features and limitations. We indicate -- but do not yet pretend to have solved -- some of the problems associated with their practical realization.

4.1 End target station

The greatest degree of freedom is evidently obtained with a target station where no further use of the EPB branch is required after the target, i.e. at the end of an EPB branch. The principle of such a target station is illustrated in Fig. 6a. The EPB is incident on a target T which is followed by an analysing magnet M; a beam of secondary particles of chosen central momentum ±p produced at zero angle is deflected through an angle α to emerge along a fixed line OS independent of p; the unused EPB will be deflected through an angle ε ($\varepsilon_1 \geq \varepsilon \geq -\varepsilon_2$) and emerges in a direction OP which depends on the choice of p.

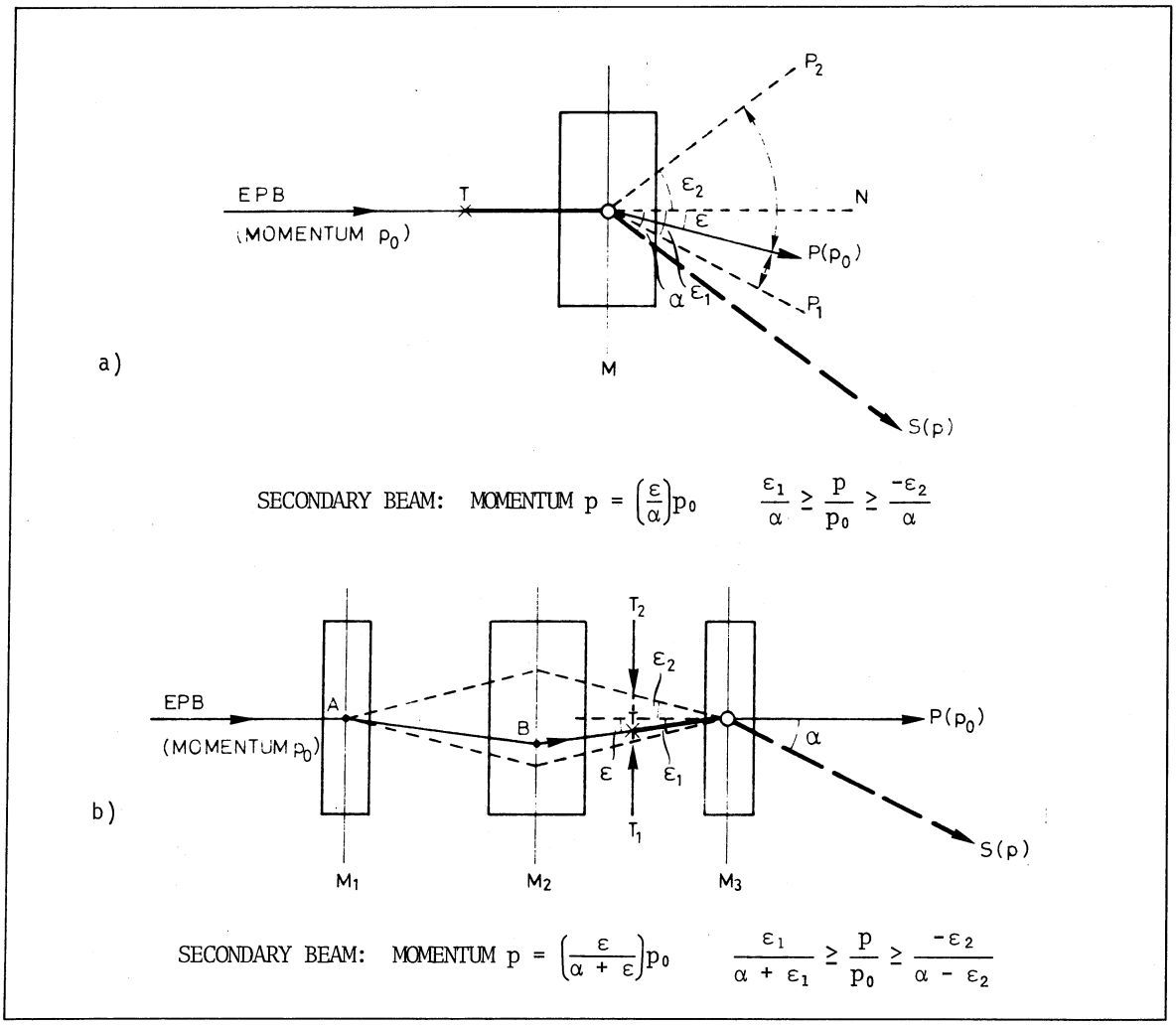

Fig. 6 Principles of target stations: a) End target station; b) Transmission target station

Figure 7 shows a possible example of a target station of this type; an additional (C-type) magnet M_C is used to increase the separation of the secondary beam line from the extreme EPB trajectory at P_1. In this example positively or negatively charged particles of momentum p in the range

$$+0.8\ p_0 \gtrsim p \geq -0.9\ p_0 \quad \text{(in principle } -p_0 \text{ is possible)}$$

can be selected at zero production angle from the target.

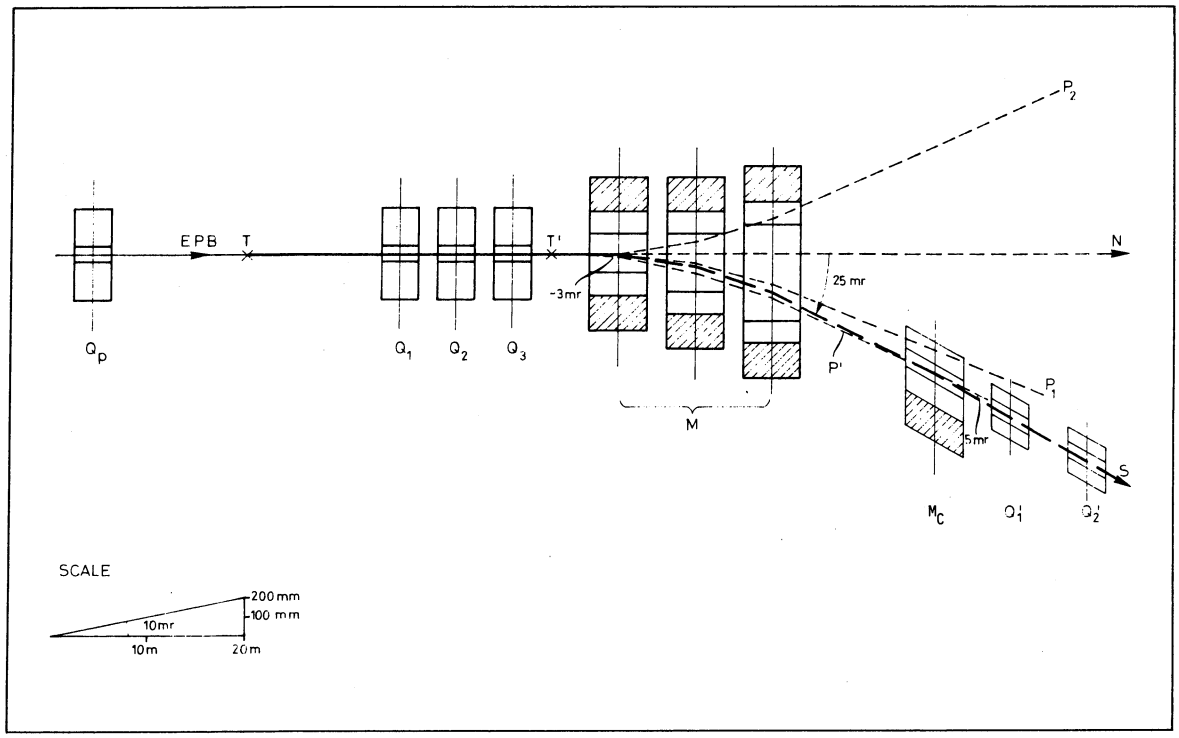

Fig. 7 Example of end target station (schematic)

Two alternative locations of the target along the incident EPB line may be considered:

i) EPB focused on target at T (using quadrupoles Q_p), followed by quadrupoles Q_1, Q_2, Q_3 in front of magnet M. In this case the acceptance angles for secondary particles are defined by the section Q_1, Q_2, Q_3 and can be made as large as is practicable. This section will, however, be common to any other beam derived from the target.

ii) EPB focused on target at T' (using Q_p, Q_1, Q_2, Q_3) immediately in front of magnets M and M_C, followed by quadrupoles Q_1' and Q_2'; these then limit the acceptance of the beam. In this case, the magnet system can be used to select particles of given momentum correlated to the production angle; in particular, a diffracted proton beam ($p = p_0$) can be derived at a scattering angle of $\sim$ 3 mrad along a trajectory T'P'S. The analysing system M can furthermore be regarded as a sweeping magnet which would allow a neutral beam (n, K_L^0, $\gamma \rightarrow e^{\pm}$) to be derived along a line T'N at zero (or near-zero) production angle from the target at T'.

4.2 Transmission target station

In order to increase the utilization of a given EPB branch without incurring the loss of flexibility inherent in deriving several beams from a single target, we consider the design of a target station which will allow the EPB to serve more than one target in series. This will in general require a system of three magnets (or "wobbling" section) to return the EPB to a fixed line independent of the momentum of the secondary beam derived. There are advantages in avoiding the use of special magnets and in leaving greater spatial freedom for the secondary beam if the target is located immediately in front of the last magnet (M_3) of the wobbling section. The principle of such a target station is illustrated in Fig. 6b.

The secondary beam (of central momentum ±p) and the unused EPB leave the analysing magnet M_3 along fixed lines OS and OP, respectively, at angle α to each other, independent of p; the trajectory ABT of the incident EPB and the lateral position of the target T can be varied between two limits given by T_1 and T_2 ($\varepsilon_1 \geq \varepsilon \geq -\varepsilon_2$) according to the choice of p. Figure 8 shows a possible example of a target station of this type in which positively or negatively charged particles of momentum p in the range

$$+0.6\ p_0 \geq p \geq -p_0$$

can be selected at zero production angle from the target with an acceptance defined by the quadrupoles Q_1 to Q_4. Positive particles of momentum $p > 0.6\ p_0$ can be collected at non-zero production angle if an additional (C-type) magnet is inserted between M_3 and Q_1. It should be noted that the initial angle of deflection of the secondary beam and hence the momentum dispersion introduced by the analysing magnets M_3 will be a function of momentum p; this can be taken into account in designing the secondary beam. The scheme permits the beam of protons not consumed in the target to be refocused by the quadrupoles Q'_p essentially independently of the operation of the secondary beam. Only marginal (∿ 20%) loss of possible secondary particle flux is incurred by restricting the target length to allow roughly equal utilization of the transmitted protons on a second target in series*).

4.3 Comparison of target stations

Some parameters relating to the examples of the two types of target station (Figs. 7 and 8) are compared in the following table.

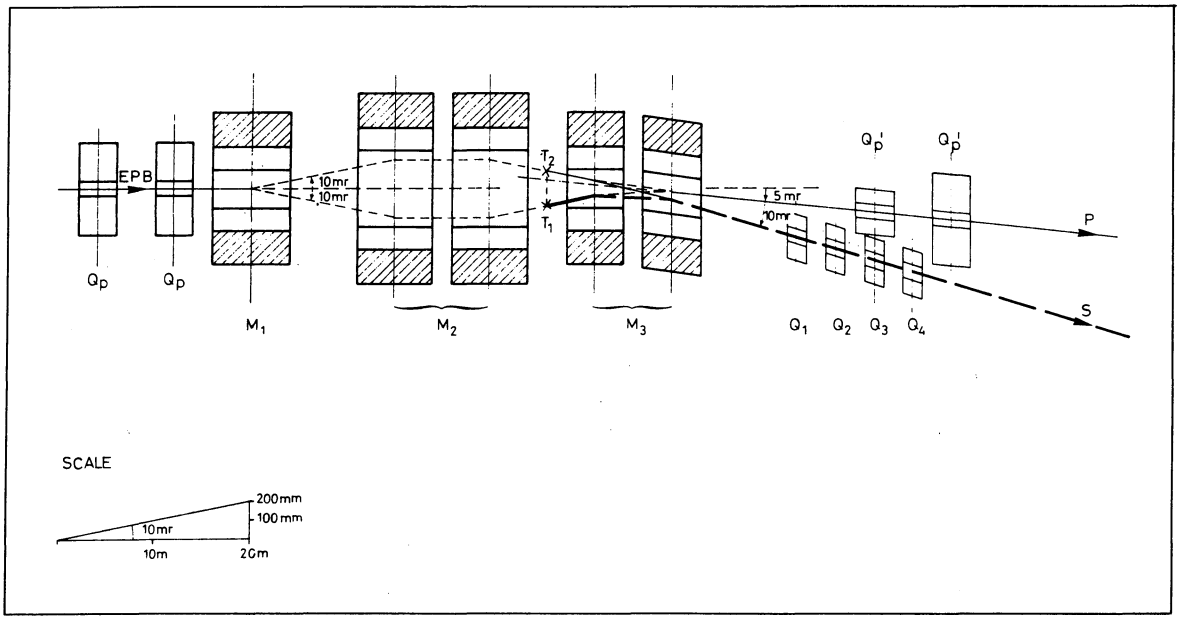

Fig. 8 Example of transmission target station (schematic)

*) It may be noted that the r.m.s. scattering angle introduced by the presence of as much as one interaction length of material in the EPB at 400 GeV/c is small (∿ 0.05 mrad for Be, ∿ 0.15 mrad for Cu) compared with a typical divergence of ∿ ±0.5 mrad for the focused EPB.

	End target station		Transmission target station
	Target at T	Target at T'	
Limiting angles (mrad) α	25		10
ε_1	∿ 20		15
ε_2	22.5		5
Maximum momentum of secondary beam[a]			
for +ve particles: p_1 (GeV/c)	+320 (280)[b]		+240 (200)[b]
for -ve particles: p_2 (GeV/c)	-360		-400
Acceptance of secondary beam[c] (μsr)	∿ 2.2	∿ 0.8 (∿ 1.5) [b]	∿ 2.2 (∿ 3.1) [b]
Total bending power[d] (T·m)			
required for p_1	∿ 32.0		60.0
required for p_2	36.0		46.7

a) For momentum of EPB, p_0 = 400 GeV/c.

b) The numbers in brackets illustrate the correlation between the acceptance of the secondary beams and the maximum momentum of positive particles collected at zero production angle. For example, in the case of an end target, the acceptance almost doubles if the maximum positive momentum is limited to 280 GeV/c instead of 320 GeV/c.

c) Assuming "slim" quadrupoles, aperture 80 mm (useful aperture ∿ 65 mm), and maximum field on pole face ∿ 1.0 T.

d) Assuming conventional magnets of gap ∿ 50 mm and maximum field ≳ 1.6 T.

For both types of station, additional charged secondary beams could be derived along lines at different angle α from the analysing magnet. They would in general be at a lower momentum, which would be coupled in sign and (to some extent) in magnitude to that of the principal beam. However, the increase in pole width of the analysing magnet which this would entail, and the additional requirements on space around the target station, may make this facility of limited use for a practical layout.

It should be noted that the target station schemes considered here are based on the use of iron magnets of conventional type, in the belief that these offer the greatest degree of simplicity, reliability, and resistance to radiation under the especially severe conditions close to a target. These factors will be paramount in continuing the study of practical designs of target stations.

5. TENTATIVE LAYOUT

In addition to the NA being complementary to the WA as already mentioned, our studies have been guided by the following considerations and assumptions:

i) We shall limit ourselves to the first half of the area extending to about 1.4 km from point 0 (see Section 2). In fact, all experimental facilities discussed so far can be contained in this part. In any case it would be wrong to plan now for the facilities occupying the entire area; it is more advisable to reserve the rest for future development, either of the primary proton energy beyond 400 GeV or for second-generation experiments still at 400 GeV.

ii) There will be only slow extraction.

iii) There will be about six beams operating simultaneously and making the most efficient use of protons (all capable of reaching zero production angle).

As mentioned in Section 1, it is our belief that it is advantageous and almost compelling to locate the various parts of the layout (beam splitter and primary targets, secondary beams, and experimental zones) in different and specialized building enclosures adapted to the particular needs of each part.

Figure 9 shows a possible layout.

The targets, placed in the various EPB branches, are at a level of 441.2 m (∿ 10 m below the natural ground level). The charged secondary beams rise to the main experimental zone (Exp. Zone 1), located at a level much closer to the surface (beam height 451.2 m). On the other hand, the muon-neutrino beam(s) will rise more gently with an inclination of ∿ 10 mrad, to a specialized experimental zone (Exp. Zone 2) reserved for muon and neutrino detectors beyond the river "Le Lion". In addition to the secondary beams already mentioned, a possible continuation of the EPB to other experimental zones is also indicated. It can be fed by either the first (from top) or the second EPB branch.

The justification for such a layout is as follows:

i) The primary targets, which are designed to receive globally 10^{13} ppp, must be shielded transversely by an amount of material of ∿ 1600-1800 g/cm^2. In addition, the forward muon cone, whose range in earth is ∿ 400 m from the target, has also to be stopped. By placing the targets at 441.2, both shields are obtained in a rather natural and

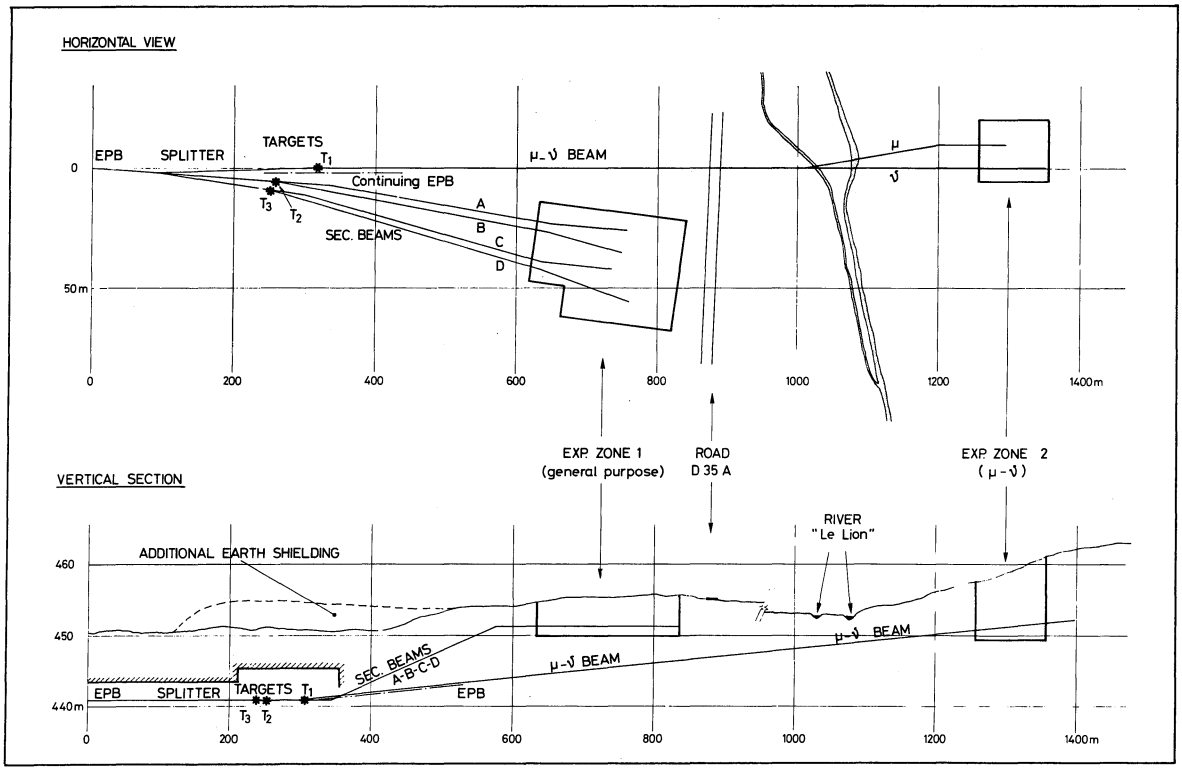

Fig. 9 North Area layout

inexpensive way; the former by filling back the earth on top of the target enclosure (some additional volume is needed, however), the latter by the untouched earth below the rising secondary beams.

ii) The Experimental Zone 1, which is meant as a general-purpose zone, should be as close as possible to the surface; and indeed it can be so since, in general, only beams carrying $\leq 10^8$ ppp will be admitted into it. An exception will be the attenuated proton beam, which could go up to 10^{10} ppp by taking appropriate precautions.

iii) As a consequence of (i) and (ii), the secondary beams must cover a difference in level of 10 m, and for practical reasons must be horizontal again in the Experimental Zone. It therefore appears most natural to use the two bending sections required for momentum selection, measurement, and recombination[3]. The secondary beams can be achromatic in both transverse and angular coordinates at entry in the Exp. Zone.

iv) The muon-neutrino beam(s) cannot follow the same path as the other secondary beams for at least two reasons. The first is that the neutral line (prolongation of the EPB branch) must reach the Exp. Zone for a wide-band neutrino beam. The second is that the beams must pass under the river at sufficient depth to comply with the radiation safety regulations.

The secondary beams A, B, C, and D are charged beams and should be determined in relation to a possible experimental programme.

However, as an illustration of what could be done, the following set of beams seems to be mutually compatible:

A - Attenuated proton beam ($\leq 10^{10}$ ppp) to be brought onto a target in Exp. Zone 1 to produce, for example, beams of short-lived particles.

B - Charged beam ($\pi^{\pm}$, $K^{\pm}$, $\bar{p}$) with good resolution and DISC counter for particle identification.
Momentum range +240 GeV/c $\gtrsim p_{sec} \gtrsim$ -400 GeV/c.

C - Electron beam (by conversion of γ's from target). Can be reconverted to tagged photon beam in Exp. Zone 1.
Electron momentum $\leq$ 200 GeV/c.

D - Charged beam ($\pi^{\pm}$, $K^{\pm}$, $\bar{p}$) similar to B.
Momentum range +300 GeV/c $\gtrsim p_{sec} \gtrsim$ -400 GeV/c.

Of course, a gradual development of the NA is possible. The muon-neutrino facility could be started first, and beams A, B, C, D would follow in due course.

One has, however, to be aware of the fact that the civil engineering of the target enclosure and of the best part of the tunnels housing the beams A, B, C, and D has to be completed prior to any utilization of the area.

Finally, it is worth while noting that a layout including the same beams but with all the parts at the same level, chosen to be intermediate between 441 m and 451 m (for example 446-447 m), was also considered in some detail. The incentive to make such a study was the belief that this solution might be more flexible. It was found that this one-level solution is disadvantageous in many respects, since:

i) the targets would have to be placed further downstream and hence the available distance to the river would be reduced by $\sim$ 50-100 m;

ii) the width of the Exp. Zone 1 should be wider by 30-40 m for the same number of facilities, since the offset necessary in the secondary beams to provide the required momentum resolution should be horizontal instead of vertical;

iii) the background at the experiments produced by the primary targets may be greater and such as to limit the freedom of placing experiments in the Exp. Zone 1;

iv) a higher cost may be incurred because of the greater total excavation needed by the depth of the large Exp. Zone 1;

v) finally, we do not believe this one-level solution to be more flexible. The basic "inflexibility" is given by the separate building enclosures and the earth shielding, whose transverse thickness must be the same in either solution. As mentioned earlier, we believe that a "comprehensive hall" simply cannot be afforded and would also be inflexible when buried by concrete and iron blocks.

6. SOME FEATURES OF A HIGH-ENERGY CHARGED SECONDARY BEAM

In order to acquire some ideas on the distance needed between targets and Exp. Zone 1 and on a possible beam layout, we undertook to design a high-energy charged beam with the characteristics indicated below. Clearly, should such a beam be of interest, these characteristics should be revised and more clearly defined in the light of proposals for specific experiments.

i) Particles/Flux/Momentum : $\pi^{\pm}$, $K^{\pm}$, p, $\bar{p}$ with maximum fluxes of $\sim 10^6$-10^8 ppp over a wide range of momenta extending as high as possible towards the primary momentum (p_0 = 400 GeV/c) of the EPB.
$\Delta p/p \sim 1\%$.

ii) Background : acceptable fluxes of hadrons and muons accompanying the beam at positions where detectors may be placed.

iii) Momentum selection/ recombination : high intrinsic resolving power of the beam at the position of momentum-defining slits.

iv) Momentum (energy) measurement on individual particles : detector spacing allowing resolution of $\sim \pm m_\pi c/2 \simeq \pm 70$ MeV/c at the highest possible momentum.

v) Particle identification : velocity measurement permitting π-K separation at the highest possible momentum ($\Delta\beta_{\pi K} \sim 10^{-6}$ at 300 GeV/c).

vi) Matching of the beam size and divergence to the experimental set-up.

If produced from an end target station similar to that shown in Fig. 7, the following set of parameters could be obtained:

i) Maximum momentum : $|p_{max}|$ = 400 GeV/c

ii) Production angle : δ = 0 for +320 GeV/c $\gtrsim p_{sec} \gtrsim$ -360 GeV/c
$\delta \simeq 3$ mrad for p = +400 GeV/c

iii) Acceptance from a target of 2 mm Ø : $\theta_x \simeq \pm 0.8$ mrad
$\theta_y \simeq \pm 0.3$ mrad
$(\Delta p/p)_{FWHM} = 1.2\%$
$\Omega \cdot \Delta p/p \simeq 1$ μsr · %

iv) Fluxes : shown in Fig. 10

v) Resolution for momentum measurement : ∿ 2800 (or ±70 MeV/c at 400 GeV/c)

vi) Velocity measurement : DISC counter set for π/K identification up to $|p_{max}|$ and accepting ≳ 80% of particles in the beam[4]

vii) Design emittance at experiment : horizontal (x) plane ∿ ±1.0 mm · mrad
vertical (y) plane ∿ ±0.6 mm · mrad

viii) Total length : ∿ 500 m.

It should be noted that to comply with (vi) and (vii) above, it is necessary to correct systematically the chromatic aberrations along the beam[5].

A more complete description of the optics of such a beam is in preparation[3].

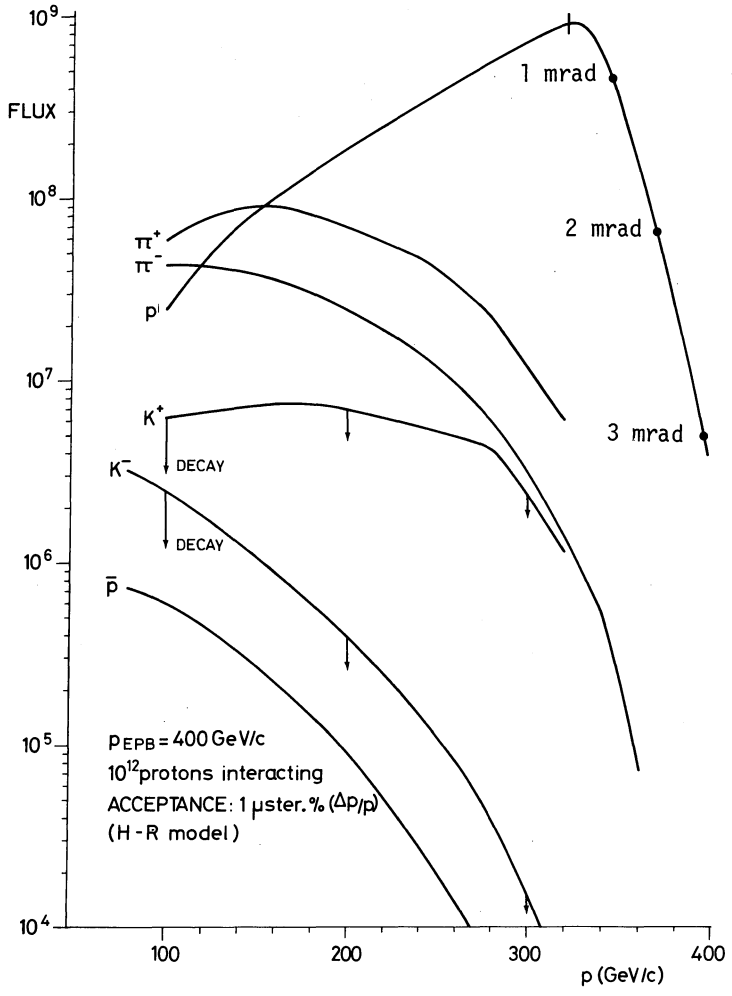

Fig. 10 Flux of particles in beam produced from the end target station shown in Fig. 7

7. CONCLUSIONS

It may be noticed that some important questions are not adequately answered or even mentioned in this report. They concern mainly the experimental zones themselves, civil engineering solutions for the various parts of the layout, radiation problems, beam elements, construction of targets, etc. Many of these questions have not yet been studied in sufficient detail to justify a meaningful presentation.

We also consider it essential that more information on possible experimental detectors should be obtained very soon in order to assess in a better way the facilities needed in the Experimental Zones.

Finally, a general comparison can be made between the West and the North Areas. The North Area has the following distinctive features (with respect to the WA):

i) The EPB energy can always be equal to the maximum accelerator energy.

ii) The maximum length available to secondary beams and experiments between targets and maximum extension of Exp. Zone 1 is $\sim$ 900 m (three times more than in the WA).

iii) The secondary beams become longer (higher energy) and are more rigidly fixed (at least in the first part).

iv) However, the experiments are less likely to be disturbed by background, and their location may be more independent of the primary targets and may thus be changed more freely.

v) There are ample possibilities of extension to the second part of the area.

It is therefore our belief that the utilization of both the NA and the WA will allow a comprehensive and versatile experimental programme to be carried out.

* * *

REFERENCES

1) H. Atherton, G. Brianti and N. Doble, CERN/ECFA/72/4 (1972), Vol. I, p. 394.

2) H. Grote, R. Hagedorn and J. Ranft, Atlas of particle spectra (CERN, Geneva, 1970). The parameters used are those contained in the CERN computer ISR production program ISPRO.

3) N. Doble, A high-energy charged beam for the North Area. To be published.

4) M. Benot, J. Litt and R. Meunier, Čerenkov counters for particle identification, paper presented to the ECFA Working Group on particle identification, May 1972.

5) K.L. Brown, A systematic procedure for designing high resolving power, beam transport systems or charged particle spectrometers, SLAC-PUB-762, June 1970.

POINTS ARISING IN THE DISCUSSION AFTER G. BRIANTI'S TALK

1. HIGH-INTENSITY PRIMARY TARGET AS A SOURCE OF SHORT AND SPECIAL BEAMS (e.g. NEUTRON BEAM)

The remark was made that in the tentative layout no provision exists for such cases.

Indeed it is very difficult and expensive to provide such a facility in the immediate neighbourhood of the target enclosure. It was thought, however, that since such a facility can be inserted easily in the West Area, one could avoid constructing it in the North Area from the very beginning. Obviously, in a second phase of the NA development, it would be possible to combine it with the EPB continuing to the second part of the area.

It was also stressed that the attenuated proton beam ($\lesssim 10^{10}$ ppp) which can reach the Exp. Zone 1 via, for example, beam A, will already be very useful for the production of hyperon beams and of beams of short- (and long-) lived neutrals.

2. HIGH-INTENSITY PROTON BEAM TRAVERSING A (LIQUID HYDROGEN) TARGET, AND OBSERVATION OF EVENTS AT LARGE TRANSVERSE MOMENTUM

This requires the observation of particles produced in the laboratory system in a cone whose angular semi-aperture may extend up to $\sim$ 100 mrad or so.

In principle, this could be done in the primary target enclosure itself, but the main difficulty will be to install sizeable experimental equipment in a zone which is the heart of the NA (it should be in operation whenever the machine operates) and which contains hot equipment.

A better solution could be to combine this facility with the one mentioned under point 1 above, e.g. on the EPB continuing onto the second part of the area.

3. USE OF A SECONDARY BEAM FOR MORE THAN ONE EXPERIMENT

The remark was made that, since high-energy beams are long, costly, and necessarily limited in number, it would be quite appropriate to use them for more than one experiment at a time.

It certainly looks feasible to have two experiments, e.g. one data-taking and the other setting-up, at the end of any of the beams A, B, C, D. The beam could then be shared in time between the two experiments as appropriate.

Whether or not more sophisticated schemes could be applied (more than two experiments, more elaborate particle sharing, etc.) will be studied in due course, when actual experiments are designed.

4. PROVISION OF A PION BEAM OF THE HIGHEST POSSIBLE INTENSITY

Interest was expressed in deriving a beam of $\gtrsim 10^9$ π's at medium energies (100-200 GeV/c) for experiments in which detectors would be placed outside the beam to observe reaction products at large transverse momentum.

The similarity of these requirements with those of the muon beam included in the layout (large acceptance, wide momentum-band transmission, possibly a common detector system, natural earth shielding around Exp. Zone 2) suggests that a combined π/μ beam facility might merit closer study.

COMMENTS ON THE HADRONIC BEAM SESSION

M. Steuer*)
CERN, Geneva, Switzerland

D. Treille
Laboratoire de l'Accélérateur linéaire, Orsay, France

Possible solutions for the set-up of charged hyperon beams, long- and short-lived neutral beams, and a polarized proton beam were discussed. The question of RF separated beams for counter experiments was treated, and general constraints on beams when identifying particles with a Čerenkov counter were presented.

1. CHARGED HYPERON BEAMS

There exist two solutions for a charged hyperon beam, one with fixed incident proton energy and one where the incident protons can vary over a wide energy range, thus permitting adjustment of the γ-value of the hyperons to specific experimental requirements. This flexibility reduces the acceptance, but the main limitation in constructing a hyperon beam seems to be due to π, μ (or p) contamination. A detailed study has therefore to be made to decide whether a longer beam with a momentum slit is better than a high acceptance short beam. The fixed incident energy hyperon beam is designed for 200 GeV/c or eventually 400 GeV/c primary protons and has therefore a narrower range of secondary momenta than that of the variable incident energy hyperon beam. The channel is as short as possible in order to allow a large hyperon flux. The muons are bent away from the experimental zone by a wide-gap magnet filled with heavy shielding.

J. Lefrançois asked for a comparison of the relative merits of a diffracted proton beam and a secondary variable energy proton beam. J. Allaby answered that a diffracted (or rather attenuated) proton beam could provide more protons (up to 10^{11}) and a better spot size than a secondary one. P. Lehmann pointed out that varying the momentum of the primary protons might affect other users of the area in which the hyperon beam is located.

2. POLARIZED PROTON BEAM

The polarized proton beam and the neutron beam can work simultaneously when using a 30 cm Be target having the transverse dimension of the beam. A primary proton intensity of 3×10^{12} ppb is necessary for the polarized proton beam; at lower intensities it might be used as an unseparated charged particle beam[1].

W. Koch asked how the p polarization would be affected by a Λ polarization at production. P. Dalpiaz recalled that the Λ, being taken at 0 mrad, cannot be polarized.

G. Coignet stressed that the total beam acceptance is ±8%, whereas the rates indicated in Figs. 7.11a and 7.12a of their contribution to this meeting[2] are given per GeV/c: thus, for 100 ± 8 GeV/c a transverse polarization of $\simeq$ 55% is achieved with a total beam intensity $\simeq 10^6$ ppp.

---

*) Visitor from the Institute for High-Energy Physics, Austrian Academy of Sciences, Vienna, Austria.

3. RF SEPARATED BEAM

A. Michelini (with G. Petrucci) gave the main features of a possible RF separated beam for counter experiments in the Hall E1. Such a beam of maximum momentum 40 GeV/c would have a length of 230 m, an acceptance of 70 μsr, and a momentum bite of ±1%. At 0° it would collect the secondaries from around 3×10^{11} protons of 200 GeV/c per pulse. The mass separation would be obtained with two RF superconducting cavities (S band, > 6 MeV/c transverse momentum produced per cavity, 4 cm diameter).

A comparison of the yield of K^- between this beam and unseparated ones was performed. For the unseparated beam the useful beam intensity, limited by the time resolution of the detector, was set to 5×10^6 particles/burst; two lengths of unseparated beam (230 m and 130 m) were considered. The general result is that factors of $\sim$ 10 in gain of K^- seem possible by going from an unseparated to a separated beam. However, to ensure this gain, strict conditions for the background have to be imposed and a lower limit of 2 MeV/m for the deflecting power of the cavities is required, 4 MeV/m being strongly recommended.

M. Martin pointed out that up to now no use has been made of the unwanted pions removed from RF separated beams by stopping them in a beam stopper. If these pions, which have been momentum analysed, can be extracted by a septum magnet, a very intense pion beam could be extracted from the Ω beam line. Although the energy is not too high, the beam could be used for high intensity experiments at little extra cost.

4. n-K^0_L

N. Doble asked whether both beams could be taken at the same angle ($\sim$ 0°) provided that an absorber is set to reduce the neutron/K^0_L ratio and give more favourable background conditions for K^0_L physics. However, the people interested in K^0_L (Wahl et al.) seem to stick to a larger production angle ($\sim$ 5 mrad) and prefer a duplication of beams.

5. IDENTIFICATION OF PARTICLES IN A CHARGED BEAM

R. Meunier described the calculations which were performed on a beam transport system containing a production target and a differential Čerenkov counter (DIFC). Such a system is capable of selecting and performing a mass identification of the charged particles within the produced secondary beam.

The whole set-up will, of course, comprise the target in which the particles are produced, collimators limiting the aperture of the particle beams emerging from the target, beam transport elements such as bending and quadrupole magnets, possibly momentum-analysing slits, and the differential Čerenkov counter, which provides identification of the particle, without modifying its velocity and trajectory. Scintillation counters can be added if required, in particular to define the apertures.

The whole system can also be considered as a spectrometer, which would not absorb the particle to be measured or modify its flight. The distinction between a secondary beam or a spectrometer is irrelevant for our purpose.

The aim of this work has been to investigate and evaluate the fundamental properties of analysis systems making use of a Čerenkov detector, with a view to making an optimum design

in each particular case. In particular, we have examined a) the conditions for mass separation, b) the beam acceptance, c) the momentum bandwidth, and d) detection and rejection efficiencies.

It is found that the problem is completely determined if one specifies initially the mass M and momentum p of the particle to be electronically identified, and the mass difference ΔM for which another particle is to be electronically rejected. The basic design quantities of the whole system are shown to be the target dimensions, some of the beam transport matrix elements, beam apertures, momentum-slit width, and the Čerenkov angle of the DIFC. Relations between these quantities, which are in fact more easily expressed using non-dimensional variables, allow one to optimize the system and to calculate its detection efficiency, i.e. the number of particles identified per incident interacting particle on the production target.

These relations, obtained from first-order theory, can be taken as a starting point in the design of the charged particle beam (or spectrometer) for mass identification with Čerenkov counters. The effects of optical aberrations and of the limiting velocity resolution of the DIFC or the electronics detection efficiency are also evaluated. The derivations of these relations are to be published

* * *

REFERENCES

1) J.A. Jansen, P. Dalpiaz and G. Coignet, this volume, p. 83.

2) P. Dalpiaz, J.A. Jansen and G. Coignet, CERN/ECFA/72/4 (1972), Vol. I, p. 289.

ALTERNATIVE USE OF THE POLARIZED PROTON BEAM LAYOUT FOR A CHARGED PARTICLE BEAM*)

J.A. Jansen and P. Dalpiaz
CERN, Geneva, Switzerland

G. Coignet
Division des Hautes Energies, Institut de Physique nucléaire, Orsay, France

The beam transport system of the polarized proton beam proposed elsewhere[1] can be used to provide other charged particles on an experimental target, if it will not be possible to obtain on the production target a direct beam intensity of some 10^{12} ppb.

i) The first possibility is to accept all azimuthal angles for the protons from the Λ^0 decay and to focus them on the experimental target, where the net polarization will be very small. In the momentum range from 80 to 140 GeV/c, the proton flux thus obtained will be of the order of 10^7 ppb for 10^{12} direct 200 GeV/c protons on a 30 cm Be target, increasing the Λ^0 solid angle to 10^{-6} sr and decreasing the proton momentum bite to $\Delta p/p = \pm 4\%$.

ii) The second possibility is to use the set-up as a normal hadron beam line, where probably only one section for particle identification has to be added (see Fig. 1). The small acceptance of this system, caused by the large distance between the first focusing element (QP_1-QP_2) and the target ($\sim$ 30 m), can be overcome by placing two quadrupoles immediately behind the sweeping magnet (SM) as indicated in Fig. 1 by QP_H, QP_V thus increasing the solid angle from 2 to 15 μsr. The momentum resolution of this beam is of the order of $\Delta p/p = \pm 0.2$-0.4% and the momentum acceptance is approximately $\Delta p/p = \pm 4\%$.

Under these experimental conditions,

target	:	10 cm Be (10^{25} p/cm^2)
beam	:	10^{12} ppb
$\Delta p/p$	:	$\pm 4\%$
$\Delta\Omega_{acc}$	:	2 μsr,

the particle intensities for 200 GeV/c and 400 GeV/c direct proton beams are given in Table 1.

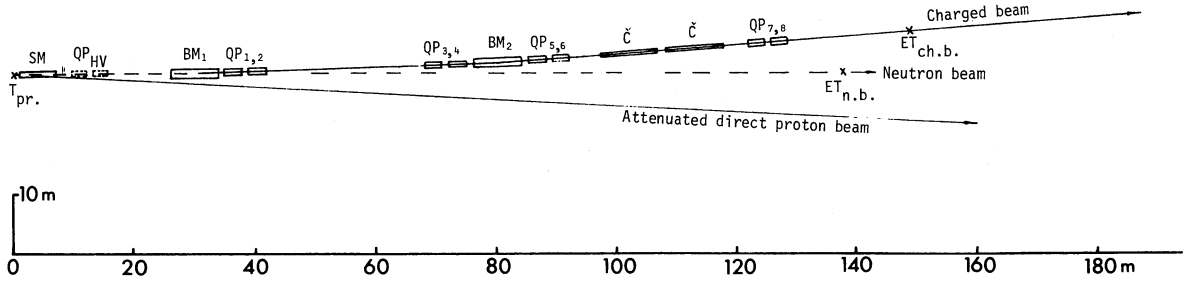

*) Contributed paper

Table 1

Particle intensities calculated with the thermodynamical model

	Incoming proton energy			
	200 GeV/c		400 GeV/c	
	100 GeV/c	150 GeV/c	200 GeV/c	300 GeV/c
p	2.7×10^8	1.2×10^9	1.1×10^9	4.9×10^9
$\bar{p}$	8.4×10^4	1.3×10^3	3.6×10^5	6.5×10^3
π^+	5.2×10^7	7.1×10^6	2.2×10^8	3.2×10^7
π^-	2.3×10^7	2.7×10^6	1.0×10^8	1.2×10^7
K^+	4.9×10^6	1.7×10^6	2.2×10^7	7.8×10^6
K^-	3.6×10^5	1.3×10^4	1.5×10^6	6.2×10^4

We want to remark that using the SM immediately behind the target, the production angle of the charged particles may change from 0 to about 10 mrad. This feature is particularly convenient for operating with positive mesons, since although the intensities of the secondary particles are reduced by a factor of 3 to 5, operating at angles of 5 to 10 mrad the ratio of mesons to protons increases significantly with respect to the ratio at 0° production angle.

In the case of simultaneous use of the neutron beam and the polarized proton beam as described in another paper[2], the SM immediately behind the production target is used to clean the neutron beam of charged particles. In the case of the alternative use of the polarized proton beam described in this paper the SM has a low field, or it is switched off and the first bending magnet BM1 can be used to clean the neutron beam.

* * *

REFERENCES

1) P. Dalpiaz, J.A. Jansen and G. Coignet, CERN/ECFA/72/4 (1972), Vol. I, p. 284.

2) J. Engler, F. Mönnig and H. Schopper, CERN/ECFA/72/4 (1972), Vol. I, p. 267.

CHAPTER III

NEUTRINO PHYSICS

NEUTRINO PHYSICS

C.H. Llewellyn Smith
CERN, Geneva, Switzerland

1. INTRODUCTION[1)]

It is now more than 12 years since Lee and Yang, Cabibbo and Gatto, Yamaguchi and others spelled out the theoretical reasons for studying neutrino reactions. In their Phys. Rev. Letter, Lee and Yang posed the nine questions which are listed in Table 1. It is interesting to examine them and ask how many have been answered. It will be seen that only one question has been completely answered, while neutrino experiments have so far yielded essentially no information about five of them.

Table 1

Questions raised by Lee and Yang [Phys. Rev. Letters 4, 307 (1960)]	Experimental answers from ν experiments
1) $\nu_\mu = \nu_e$?	$\nu_\mu \neq \nu_e$
2) Lepton conservation $\nu \to L^+$ and $\to L^-$?	$\sqrt{\frac{\sigma(\nu_\mu \to \mu^+)}{\sigma(\nu_\mu \to \mu^-)}} \leq 0.068$ But several different forms of conservation law still allowed
3) Neutral currents?	$\sqrt{\frac{\sigma(\nu n \to \nu n\pi^0) + \sigma(\nu p \to \nu p\pi^0)}{2\sigma(\nu n \to \mu^- p\pi^0)}} \leq 0.37$
4) "Locality" (vector nature of weak interactions)	-
5) Universality between ν_μ and ν_e, μ and e?	-
6) Charge symmetry?	-
7) CVC; isotriplet current?	-
8) W ?	$M_W > 1.8$ GeV
9) What happens at high energy ($E_\nu \to$ "unitarity limit")?	-

Thus we are still ignorant about many fundamental questions concerning the weak interactions, and the table defines a large experimental programme even without the additional questions which have been raised in the last 12 years. In any case, much recent work --

particularly that concerning the deep inelastic region -- presupposes answers to the original questions, which should really be tested first. I intend to begin by stressing how little evidence there is for many of the ideas which are commonly taken for granted and then turn to more interesting recent developments.

Apart from ν reactions, all our knowledge of weak interactions has been derived from studying the decays of only eight stable particles -- μ, π, K, N, Λ, Σ, Ξ, Ω -- and from μ capture. (This shows the fundamental reason for doing neutrino experiments -- to study other processes and investigate the weak interactions at large energy/momentum transfer.) Most of these data can be satisfactorily described by a simple phenomenological theory involving only a few parameters. Thus we can distinguish a first goal of neutrino experiments:

i) to establish the domain of validity of the phenomenological theory and test the selection rules embodied in it.

It is well known, however, that the phenomenological theory cannot give a correct description at very high energies (we review the reasons for this in Section 3). Thus a second goal is:

ii) to provide clues for the construction of an alternative theory of weak interactions.

A third is:

iii) given a theory, to use neutrinos to probe the structure of hadrons.

The rest of this talk is divided into three parts in which these goals are considered in more detail.

2. THE PHENOMENOLOGICAL THEORY

The phenomenological theory can (in part) be stated thus: apart from T violation, all known reactions involving neutrinos can be described by the effective interaction

$$\mathscr{L}_{\text{eff}} = \frac{G}{\sqrt{2}}\left[(j^{e}_{\lambda} + j^{\mu}_{\lambda})^{+}\, J^{h,\lambda} + j^{e^{+}}_{\lambda} j^{\mu,\lambda} + \text{h.c.}\right], \tag{1}$$

where

$G = 1.0 \times 10^{-5}/\text{Mp}^2$

$j^{\mu}_{\lambda} = \bar{\psi}_{\mu}\, \gamma_{\lambda}(1 - \gamma_5)\psi_{\nu_{\mu}}$

$j^{e}_{\lambda} = \bar{\psi}_{e}\, \gamma_{\lambda}(1 - \gamma_5)\psi_{\nu_{e}}$

J^{h}_{λ} is a current which depends on hadronic variables and behaves <u>as if</u> it were constructed from quark fields (p,n,λ); thus

$$J^{h^{+}}_{\lambda} = \bar{p}\, \gamma_{\lambda}(1 - \gamma_5)n \cos\theta_C + \bar{p}\, \gamma_{\lambda}(1 - \gamma_5)\Lambda \sin\theta_C ,$$

where θ_C is the Cabibbo angle,

and the notion of an effective interaction will be defined in the next section.

The point I wish to stress is that this is a minimal scheme. Interactions certainly exist with the quantum numbers of all the terms in $\mathscr{L}_{\text{eff}}$, which is probably the simplest form which can describe the existing data. However, the limits on other possible terms are actually very bad. Thus the data allow quite different forms of lepton conservation

laws from the one implied by Eq. (1), neutral currents (purely leptonic or with $\Delta S = 0$) with appreciable strength, etc.; the relevant data are reviewed elsewhere[1]. Here we mention just three examples of badly tested "principles" embodied in $\mathscr{L}_{\text{eff}}$:

1) Semileptonic processes with $\Delta S > 1$ should not occur in lowest order. However, the best limit is

$$\frac{|A(\Xi^0 \to pe^-\bar{\nu}_e)|}{|A(\Xi^- \to \Lambda e^-\bar{\nu}_e)|} < 0.27 \ .$$

The $\Delta S \leq 1$ hypothesis can, of course, be tested in neutrino reactions since it implies

$$\bar{\nu}n \not\to \mu^+\Omega^-$$

in

$$\bar{\nu}p \to \mu^+\Lambda^0(K^0 + y\bar{K}^0) \ , \qquad y = 0 \ , \quad \text{etc.}$$

2) $\Delta S = 0$ semileptonic processes should obey a $\Delta I = 1$ rule. Examination of possible semileptonic decay processes shows that they put no constraints whatsoever on terms with $\Delta I \geq 2$ (in electromagnetic interactions a $\Delta I \leq 1$ rule is also usually assumed, but there are no good limits on currents with $I \geq 2$ at present). Again, neutrino reactions can provide tests since this "rule" implies:

$$\frac{\sigma(\nu p \to \mu^-\Delta^{++})}{\sigma(\nu n \to \mu^-\Delta^+)} = 3 \ , \text{ etc} \ .$$

3) J^h_λ satisfies the "charge symmetry condition"

$$J^{h+}_\lambda = -e^{-i\pi I_2} J^h_\lambda e^{i\pi I_2}$$

(this is equivalent to assuming that there are no second-class currents in the approximation that T is conserved). This hypothesis predicts

$$\frac{\Gamma(\Sigma^- \to \Lambda e^-\bar{\nu}_e)}{\Gamma(\Sigma^+ \to \Lambda e^+\nu_e)} = 1.64$$

with which the experimental ratio of 1.60 ± 0.56 is obviously compatible. However, if we attribute significance to the data [compiled by Wilkinson et al.[2]] suggesting asymmetries in the ft values for β-decays of mirror nuclei, then we would conclude that the charge symmetry condition is wrong. Luckily it can be tested by comparing ν with $\bar{\nu}$ interactions on D, Ne, or any $I = 0$ target.

It is commonly supposed that the weak interactions are mediated by charged vector bosons ($W^\pm$) which interact thus:

$$\mathscr{L} = g_W(J_\lambda W^\lambda + \text{h.c.}) \ , \tag{2}$$

where $J_\lambda = J^h_\lambda + j^\mu_\lambda + j^e_\lambda$, which reduces to

$$\mathscr{L}_{\text{eff}} = \frac{G}{\sqrt{2}} J^+_\lambda J^\lambda \ , \qquad \left(\frac{G}{\sqrt{2}} = \frac{g_W^2}{M_W^2}\right), \tag{3}$$

at low momentum transfers. In addition to the properties already implied by Eq. (1), Eqs. (2) and (3) imply the following:

1) *Additional "diagonal" leptonic processes:*

$$\nu_e + e \to \nu_e + e$$
$$\nu_\mu + \mu \to \nu_\mu + \mu\,, \quad \text{etc.},$$

with definite cross-sections. Sixteen years have passed since this was first predicted, but these cross-sections have not yet been measured. These processes are, of course, extremely hard to observe directly [note that $\sigma(\nu_e e) \sim G^2 s = 2G^2 m_e E_\nu^{lab} = 5 \times 10^{-43}\ E_\nu^{lab}\ (\text{GeV})^{-1}\ \text{cm}^2$] but they could perhaps be seen indirectly by observing:

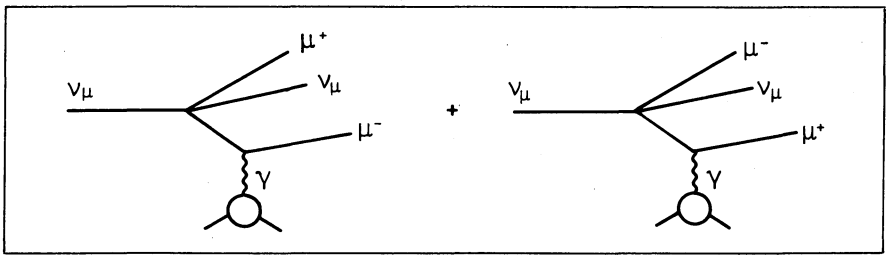

If there are neutral leptonic currents (as required by various theories discussed below) the predictions for these "diagonal" processes would change. In any case it is extremely important to try to observe them.

2) *Non-leptonic processes.* These are really outside the scope of this talk, but we observe that: a) $\Delta S = 0$ processes with the order of magnitude required by the current-current theory are known to exist; b) the well-known $\Delta S = 1$ processes present some problems. Their gross features can be described by $I = \frac{1}{2}$ amplitudes; small $I = \frac{3}{2}$ amplitudes are needed, but in no case are they required to be > 5% *). This is not really understood, in my opinion, and is a problem for the current-current model. Furthermore, the model naively predicts amplitudes that are about a factor of five too small for these processes.

3) *The existence of W's.* One of the primary aims of neutrino experiments is to observe the process:

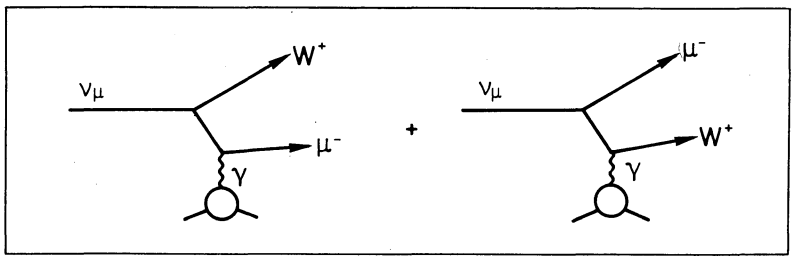

In this way, W's of up to 15 GeV could perhaps be seen at NAL and the CERN SPS. The clearest way to observe W's is in $e^+e^- \to W^+W^-$, but there are no machines approved which could reach $M_W \gtrsim 4.5$ GeV. If theoretical calculations based on the parton model are not badly wrong,

---

*) Since this was written I have discovered that substantially larger $I = \frac{3}{2}$ amplitudes are now needed in $K \to 3\pi$. See the discussion of the papers submitted by Pirone et al., and Hitlin et al., at the Batavia conference in the article by Zakharov in the parallel session led by M.K. Gaillard (to be published in the Proceedings).

W's of up to about 40 GeV could perhaps be observed in the process $pp \to W + \ldots$ at the new accelerators and the ISR. The existence of W's of even higher mass might be inferred from characteristic deviations from scaling in deep inelastic neutrino reactions.

To summarize this section: there is a phenomenological theory which describes most decay processes satisfactorily in terms of a few parameters. Nevertheless, many fundamental questions first posed many years ago are still open. In particular, we would like further information concerning

i) the validity of selection rules, neutral currents, form of lepton conservation law, isospin properties, etc. (Note that ideally we would like tests at high as well as low energy; currents with, for example, $\Delta S = 4$ or $\Delta I = 10$ could not show up below the $4K$ and the 9π thresholds, respectively.)

ii) "Diagonal" cross-sections.

iii) W's.

3. POSSIBLE THEORIES OF WEAK INTERACTIONS

3.1 Problems with the conventional theory

If we take the current-current form and try to calculate second-order effects, we immediately encounter divergent integrals:

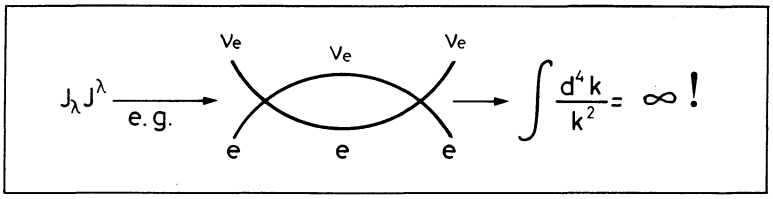

Divergent integrals also occur in quantum electrodynamics, but in that case they can be absorbed by renormalization. Here, however, we are dealing with a "non-renormalizable" theory, and it turns out that an increasing number of arbitrary constants must be introduced in each successive order to render all matrix elements finite. An alternative way of looking at the problem of the divergent second-order amplitude above is to consider calculating it by writing a dispersion integral over the imaginary part, which is proportional to the lowest-order cross-section for $\nu_e + e \to \nu_e + e$. It is a safe approximation to neglect the electron mass at high energy in this case, and therefore (on dimensional grounds)

$$\sigma(\nu_e + e \to \nu_e + e) \sim G^2 s \qquad (s \gg m_e^2) \ . \tag{4}$$

Consequently the dispersion relation requires two subtractions[3], the subtraction constants being the first of the arbitrary constants alluded to above.

Faced with this proliferation of arbitrary constants, an "effective Lagrangian philosophy" is usually adopted according to which higher-order terms are simply discarded and the matrix elements of $\mathscr{L}_{\text{eff}}$ are supposed to describe the data completely. However, as is well known, this "philosophy" must fail at high energies. In the current-current model the interaction $\nu_e + e \to \nu_e + e$ occurs at a point (zero impact parameter). It is purely s-wave and is bounded

by unitarity to be $\leq$ const/s. The predicted cross-section [Eq. (4)] overtakes this bound at the so-called "unitarity limit". The most stringent bound is actually obtained in the inelastic process $\nu_\mu + e \to \mu + \nu_e$ where the limit is reached at $E^\nu_{cm} \sim 320$ GeV (corresponding to $E^\nu_{lab} \sim 10^5$ GeV).

In these processes, the situation can be improved by introducing a W which "spreads out" the cross-section over many partial waves:

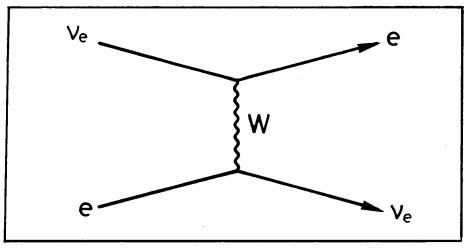

The lepton masses can again be neglected at high energies and, since the coupling g_W [Eq. (2)] is dimensionless,

$$\frac{d\sigma}{dQ^2} \sim \frac{g_W^4}{(Q^2 + M_W^2)^2}, \qquad \sigma \sim \frac{g_W^4}{M_W^2}$$

for $s \gg M_W^2$. The dispersion relation now converges[3] and we can calculate the second-order amplitude. [The s-wave cross-section, which behaves as

$$\sigma_{s\text{-wave}} \sim \frac{g_W^2}{s} \log\left(\frac{s}{M_W^2}\right),$$

still violates unitarity at some astronomical energy, but this is only a problem if we adopt an "effective philosophy" and reject higher orders; even renormalizable theories eventually violate exact unitarity if we work in a fixed order.]

Although in processes such as $\nu_e + e \to \nu_e + e$ the high-energy behaviour is greatly improved by the introduction of a W, we are now faced with disaster in other diagrams such as

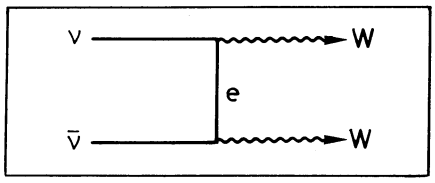

The problem occurs when the W is longitudinally polarized. In its rest frame the W's polarization is described by three vectors:

$$\begin{matrix} t \\ x \\ y \\ z \end{matrix} \quad \begin{pmatrix} 0 \\ 1 \\ 0 \\ 0 \end{pmatrix}, \quad \begin{pmatrix} 0 \\ 0 \\ 1 \\ 0 \end{pmatrix}, \quad \begin{pmatrix} 0 \\ 0 \\ 0 \\ 1 \end{pmatrix}.$$

Under a Lorentz transformation along the z-axis the transverse (T), x and y, components are unchanged, dimensional analysis still governs at high energies and

$$\sigma(\nu\bar{\nu} \to W_T W_T) \sim \frac{g_W^2}{s} , \qquad (s >> M_W^2) .$$

However, the longitudinal (L) polarization vector becomes

$$\varepsilon_\mu^L = \frac{1}{M_W} \left(|\vec{k}|, 0, 0, k_0\right) = \frac{k_\mu}{M_W} + 0\left(\frac{M_W}{k^0}\right)$$

so that

$$\sigma(\nu\bar{\nu} \to W_L W_L) \sim \frac{g_W^2}{M_W^4} s , \qquad (s >> M_W^2)$$

rendering the contribution of the WW state to the fourth order (in g_W) amplitude for $\nu\bar{\nu} \to \nu\bar{\nu}$ uncalculable except in terms of arbitrary constants.

Another way to exhibit this problem is to note that the spin projection operator (obtained by summing over the polarization vectors above and writing the result covariantly) is

$$\sum \varepsilon_\mu \varepsilon_\nu = -g_{\mu\nu} + \frac{k_\mu k_\nu}{M_W^2} .$$

The $k_\mu k_\nu$ term (due to the longitudinal component) prevents the propagator

$$\frac{-g_{\mu\nu} + \dfrac{k_\mu k_\nu}{M_W^2}}{k^2 - M_W^2}$$

from falling off as $k_\mu \to \infty$, thus making higher-order terms unrenormalizably infinite.

Before discussing possible ways out of this apparent dilemma, we consider *attempts to estimate the cut-off energy/momentum* λ *beyond which the conventional weak interaction theory is expected to fail* (the strong interactions do not provide a cut-off according to current algebra -- light cone -- parton ideas). Estimates of the most divergent contributions (due to Ioffe et al.) to $K_L^0 \to \mu^+\mu^-$ yield $\lambda \lesssim 23$ GeV, while (yet more model-dependent) calculations of the $K_L^0 - K_S^0$ mass difference give $\lambda \approx 4$ GeV. This suggests that the conventional theory may fail at quite modest momentum transfers and is therefore very encouraging for experimentalists. However, it has to be said that the details of the calculation would make no sense in finite theories, although they are probably valuable as order of magnitude estimates. (We shall see below that these results are embarrassing for theories which unify weak and electromagnetic interactions in which $\lambda \sim M_W \sim e/\sqrt{G}$ is expected.)

3.2 Some possible theories

We have discussed the fact that with the simple current-current form or the traditional picture with W's [Eqs. (2) and (3)] we cannot calculate to all orders without introducing an infinite number of arbitrary constants. In the latter case trouble first occurs in diagrams such as

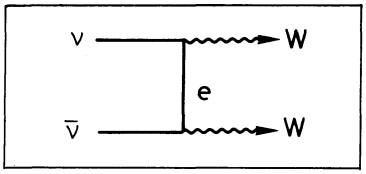

We now consider some possible ways out of this problem:

1) It can be asserted that "perturbation theory is irrelevant". If this were so, it is not clear that $\mathscr{L}_{\text{eff}}$ would be connected in any way with the "true" Lagrangian. In any case, such an assertion on its own is scarcely scientific, being without predictive powers.

2) Salam et al. have considered "non-polynomial Lagrangians" which are closely related to Eq. (2) [4]. Techniques have been developed for handling such Lagrangians (at least in simple cases); the method amounts essentially to giving a "minimal" prescription for assigning values to the arbitrary constants encountered in the usual approach. It would be nice if advocates of this approach could commit themselves to definite predictions for higher-order weak interactions and high-energy behaviour.

3) As observed by Gell-Mann, Goldberger, Kroll and Low, the propagator $\Delta^{ij}_{\mu\nu}$ which connects currents j^i_μ and j^j_ν can be made to behave as $1/k^2$ as $k \to \infty$, provided $i \neq j$, by introducing additional scalar bosons with a derivative coupling to j_μ thus:

$$\Delta^{ij}_{\mu\nu} = \frac{-g_{\mu\nu} + (k_\mu k_\nu / M_W^2)}{k^2 - M_W^2} + \frac{g_i^* g_j \, k_\mu k_\nu}{k^2 - M_S^2} .$$

(This led these authors to stress the importance of measuring the diagonal -i = j -- matrix elements which, they suggested, might be described by something quite different from the conventional theory.) The non-renormalizable divergences of higher-order diagrams could all be removed if the second term entered with a minus sign. This means abandoning the notion of positive metric and seems to lead to violations of unitarity, e.g. the amplitude corresponding to the diagram

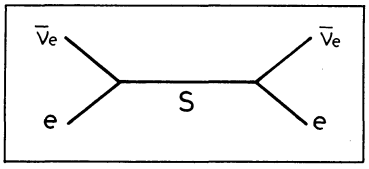

has the opposite sign than in usual theories; the imaginary part of this amplitude gives the probability for producing the particle S which is now negative! Lee and Wick observed [5] that this does not matter if all negative metric particles (such as S) are unstable and therefore cannot really be produced. With four new bosons in place of each one in the conventional theory, all amplitudes can be made not only renormalizable but actually finite; similarly, a negative metric "heavy photon" can be introduced to make electromagnetic amplitudes finite. The most important experimental implications of this model are the existence of scalar bosons, which should be produced by neutrinos (note, however, that if $M_W > M_S$ we expect

$$W \to S + \gamma$$
$$\quad\quad \hookrightarrow \text{hadrons}$$

to be the dominant decay mode), and a "heavy photon" which should be seen, for example, in $e^+e^- \to \mu^+\mu^-$ and $pp \to \mu^+\mu^- + \ldots$.

4) "Conspiracy". Models can be devised[6] in which the weak interactions are mediated by scalar bosons (so that the theory is renormalizable) whose couplings are arranged so as to simulate the usual V-A interaction at low energies. For example, in the theory of Kummer and Segrè[6], μ decay is a fourth-order process, described by the diagram:

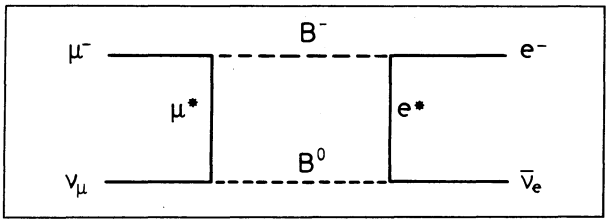

where $B^{\bar{0}}$ are heavy scalar bosons and $\mu^*(e^*)$ is a heavy muon (electron). A large menagerie of new particles must be introduced, whose couplings must conspire to satisfy many relations, in order to reproduce the successful aspects of the usual theory, such as -- for example -- CVC (which in this model appears to be an accidental small momentum transfer effect). The existence of these models is of considerable interest but, in view of their inelegant features, I personally would only advocate them as a last resort.

5) "Evasion". It has been suggested that W's may interact strongly with each other[7] (some models have been proposed in which they also interact strongly -- in pairs -- with hadrons). These strong interactions could damp out the bad high-energy behaviour encountered in the usual theory, e.g. by a final state interaction in the example considered previously:

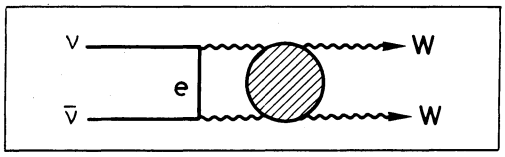

This suggestion is evasive in the sense that it shifts the problem into the intractable realm of the strong interactions. Presumably strongly interacting W's should exhibit typical strong interaction phenomena -- bound states, resonances, Regge recurrences, etc. Thus there may be large families of new particles dubbed "sthenons" by Appelquist and Bjorken[8] at the insistence of the editor of Phys. Rev. (in place of the earlier name "nguvons" which replaced the original term "Garryons" -- in honour of Garry Feinberg who was one of the first to consider strongly interacting W's).

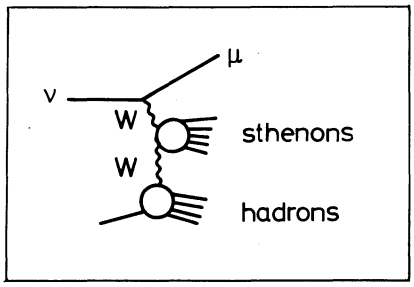

Experimentally these models imply that for $s \gg M_W^2$ diagrams like the one opposite become important and

$$\frac{\sigma(\nu A \to \mu^- + \text{sthenons} + \text{hadrons})}{\sigma(\nu A \to \mu^- + \text{hadrons})} \sim 1 \ .$$

(the linearly rising total cross-section having flattened out at $s \sim M_W^2$, as in all models with W's). Further implications are considered by Appelquist and Bjorken[8].

6) "Cancellation". The last possibility which we shall consider is to introduce new contributions which cancel the bad high-energy behaviour encountered previously. Systematic attempts to do this lead more or less inexorably to spontaneously broken gauge theories of the Higgs type. In view of the recent interest in these theories, we shall now discuss them at some length.

3.3 Spontaneously broken gauge theories[9]*)

3.3.I Motivation[10]

In order to cancel the bad high-energy behaviour encountered in $\nu\bar{\nu} \to WW$ with other contributions in the same order, we must introduce new exchanges in the s-channel or the t- (or u-) channel (whose couplings can be adjusted to cancel the offending terms):

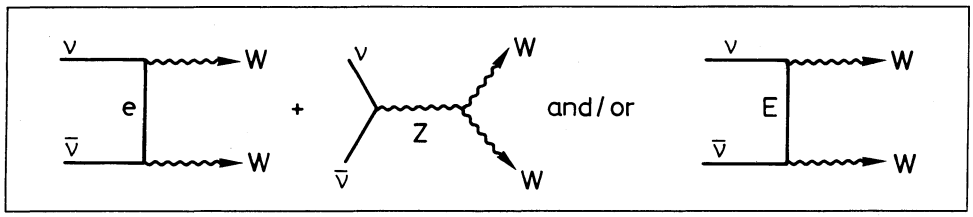

Thus cancellation requires the existence of either neutral currents or heavy leptons (with $Q = \pm 1$) or both.

Next consider the reaction $e^+e^- \to W_L^+W_L^-$ in which the diagram

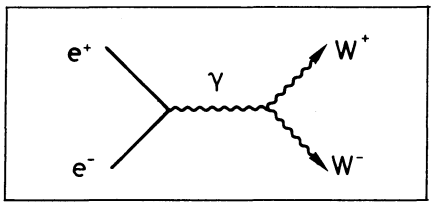

leads to disaster. In this case there exists another contribution with which it might be thought that cancellation could be arranged:

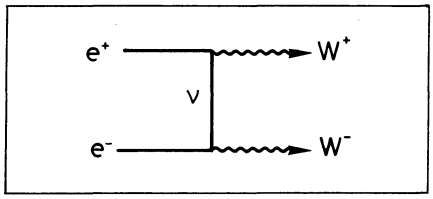

*) We follow convention and use the term "spontaneously broken" symmetry but note that it is misleading. The symmetry is not broken (the corresponding Ward identities are satisfied) but it is realized in a relatively unfamiliar way (without degenerate multiplets).

However, because of the V-A vertex structure, this is impossible since we can always polarize the electrons so that this contribution vanishes. Once again, cancellation requires the introduction of new exchanges:

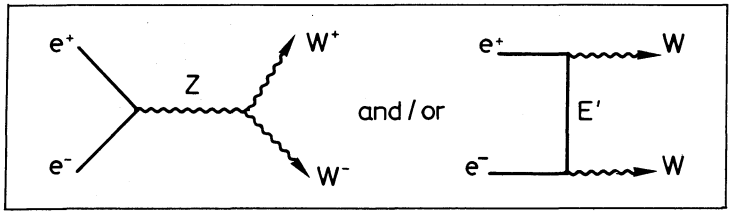

(where $|Q_{E'}| = 0$ or 2). If, in the interest of economy, we wish to use the same Z (and/or related particles E and E') to effect the cancellation in the case of $e^+e^- \to W^+W^-$ and $\nu\bar{\nu} \to W^+W^-$ then there must be a relation between the strengths of the weak and electromagnetic interactions.

If we actually pursue this cancellation idea systematically in processes of the type $L\bar{L} \to W\bar{W}$, then we are led to relations between the couplings which are characteristic of Yang-Mills theories[10] (i.e. the "conspiracy relations" needed to give the desired cancellation look rather natural since they have a Clebsch-Gordan-like character). It is well known that the electrodynamics of charged vector bosons is best behaved at high energies when the gyromagnetic ratio has the Yang-Mills value $\lambda = 2$ [e.g. in lowest order $\sigma(\gamma\gamma \to WW) \sim s$ for $\lambda \neq 2$, $\sim \ln s$ for $\lambda = 2$].

It turns out that renormalizable theories involve one more new type of particle -- scalar mesons (ϕ) coupled to W's and to fermions. The necessity of the ϕ can be motivated by considering $\bar{\nu}_e e \to 3W$; with the couplings introduced so far, this process makes a divergent contribution to $\bar{\nu}_e e \to \bar{\nu}_e e$. The introduction of ϕ's is the simplest way of achieving convergence [a more detailed discussion of this argument, which is due to H. Quinn, is given in the Appendix to B.W. Lee's article[9]].

To sum up: the demand that all Born terms are well behaved at high energy in a theory with W's requires the existence of neutral currents and/or heavy leptons with couplings of the Yang-Mills type; in higher orders, new scalar mesons are needed. [Further: it is most economical to unite the weak and electromagnetic interactions. This leads to a relation of the form $M_W \sim \alpha/\sqrt{G} \sim 100$ MeV. Thus in Weinberg's model $M_W = 37$ GeV/sin $\theta \geq 37$ GeV, while in the Georgi-Glashow model $M_W = 53$ GeV $\times$ sin $\beta \leq 53$ GeV when θ and β are parameters in these theories.] These, then, appear to be necessary conditions for the construction of a renormalizable theory of this type. It is now believed that they are also sufficient conditions and that spontaneously broken gauge theories with these ingredients are renormalizable [these developments are associated with the names of Higgs, Kibble, 't Hooft, B.W. Lee, Weinberg, Salam, and others[9]].

Technical aside: What is a spontaneously broken gauge theory? Recall that the invariance of Lagrangians under phase transformations $\psi \to e^{ie\chi}\psi$ leads to charge conservation. If we allow χ to become an arbitrary function of space time $\chi(x)$ and still demand invariance, then we must introduce a new massless field A_μ which transforms as $A_\mu \to A_\mu + \partial_\mu \chi$ and (as a minimal requirement) make the replacement $\partial\mu\ \psi \to (\partial\mu - ieA\mu)\psi$ in the Lagrangian. This gauge invariance leads to the well-known result that in an amplitude involving a photon with

momentum k we can make the replacement $\varepsilon_\mu(k) \to \varepsilon_\mu(k) + \beta k_\mu$ without changing any physical results. Recall that the origin of the problem with W's was that

$$\varepsilon_\mu^L(k) = \frac{k_\mu}{M_W} + O\left(\frac{M_W}{k^0}\right).$$

If there was some sort of gauge invariance for the charged W's, so that we could change ε_μ by terms proportional to k_μ with impunity, then the k_μ term in ε_μ^L would have to be totally ineffective and our problems would be solved. Yang and Mills showed that the required gauge invariance can be obtained by generalizing invariance under such transformations as, for example, isospin ($\psi \to e^{i\vec{\tau}\cdot\vec{\Lambda}}\psi$) to space time dependent transformations [$\psi \to e^{i\vec{\tau}\cdot\vec{\Lambda}(x)}\psi$]; this requires the introduction of isospin multiplets of vector mesons (W's). The problem is that the invariance requires that $M_W = 0$. This is avoided by producing a "spontaneous breakdown" of the symmetry so that the solution (in which $M_W \neq 0$) does not have the full symmetry of the Lagrangian (in which $M_W = 0$) [11]; traces of the symmetry remain in the relations between the couplings, which give rise to systematic cancellations in divergent amplitudes (in the way discussed above). The spontaneous breakdown is implemented by introducing scalar mesons ϕ coupled to the W's (as already encountered above); the ϕ's have a self-interaction such that at the classical potential minimum $\phi = \lambda \neq 0$. Thus in the ground state the coupling ($\sim \phi^2 W^2$) becomes a mass term ($\sim \lambda^2 W^2$).

Problems: The introduction of neutral currents and/or heavy leptons and ϕ's seems a small price to pay for a renormalizable model which unites weak and electromagnetic interactions. Why then has no model emerged which has gained general acceptance? The problem is that in all models considered so far the baryon structure is a mess. It turns out that models with three quarks are essentially impossible [12]. Since we do not want a $\Delta S = 1$ neutral current, the badly behaved quark amplitude

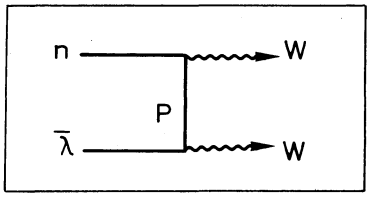

cannot be cancelled with an s-channel exchange. New t- (or u-) channel exchanges require that the number of "quarks" is increased to at least four; thus schemes with 4, 5, 8, 11, etc., "quarks" have been considered. These schemes go beyond SU(3); a new quantum number, conserved by strong interactions, called "charm" (a sort of new strangeness) is introduced and SU(3) is supposed to hold as a low-energy remnant of some higher symmetry. The non-appearance of "charmed particles" is explained by attributing large masses to them. (We consider the phenomenological implications of charm very briefly below.)

Another problem is that those second-order effects which are quadratically divergent in the phenomenological theory are of order $G(GM_W^2) \sim G\alpha$ in these theories. The fact that $K_L^0 \to \mu^+\mu^-$ does not occur above the $G\alpha^2$ level can generally be arranged at a price [e.g. in the O(3) model of Georgi and Glashow this can be done by increasing the original choice of five quarks to eight [13]]. However, the fact that

$$m_{K_L^0} - m_{K_S^0} \approx \frac{1}{2}\Gamma_{K_S^0} \sim G^2 M^5$$

is harder to explain; again it is easy to suppress the natural magnitude ($\sim G\alpha$), but the fact that it is suppressed to exactly the conventional second-order level has to be put in by hand.

3.3.2 Phenomenology

Regardless of the validity of the theories considered above, they have already played an important role in stimulating experimentalists to improve the limits on neutral currents. It is to be hoped that they will also stimulate searches for heavy leptons and charmed particles. We now examine some relevant phenomenology.

i) Neutral currents: The failure to observe neutral currents in neutrino reactions has cast considerable doubt on the only known model [the SU(2) × U(1) model of Weinberg] which has no heavy leptons[14]. However, there are plenty of models with neutral currents as well as heavy leptons*). In some of these the neutral current is not coupled to the neutrino, so its only observable effects might be in e^+e^-, eN, and μN collisions. Unfortunately the effects are probably small; the interference term in

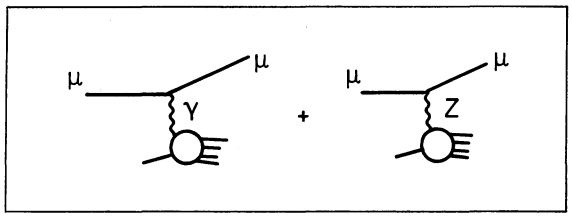

is of order $GQ^2/4\pi\alpha$ relative to the purely electromagnetic contribution, e.g. a simple guess for the parity-violating difference of cross-sections for left- and right-handed μ's (e's) gives

$$\frac{|d\sigma^L - d\sigma^R|}{d\sigma^L + d\sigma^R} \sim 10^{-4} \left(\frac{4\omega}{3 + \sqrt{\omega}}\right) \frac{Q^2}{M_p^2} \frac{Q^2}{2M_p E_\mu^{lab}}$$

(where $\omega = 2\nu/Q^2$). Despite the smallness of the effect, the apparent violation of scale invariance produced by the Z might be detectable at very high energies; see Ref. 15, where more serious estimates are given.

ii) Heavy leptons[16]*:* We only consider here heavy leptons of the type encountered in gauge theories, which have the same lepton numbers as those of muons or electrons; a review of some ideas and evidence about these and other species of heavy leptons has recently been given by Perl[17]. When we considered cancelling part of the electron exchange contribution to $\nu\bar{\nu} \to W\bar{W}$ we were led to contemplate the introduction of a heavy lepton in either the t- or the u-channel. In simple models, it turns out that in this case the appropriate choice is

*) A survey of several models has been given by J.D. Bjorken [to be published in Proceedings of the 1972 International Conference on High-Energy Physics (Batavia)]. See also the Appendices in Ref. 16.

such that there is an M^+ with the same lepton numbers as ν_μ and μ^-. Cancellation in $\mu^+\mu^- \to$ $\to W^+W^-$ is likewise achieved with an M^0. Thus the fundamental vertices are

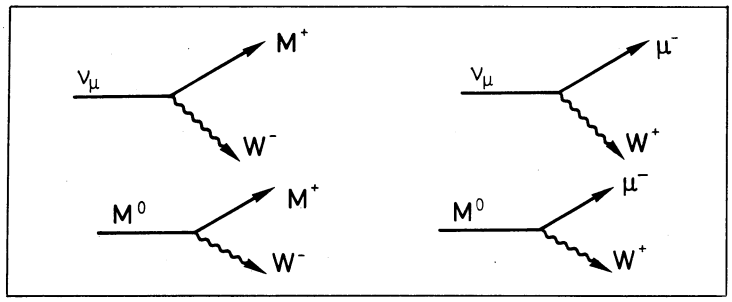

[more technically, when we augment the simplest "isodoublet" structure (ν_μ, μ^-) we are led, e.g. to consider "isotriplets" (M^+, ν_μ, μ^-), and M^0's mixed with ν_μ]. The fact that M^+ and μ^- have the same lepton number will be seen to lead to very good signatures for $M^\pm$ production.

The decays are simple to investigate. The main results are as follows:

a) According to currently popular ideas

$$\frac{\Gamma(M^\pm_0 \to \text{leptons})}{\Gamma(M^\pm_0 \to \text{lepton} + \text{hadrons})} \sim 1 \ ,$$

thus making it easy to identify M's from their leptonic decays. [If $M_{\text{heavy lepton}} > M_W$, then the dominant decay mode is $M \to W +$ lepton.]

b) For masses $\gtrsim$ 800 MeV [18], the lifetime of this particular species of heavy lepton is such that they would not leave visible tracks.

Several production processes might be contemplated:

1. $e^+e^- \to M^+M^-$

$$\begin{cases} \bar{\nu}_\mu \mu^- \bar{\nu}_\mu \\ \bar{\nu}_\mu e^- \bar{\nu}_e \\ \bar{\nu}_\mu + \text{hadrons} \end{cases}$$

$$\begin{cases} \nu_\mu \mu^+ \nu_\mu \\ \nu_\mu e^+ \nu_e \\ \nu_\mu + \text{hadrons} \end{cases}$$

In this process M's with mass almost up to the beam energy should be seen with the design luminosity of machines under construction (giving limits of $\sim$ 4.5 GeV in a few years).

2. $\gamma A \to M^+M^- + \ldots$ by the mechanism

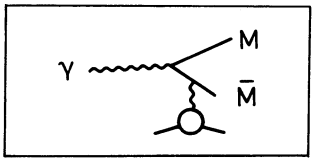

The cross-section can be calculated exactly [19]. It seems unlikely that mass limits of $\gtrsim$ 3 GeV can be set from this process with machines under construction.

3. $\nu_\mu A \to M^+ + \ldots$

$$\nu_\mu A \to M^+ + \ldots \quad \Big\lfloor \begin{cases} \nu_\mu e^+ \nu_e \\ \nu_\mu \mu^+ \nu_\mu \\ \nu_\mu + \text{hadrons} \end{cases}$$

The results of a (model-dependent) calculation of the cross-section are shown in Fig. 1. From this figure we may probably conclude that $M_{M^+} > 1$ GeV. In the CERN 1967 HLBC experiment over 100 events with $E_\nu > 4$ GeV were observed. Were M^+ to exist with mass ~ 1 GeV, there would have been $\gtrsim 25$ M^+ production events as well. Were M^+ to have a mass ~ 1.5 GeV, this number would drop to ~ 5, probably consistent with the data. On the basis of this figure we conclude that heavy leptons with masses up to somewhere in the 5-10 GeV range could perhaps be seen in neutrino experiments at NAL and the CERN SPS.

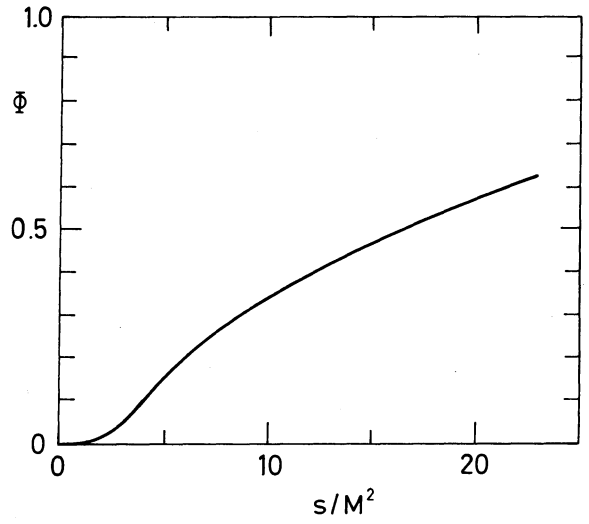

Fig. 1 Model-dependent calculation of

$$\Phi = \frac{\sigma(\nu A \to M^+ + \ldots)}{\sigma(\nu A \to \mu^- + \ldots)}$$

as a function of s/M_M^2 (taken from Ref. 16)

4. $\mu^+ N \to M^0 + \ldots$. In models examined by us:

$$4 \times 10^{-37}\ \text{cm}^2 \lesssim \sigma \lesssim 2.5 \times 10^{-35}\ \text{cm}^2$$

for a fully polarized μ^+ beam (the best case) of 100 GeV, and $M_{M^0} \leq 4$ GeV. This experiment looks possible but very difficult.

5. $e^+e^- \to M^0\bar{\nu}_\mu$. The cross-section is very model-dependent, e.g. for E/beam = 4 GeV and $M_{M^0} \leq 2$ GeV it is nominally $\sim 2 \times 10^{-37}$ cm^2, but it turns out to be actually $\sim 10^{-35}$ cm^2 in one model.

6. $pp \to M^+M^- + \ldots$. The cross-section is given by:

$$\frac{\sigma(pp \to M^+M^- + \ldots)}{\sigma(pp \to \mu^+\mu^- + \ldots)} = \left(1 - \frac{4M_M^2}{Q^2}\right)^{1/2} \left(1 + \frac{2M_M^2}{Q^2}\right).$$

The feasibility of finding M's (or heavy electrons) this way depends on how large $\sigma(pp \to \mu^+\mu^- + \ldots)$ turns out to be.

iii) Charm: As discussed above, fashionable theories suggest the existence of a new "charm" quantum number. The properties of "charmed" particles are quite analogous to those of "strange" particles except that the lightest charmed particle is probably heavier than 1 GeV. A guess would be that hadronic ($C \to$ hadrons) and leptonic ($C \to \mu\nu$ + hadrons) decays are roughly equally probable (within a factor of 10?). In strong interactions there must be "associated production":

$$p p \to C\bar{C}' + \ldots$$
$$p\bar{p} \to C\bar{C}' + \ldots .$$

They could be copiously produced in the reaction

$$e^+e^- \to C^+C^- .$$

Single C's could be produced by neutrinos:

$$\nu A \to \mu C + \text{hadrons}$$

which may make neutrino experiments the best place to search for them if they are heavy*).

3.3.3 *Conclusions*

Many experiments can look for heavy leptons and charmed particles, and it is, of course, important to try to do this independently of present theory. [Unfortunately, in most gauge models there is no upper limit on the heavy lepton mass[20] so theorists can -- and will -- retreat by increasing the mass if they are not found.]

4. NEUTRINOS AS PROBES OF HADRON STRUCTURE

If the usual description of the ν_μ - μ current is correct, then we can use neutrinos to probe the structure of the hadronic current with which it interacts (via a W or not). For example, we can measure form factors, test the Cabibbo theory, test PCAC using Adler's theorem [$\sigma^{\nu+A\to\mu+F}(\theta_{\mu\nu} = 0) \propto \sigma^{\pi^+ + A\to F}$], test current algebra sum rules, etc. We will return to the question of the fundamental Adler sum rule later; first we consider the scaling property discovered in the SLAC-MIT inelastic electron scattering experiments, which suggests that it might be possible to obtain fundamental information about the structure of hadrons by studying deep inelastic neutrino reactions. We will consider just one illustrative example of the sort of results that have been obtained.

All our discussion will be based on the supposition that scaling continues to hold at much larger Q^2, and also that it holds in weak as well as in electromagnetic interactions. It is, of course, very important to test scaling; it is broken by factors log (Q^2/M^2) in perturbation theory, and we have no soluble models to test the assertion that the same might not be true in exact solutions of field theories and/or in the real world. [The absence of the photon propagator means that relative to electron scattering a much larger fraction of the neutrino events are at large Q^2 so that quite good tests of scaling may be obtained: note that a W propagator would break scaling in a trivial way -- by a factor $1/(1 + Q^2/M_W^2)^2$ -- which may provide a sensitive test for W's[21].] If the (expected?) log Q^2 factors do not show up then we can reject arguments based on perturbation theory and perhaps even have a

---

*) The introduction of charm deprives SU(3) symmetry of a fundamental role and should therefore stimulate interest in checking the Cabibbo theory in ν reactions and to greater accuracy in decay processes.

little confidence in formal calculations of the light-cone commutator of currents or (equivalently for the predictions discussed below) the parton model, which give a simple picture of the SLAC-MIT results but are invalid in perturbation theory.

If the current-current picture is correct then we can measure the total current (W?)-nucleon cross-section in inelastic neutrino scattering. According to the parton model, the "deep inelastic" cross-section is given by adding incoherently the contributions from all the constituents:

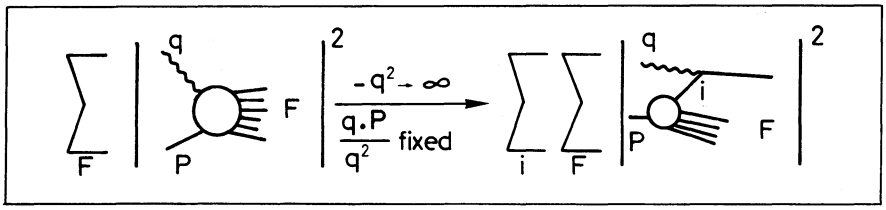

Consider models in which the constituents with which the current interacts have spin ½ (as suggested by the small value of σ_S/σ_T observed in the SLAC-MIT experiments), isospin $\leq$ ½, and a weak current of the form $\bar{\psi}\gamma_\lambda \times (1 - \gamma_5)\tau^+\psi$. At high energies, the $(1 - \gamma_5)$ structure implies that the left-handed (right-handed) current interacts only with particles (anti-particles). Thus the parity-violating quantity $\sigma_{left} - \sigma_{right}$ (which is proportional to the structure function W_3 whose scaling limit is called F_3) is proportional to the difference of the distributions of particles and antiparticles in the nucleon. Integration over these distributions leads in these models to the sum rule

$$-\frac{1}{2}\int [F_3^{\nu p}(x) + F_3^{\nu n}(x)]\,dx$$

= (No. of I = ½ spin ½ particles - No. of I = ½ spin ½ antiparticles) in the nucleon

= 3 [quark model]

= 1 ["sensible" (?) models] ,

where $x = Q^2/2q \cdot p$ and we have made the (presumably good) approximation $\theta_{Cabibbo} = 0$. This is an example of just one of several relations which can be derived in such "free field" models (and also, of course, from the light commutators abstracted from them) which can test very directly the properties of any underlying field theory (theoretically it would be very interesting to have measurements of the other two structure functions which can only be separated by measuring the outgoing lepton's polarization to order $m_L^2/E_\nu M_p$ -- here we need heavy leptons!).

The F_3 sum rule is the only sum rule for $\nu p + \nu n$ (rather than $\nu p - \nu n$) data and hence can be tested in experiments on heavy nuclei. However, if the quark value is correct then the sum rule must converge very slowly (i.e. large Q^2 data are needed at very small x - large ω) [22]. There are also reasons to fear that the much more fundamental Adler sum rule (which is true in any "reputable" model) may converge very slowly or even be wrong.

In view of its fundamental importance, we will review the arguments advanced by Bjorken, Tuan, Sakurai and Thacker, which cast doubt on the validity of the Adler sum rule[23]. Separate sum rules can be written for the vector and axial vector contributions to the structure function F_2. Consider the vector sum rule which may be written

$$\int_1^\infty [F_2^{\nu n}(\omega)_{VV} - F_2^{\nu p}(\omega)_{VV}] \frac{d\omega}{\omega} = \int_0^1 [F_2^{\nu n}(x)_{VV} - F_2^{\nu p}(x)_{VV}] \frac{dx}{x} = 1 ,$$

in the deep inelastic region. CVC gives the inequality

$$(F_2^{\nu n} + F_2^{\nu p})_{VV} \leq 2(F_2^{ep} + F_2^{en}) .$$

Hence, according to the SLAC data, the average of $F_2^{\nu p} + F_2^{\nu n}$ never exceeds ~ 0.6 -- but the difference weighted by ω^{-1} must integrate to unity. There are two extreme ways of achieving this:

i) The sum rule may converge very slowly. This happens in many simple models (fitted to the SLAC data) in which the sum rule holds[24]; e.g. in the Kuti-Weisskopf model we must integrate up to $\omega = 476.51$ to get 0.9 on the right-hand side. This is certainly rather unexpected and according to some people's intuition it is unreasonable [if we accept Rittenberg and Rubinstein's claim that $Q^2 = 0$ data can be translated to all Q^2 with a "modified scaling" variable, then the convergence of the ($Q^2 = 0$) Alder-Weisberger relation implies that we should get 0.9 by integrating only up to $\omega \approx 34$].

ii) The so-(emotively)-called "bizarre behaviour" $F_2^{\nu n} >> F_2^{\nu p}$ holds for $\omega \lesssim 5$, which probably implies the (already excluded?) result

$$\frac{\sigma^{\nu n}}{\sigma^{\nu p}} \gtrsim 2.5 .$$

The second option has also been considered unreasonable (I personally would not find an intermediate result -- quite slow convergence and "rather bizarre" behaviour -- at all repugnant; firstly, I do not know what is a reasonable rate of convergence and, secondly, the fact that F_2^{en}/F_2^{ep} seems to be small for $\omega \sim 1$ suggests models in which $F_2^{\nu n} >> F_2^{\nu p}$ for $\omega \sim 1$)[25]. In any case these results invite us to entertain further alternatives:

iii) Perhaps at large missing mass a new threshold is reached (quarks?) which gives rise to a dramatic increase in the scaling functions, which is needed to satisfy the sum rule in the scaling limit (but not to satisfy the Adler-Weisberger relation at $Q^2 = 0$!).

vi) Perhaps the sum rule is wrong because either

a) the attractive (but very badly tested) current algebra hypothesis is wrong, or perhaps the weak current has pieces with $I \geq 1$, etc. (in these cases we would wonder why the Adler-Weisberger relation works), or

b) something is technically wrong with the derivation of the Adler sum rule; this sounds boring but it would mean that the light-cone algebra, parton model, etc., are all quite irrelevant.

In any case, it is clear that accurate high-energy neutrino experiments on hydrogen and deuterium are of crucial importance for testing current algebra sum rules.

5. SUMMARY AND CONCLUSIONS

It is very likely that high-energy neutrino experiments will reveal surprises which are quite unanticipated. At the very least, they will be of crucial importance for "traditional" weak interaction theory. They may also unveil fundamental information about hadron structure. I wish to end by stressing that in addition to heavy-liquid bubble chamber and counter experiments (which are best suited for some things, such as search experiments -- W's, heavy leptons, etc. -- and measuring the "diagonal" cross-sections), neutrino (and antineutrino) experiments on hydrogen and deuterium with track-sensitive targets (or perhaps mono-energetic beams or other devices) will be of crucial importance in testing the Adler (and other) sum rules, testing selection rules, and eventually in unravelling detailed information about the behaviour of weak interactions at high energy.

Acknowledgements

I am grateful to J.S. Bell, D.G. Sutherland, and K. Winter for comments on the manuscript, and to J. Prentki for discussions.

* * *

REFERENCES AND FOOTNOTES

1) Detailed references and bibliographies may be found in, for example:
R.E. Marshak, Riazzuddin and C.P. Ryan, Theory of weak interactions (Academic Press, Inc., New York, 1969).
A. Pais, Ann. Phys. 63, 361 (1971).
C.H. Llewellyn Smith, Phys. Reports 3C, No. 5 (1972).
No attempt has been made to give systematic references assigning correct priorities, etc., in the present paper; most of the ideas cited without reference are "well known".

2) The evidence is not so compelling as it was a year ago; for a recent discussion, see D.H. Wilkinson, to be published in Proceedings of the Few-Nucleon Problem Conference, Los Angeles (1972). References may be traced from this paper, or from B. Eman, D. Tadić, F. Krmpotić and L. Szybisz, Phys. Rev. 6C, 1 (1972).

3) The relevant integral is

$$\int_0^\infty ds' \left(\frac{\sigma^{\nu e}(s')}{s' - s} - \frac{\sigma^{\bar{\nu} e}(s')}{s' + s} \right).$$

In the $j_\lambda j^\lambda$ theory

$$\lim_{s\to\infty} \left(\frac{\sigma^{\nu e}}{\sigma^{\bar{\nu} e}} \right) \neq 1 ,$$

so with $\sigma \sim s$ two subtractions are needed. With W's the behaviour of σ changes by one power ($\sigma \to$ const), but nevertheless no subtractions are needed since

$$\lim_{s\to\infty} \left(\frac{\sigma^{\nu e}}{\sigma^{\bar{\nu} e}} \right) = 1$$

in this case.

4) For a review, see
A. Salam, Proceedings of the Rochester Meeting of the APS (eds. A.C. Melissinos and P.F. Slattery) (American Institute of Physics, New York, 1971).

5) For an introductory account, see
T.D. Lee, in Elementary processes at high energy, Part B (ed. A. Zichichi) (Academic Press, Inc., New York, 1971).

6) See, for example,
Y. Tanikawa and S. Watanabe, Phys. Rev. 113, 1344 (1959).
Y. Tanikawa and S. Nakamura, Progr. Theor. Phys. Suppl. 37, and 38, 306 (1966).
E.P. Shabalin, Yadernaya Fiz. 8, 74 (1968).
W. Kummer and G. Segrè, Nuclear Phys. 64, 585 (1965).
N. Christ, Phys. Rev. 176, 2086 (1968).
E.P. Shabalin, Yadernaya Fiz. 13, 411 (1971).
Further references may be found in Ref. 1.

7) For a recent discussion, see
R.E. Marshak, City College New York preprint, to be published in Proceedings of the "Neutrino 1972" Conference, Lake Balaton, Hungary, June 1972.

8) T. Appelquist and J.D. Bjorken, Phys. Rev. D4, 3726 (1971).

9) For references to the original literature on this subject, see the talks by B.W. Lee and others in the Proceedings of the 1972 International Conference on High-Energy Physics, Batavia, to be published.

10) The approach outlined here is known to many people (it was first impressed on me by J.D. Bjorken, who has pursued it fairly systematically). More detailed work on these lines can apparently be found in a paper by Khriplovitch and Vainstein (submitted to Nuovo Cimento Letters), in the Leningrad Winter School Lectures by Vainstein and Khriplovitch (I was informed of these Russian works by Bjorken), and in the Copenhagen Summer School Lectures by J.S. Bell.

11) In theories formulated in a manifestly covariant way, "spontaneous symmetry breaking" requires the existence of zero mass "Goldstone" bosons. In this case, however, we can say that these bosons are absorbed by the W to give it the extra degree of freedom it needs when it acquires a mass.

12) Exceptions with unacceptable properties (such as $\theta_{\text{Cabibbo}} = 45°$) can be contrived.

13) B.W. Lee, J.R. Primack and S.B. Treiman, NAL preprint NAL-THY-74 (1972).

14) Wongyong Lee, Phys. Letters 40 B, 423 (1972).
Report of Gargamelle group, presented at the 1972 International Conference on High-Energy Physics, Batavia.
Theoretical estimates of neutral current cross-sections in these models have been made by:
B.W. Lee, Phys. Letters 40 B, 420 (1972).
E.A. Paschos and L. Wolfenstein, NAL preprint NAL-THY-69 (1972).

15) A. Love, D.V. Nanopoulos and G.G. Ross, Rutherford preprint RPR/T/26 (1972).

16) The discussion here is based on
J.D. Bjorken and C.H. Llewellyn Smith, SLAC-PUB 1107 (1972). This paper compiles relevant phenomenology, much of which is already known to many people (see, for example, the references to works by Tsai and Gerstein and Folomeshkin).

17) M. Perl, SLAC-PUB-1062 (1972).

18) A limit of 900 MeV has been given by Zichichi et al., from e^+e^- colliding beam experiments at Frascati. (Contribution to the 1972 High-Energy Conference, Batavia.)

19) See, for example, K.J. Kim and Y.S. Tsai, Phys. Letters 40 B, 665 (1972).

20) An exception is the Georgi-Glashow model. See H. Quinn and J.R. Primack, to be published in Phys. Rev.

21) A W would cause the famous linearly rising ν cross-section to begin to flatten out at $s \sim M_W^2$. If the Pomeron contributes, the linear rise is replaced by $\ln(s/M_W^2)$; if it does not contribute, $\sigma \to$ const. In either case

$$\frac{\sigma^{\nu p}}{\sigma^{\bar{\nu} n}} \xrightarrow{s >> M_W^2} 1 \ , \qquad \frac{\sigma^{\bar{\nu} p}}{\sigma^{\nu n}} \xrightarrow{s >> M_W^2} 1$$

is expected.

22) In the quark model

$$|F_3^{\nu p+\nu n}| \leqslant \frac{18}{5}\, \omega\, F_2^{ep+en} \ .$$

Hence (using the SLAC data)

$$\int_1^{12} |F_3^{\nu p+\nu n}|\, \frac{d\omega}{\omega^2} \lesssim 3.6 \ .$$

To reach the required value, we must clearly go to $\omega >> 12$. This does not mean that the sum rule is wrong. With data limited to $\omega \lesssim 20$, we could devise different extrapolations which give the desired value or fail by large amounts (note that if Regge behaviour holds, $F_3 \sim \sqrt{\omega}$ as $\omega \to \infty$). Models exist (e.g. the Landshoff-Polkinghorne or Kuti-Weisskopf models) which fit existing data and satisfy the quark sum rule (but the convergence is, of course, extremely slow).

23) J.D. Bjorken and S.F. Tuan, SLAC-PUB-1049 (1972), submitted to Comments on Nuclear and Particle Physics.
J.J. Sakurai, H.B. Thacker and S.F. Tuan, UCLA preprint, UCLA/72/TEP/58 (1972), submitted to Nuclear Phys.

24) H. Pagels, Phys. Rev. D3, 1217 (1971), was the first to point out that Regge fits to the SLAC data implied that the Adler sum rule would have to converge very slowly.

25) In the quark parton model if $F_2^{en}/F_2^{ep} \to 1/4$ as $\tilde{\tilde{\omega}} \to \tilde{\tilde{1}}$, this means that the virtual photon "sees" the neutron as an n quark and the proton as a p quark in this limit, which would imply $d\sigma^{\nu p}/d\sigma^{\nu n} \xrightarrow{\omega \to 1} 0$. More quantitatively, Paschos (NAL preprint NAL/THY-87, 1972) has pointed out that the Nachtman inequalities imply

$$\frac{F_2^{\nu n}}{F_2^{\nu p}} \geqslant \frac{1}{2} + \frac{1}{2}\,\frac{6 - 9y}{4y - 1}$$

for $y = F_2^{en}/F_2^{ep} < 2/3$. The SLAC-MIT results for y then give $F_2^{\nu n}/F_2^{\nu p} > 2$ (3) for $x > 0.7$ (0.8). Similar conclusions hold in many other parton models. Note also that the arguments of Bloom and Gilman (taken literally, in a way which is actually incompatible with parton-like models) also imply $d\sigma^{\nu p}/d\sigma^{\nu n} \xrightarrow{\omega \to 1} 0$.

COMMENTS ON THE NEUTRINO SESSIONS

D. Treille
Laboratoire de l'Accélérateur linéaire, Orsay, France

H. Wachsmuth
CERN, Geneva, Switzerland

1. DETECTOR QUESTIONS

1.1 BEBC

Bare BEBC is considered to be a useful neutrino detector, in which neutrino interactions with only charged secondaries ($\sim$ 20% of all interactions) could be fully analysed, missing neutrals could be treated statistically by balancing the transverse momentum distribution in the hadron jet (see G. Myatt, p. 117 of this chapter), and the muon might be identified kinematically by moving outside the hadron jet.

However, as was already recommended in the Working Party Report[1] and stressed in several discussion remarks and contributions to the parallel session of the present meeting, much more information, which is necessary in order to analyse ν events completely, can be obtained by complementing BEBC by an external muon identifier (EMI) and by a track-sensitive target (TST). More than 50% of the 3C events above 10 GeV will be self-ambiguous ($\mu^-\pi^-$ ambiguity)[2] and little physics can be done unless the muon is identified[3]. D. Haidt reported about preliminary calculations of muon identification efficiencies for a Gargamelle EMI; a study was made by Eisele[4], showing that the BEBC body, magnet coils, etc., provide adequate π-μ discrimination for $p_\mu > 1$ GeV/c, and a $\sim$ 30 m^2 detector (multiwire proportional chambers) could accept muons with 60% to 85% efficiencies from 10 to 80 GeV. In this context another study[5] may be mentioned, predicting the performance of the EMI proposed[6] for the 15' NAL bubble chamber. J. von Krogh summarized the arguments which had led to a strong recommendation to develop a TST for BEBC neutrino physics (see p. 121 of this chapter). It was also asked (J. Meyer, H. Wachsmuth) that -- in view of the need for a TST for hadron physics -- a study should be made of the possibility of a TST which would be compatible for both neutrino and hadron physics.

1.2 Gargamelle

Several questions were asked concerning the usefulness of moving Gargamelle behind BEBC (costs estimated for transport and annual operation are 3 and 3.5 MSF, respectively, personnel not included). The reasons for the use of Gargamelle behind BEBC were summarized by P. Petiau as follows:

i) the existence of Gargamelle and its analysis equipment;

ii) Gargamelle has been proven to be a good neutrino detector at present energies, and is expected to be comparable to BEBC (filled with neon) at higher energies;

iii) the multitude of (complementary) ν experiments to be done (ν, $\bar{\nu}$ in H_2, D_2, heavy liquid).

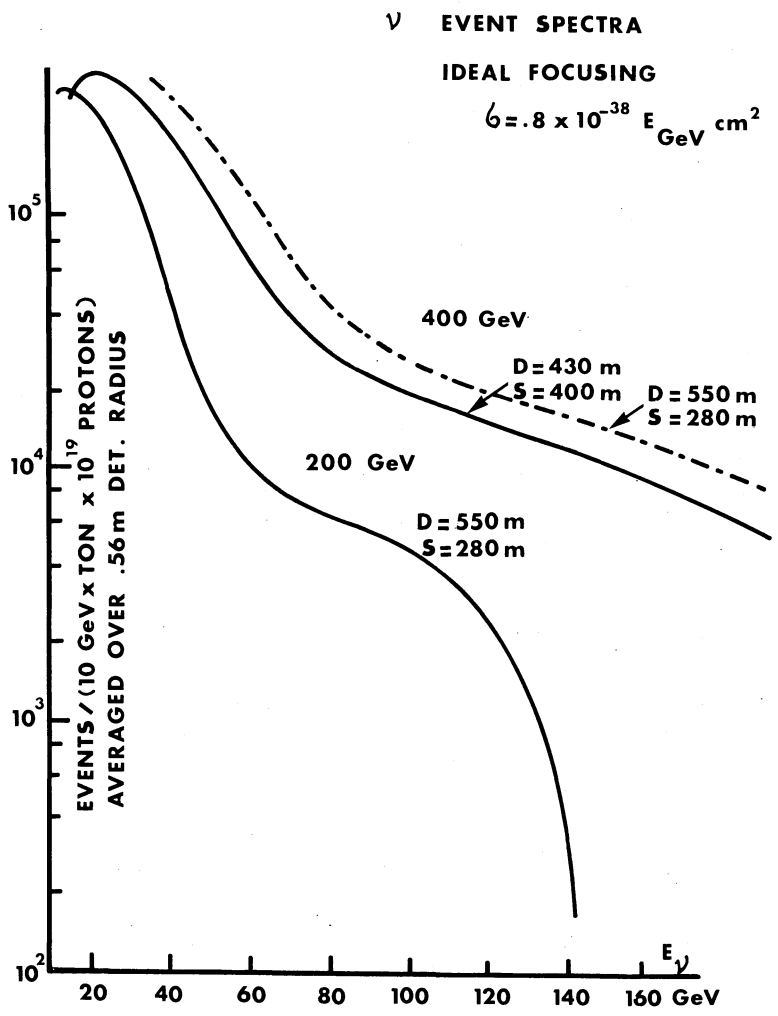

Fig. 1 Neutrino event spectra from a π, K pencil beam (ideal focusing) in a 1 m^2 detector for 200 and 400 GeV protons in the West Area neutrino beam line (830 m distance between target and detector).

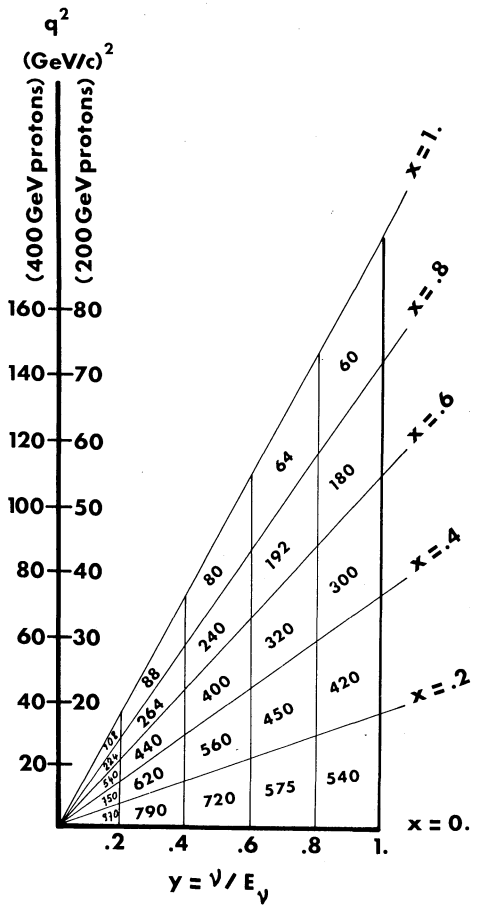

Fig. 2 Distribution of 10,000 neutrino events in $q^2 = 2M\nu x$ and $\nu = yE_\nu = E_\nu - E_\mu$ according to $\partial^2\sigma/dxdy = (G^2ME_\nu/\pi)\ (1 - x)\ [1 - y + (y^2/2)]$ [diffraction model[8]; the spin-½ parton model predicts constant y distribution]. In a realistically focused "tunnel" beam 10,000 events could be obtained in BEBC (H_2) for
a) $45 < E_\nu < 55$ GeV with 10^{19} 200 GeV protons,
b) $95 < E_\nu < 105$ GeV with 10^{19} 400 GeV protons.

1.3 Electronic neutrino detectors

In connection with electronic neutrino detectors, the detailed design of which will depend on early NAL results, the possibility was discussed of planning a neutrino counter set-up in the West Area in the bubble chamber beam line (underground neutrino beam, see Vol. I, chapter 5, p. 148). The implications on the beam are discussed below.

2. 400 GeV PROTONS FOR THE WEST AREA NEUTRINO BEAM

Despite the difficulties of complete event analysis at very high energies, bubble chambers are powerful neutrino detectors also in 400 GeV neutrino beams. At present only bubble chambers have the spatial resolution required for a large class of measurements, combined with a large target mass (20 tons of neon in the visible BEBC volume) which is necessary for low cross-section interactions, and good energy resolution. The discovery of any new feature of weak interactions (W production, weak interaction structure effects other than W exchange, etc.) can be expected only at highest energies, and then powerful analysis tools such as bubble chambers will be needed in order to study details of the hadronic final state. At 400 GeV and with suitable ancillary equipment (EMI, TST), q^2-ν plots could be examined covering twice the range of those obtainable at 200 GeV, as is shown in Figs. 1 and 2 which compare neutrino event spectra for 200 and 400 GeV ideal neutrino beams in the West Area [see also Tables 1 and 2*)].

3. BEAM QUESTIONS

3.1 Wide-band beam

Until more precise plans for neutrino counter physics exist (which may merge from NAL experience), people interested in this field think that one must keep open the possibility of using a wide-band beam.

The spill required is still an open question. A spill length longer than 60 μsec (requiring multiturn extraction) cannot be obtained in the West Area for the BC neutrino line without stopping counter physics in the West Hall. This also implies that the fast switch which is planned would have to be changed to a slow one (Brianti). If this 60 μsec is too short a spill to perform good electronic neutrino physics behind BEBC, an early start on a neutrino programme in the North Area would be desirable (Steinberger, Gregory, Winter et al.).

Several people (Steinberger et al.) consider that a spill of $\sim$ 1 msec can be sufficient, and a recent study[7] shows that horns can be made for such pulse lengths without increasing the conductor wall thickness appreciably.

A wide-band neutrino beam in the North Area could share a common tunnel with the muon beam; but these beams would be derived from different targets and would run parallel to one another.

The yield of neutrinos can be inferred from Table 1.

---

*) These are amended versions of Tables 5.1 and 5.2 of Vol. I where some of the 400 GeV figures are wrong.

Table 1

Amendment to page 162 of Vol. I

TABLE 5.1: νEvent rates (per ton and 10^{19} protons) in ideal beams for various decay (D) and shielding (S) lengths and proton momenta (σ_{tot} = 0.8 x E(GeV) 10^{-38} cm^2).

p_{proton} (GeV/c)		(1)	(2)	(3)	(4)	(5)	(6)	(7)	(8)	(9)	(10)
		24	150*) $p_{\pi,K<40}$	100	150	200			400 ($\frac{1}{2}$ repetition rate !)		
E (GeV)	D(m)	75	100	200	170	550	400	680	430	400	1250
	S(m)	25	43	80	113	280	1000	150	400	1000	250
⩽ 5		90.000	260.000	95.000	58.000	20.000	3.600	33.000			
⩽ 10		96.000	520.000	320.000	300.000	120.000	23.000	250.000	80.000	14.000	80.000
⩽ 20		100.000	670.000	430.000	600.000	470.000	70.000	840.000	350.000	75.000	500.000
⩽ 30		100.000	730.000	450.000	670.000	690.000	110.000	1.000.000	725.000	183.000	1.233.000
> 50		-	-	3.000	28.000	45.000	8.000	76.000	260.000	120.000	450.000
> 80		-	-	-	3.000	19.000	4.000	28.000	150.000	44.000	210.000
> 100		-	-	-	100	8.000	1.600	10.000	100.000	30.000	150.000
> 200		-	-	-	-	-	-	-	9.000	4.000	15.000
Total		100.000	750.000	460.000	770.000	860.000	160.000	1.400.000	1.500.000	470.000	2.500.000
		West Hall Surface				Under-ground	NAL	Best	Under-ground	NAL	Best

*) 100 % acceptance assumed (see section 5.2.1.2.). For other assumptions see text.

Table 2

Amendment to page 170 of Vol. I

TABLE 5.2

BEAM	W. HALL SURFACE Ep = 150 GeV D = 170 m S = 113 m			W. HALL TUNNEL Ep = 200 GeV D = 550 m S = 280 m			W. HALL TUNNEL Ep = 400 GeV D = 430 m S = 400 m		
CHAMBER / REACTION	BEBC(Ne)	GGM(CF_3Br)	BEBC(H_2)	BEBC(Ne)	GGM(CF_3Br)	BEBC(H_2)	BEBC(Ne)	GGM(CF_3Br)	BEBC(H_2)
Total events	7.600.000	3.100.000	380.000	9.000.000	3.700.000	450.000	16.500.000	6.700.000	840.000
$\nu_\mu + n \rightarrow \mu^- + p$	310.000	140.000	-	220.000	100.000	-	270.000	130.000	-
$\nu_\mu + p \rightarrow \mu^- + \pi^+ + p$	570.000	210.000	60.000	410.000	150.000	40.000	480.000	180.000	50.000
W bosons, M=7 GeV	2.600	1.100	200	7.200	5.800	640	53.000	21.000	4.800
$\nu_\mu + e^- \rightarrow \mu^- + \nu_e$	770	290	80	1.700	640	170	5.100	1.900	500
$\nu_\mu + Z \rightarrow \mu^- + e^+ + \nu_e + Z$	100	70	-	140	90	-	270	180	-
$\nu_\mu + Z \rightarrow \mu^- + \mu^+ + \nu_\mu + Z$	42	39	-	64	40	-	135	80	-

GGM - 6 m^3 , CF_3Br = 9 tons

BEBC(Ne) - 18 m^3 , Ne = 22 tons

BEBC(H_2) - 18 m^3 , H_2 = 1.1 tons

Gargamelle is 80 m downtream of BEBC

These event rates correspond to 10^{19} protons on target with the neutrino spectra used in section 5.3.2, assuming real focusing $\sim \frac{1}{2}$ ideal.

3.2 Muon-neutrino facility

The neutrino yield from a quadrupole channel was discussed (Vannucci, Brasse), and the following remarks were made:

- The quadrupole channel (without primary analysis of the hadrons) gives a wide-band neutrino beam which is severely truncated at low neutrino momenta and therefore is not the best possible wide-band beam that neutrino counter experiments may eventually require (Rubbia et al.).
- If the primary analysis of hadrons is performed (giving polarized muons), one gets a narrow band beam of neutrinos. But the wavy trajectory of the parents in the channel gives a broadening of the neutrino spectrum (Rubbia). In fact this seems to be a small effect (curves shown by Brasse).
- A channel of large-aperture quadrupoles arranged in triplets is extremely power-consuming (Brianti); it would be more reasonable to consider standard quadrupoles ($\varnothing \lesssim 20$ cm) and a FODO configuration. The dependence of the neutrino output on the quadrupole diameter is required (Brianti) and is under study.
- Several people seem to prefer to disconnect muon and neutrino beams to facilitate both experimental programmes.

3.3 ν_e beams

The authors (Turlay et al.) feel that more precise computations are needed: yield of ν_μ contamination; backgrounds of μ and the way to decrease it; background due to hadrons, if any; refinement of the production formulae.

The problem of the possible location of such a beam was raised (Brianti). The yield of ν_e from 200 GeV protons (instead of 400 GeV) was asked for, in view of a hypothetic installation to be made in the West Hall (Brianti).

3.4 Tagging of high-energy neutrinos*)

(summarized by rapporteurs)

Spillantini made some computations on the tagging of high-energy ν ($E_\nu \geq 0.3\, E_{proton}$) from K decay (ECFA file 72/168).

A toroidal muon detector located at the end of the decay tunnel has to measure p_μ ($\Delta p_\mu/p_\mu \sim 8\%$) and θ_μ ($\Delta\theta_\mu \sim 0.2$ mrad) in order to give E_ν with reasonable accuracy (±2% to ±15%). It is made of two groups of scintillation counter hodoscopes (θ and ϕ elements in each group, 10 nsec of resolution time) with a toroidal magnetic field between them (magnetized iron). The useful region of the detecting system is located between $R_1 = 0.5$ m (to avoid the huge flux of μ close to the axis) and $R_2 = 1.5$ m.

The author first shows that a normal wide-band beam would bring too many μ to the detector, and he considers the case of a high-band beam in which all hadrons below 150 GeV (from 400 GeV protons) are removed. Such a beam would give $\sim 2 \times 10^{10}$ ν in a ν detector of 1 m^2: the loss below $E_\nu = 50$ GeV, when compared to that of a wide-band beam, is ~ 10. He assumes that 10^{13} protons interact during 1 sec flat top.

---

*) Paper contributed by P. Spillantini, Laboratori Nazionali del CNEN, Frascati, Italy.

In any case the μ detector still receives 1.6×10^{10} μ and therefore has to be split into a large number of elements. Among these μ, only 2.4×10^{7} are "candidates": these candidates, associated to neutrinos of high momentum (> 0.3 p_{proton}), must be selected by a fast on-line analysis. Getting the precision quoted on p_μ and especially θ_μ seems extremely difficult.

At each ν event, one has a probability of 0.24 to find one candidate within 10 nsec. But this candidate has only a very small chance of being associated to the interacting ν: the tagging efficiency (fraction of ν events with a "candidate" μ on the μ detector) is indeed only $\sim 3 \times 10^{-2}$. So a very powerful off-line analysis has to be performed afterwards (accurate time correlation, coplanarity check, etc.) and one must study more carefully the rejection factor one can expect. The rate of events from tagged ν is $\sim 1.5 \times 10^{-2}$ event/ton per 10^{13} protons.

3.5 Shielding

It seems that a magnetic shield (Leutz et al.) can reduce the weight (and cost) of iron needed to stop muons by a factor of 3-4. But the decay channel shielding and hadron stopper stay the same.

4. CERN-NAL COLLABORATION

At present there are links between CERN and NAL on the basis of individual participation. A collaboration on a larger scale and even a physics programme co-ordination (Giacomelli) would be desirable.

* * *

REFERENCES

1) Status Report of the Working Parties, CERN/ECFA/72/4 (1972), Vol. I.

2) D.H. Perkins, CERN/ECFA/WG/72-72 (1972).

3) NAL proposals 9, 28, 44, 53, 92; NAL Summer Studies SS69, p. 207 and SS70, pp. 255, 279, 295.

4) F. Eisele, CERN/ECFA/WG/72-123 (1972).

5) A.D. Johnson, M.W. Peters and V.J. Stenger, University of Hawaii, preprint UH-511-97-71, April 1971.

6) NAL proposal 155.

7) B. Langeseth, J.M. Maugain and F. Völker, CERN Internal Report, TC-L/TF 72-2 (1972).

8) See, for example, H. Harari, Phys. Rev. Letters 22, 1078 (1969).

THE USE OF TRANSVERSE MOMENTUM BALANCE AS A MEANS OF ESTIMATING THE ENERGY OF INTERACTING NEUTRINOS *)

G. Myatt
Nuclear Physics Laboratory, University of Oxford, England

A study of positive pions produced in neutrino interactions in freon[1] and propane[2] has shown that whereas the average transverse momentum relative to the neutrino direction increases with pion momentum, the average transverse momentum relative to the direction of the laboratory three-momentum transfer $\vec{q}$ (Fig. 1) tends to a limiting value of $\sim$ 440 MeV/c independent of q^2. These features are shown in Figs. 2 and 3. A similar behaviour has recently been observed in inelastic electron scattering[3,4].

It is probable that π^0's have similar properties, although present neutrino experiments have been unable to verify this because of either poor measurement of π^0 momenta in freon or low detection efficiency in propane. If this is the case, then the π^0's which are not observed in detector such as BEBC with H_2 or D_2 filling will carry off on the average only a small momentum transverse to $\vec{q}$. Therefore it may be that the vector addition of the observed charged pion momenta gives a fairly good approximation to the direction of $\vec{q}$. From Fig. 1 we can see that if θ_q is known (or estimated), then we can obtain an estimate E_c of the neutrino energy E_ν from the following relation obtained by balancing the transverse momenta relative to $\hat{\nu}$, of the muon and the hadrons:

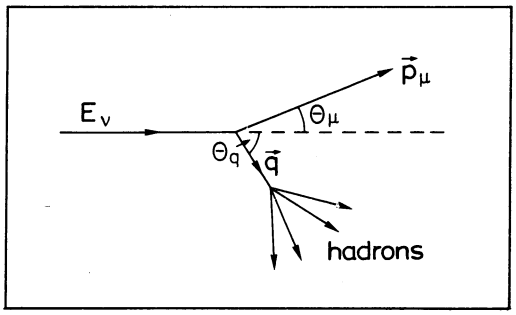

Fig. 1

$$E_c = p_\mu \frac{\sin \theta_\mu}{\tan \theta_q} + p_\mu \cos \theta_\mu \, . \qquad (1)$$

In order to test if these ideas are useful, we have made Monte Carlo calculations using a model which incorporates the features of neutrino interactions as they have been observed in the few GeV region[5] and assumed that scaling holds at higher energies. In particular, we have taken

$$\bar{n}_\pi = 1.9 \log \nu + 1.3 \; ; \quad n_{\pi^0}/n_\pi = 1/3$$

$$\frac{dN}{dp_T} \propto e^{-bp_T^2} \; ; \quad \frac{dN}{dp_L} \propto e^{-cp_L/p_{L,max}} \, ,$$

where the constants b and c have been taken to be the same as those determined from inelastic electron scattering[3]:

*) Contributed paper

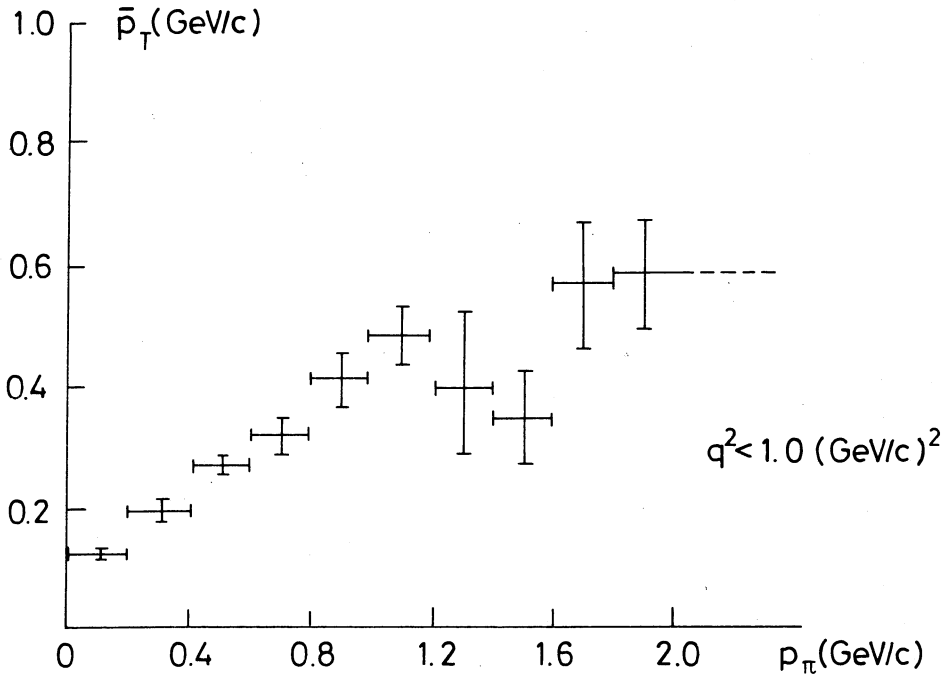

Fig. 2 Distribution of average transverse pion momenta with respect to the direction of the laboratory three-momentum transfer $\vec{q}$ to all hadrons as a function of pion momentum for $q^2 < 1.0$ (GeV/c)^2.

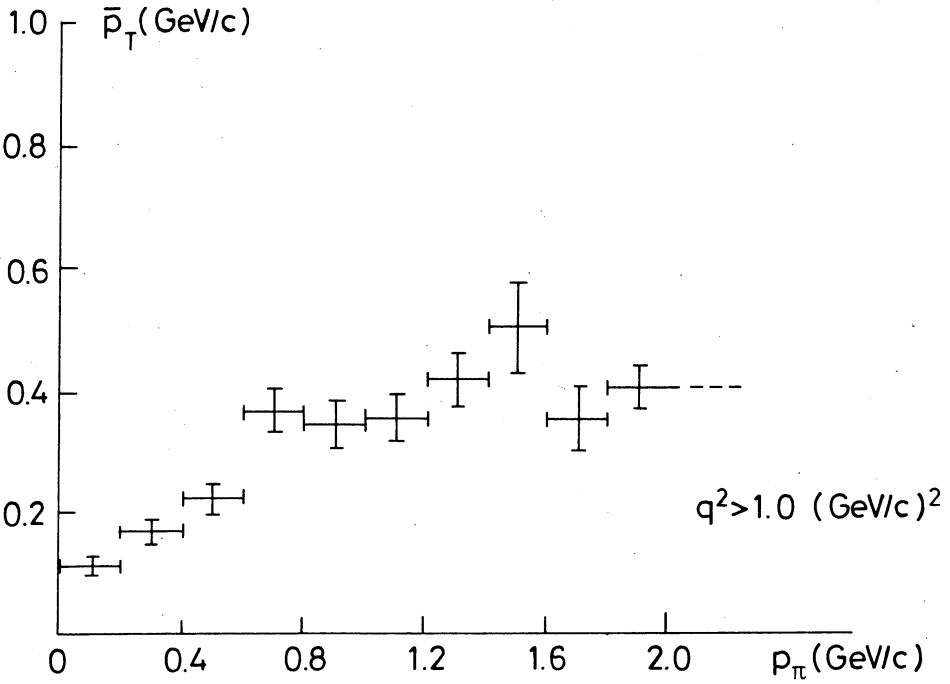

Fig. 3 Distribution of average transverse pion momenta with respect to the direction of the laboratory three-momentum transfer $\vec{q}$ to all hadrons as a function of pion momentum for $q^2 > 1.0$ (GeV/c)^2.

$$b = 4.7$$
$$c = 3.0 \quad \text{(average of } \pi^+ \text{ and } \pi^-\text{)} .$$

The structure factors[6] F_1, F_2, F_3 have been assumed to obey the relation

$$2xF_1 = F_2 = xF_3 .$$

The pions were generated according to a Poisson distribution, the π^0's removed, and the resultant momenta of the charged particles used to estimate θ_q. It was assumed that the nucleon in the final state had an equal probability of being a proton or a neutron. The nucleons were taken to have the same distributions in p_T and p_L as the pions, and when the final nucleon was a neutron it was assumed to be unobserved and its momentum subtracted from that of the hadron shower. It should be noted that it is not necessary to identify the final-state charged hadrons in order to perform the present analysis, since only their observed momenta are used.

It was found that in a small proportion of cases (6% at 20 GeV, 3% at 200 GeV), Eq. (1) gave unphysical answers because the estimated θ_q lay outside the range $0 < \theta_q < \pi/2$. For the remaining cases of the calculated neutrino energy E_c to the input neutrino energy E_ν is shown in Fig. 4. It can be seen that the majority of events give E_c quite close to E_ν with full widths at half maximum of

10% at 40 GeV
8% at 100 GeV
7% at 200 GeV .

Not shown are those events with no neutral particle in the final state, in which case E_c is correctly estimated. These amount to 7% at 40 GeV and 2.5% at 200 GeV. It may be noticed that the peak in E_c/E_ν is slightly displaced from unity. This shift is $\sim$ 1% at 40 GeV and less for higher energies, and is due to a difference in the sensitivity of E_c to changes of θ_q towards or away from the neutrino direction.

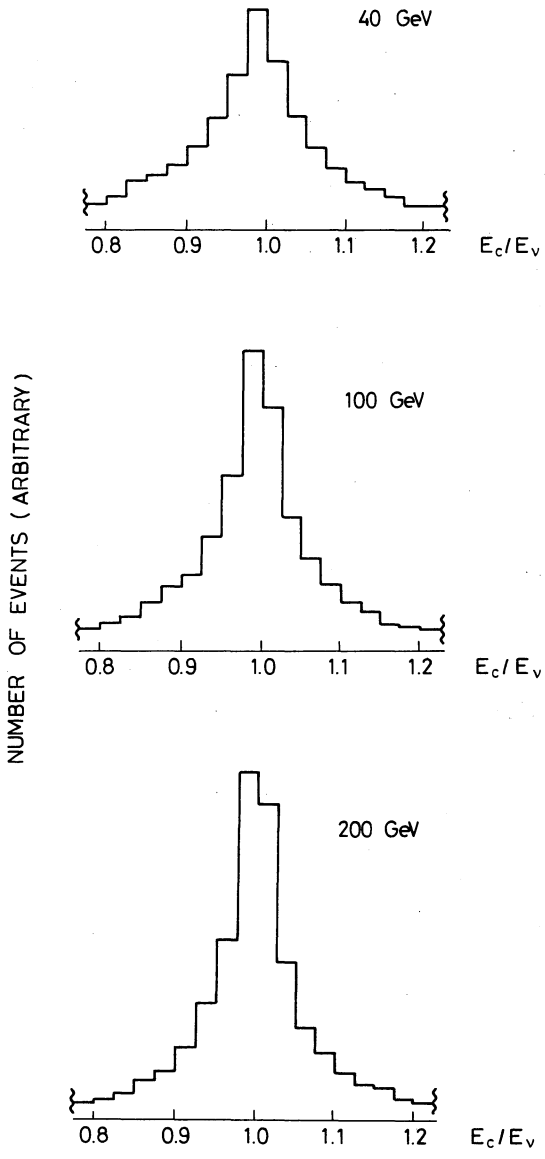

Fig. 4
Distribution of the ratios of calculated to input neutrino energy for three neutrino energies (40, 100, and 200 GeV).

The errors on E_c will in general be too large to enable accurate absolute cross-sections to be determined because of the rapid variation of neutrino flux with energy in wide-band beams. However, they may be adequate enough to determine the regions of the kinematic variables q^2 and ν $(= E_\nu - E_\mu)$, and hence $\omega = 2M/q^2$, $y = \nu/E_\nu$ in which one may use the HBC to study, for example,

- charged pion multiplicities
- π^+/π^- ratio
- $\nu n/\nu p$ cross-section ratios
- vector meson production,

etc.

In order to make estimates of the neutrino energy by means of the above method, it is essential to identify the muon among the charged secondaries. At high energies therefore, BEBC would need to be supplemented by an external muon identifier.

* * *

REFERENCES

1) M. Paty, CERN 65-12 (1965).

2) J.L. Masnou, L.A.L. 1245, Orsay (1971).

3) J.T. Dakin, G.J. Feldman, W.L. Lakin, F. Martin, M.L. Perl, E.W. Petraske and W.T. Toner, Phys. Rev. Letters 29, 746 (1972).

4) E. Lazarus, D. Andrews, K. Berkelman, G. Brown, D.G. Cassel, W.R. Francis, D.L. Hartill, J. Hartmann, R.M. Littauer, R.L. Loveless, R.C. Rohlfs, D.H. White and A.J. Sadoff, Phys. Rev. Letters 29, 743 (1972).

5) G. Myatt and D.H. Perkins, Phys. Letters 34 B, 542 (1971).

6) J.D. Bjorken, Phys. Rev. 179, 1547 (1969).

TRACK-SENSITIVE TARGETS FOR NEUTRINOS IN BEBC*)

J. von Krogh,
III. Physikalisches Institut, Technische Hochschule, Aachen, Germany

The aim of future neutrino experiments will be a detailed study of interactions off protons and neutrons separately (see C.H. Llewellyn-Smith, p. of this chapter). Hence it will be necessary to use both hydrogen and deuterium as target liquids so as to minimize nuclear effects.

In order to calculate neutrino cross-sections as a function of energy E_ν, it is imperative to know E_ν as accurately as possible, since a small error in E_ν causes relatively large errors in the cross-section owing to the rapidly falling neutrino spectrum. Unless one works with a narrow-band neutrino beam of known energy, the only way to obtain E_ν is by calculating or fitting it from the information one has about the final state. Hence it is even more important than in hadron physics to detect and measure all neutrals in the final state.

The most attractive way to do this is to use a track-sensitive target (TST). Since we deal with very small cross-sections, however, we cannot use the flat TST, developed for hadron physics[1]. For neutrinos, large massive targets are required.

On the one hand, such a target has to be large enough so that the event rate in hydrogen is as high as possible; on the other hand, a sufficient amount of heavy liquid (Ne/D_2 mixture) has to surround it in order to ensure good detection efficiency for neutrals.

Fortunately, neutrinos are sufficiently concentrated in the centre of the beam to make possible a reasonable compromise between these seemingly contradictory requirements[2].

In Fig. 1 we give the number of neutrino interactions plotted versus E_ν in bare BEBC filled with H_2 and in the TST.

We see that even though the ratio of volumes $V_{TST} : V_{BEBC} \approx 1 : 9$, in certain energy ranges the ratio of interactions in the TST to those in bare BEBC is better than 1 : 4. The spectrum is based on the tunnel solution (shielding = 280 m, decay length = 550 m) with a conventional horn-reflector system scaled to these energies[3]. This can be improved upon by using elliptical lenses[4].

In Table 1 we make a detailed comparison of neutrino event rates for this spectrum, considering an energy region $10 < E_\nu < 40$ GeV, where neutrinos are focused in an optimum way.

The detection efficiency was calculated by the Monte Carlo method for single π^0 production by neutrinos in a D_2 target with a mixture of 30 cm radiation length outside. The efficiency for seeing both γ's from the π^0 is 74%. For comparison, the efficiency for seeing both γ's from the π^0 in bare BEBC filled with D_2 is about 1.5%. In the table we present a comparison of event rates in bare BEBC and in the TST.

---

*) Contributed paper

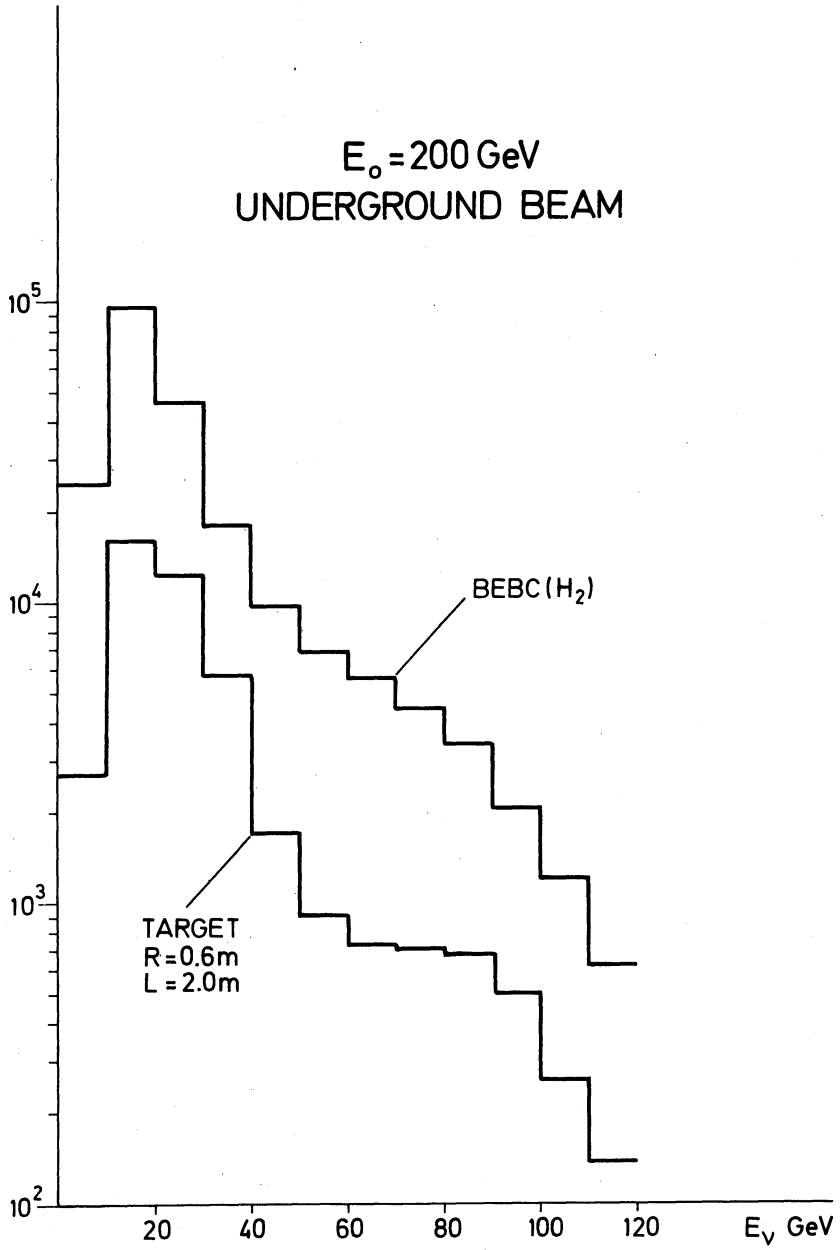
$E_o = 200$ GeV
UNDERGROUND BEAM
10^5
10^4
10^3
10^2
BEBC (H_2)
TARGET
R = 0.6m
L = 2.0m
20
40
60
80
100
120
E_ν GeV

Fig. 1

Table 1

Comparison*) of neutrino event yields in a 2 m^3 TST and in bare BEBC/H_2

	TST (2 m^3)	BEBC/H_2 (18 m^3)
Detection efficiency for single π^0	74%	1.5%
Total events $10 < E_\nu < 40$ GeV	34,000	159,000
Useful (E_ν known)	20,000 All final states	32,000 Charged final states only
Less useful (E_ν not known)	14,000 Unknown fraction of neutrals escaped	127,000 Unknown fraction of neutrals escaped
Plus	$\sim$ 3,000,000 Events in neon	-

*) for underground wide-band beam (200 GeV) focusing by horn and reflector scaled to 200 GeV (for 10^{19} protons)

We see that if we compare the useful number of events (with E_ν known) the TST compares very favourably with bare BEBC.

Acknowledgements

This report is based on the work of F.J. Hasert, W. Krenz, K. Schultze and H. Wachsmuth.

* * *

REFERENCES

1) D.J. Miller, CERN/ECFA/72/4 (1972), Vol. I, p. 13.

2) K. Schultze, Massive TST for BEBC neutrino experiments, CERN/ECFA/WG/72-122 (1972).

3) H. Wachsmuth, private communication.

4) H. Faissner, F.J. Hasert, J. von Krogh and W. Thomé, Aachen report PITHA-59 (1972).

CHAPTER IV

ELECTRON, MUON, AND PHOTON PHYSICS

POSSIBILITIES IN ELECTRON AND PHOTON BEAMS AROUND THE WORLD IN 1977

B.H. Wiik
Deutsches Elektronen-Synchrotron (DESY), Hamburg, Germany

1. INTRODUCTION

To do justice to the title of this talk one clearly needs to have a fair amount of clairvoyance. Although sadly lacking in this commodity, I will still venture the prediction that in 1977 the experimental facilities available for electron and photon physics will be very good indeed. This optimism is based in part on the proposed improvements both in energy and intensity of existing facilities, and in part on the new high-energy photon and electron beams to become available at NAL and the CERN SPS. Moreover, not only the increase in energy and intensity, but also the use of more sophisticated techniques employing both polarized beams and polarized targets will greatly add to the range of possible experiments.

A new and exciting accelerator for electron and photon physics at extremely high energies is the electron-proton colliding ring now under consideration both at SLAC (Berkeley) and BNL. These high-energy accelerators will most likely not be available in 1977, but such a device, providing a maximum centre-of-mass energy of up to 9 GeV, will be built at DESY before this date.

In this talk I will first briefly remind you of the properties of the existing electron accelerators above 4 GeV, and then discuss in more detail the extensions planned at the various facilities. In the second half of the talk some typical experiments in electron and photon physics will be discussed. Since the subject to be covered is rather large for a one-hour talk, I also apologize for the cavalier treatment of many topics.

2. PRESENT STATUS

Some of the relevant properties for the electron accelerators are listed in Table 1.

Table 1

	Cornell	Erevan	DESY	NINA	SLAC
Energy (GeV)	12	6	7.5	5	22
Current ($\times 10^{12}$) a)	0.3	-	3	3	200
Duty cycle (%)	5	-	5	11	0.06
Polarized photons up to (GeV)	$\sim$ 8	-	$\sim$ 4.5	$\sim$ 3	22
Polarized electron beam			b)		1973

a) extracted current.

b) under development.

A few miscellaneous remarks to this table: the maximum energy available at SLAC has been slowly increasing over the past few years and has now reached 22 GeV. This increase is due to the replacement of the old 20 MW klystrons by new 30 MW klystrons. A full complement of these tubes will yield an end-point energy of 25 GeV. The maximum energy of the Cornell Synchrotron[1] has also recently been increased from 9 GeV to 12 GeV. This was done by installing an additional RF cavity providing an energy gain of about 9 MeV/turn.

The duty cycle obtained at the electron synchrotrons is typically around 5-10% as compared to a design value of around 25% at NAL and the CERN SPS. The duty cycle at SLAC, however, is only 6×10^{-4}. This low duty cycle sets severe limits on the type of coincidence experiments which can be done profitably at SLAC.

The average current extracted from an electron synchrotron is of the order of 10^{12} e/sec, or more than two orders of magnitude less than the current available at SLAC. This very high current has made it possible to investigate reactions with differential cross-sections down to 10^{-39} cm^2/GeV^2 at SLAC.

Since most of you are mainly familiar with hadron beams, let me briefly discuss the various types of photon beams available. A photon beam is generally produced by passing an electron beam through an amorphous radiator, typically about 3% of a radiation length thick. After the radiator, the electrons are swept out of the beam by a bending magnet and the photons continue on to the target.

Such a bremsstrahlung beam contains photons of all energies, from the incident electron energy on downwards. The number of photons with a certain energy k is proportional to 1/k. The problems introduced by such a continuous spectrum can be avoided by measuring the energy of the outgoing electron. Since the energy of the incident electron is known, this determines the energy of the photon. The intensity of such a tagged photon beam is, however, rather low -- typically of the order of 5×10^5 photons/sec.

A polarized photon[2] beam can be made by replacing the amorphous radiator by a crystal, say a thin diamond. The photon spectrum from a suitably oriented diamond in a well-collimated electron beam is plotted in Fig. 1.

The spectrum is a superposition of an unpolarized non-coherent part ($\sim$ 1/k) and spikes resulting from the coherent scattering from individual reciprocal lattice points. The non-coherent part of the spectrum can be substantially reduced by using an extremely thin diamond and demanding a tight collimation of both the incident electron beam and the emerging photon beam. Using a diamond roughly $\sim$ 0.01 mm thick, SLAC[3,4] hopes to produce a beam with 45%

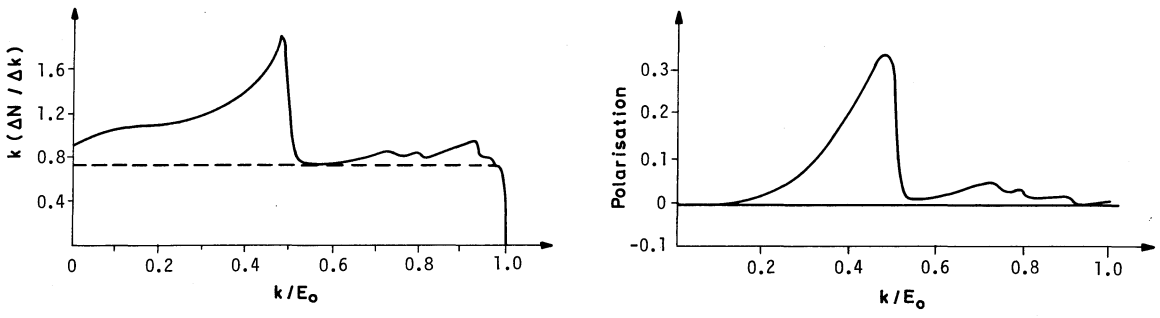

Fig. 1

polarization at a photon energy which is 3/4 of the incident electron energy. The intensity would be 2×10^9 photons/sec, and 50% of the photons would be within $\Delta k/k = \pm 2\%$. The beam is scheduled to be installed by the end of the year.

For completeness let me mention that also the end point of a bremsstrahlung spectrum can be polarized[5], something which is crucial for single-arm experiments. In this case an unpolarized photon beam is passed through a long slab of a suitably oriented carbon crystal. Since the absorption cross-section depends upon the orientation of the spin of the photon relative to the lattice, a polarized photon beam will emerge after the absorber. Such a beam[6] has recently been employed in a first experiment at SLAC. They achieved an average polarization of 24% at 16 GeV using a carbon crystal 61 cm long. This method becomes more advantageous at higher energies; for example, at 50 GeV the photons would be more than 50% polarized.

A low-intensity, highly polarized photon beam resulting from the Compton scattering of laser light on the electron beam[7] is also in use at SLAC. The highest energy reached so far is 9.3 GeV with a flux as high as 2×10^3 photons/sec.

There is great interest in experiments using polarized lepton beams. Such beams are under development both at SLAC and at DESY. The SLAC beam[8] will be produced by photoionization of polarized ^{6}Li atoms. They hope to be able to reach a polarization of 90% with an average current of about 2×10^{11} e^-/sec. It is planned to install the source by the end of the year. The source under development at DESY[9] is based on spin exchange between polarized hydrogen atoms and low-energy electrons.

3. PROJECTED STATUS IN 1977

3.1 Cornell

The energy of the present synchrotron could be raised still further by adding more RF to the accelerator to compensate for the losses due to the synchrotron radiation of the electrons. However, since the potential gain in energy is rather small, Cornell has asked the National Science Foundation to finance a design study of a new synchrotron[1] with an end-point energy around 35 to 40 GeV and an intensity of around 10^{12} e^-/sec. The accelerator would be situated in a new tunnel and the present synchrotron would be used as an injector. This has the advantage of reducing the magnet aperture and hence the cost. The circumference of the machine would be 1500 m with a bending radius of roughly 130 m. At the highest energy the loss due to synchrotron radiation is about 2 GeV/turn. Therefore a large, high duty cycle, RF system is needed, and the most economical solution seems to be to use superconducting RF cavities. Cornell has therefore also requested the NSF to support a program to develop such cavities suitable for synchrotron use. The plan is to use S-band cavities (2856 MHz). The required gradient of 3 MeV/m should be well within the state of the art[10].

Cornell has initiated the superconducting program and hopes to be able to submit a final proposal in 1973-1974. It is estimated that the construction time for the first stage of the project (25 GeV) will take between 2 and 3 years.

Another option, also under consideration, is to build a new ring in the present tunnel, employing the present synchrotron as an injector. In this case the energy will be limited to 27 GeV.

3.2 DESY

With the ee colliding ring scheduled to come into operation by the end of 1973, there are no concrete plans for increasing the energy of the present DESY synchrotron. However, a program to increase both the intensity and the duty cycle of the synchrotron is well under way. With the installment of the new injector, circulating currents of 30-50 mA are now routinely achieved, and with a long flat top -- soon to be available -- a duty cycle as high as 15% can be reached.

Since the colliding ring consists of two independent rings, it is possible to inject electrons (or positrons) into one ring and protons into the other and observe electron-proton collisions[11]. The initial centre-of-mass energy will be 7 GeV and it can be extended, by adding more RF power to the electron ring, to 9 GeV. This is equivalent to an incident electron energy in the laboratory of 46 GeV. The luminosities will be of the order of 10^{30}-10^{31} cm^{-2} sec^{-1}. This corresponds to 10^{6}-10^{7} e/sec incident on a hydrogen target 20 cm long. The construction will start in 1973 and should be finished by 1976.

3.3 NINA

The plans[12] are to continue to run NINA at 5 GeV and to increase the intensity gradually.

3.4 NAL

It seems likely that for the foreseeable future, photon and electron physics above 60 GeV can only be done using the secondary beams at NAL and CERN SPS. To remind you of the complexities involved in constructing such a beam and the intensities which will be available, let me briefly describe the beam proposed by Halliwell et al.[13] for NAL. The layout of the beam, which is more or less typical, is shown in Fig. 2.

A high-energy proton beam is focused on to a low-Z target, typically beryllium, producing, among other particles, π^0's. The photons from the π^0 decay travel for about 22 m before striking a high-Z converter. Between the production target and the conversion target, the primary beam and the charged secondaries are swept out of the neutral beam by several bending magnets. After the high-Z converter, a negatively charged beam is selected, momentum-

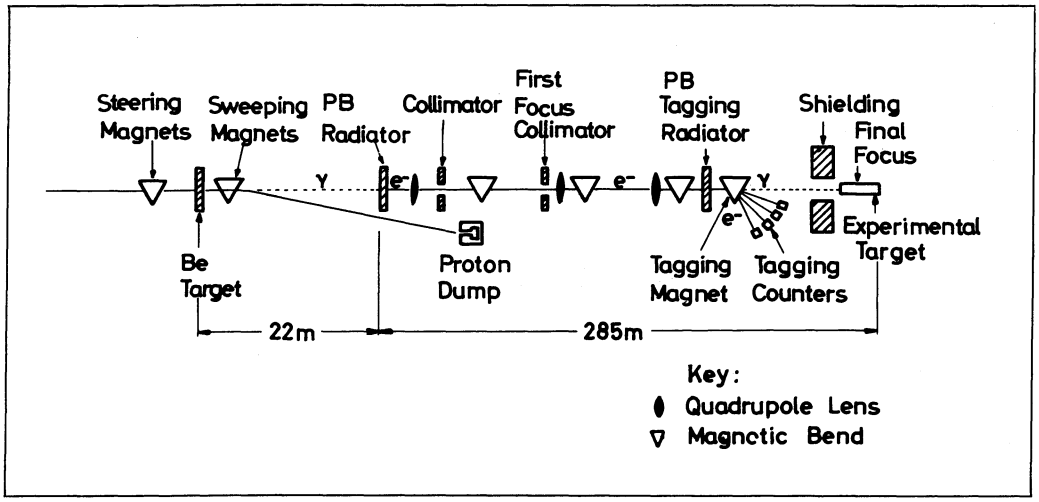

Fig. 2

analysed, and focused on to a target located some 300 m downstream. Such a long distance is needed in order to provide sufficient shielding against the muons. About 40 m upstream of the target, the electrons may be converted to photons in a second thin (0.01 X_0) lead radiator. The recoiling electrons are detected and momentum-analysed in order to determine the energy of the primary photon.

For 10^{13} incident protons with an energy of 500 GeV they expect an electron intensity of typically 1.5×10^8 electrons at 150 GeV and 5×10^5 photons with energies between 100 and 150 GeV. The computed electron yield is shown in Fig. 3 together with the computed π/e ratio. The π/e ratio can be further reduced by going to a finite π^0 production angle at some loss in electron intensity.

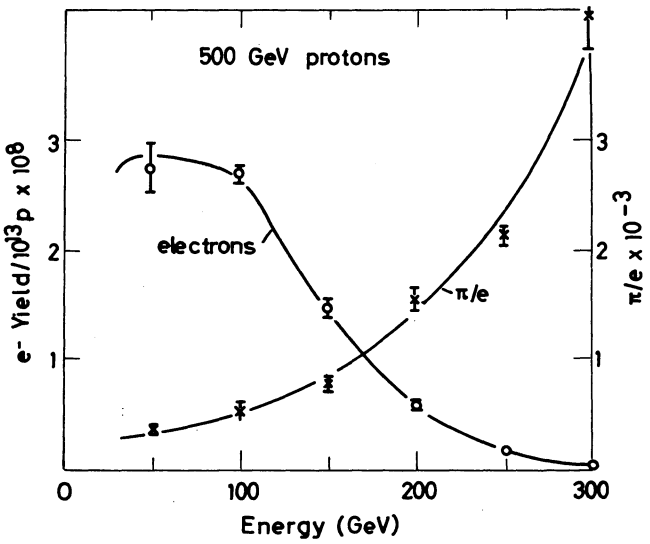

Fig. 3

NAL is now proceeding with the construction of such a beam, and it is expected that the first stage of the beam will become operational sometime in 1974[14].

3.5 SLAC

As noted earlier, SLAC has a gradual improvement program implemented by replacing the 20 MW klystrons with 30 MW klystrons. A 60 MW klystron is also under development. With a full complement of these tubes an energy of 35 GeV can be reached. However, since the energy gain in a linear accelerator is only proportional to the square root of the input power and furthermore the duty cycle would remain low, SLAC is pursuing another project[3] to achieve both high energy and high duty cycle, albeit not at the same time.

The layout of the project, christened a recirculating linear accelerator (RLA), is shown in Fig. 4.

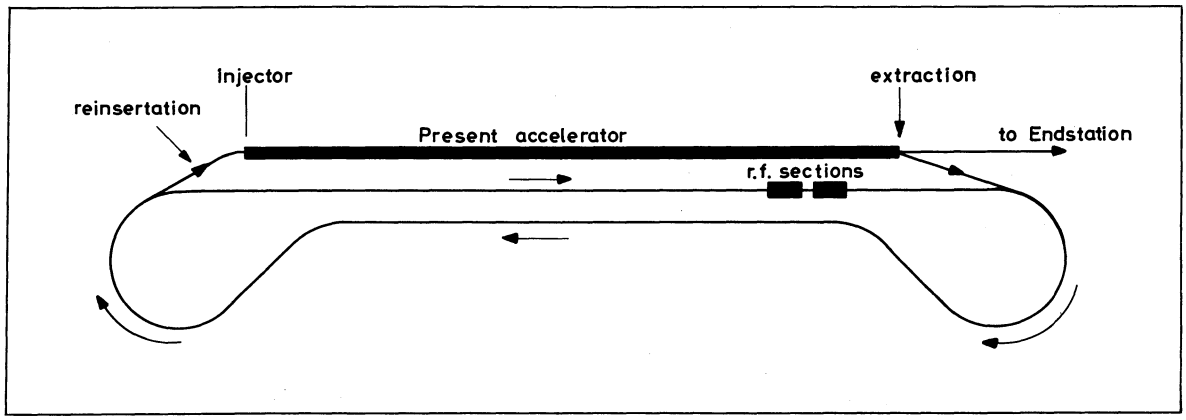

Fig. 4

Electrons injected into the present linear accelerator are accelerated up to an energy of 17.5 GeV or less. Emerging from the end of the accelerator they are switched into a storage ring consisting of two long straight sections and two bends of 210° and 198°, respectively. The total path length for each revolution is about 6900 m, corresponding to a revolution time of 23 μsec. At 17.5 GeV an electron is losing a total of 125 MeV per revolution, and this energy is being restored by means of two conventional accelerator sections, each 100 m long.

With this device there are three possible modes of operation:

i) The trivial one -- just use the linear accelerator.

ii) The beam is injected into the ring and stored for about 2.8 msec -- the time between two RF pulses in the linac. The beam is then reinjected into the accelerator, gaining another 25 GeV, and emerges at the end of the accelerator with a total energy of 42.5 GeV. Since concurrently with this beam a new beam of electrons is being injected into the storage ring, the duty cycle and the average current remains as before. In this mode of operation, the storage ring in effect serves as an energy doubler.

iii) In this mode of operation the electrons are again injected into the ring, but now they are slowly peeled off during each transit around the loop so that after 2.8 msec all the electrons have been extracted from the ring. The average current is as before; however, the duty cycle is now simply the ratio of the pulse length (1.6 μsec) to the revolution time (23 μsec), or roughly 7%. In this mode of operation the accelerator corresponds to a high-energy, high-intensity synchrotron.

SLAC is also considering various extensions of this scheme. These options together with other properties of the accelerator are listed in Table 2.

Table 2

	High-energy mode			High duty cycle mode		Accelerator only mode	
Final beam energy (GeV)	42.5	46	60	17.5	25	25	35
Recirculating beam energy (GeV)	17.5	21	25	17.5	25	-	-
Repetition rate (pps)	360	360	180	4×10^4	4×10^4	360	180
Duty cycle (%)	0.06	0.06	0.03	7	7	0.06	0.03
Average beam current (in units of 10^{13} e/sec)	3.6	3.6	1.8	3.6	3.6	28	14

One might also mention that with an RF system as ambitious as the one proposed for the Cornell machine, stored energies of the order of 35 GeV can be reached. This ties up nicely with the fact that with a full complement of 60 MW klystrons, the energy gained for a single pass through the linear accelerator is also 35 GeV.

A proposal has been submitted to the Atomic Energy Commission, and SLAC is hoping for a favourable decision this year. The construction time is estimated to be about 3 years.

In comparing the electron fluxes at an electron accelerator with those that will be available in secondary electron and photon beams (at NAL and CERN SPS), it is clear that there is a factor of roughly 10^5 in favour of the electron accelerators. Of course this factor renders these accelerators highly advantageous in the case of single-arm experiments such as $e + p \to e' + X$, or for certain classes of simple coincidence experiments such as $e + p \to e' + n + \pi^+$. However, even for such experiments, we should bear in mind that the highest energies can only be reached in secondary beams, and that the rates are sufficiently high with these beams to exploit a large kinematic region. In experiments where a complicated final state must be measured, the situation is much more favourable for secondary beams. At electron machines the maximum current which has been used so far in large solid-angle experiments is of the order of 5×10^6 e^-/sec. The fluxes which will be available at CERN SPS and NAL -- in particular with μ beams -- are higher than these numbers. This, together with the good duty cycle at NAL and CERN SPS, will make these accelerators very competitive indeed for experiments involving a large solid-angle apparatus.

4. PHYSICS

4.1 Photoproduction

Perhaps the most important feature to emerge from the study of the photoproduction reactions[15] is the remarkable similarity between these reactions and purely hadronic reactions. This finding has been expressed formally in the vector-meson dominance model (VDM). In this model the purely electromagnetic interaction of a photon is assumed to be proportional to the sum of the strong interactions of 1^- states (ρ, ω, ϕ, ...). This implies that a photon beam can be looked upon as a beam of strongly interacting bosons, and that all the theories which have been developed for pure hadronic interactions can now be applied and tested with photons. Furthermore, since the photon has helicities of ± 1, several crucial experiments which are difficult to do with an incident pion beam can be done with relative ease using a photon beam. Although these similarities between photons and hadrons have been exploited very successfully over the past few years, one should keep in mind that the photon might possess some special properties and that these might show up more clearly at high energies. In fact one major motivation for doing photon physics at high energies is just to search for such effects.

In the next part of the talk I would like to discuss some typical photoproduction experiments to remind you of both the physics interest and the problems one might encounter when extending these experiments to higher energies. The experiments to be discussed are the following:

1) Total photoabsorption cross-section on hydrogen and deuterium
2) Total photoabsorption cross-section on complex nuclei
3) Elastic Compton scattering
4) Production of ρ, ω, ϕ and a search for heavy vector mesons
5) Photoproduction of pseudoscalar mesons
6) Inelastic Compton scattering

In discussing these rates we will assume a tagged photon beam with 10^5 photons/sec incident on a liquid-hydrogen target 1 m long.

4.1.1 Total photoabsorption cross-section on hydrogen and deuterium

The total photoabsorption cross-section has now been measured[15,16] from close to threshold up to 18 GeV. The energy dependence of the cross-section was found to be well represented by the form $a + b(\nu)^{-1/2}$ as expected from a simple Regge theory and also observed in purely hadronic interactions at these energies (ν is the laboratory energy of the incident photon). Also, the difference between the proton and neutron total cross-sections seems to disappear with increasing energy as $(\nu)^{-1/2}$. Using these data as input to dispersion relations, Damashek and Gilman[17] have evaluated the real part of the forward Compton amplitude. These computations all indicate the presence of a constant term in the real part of the amplitude. In Regge theory this could correspond to a fixed J = 0 pole if $\alpha(t) = 0$. Such a fixed pole is in principle allowed in electromagnetic interactions, although forbidden for purely hadronic amplitudes. The presence of a fixed pole would violate a strict VDM and demonstrate that a photon is indeed different from a hadron. However, the existence of a constant real part in the forward Compton amplitude is crucially dependent on the assumption that $\sigma_T = a + b \cdot (\nu)^{-1/2}$, and that the amplitude behaves like a simple Regge amplitude at high energies. It should be noted that the energy dependence of the total cross-sections measured at Serpukhov[18] is no longer consistent with $a + b \cdot (\nu)^{-1/2}$. A measurement of the total photoabsorption cross-section is therefore important, both as a test of the Regge models, and as an input to the dispersion relations. Experimentally there should be no problems in performing the measurement at any of the proposed facilities. With the standard conditions and assuming a cross-section of 100 μb, the data rate will be of the order of 40 events/sec, i.e. a measurement with high statistical accuracy will be possible both at NAL and CERN SPS up to very high energies.

4.1.2 Total photoabsorption cross-section on complex nuclei

The measurement of the total photoabsorption cross-section on complex nuclei provides us with a paradox which can be nicely resolved assuming the photon to behave like a hadron. The problem is as follows. The total photoabsorption cross-section is of the order of 100 μb, which implies a mean free length of a photon in nuclear matter of several hundred fermi. The total photoabsorption cross-section should thus be the sum of the cross-sections on the individual nucleons: i.e. $\sigma_T(\gamma,A) \simeq A\,\sigma_T(\gamma,N)$. Experimentally[15,19] we find that $\sigma_T(\gamma,A) < A\,\sigma_T(\gamma,N)$, i.e. some unexpected shadowing occurs. A very lucid explanation of this phenomena has been given by Gribov[20] and can be sketched as follows:

The photon can dissociate into virtual 1^{-1} states such as the ρ, ω, ϕ, $K\bar{K}$, $p\bar{p}$, ... as indicated in Fig. 5. This virtual state violates energy conservation by an amount $\Delta E = (m^2/2\nu)$, i.e. the lifetime, and hence the distance this state can travel before decaying back into a photon is $\ell \sim (\Delta E)^{-1} = 2\nu/m^2$. Now if this distance ℓ is greater than the mean free length of this particle in nuclear matter, then the hadron will be absorbed and the photon will have disappeared. At large energies the photon will be able to travel as large a distance as will a hadron, and we should thus expect to find a total cross-section proportional to $A^{2/3}$ as observed in hadrons on nuclei. Experimentally[19] a cross-section proportional to $A^{0.9}$ is found. Such a discrepancy could, for example, be understood if the

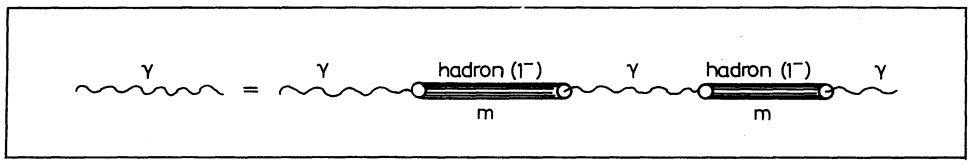

Fig. 5

photon couples to a heavy vector meson (or the continuum), or to a relatively light vector meson with a small total cross-section. The difference could also of course indicate a large breakdown of the VDM. To settle these questions, data at higher energies are needed. Since the purely electromagnetic background increases strongly with A, these measurements are much more difficult than the measurements on hydrogen. For example, using lead as a target the electromagnetic background is roughly three orders of magnitude larger than the total photoabsorption cross-section. However, since such an experiment was successfully completed at SLAC in spite of the poor duty cycle, it should presumably be rather straightforward to extend the experiment to higher energies at Cornell, CERN SPS, or NAL.

4.1.3 Compton scattering

The cross-section for the reaction $\gamma p \to \gamma p$ has been measured[15,21] for photon energies up to 19 GeV and for values of the momentum transfer t out to $|t| \leq 1.2$ (GeV/c)^2. Also, this process has an s- and t-dependence as observed in hadronic elastic scattering processes, i.e. a slowly decreasing forward cross-section with increasing energy and a t-dependence of the form e^{At}. Now what can be learned from this reaction at higher energies?

i) A comparison between the total photoabsorption cross-section and the forward Compton cross-section at $t = 0$ is very important as a check on the forward dispersion relation. Such tests are rather interesting in the case of photons, since here additional terms[22] of the form $a \cdot \Lambda^2 + \ldots$, which must be absent in πN scattering, can in principle be added to the real part of the diffractive amplitude.

ii) The result of this experiment is particularly useful within the context of the vector-meson dominance model. In this model the Compton cross-section is directly related to the cross-section for photoproduction of vector mesons as indicated in Fig. 6.

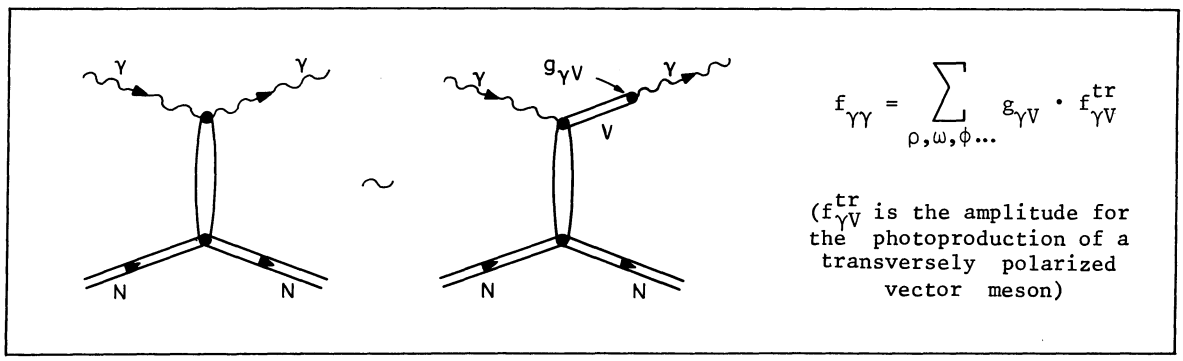

Fig. 6

iii) Brodsky, Close and Gunion[23] have extended the parton model, normally used for large q^2 processes, to $q^2 = 0$. They find that a gauge-invariant treatment of the parton model leads to a constant in the real part of the Compton amplitude. Some predictions of this model are:

a) the Compton amplitude will become predominantly real at large values of t;

b) s-channel helicity conservation will break down at large values of t -- this will result in a positive asymmetry $A = (\sigma_\perp - \sigma_\parallel)/(\sigma_\perp + \sigma_\parallel)$ in experiments with linearly polarized photons;

c) Compton scattering should have a more gentle fall-off with t than ρ production.

Now how far can the experiment be extended on to higher energies? The main difficulty at lower energies is to separate Compton scattering from the much more abundant single π^0 production. At high energies, however, this should be no problem, and the maximum energy reached will probably be limited by the absolute counting rate rather than by the background. For the rate estimate let us assume the standard conditions and a cross-section of

$$\frac{d\sigma}{dt} = 0.7\ (\mu b/GeV^2)\ e^{7t}\ .$$

Let us further make the assumption that the φ acceptance is 2π. Since the recoil proton must be detected in coincidence with the scattered photon, both to determine the t-value and to reject the background, this is a very optimistic assumption. However, with this assumption and our standard conditions, we have 4.5 events/hour for $|t| \geq 0.5\ GeV^2$.

At SLAC it should be possible to extend the data out to a t-value of roughly 1.5 $(GeV/c)^2$ at high energies.

4.1.4 Production of ρ, ω, and φ mesons and a search for new heavy vector mesons

Since the vector mesons have the same quantum numbers as those of the photon, one would expect, on general grounds, that the process $\gamma + p \to V + p$ is mainly diffractive at higher energies. This is indicated in Fig. 7. Therefore photoproduction of vector mesons offers a unique opportunity of studying the elastic scattering of vector mesons on nucleons.

Using a linearly polarized photon beam and measuring the angular distribution of the decay products, important quantities such as the ratio of natural to unnatural parity

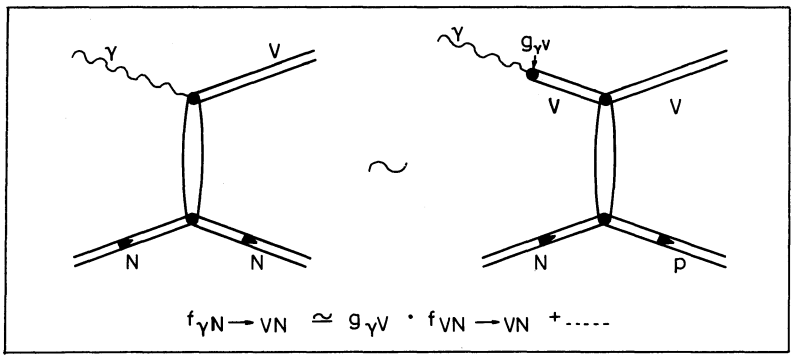

Fig. 7

exchange (t-channel) or the amount of helicity conservation can be directly determined. The ϕ photoproduction further offers a unique opportunity of determining[24] the properties of the Pomeron without any interference from lower trajectories. That ϕp elastic scattering can only proceed by Pomeron exchange follows directly from the quark model with the ϕ made up of two strange quarks, and is supported by experimental evidence showing the ϕ to be remarkably decoupled from non-strange hadrons.

The counting rates evaluated for the standard conditions and assuming a ϕ acceptance of 2π (too optimistic since we have to detect the proton) are listed in Table 3 for $|t| \geq 0.1$ (GeV/c)^2 (lower limit on t if the proton must be measured) and for $|t| \geq 1.0$ (GeV/c)^2. The cross-section for ρ photoproduction was assumed to be

$$\frac{d\sigma}{dt} = 100\ [\mu b/(GeV/c)^2]\ e^{7t} .$$

The yield of ω's was taken to be 1/9 of the ρ yield, and the cross-section for ϕ production was set equal to

$$\frac{d\sigma}{dt} = 2\ (\mu b/GeV^2)\ e^{4.5t} .$$

Table 3

	$\|t\| \geq 0.1$ GeV^2	$\|t\| \geq 1.0$ GeV^2
$\gamma + p \to \rho + p$	$\sim$ 11000 counts/hr	$\sim$ 20 counts/hr
$\gamma + p \to \omega + p$	$\sim$ 1200 counts/hr	$\sim$ 2 counts/hr
$\gamma + p \to \phi + p$	$\sim$ 400 counts/hr	$\sim$ 8 counts/hr

It is also advantageous to search for new vector mesons using a high-energy photon beam. The reason for this is twofold: since the 1^- states are diffractively produced they will become increasingly prominent at higher energies. Furthermore, the minimum momentum transfer squared to the nucleon $t_{min} = (m^2/2k)^2$, needed in order to produce a state with the mass m, will become very small even for very massive states. However, despite these advantages, my own personal prejudice is that these states will be more easily found in e^+e^- colliding beams.

4.1.5 Photoproduction of pseudoscalar mesons

The measurements on photoproduction of pseudoscalar mesons[15] have been very important for present-day electron accelerators. Owing to the high photon fluxes available (equivalent of about 10^{10} pions/sec), and the use of polarized beams and polarized targets, these reactions have provided crucial tests of various models.

However, the experiments found that the cross-sections are decreasing with increasing energy roughly proportional to $1/k^2$, leading to very low cross-sections at high energies. For example, with 10^5 photons/sec at 100 GeV incident on a hydrogen target 1 m in length, the total rate for the reaction $\gamma + p \to \pi^+ + n$ would be roughly 3 events/hr. The rates for

the other reactions are similar. These are rather low rates and, with the exception of survey-type experiments, my guess is that the photoproduction of pions and kaons will remain the domain of SLAC and Cornell.

An amusing example of a certain type of reaction which it might be possible to measure at high energies is $\gamma + p \to B + p$. This process seems to be predominantly diffractive[15] at lower energies. Since the B has the quantum numbers 1^+, this is only possible if the photon and the Pomeron couple in a relative p-state. Assuming the cross-section to be independent of energy, we would expect about 800 events/hr for $|t| \geq 0.1$ GeV^2. The search for other such diffractive states should become easier at high energies.

4.1.6 Inelastic Compton scattering

A reaction which has some bearing on the question of possible substructure within the proton is inelastic Compton scattering: $\gamma + p \to \gamma' +$ "anything". This process has been evaluated within the parton model by Bjorken and Paschos[25] using the graphs as shown below in Fig. 8. They find this reaction to be closely related to deep inelastic electron-nucleon scattering:

$$\left.\frac{d^2\sigma}{d\Omega dE'}\right|_{\gamma p} = \frac{\nu^2}{EE'} \cdot \left.\frac{d^2\sigma}{d\Omega dE'}\right|_{e'p} \frac{\Sigma_i \langle Q_i^4 \rangle}{\Sigma_i \langle Q_i^2 \rangle} \cdot$$

Here Q_i^n is the n^{th} power of the charge of the constituents (partons) averaged over the constituents. For example, for three quarks in a sea of quark-antiquark pairs this ratio is bounded:

$$\frac{1}{3} \leq \frac{\Sigma_i \langle Q_i^4 \rangle}{\Sigma_i \langle Q_i^2 \rangle} \leq \frac{5}{9} \cdot$$

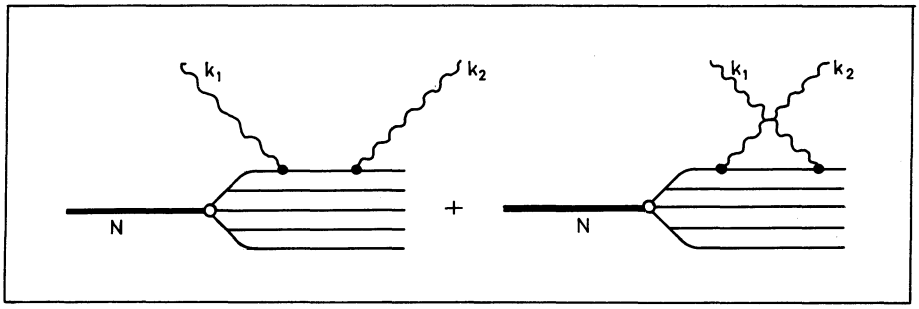

Fig. 8

Hence in principle this experiment can give some information on the charge of the constituents. The experimental problems are obvious; to be sure that the measured photons are from the diagrams shown above, large values of transverse momenta with correspondingly small cross-section are required. This can be partially offset by the fact that a good energy definition of the photon is not needed, i.e. we should be able to increase the photon fluxes considerably by using a thick radiator. Furthermore, the background due to photons from π^0 decay tend to bury the contribution from inelastic Compton scattering. At high energies, however, the situation becomes much more advantageous. The inelastic Compton cross-section

will decrease slowly with t (the photon scatter off point-like particles), whereas π^0 production should have a more rapid decrease with increasing values of t. Of course it is likely that the π^0 spectrum has a smaller slope at large values of t, so that a substantial background will remain even at high energies. However, the good duty cycle at CERN SPS and NAL will make it possible to measure the π^0 spectrum concurrently with the measurement of the Compton process. The background from π^0 decays can be avoided by demanding the scattered photon to be off the mass shell and to decay into μ pairs[24]. Experimentally a μ pair of low invariant mass but large angles must be measured[25,26]. The problem here is the low counting rate and the contamination due to the Bethe-Heitler process.

In addition to the more obvious photoproduction experiments discussed here, there is also a large class of more speculative experiments. As examples, let me just mention the proposed[27] search for heavy leptons and intermediate bosons in a pair production experiment, or a measurement of μ pairs with large invariant masses as a test of parton models[28]. It is therefore clear that a high-energy secondary photon beam at CERN SPS would be a very valuable tool.

4.1.6 Inelastic electron scattering

The results of the SLAC-MIT Collaboration[29] on deep inelastic electron-nucleon scattering have received much attention[15] over the past few years. The kinematics of this inclusive reaction is defined in the one-photon approximation in Fig. 9. The properties of the virtual photon (mass q^2, energy ν, and polarization ε) are all determined by the electron kinematics, as shown in the figure, and can therefore be varied continuously in a well-defined manner.

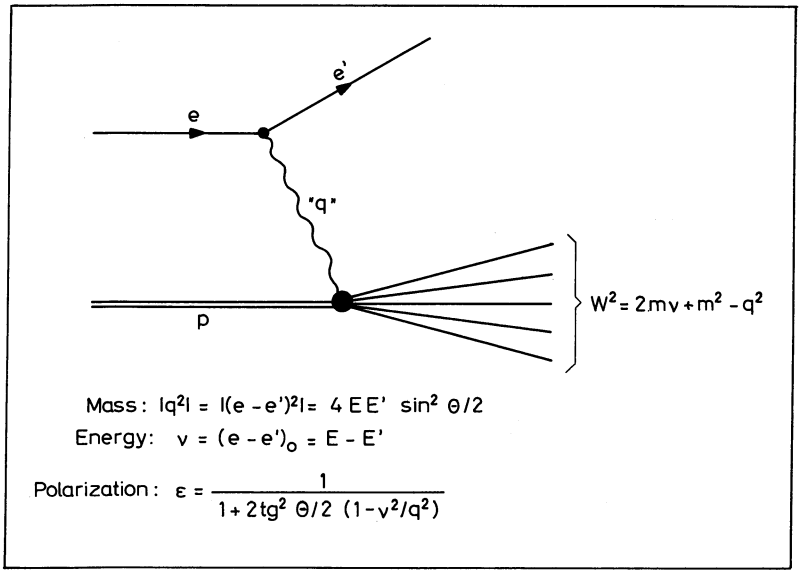

Fig. 9

In this type of inclusive experiment, where only the scattered electron is detected, the quantity measured is the total absorption cross-section for a "virtual" photon with mass q^2 on a nucleon. In the case of an unpolarized electron beam scattered on an unpolarized

nucleon, this total cross-section can be written in terms of two unknown structure functions $W_1(\nu,q^2)$ and $W_2(\nu,q^2)$ as:

$$\frac{d^2\sigma}{d\Omega dE'} = \left(\frac{4\alpha^2 E'^2}{q^4}\right) \cdot \left\{2W_1(\nu,q^2) \sin^2\frac{\theta}{2} + W_2(\nu,q^2) \cos^2\frac{\theta}{2}\right\}.$$

Roughly speaking, at small scattering angles $W_2(\nu,q^2)$ is measured, at large scattering angles $W_1(\nu,q^2)$.

The SLAC-MIT Collaboration has collected data in the kinematical region shown in Fig. 10. To separate $W_1(\nu,q^2)$ and $W_2(\nu,q^2)$, measurements at fixed ν and q^2 but for different angles of the scattered electron are needed. The kinematical region, where this has been done is shown as the hatched part in Fig. 10.

The main results of these measurements can be summarized as follows:

i) The measured cross-section in the deep inelastic region is large and decreases only slowly with q^2. In fact the cross-section for fixed q^2 integrated over ν gives a result which is of the same order of magnitude as the point (Mott) cross-section (Fig. 11).

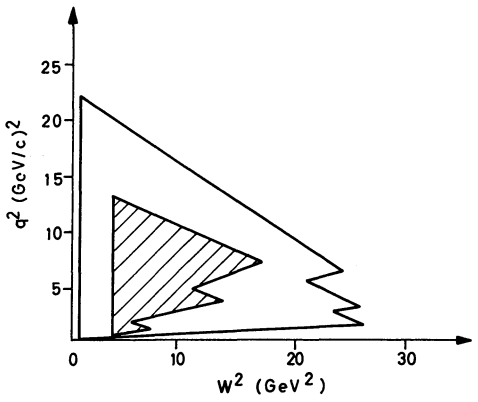

Fig. 10

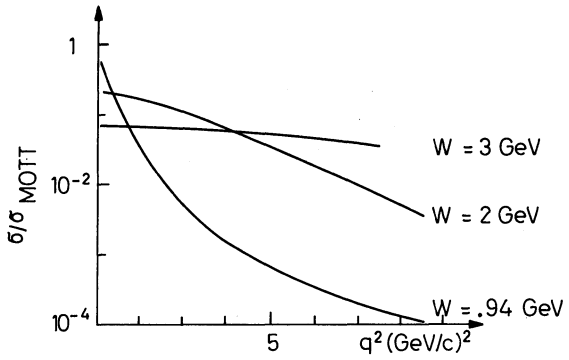

Fig. 11

ii) $W_1(\nu,q^2)$ and $W_2(\nu,q^2)$ shows scaling, i.e. for fixed $\omega = 2M\nu/q^2$ the structure functions are independent of q^2. The threshold for scaling is at surprisingly low values of q^2 and W, i.e. $q^2 \geq 1$ (GeV/c)^2, $W \geq 2.6$ GeV (Fig. 12).

iii) $W_2^p(\nu,q^2) \neq W_2^n(\nu,q^2)$, i.e. the structure function has a non-diffractive component, at least for $\omega \leq 10$ (Fig. 13).

These features were predicted on general grounds prior to the experiments by Bjorken[30] in the so-called scaling limit, i.e. $q^2 \to \infty$, $\nu \to \infty$, but $\omega = 2M\nu/q^2$ finite. Feynman[31] then showed that a natural explanation of scaling could be given in terms of point-like objects within the proton. This, of course, is a very exciting possibility, although more mundane explanations of the data are certainly also possible. One of the surprises of these data is the early onset of scaling. The crucial question is, then, Is the scaling observed at present energies an accident or not? This question of course can only be decided by extending the experiments to higher energies.

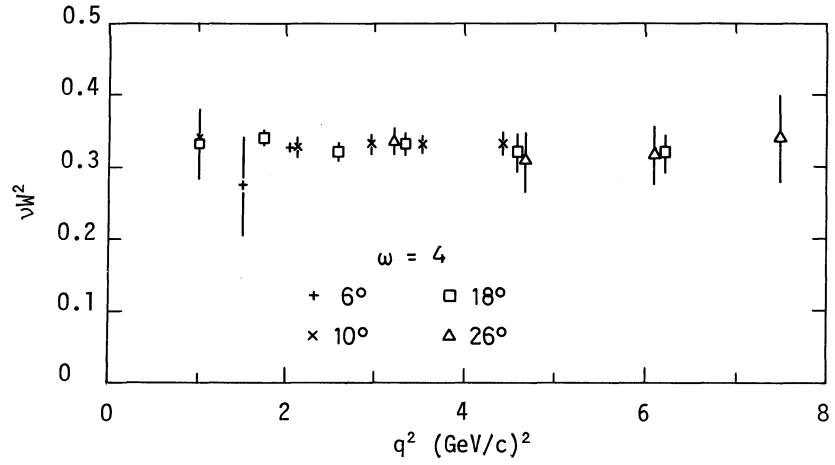

Fig. 12

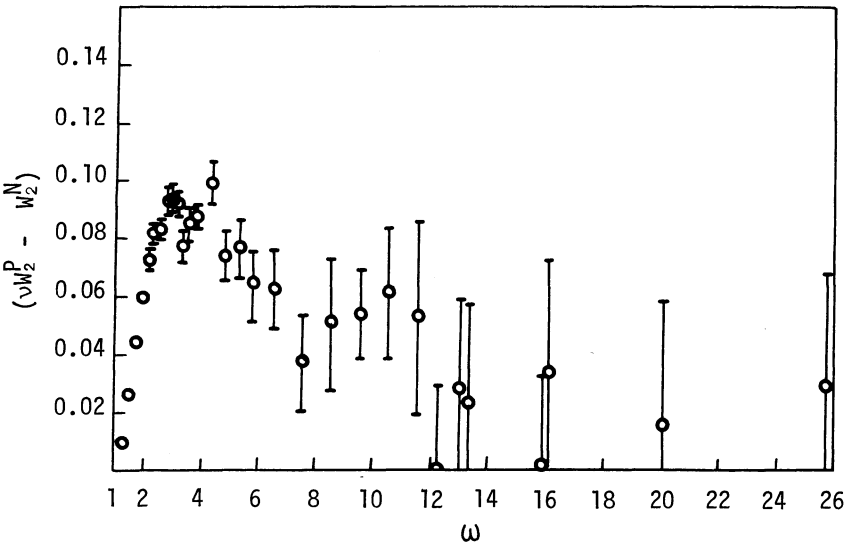

Fig. 13

The kinematical region which will become available at the new accelerators is shown in Fig. 14 for incident electron energies of 40 GeV (SLAC I, Cornell), 60 GeV (SLAC II), and for 200 GeV (CERN SPS, NAL). All the present data lie in the hatched region.

It is clear that in principle these new accelerators allow us to extend the measurements substantially both in q^2 and in W^2. To see which part of the kinematical region can be exploited experimentally, we have evaluated the counting rates assuming a ratio between the longitudinal and the transverse cross-section σ_L/σ_T of 0.2. We further assume scaling, and for $\nu W_2(\nu,q^2)$ the form suggested by Bloom and Gilman[32] was used.

In Fig. 15 the counting rates, using one of the three SLAC spectrometers, is shown. As incident energy 60 GeV was chosen with 1.8×10^{13} electrons/sec incident on a target 15 cm long. In this figure is plotted the counting rate per hour at the corresponding value of q^2 and W^2. It is clear that the experiments will be able to cover most of the available kinematical region.

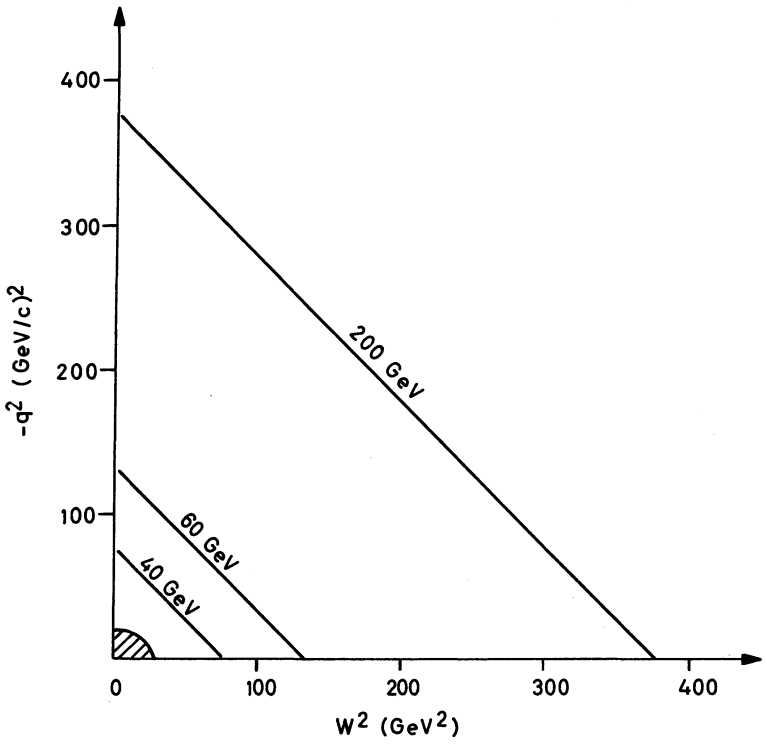
400
300
200
100
$-q^2$ (GeV/c)^2
200 GeV
60 GeV
40 GeV
0
100
200
300
400
W^2 (GeV^2)

Fig. 14

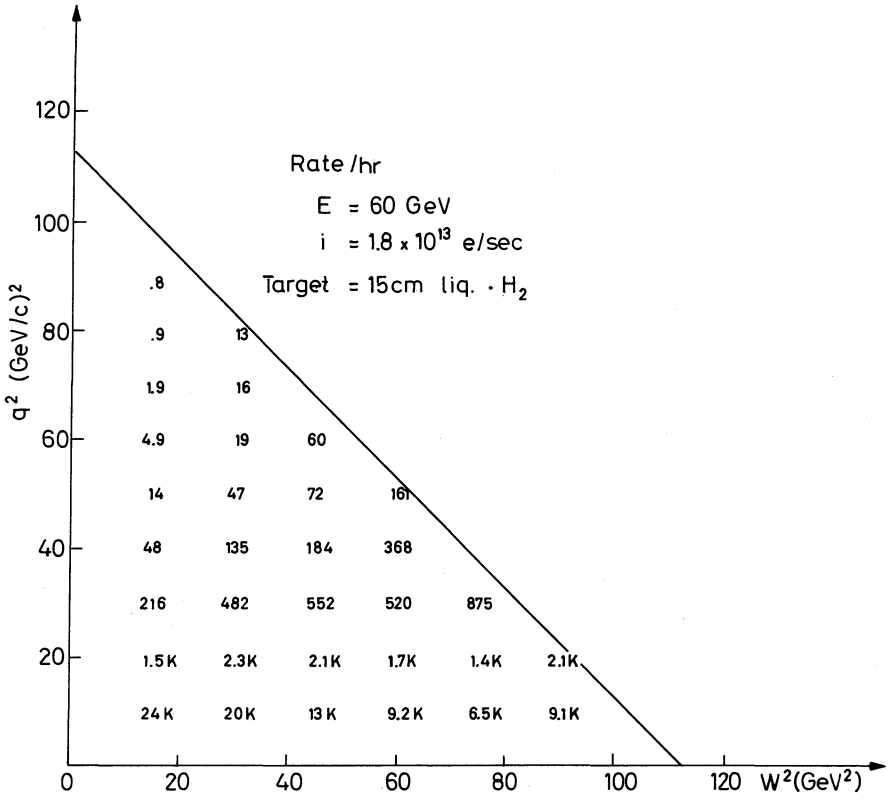
120
100
80
60
40
20
q^2 (GeV/c)^2
Rate /hr
E = 60 GeV
i = 1.8 x 10^{13} e/sec
Target = 15cm liq. · H_2
.8
.9
1.9
4.9
14
48
216
1.5K
24K
13
16
19
47
135
482
2.3K
20K
60
72
184
552
2.1K
13K
161
368
520
1.7K
9.2K
875
1.4K
6.5K
2.1K
9.1K
0
20
40
60
80
100
120
W^2(GeV^2)

Fig. 15

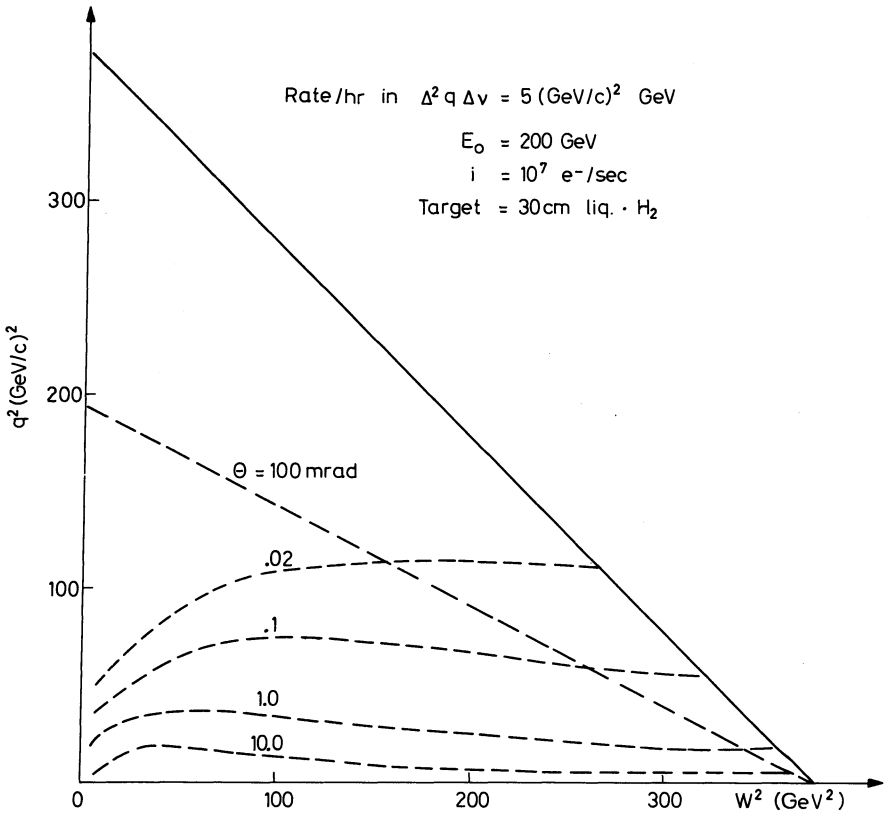

Fig. 16

The counting rate per hour in a bin $\Delta\nu$ = 5 GeV, Δq^2 = 1 (GeV/c)^2 is evaluated for CERN SPS or NAL conditions. For this estimate an electron beam with an energy of 200 GeV and a flux of 10^7 electrons/sec incident on a hydrogen target 30 cm long was used. The rates are plotted in Fig. 16 assuming the acceptance in ϕ to be 2π. The kinematical boundary of a detector with a total opening angle of 200 mrad ($\Delta\Omega \simeq 30$ sr) is also indicated in Fig. 16. Since such a detector covers most of the available kinematic area, it is probably not unreasonable to assume that a rate as low as 0.1 count/hr in $d\nu \cdot dq^2$ = 5 GeV (GeV/c)^2 is acceptable. In this case, measurements for $q^2 \geq 60$ GeV^2 will be possible. The range in q^2 is therefore roughly the same as at SLAC, but the range in ν is substantially larger.

Now what are the things we want to look for?

i) Since the measurements are being extended into a new region in q^2 and W^2, one must first make sure that the one-photon approximation is still valid. This can be done by plotting the cross-section for fixed q^2 and W^2 against $tg^2\ \theta/2$ -- deviations from a straight line will indicate a breakdown of the one-photon approximation. A more sensitive test, however, might come from comparing the e^+ and e^- rates (real part of the two-photon amplitude) or from a measurement of the asymmetry from a polarized target (imaginary part of the two-photon amplitude).

ii) Assuming the one-photon amplitude to dominate, then $W_1(\nu,q^2)$ and $W_2(\nu,q^2)$ should be determined for protons and for neutrons over as large a kinematic region as possible. This will hopefully decide the question whether the scaling observed at low ν and q^2 is an accident or not. It is also important to determine the non-diffractive part of the amplitude. Does it scale as required by the quark models? or does it disappear as permitted by various Regge models?

Assume that $W_1(\nu,q^2)$ and $W_2(\nu,q^2)$ both obey scaling. Must we then conclude that there are point-like objects within the nucleon? Scaling can be derived from several models based on quite different physical mechanisms. However, none of these models predicts the functional form of the structure functions reliably, and therefore a measurement of $W_1(\nu,q^2)$ and $W_2(\nu,q^2)$ will probably not be able to distinguish between the various models. Additional information can be gained either by measuring the properties of the produced hadron states or by doing experiments with polarized beams on a polarized target.

Now what do we measure[33] in the case of a polarized electron scattering on a polarized nucleon? In the one-photon approximation there are two asymmetries, defined in Fig. 17, which can be measured. In both cases the nucleon is polarized in the scattering plane. In the one-photon approximation, the asymmetry with the proton polarized normal to the scattering plane will disappear. These asymmetries can be expressed in terms of two new structure functions $G_1(\nu,q^2)$ and $G_2(\nu,q^2)$. The predictions for these quantities have been taken from a paper by Walsh and Zerwas[34] and are listed in Table 4.

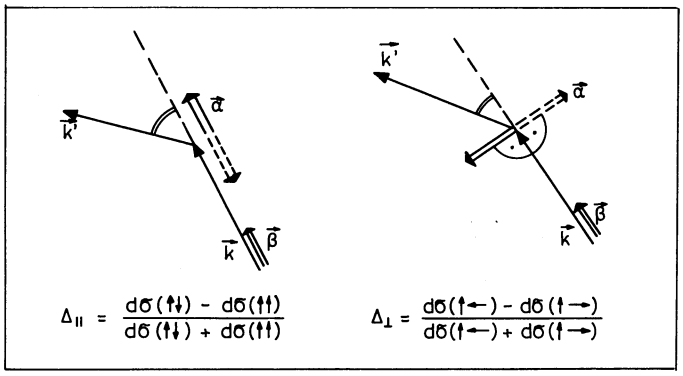

Fig. 17

As mentioned earlier, polarized lepton beams are under development both at SLAC and at DESY. However, let me digress for a moment and speak about the feasibility of doing such experiments at NAL or CERN SPS using a polarized μ beam. Since the muons originate from the decay $\pi \to \mu + \bar{\nu}$ it is possible to produce a polarized μ beam by momentum selection of the pions and the muons. The expected fluxes[35] in such a beam are of the order of 5×10^7 muons per sec at 100 GeV within a beam spot 4×4 cm^2 and with a polarization of 80%. Assuming a butanol target 8 cm long, cooled down to liquid ^{3}He temperatures, the target polarization per nucleon would be about 8%.

Table 4

		Light cone algebra	Quark-parton model	Resonance model
$G_1(\omega)$	proton	$\int_1^\infty \frac{d\omega}{\omega^2}\left[G_1^p - G_1^n\right] = \frac{f_A}{6}$	$G_1^p(\omega) \sim \omega^{+1/2}(1-\omega^{-1})^3$	$G_1^p(\omega) \simeq 0$
	neutron		$G_1^n(\omega) = 0$	$G_1^n(\omega) \simeq 0$
$G_2(\omega)$	proton	$\int_1^\infty \frac{d\omega}{\omega^2} G_2^{p,n}(\omega) = 0$	$G_2^p(\omega) = 0$	$G_2^{p,n}(\omega) \sim F(\omega)\left[\frac{\mu^2_{p,n}}{2} - \frac{\mu^2_{3/2}(\omega-1)}{\left(1+\frac{r}{2}\right)\omega - 1}\right]$
	neutron		$G_2^n(\omega) = 0$	$F(\omega) \sim \frac{\omega(\omega-1)^3}{[\omega - 1 + (r/2)]^4}$

The total μN cross-section, integrated for θ between 10 mrad and 100 mrad and for ν between 3 GeV and 60 GeV, can be written as

$$\sigma_{\mu N} \simeq \sigma_{\mu p} = \frac{4\pi}{E^2} \ln\left(\frac{\nu_{max}}{\nu_{min}}\right)\left\{\frac{1}{\theta^2_{min}} - \frac{1}{\theta^2_{max}}\right\} = 0.26\ \mu b\ .$$

This integration was done with the assumption that $\nu W_2(\nu,q^2)$ = constant = 1/3 and $W_1(\nu,q^2) = 0$. With the assumptions listed above, 2×10^5 counts/hr would be collected in such a detector. Since $\Delta_{\parallel}$ is estimated[33] to be of the order of 20% over a large region in q^2 and W^2, the expected experimental asymmetry will be of the order of 1% (beam polarization × target polarization × expected asymmetry = 0.8 × 0.08 × 0.2 = 0.013). It therefore seems possible to determine $\Delta_{\parallel}$ using a well-optimized μ beam at NAL and CERN SPS.

Another possibility of learning more about the physical reasons behind scaling is to measure the properties of the final hadron state. At low values of q^2 it might be possible to measure certain two-body channels such as ρ production or single-pion production. However, at large values for q^2 and ν, the number of available exclusive channels will become very large, i.e. the cross-section for each individual channel will become very small. It therefore seems more appropriate to concentrate on a measurement of the gross properties of the final state. For example, in the region where the minimum momentum transfer squared to the nucleon $t_{min} = [(q^2 + m^2)/2\nu]^2$ is small, one might expect the process to have a large diffractive component. In this case there might be a leading particle effect, i.e. some fraction of the events the particles in the projectile fragmentation region will have the quantum number of a photon. We would also expect that particles in the projectile region should depend on the properties of the projectile (for example, the $p_\perp$ distribution of the hadrons in this region might become flatter with increasing values of q^2). By the same token we would expect particles in the target fragmentation region to be independent of the properties of the photon, i.e. independent of q^2.

In the kinematic region where t_{min} is large, we must by definition be dealing with a central collision. One might then ask if the energy transferred to the nucleon is divided on a small number of loosely bound objects or on a large number of objects that are tightly bound. In the first case one might expect to see a non-isotropic distribution of the hadrons in the centre-of-mass frame of the hadrons, whereas in the second case a more isotropic distribution would seem likely. In the case of a parton model, we might be able to learn something about the nature of the partons by studying the final state.

The measurements to be done are:

i) distribution in rapidity and transverse momenta as a function of q^2 and ν;

ii) multiplicities as a function of q^2 and ν;

iii) particle ratios as a function of q^2 and ν.

The long spill available at NAL and CERN SPS makes these accelerators well suited for this kind of experiment.

I think it is clear that electron and photon physics is a rich field which should be rigorously exploited. I think it is also clear that CERN SPS will, for the foreseeable future, provide us with the only facility in Europe where this kind of physics can be pursued. It therefore seems reasonable to have both an electron-photon and muon beam available at the earliest possible date at CERN SPS.

REFERENCES

1) J. de Wire, private communication.
M. Tigner, private communication.

2) G. Diambrini Palazzi, Rev. Mod. Phys. 40, 611 (1968).

3) Description and physics program of the proposed recirculating linear accelerator (RLA), SLAC Report No. 139, 1972.

4) C.K. Sinclair, private communication.

5) N. Cabibbo, G. Da Prato, G. De Franceschi and U. Mosco, Phys. Rev. Letters 9, 270 (1962).
C. Berger, G. McClellan, N. Mistry, H. Ogren, B. Sandler, J. Swartz, P. Walstrom, R.L. Anderson, D. Gustavson, J. Johnson, I. Overman, R. Talman, B.H. Wiik, D. Worcester and A. Moore, Phys. Rev. Letters 25, 1366 (1970).

6) R. Siemann, private communication.

7) SLAC-Berkeley-Tufts Collaboration, Phys. Rev. D5 (1972) and references quoted therein.

8) For a description of the polarized source and the beam, see SLAC Proposal No. 80 (unpublished) and references quoted therein.

9) R.J. Krisciokaitis and Wu-Yang Tsai, Nuclear Instrum. Methods 83, 45 (1970).

10) P.B. Wilson, private communication.

11) A. Febel, H. Gerke, M. Tigner, H. Wiedemann and B.H. Wiik, Contribution to the Second ECFA Study Week on the 300 GeV CERN Accelerator, Tirrenia, Italy, 1972.

12) E. Gabathuler, private communication.

13) C. Halliwell, P.J. Biggs, W. Busza, M. Chen, T. Nash, F. Murphy, G. Luxton and J.D. Prentice, Nuclear Instrum. Methods 102, 51 (1972).

14) J.K. Walker, private communication.

15) For an excellent review of photon and electron physics, see F.J. Gilman, Photoproduction and electroproduction, Phys. Letters 4 C, 97 (1972), and references quoted therein. See also the Proc. Int. Symposium on Electron and Photon Interactions at High Energies, Ithaca, 1971 (Cornell University, Ithaca, N.Y., 1972).

16) H. Meyer, B. Naroska, J.H. Weber, M. Wong, V. Heynen, E. Mandelkow and D. Notz, Phys. Letters 33 B, 189 (1970).
D.O. Caldwell, V.B. Elings, W.P. Hesse, R.J. Morrison, F.V. Murphy and D.E. Yount, preprint University of California, Santa Barbara, September 1972, Submitted to Phys. Rev.
T.A. Armstrong, W.R. Hogg, G.M. Lewis, A.W. Robertson, G.R. Brookes, A.S. Clough, J.H. Freeland, W. Galbraith, A.F. King, W.R. Rawlinson, N.R.S. Tait, J.C. Thompson and D.W.L. Tolfree, Phys. Letters 34 B, 535 (1971).

17) M. Damashek and F.J. Gilman, Phys. Rev. D1, 1319 (1970).

18) J.V. Allaby, Yu.B. Bushnin, S.P. Denisov, A.N. Diddens, R.W. Dobinson, S.V. Donskov, G. Giacomelli, Yu.P. Gorin, A. Klovning, A.I. Petrukhin, Yu.D. Prokoshkin, R.S. Shuvalov, C.A. Ståhlbrandt and D.A. Stoyanova, Phys. Letters 30 B, 500 (1969).

19) V. Heynen, H. Meyer, B. Naroska and D. Notz, Phys. Letters 34 B, 651 (1971).
D.O. Caldwell, V.B. Elings, W.P. Hesse, R.J. Morrison, F.V. Murphy and D.E. Yount, preprint University of California, Santa Barbara, September 1972.

20) V.N. Gribov, Soviet Phys. JETP 30, 709 (1970).

21) R.L. Anderson, D. Gustavson, J. Johnson, I. Overman, D. Ritson, B.H. Wiik, R. Talman, J.K. Walker and D. Worcester, Phys. Rev. Letters 25, 1218 (1970).
G. Buschhorn, L. Criegee, L. Dubal, G. Franke, C. Geweniger, P. Heide, R. Kotthaus, G. Poelz, U. Timm, K. Wegener, H. Werner, M. Wong and W. Zimmerman, Phys. Letters 33 B, 241 (1970).
A.M. Boyarski, D.H. Coward, S. Ecklund, B. Richter, D. Sherden, R. Siemann and C. Sinclair, Phys. Rev. Letters 26, 1600 (1971).

22) S.D. Drell, in Proc. 3rd Int. Symposium on Electron and Photon Interactions at High Energies, SLAC, Stanford, 1967 (USAEC Publication, 1967).

23) S.J. Brodsky, F.E. Close and J.F. Gunion, Phys. Rev. D6, 177 (1972).

24) P.G. Freund, Nuovo Cimento 48 A, 541 (1967).
V. Barger and D. Cline, Phys. Rev. Letters 24, 1313 (1970).

25) J.D. Bjorken and E.A. Paschos, Phys. Rev. 185, 1975 (1969).

26) A first such measurement has been reported by J.F. Davis, S. Hayes, R. Imlay, P.C. Stein and P.J. Wanderer, preprint Laboratory of Nuclear Studies, Cornell University, N.Y., CLNS 196 (Aug. 1972).

27) W. Lee, J. Appel, M. Tannenbaum, D. Yount and L. Read, NAL proposal No. 87, 1970 (unpublished).

28) R.L. Jaffe, Phys. Rev. D4, 1507 (1971).

29) G. Miller, E.D. Bloom, G. Buschhorn, D.H. Coward, H. DeStaebler, J. Drees, C.L. Jordan, L.W. Mo, R.E. Taylor, J.I. Friedman, G.C. Hartmann, H.W. Kendall and R. Verdier, Phys. Rev. D5, 528 (1972).

30) J.D. Bjorken, Current algebra at small distances, Varenna School Lectures XLI, Varenna, Italy, 1967.

31) R. Feynman, Phys. Rev. Letters 23, 1415 (1969).

32) E.D. Bloom and F.J. Gilman, Phys. Rev. D4, 2901 (1971).

33) J.D. Bjorken, Phys. Rev. D1, 1376 (1970).

34) T.F. Walsh and P. Zerwas, Report DESY 72/36 (1972).

35) See, for example, H.J. Behrend, F.W. Brasse, J. Gayler and J. May, Contribution to the Second ECFA Study Week on the 300 GeV CERN Accelerator, Tirrenia, Italy, 1972.

ELECTRON VERSUS MUON PHYSICS

F. Combley*) and E. Picasso
CERN, Geneva, Switzerland

1. INTRODUCTION

Many physicists have occupied themselves for many years with a search for differences between the electron and the muon. They have searched in vain, and by now we have become so accustomed to the similarity between these two particles that we are discussing which one to use as the electromagnetic probe of hadronic matter.

In Section 2 we occupy ourselves with this choice in terms of deep inelastic scattering, and then add some observations taking into account the boundary conditions that the proposed experimental facilities will impose.

Meanwhile, the muon-electron puzzle still remains, and Section 3 is devoted to an examination of the possibilities of its resolution at the new proton synchrotron.

Finally we list what seems to us to be the best ways of exploiting lepton beams at CERN Laboratory II.

2. LEPTON-PROTON INELASTIC SCATTERING

2.1 General considerations

We believe that one of the most interesting experiments to be done with a charged lepton beam at the 300 GeV Proton Synchrotron will be to establish if the scale invariance, predicted by Bjorken[1] and discovered experimentally in inelastic electron scattering at SLAC[2], will hold as one proceeds to even higher four-momentum transfer q^2 and higher energy losses ν, or if one enters a new region of physics with, eventually, its own characteristic scaling[3].

One would like to know if scale invariance holds in the individual reaction channels, and what the multiplicity and transverse momentum distributions look like as functions of q^2 and ν, in order to provide more stringent tests for the various theoretical models[4].

One would also like to examine the inelastic nucleon structure functions for both the proton and the neutron, particularly as recent SLAC measurements of the cross-section in hydrogen and deuterium targets have shown considerable differences[5].

Finally, one would like to search for polarization effects in deep inelastic scattering and test if the spin-dependent structure functions also obey scaling. If scaling does hold, perhaps some attempt can be made to differentiate between the various predictions of light cone algebra, resonance, and quark-parton models[6].

Although the muon remains a mystery and should be studied in its own right, we are now entering an era in which the highest energy beams of both muons and electrons have to be derived from protons, and so for the first time we have more muons than electrons. It is

---

*) Permanent address: Department of Physics, University of Sheffield, United Kingdom.

therefore natural to ask ourselves if a charged lepton-proton deep inelastic scattering experiment must be designed using an electron or a muon beam. We will attempt to answer this question by comparing these two possibilities in some detail before proceeding to discuss other experiments.

2.2 Kinematics

The diagram representing one-photon exchange in inelastic lepton-proton scattering is shown in Fig. 1. The kinematic quantities $\vec{p}_0$, E_0 are the laboratory momentum and energy of the incident lepton; $\vec{p}'$, E' are the laboratory momentum and energy of the scattered lepton; q is the laboratory four-momentum of the virtual photon; m_ℓ is the lepton mass, m_p the proton mass; and M^* is the invariant mass of the total hadronic system produced in the interaction.

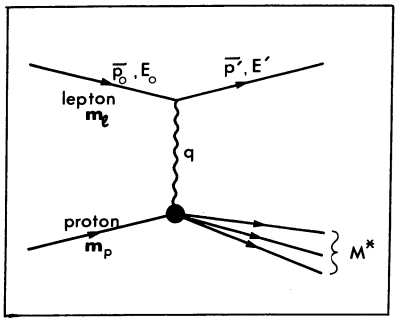

Fig. 1 Kinematical quantities for inelastic lepton-proton scattering (one-photon exchange).

The invariant q^2 is given by

$$q^2 = 4 E_0 E' \sin^2 (\theta/2) ,$$

where θ is the scattering angle in the laboratory frame. (We have assumed the condition $E_0 \gg m_\ell$ and set $m_\ell = 0$.)

The laboratory energy of the virtual photon is given by

$$\nu = E_0 - E'$$

and the total invariant mass of the final hadronic system by

$$M^{*2} = m_p^2 + 2m_p\nu - |q^2| .$$

Thus the choice of ν and q^2 determines M^*.

The double differential scattering cross-section is written in the standard form as

$$\frac{d^2\sigma}{d\Omega dE'} = \frac{\alpha^2}{4E^2 \sin^2 (\theta/2)} \left[W_2 \cot^2 (\theta/2) + 2 W_1\right] .$$

Generally the W's are functions of q^2 and ν. However, scale invariance requires that as ν and q^2 become large enough (Bjorken limit), W_1 and νW_2 depend only upon a single dimensionless variable $\omega = (2m_p\nu)/|q^2|$. As is well known, W_1 is proportional to the cross-section for virtual photons with transverse polarization, while W_2 is proportional to the sum of the cross-sections for both transverse and longitudinal polarization. Thus a separation of W_1 and W_2 is equivalent to a separation of these two cross-sections, and measurements at small q^2 permit the evaluation of $\sigma_{tot}(\gamma p)$ for real photons by extrapolation. To achieve this separation, one has to make measurements over an angular range which is sufficient to make use of the $\cot^2 (\theta/2)$ coefficient of W_2.

It should be remembered that all the analysis of deep inelastic scattering has been based on the assumption of one-photon exchange. Although no calculation of the two-photon contribution has been made, it is believed to be at the level of one or two per cent[7].

The calculations are far from simple; therefore one does not know the energy dependence of this higher-order contribution. It will be of interest to answer this query at high energies by, for example, comparing the deep inelastic cross-sections of leptons and antileptons on protons.

2.3 Comparison of experimental rates

In calculating the rates for experiments which as yet are not designed, it is necessary to make a number of simplifying assumptions. We started with muon and electron beams, which seem to be representative of what can be achieved. The electron beam is that described by the Stanford Group[8] (Hofstadter et al.) in the NAL proposal No. 164, and the muon beam is the one proposed by Aitken, Clifft and Gabathuler[9] in the ECFA Study Report. Both beams are more suitable for experiments in the North Area, and the relevant details are set out in Table 1.

Table 1

Lepton beams

Energy (GeV)		Intensity		
Proton	Lepton	Electron	Muon	
200	100	1.8×10^6	7×10^7	The proton beam has an intensity of 3×10^{12} ppp. The electron beam has $\Delta p/p \sim 2.5\%$, an area at the hydrogen target of 2.5×12.5 mm^2, and an over-all length of about 300 m. The muon beam has $\Delta p/p \sim 4\%$, an area at the hydrogen target of 50×100 mm^2, and an over-all length of about 1000 m. For the calculation of experimental rates a repetition frequency of 15 p/min is assumed for 200 GeV protons whilst for 400 GeV protons 8 p/min is taken. These rates are achieved with about 0.7 sec flat top.
400	100	6×10^7	2×10^8	
400	200	1.2×10^7	9×10^7	

Figure 2 indicates the relationship between the scattering angle and the variables q^2 and ν for incident lepton energies of 100 and 200 GeV. We have assumed that detectors can be built to cover all orientations of the scattering plane, although here there may be some difficulty with the NaI crystal electrons-shower counters. We have also assumed that the detectors which have to be placed in the muon beam can handle the rates indicated.

To accommodate the radiative corrections, the liquid-hydrogen target is 25 cm long in the electron experiment and 100 cm in the muon experiment.

The rates at which particles are scattered into bins measuring Δq^2 [= 1 (GeV/c)^2] by $\Delta\nu$ (= 1 GeV) have been calculated with the following approximate cross-section formula:

$$\frac{d^2\sigma}{d(q^2)d\nu} = \frac{4\pi\alpha^2}{q^4}\frac{E'}{E_0}\left(\frac{\nu W_2}{\nu}\right),$$

where in addition to the usual condition that $E_0 >> m_\ell$, it is assumed that $W_2 \cos^2(\theta/2) = W_2 >> W_1 \sin^2(\theta/2)$, and, for purposes of calculation, that $\nu W_2 = 0.3$.

The results of the calculation are shown in Fig. 3, where limiting curves are drawn for the six beams of Table 1. At these limiting curves the rate into the above-defined bin is one per hour. This bin size has been chosen merely for our convenience, and clearly the actual rate limit for a given experiment will depend upon its design.

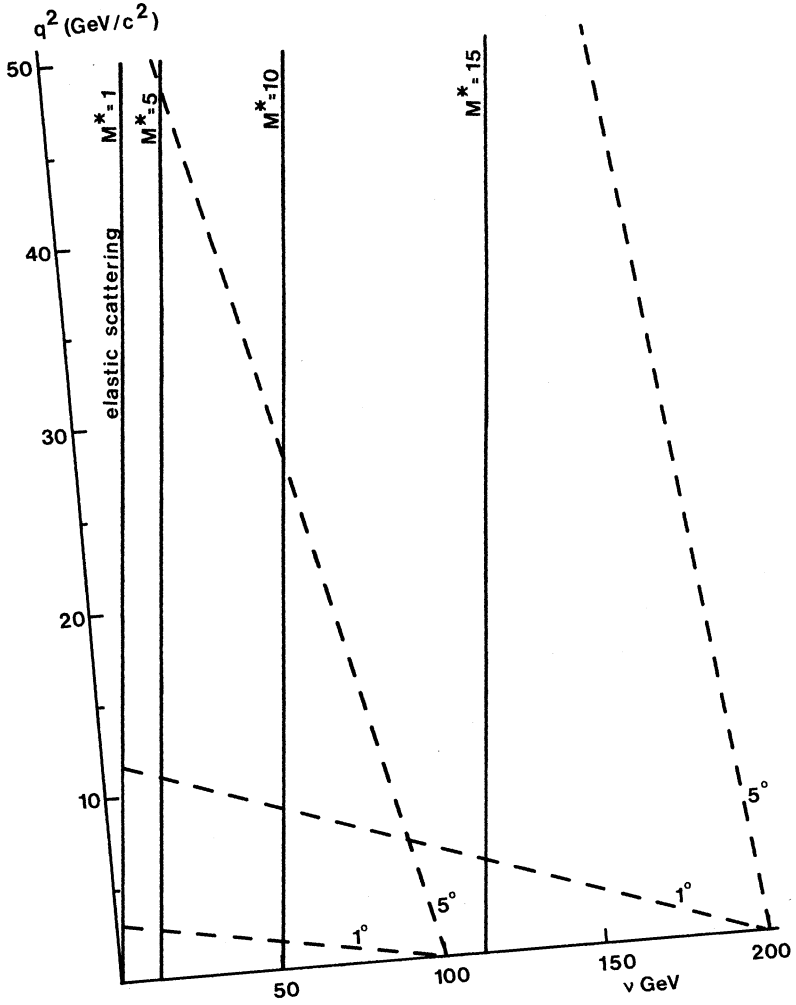

Fig. 2 Relationship between scattering angle and the variables q^2 and ν for E_0 = 100 and 200 GeV.

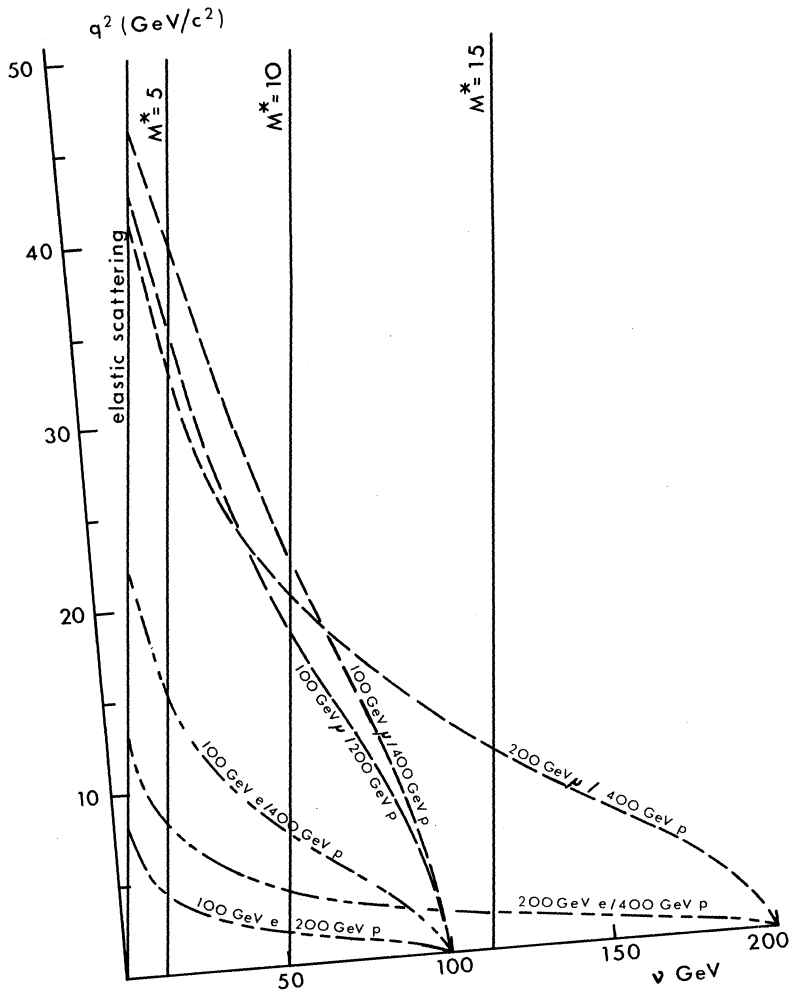

Fig. 3 Curves at which the rate drops to $(\Delta q^2 \times \Delta\nu)$ events per hour for each of the six beams given in Table 1.

From these curves we conclude that:

i) the muon beam will give access to a much larger area of the (q^2,ν) plane than will the electron beam;

ii) in order to appreciably extend the kinematical region at present covered by electron-proton scattering, it would be necessary to derive the 100 GeV electron beam from 400 GeV protons;

iii) a 100 GeV muon beam from 200 GeV protons would considerably extend the region at present covered by the SLAC electron experiments.

For comparison, the areas to be explored with electrons from the proposed Stanford Recirculating Linear Accelerator are shown in Fig. 4 [10]. In this case the rates are higher than those we have been discussing, the limit being equivalent to some 20 counts per hour into our bin size. A cut-off at this level has been found necessary at SLAC[10] in order to make radiative and other corrections, and the order of magnitude difference between the two lower limits has been considered reasonable in the light of the differences in duty cycle between the two machines and the fact that, as will be indicated below, we are really comparing electrons with muons for which the radiative corrections are generally smaller. From this comparison one is forced to conclude that even the 100 GeV electron beam from 400 GeV protons would add very little to this proposed kinematic region. Some improvement is obtained with 100 GeV muons from 200 GeV protons, but the strongest case is for a 400 GeV proton machine from which one would use 200 GeV muons.

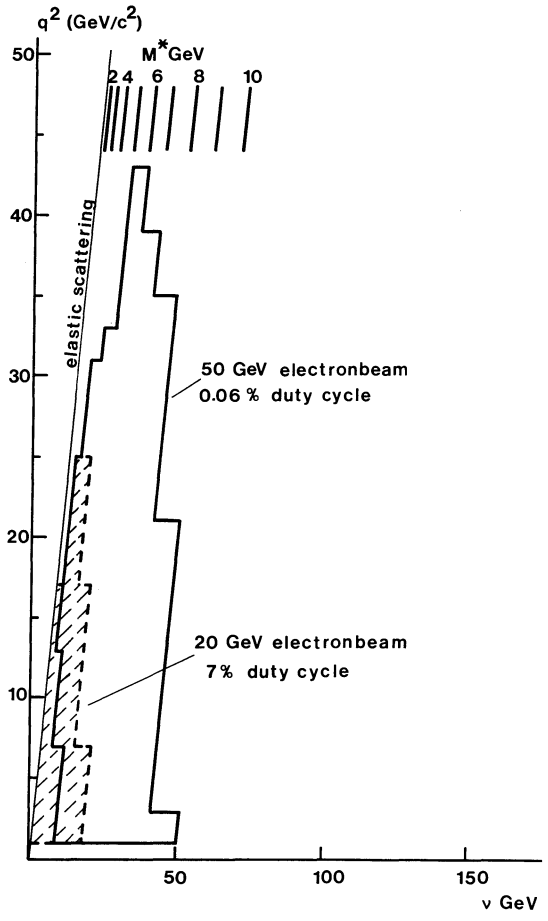

Fig. 4 Kinematical regions to be explored by the proposed Stanford Recirculating Linear Accelerator (Ref. 10).

2.4 Radiative corrections

The measured deep inelastic cross-section includes contributions from many high-order electromagnetic processes which represent an unwanted background. Theoretical analysis deals with one-photon exchange, and the experimental data are reduced to the cross-section for this process by a series of radiative corrections. The program for this reduction has been formulated in a detailed fashion[11], and here we recall only the outline, referring to the graphs of Fig. 5 where necessary.

Firstly, the measured cross-sections are corrected for the straggling of the particles in passing through the target both before and after scattering. This straggling is largely due to external bremsstrahlung, as energy loss by ionization is negligible in comparison.

This process is proportional to the square of the target thickness. Muon bremmstrahlung in the target is reduced by a factor $(m_e/m_\mu)^2$ compared with electrons.

Secondly, the cross-sections are corrected for internal bremsstrahlung; that is, emission in the same nuclear field as that of the scattering. This effect is proportional to target thickness and is roughly the same as that given by two radiators, one placed before the scattering and the other after, and each of thickness[11] given by

$$t_r = \frac{3}{4}(\alpha/\pi)\{\ln|q^2|/m_e^2) - 1\} \quad \text{radiation lengths} .$$

Thus with a target of $2t_r$ radiation lengths, the effects of straggling and internal bremsstrahlung on electrons are about the same. (This correction is represented by M7 and M8 in Fig. 5.) The muon electron ratio for this equivalent thickness is about 0.3 at a q^2 of 1 $(GeV/c)^2$ and 0.5 at a q^2 of 100 $(GeV/c)^2$.

A third correction is that originally calculated by Schwinger[12]; it contains vertex (M5) and photon propagator (M4) modifications together with some soft photon parts of diagrams M7 to M10.

Finally, the radiative tail for elastic scattering is subtracted from the cross-section. For lepton-proton scattering at energies of several GeV, only the elastic peak requires special treatment while the resonance region can be treated in the same way as the continuum.

The fully corrected cross-sections are then used to make the structure function separation and theoretical comparison.

The radiative corrections depend upon the experimental configuration, and it should be emphasized that experiments must be planned such that these calculations can be performed in a reliable manner.

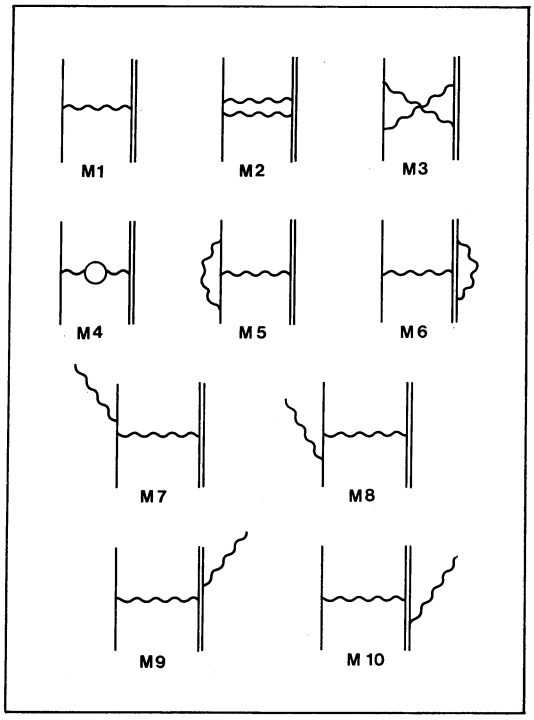

Fig. 5 Radiative corrections to lepton-proton scattering (after Ref. 19).

Drees and Leenen[13] have recently calculated the radiative corrections for inelastic electron and muon scattering off protons, assuming that only the scattered lepton is detected. Analogous calculations have been done by Hofstadter and collaborators[8]. Figure 6 is taken from the work of Drees and Leenen and shows the ratio $(d^2\sigma/d\Omega dE')_{\text{non-rad.}}/d^2\sigma/d\Omega dE')_{\text{meas.}}$ for e-p and μ-p scattering at a primary energy of 100 GeV. From this work one can see that over a large range the corrections for muon scattering are much less than those for electron scattering. However, taking a 30% correction as the limit of what is acceptable, one sees that in going from electrons to muons the range of M^* which can be explored is only extended from about 11 to 12 GeV. For 200 GeV primary energy these authors indicate that, for the same limits of 30% correction, the gain is only from 16 to 17 GeV.

In conclusion one can say that in spite of this limited gain in the useful kinematic region, the smallness of the correction for muons favours the use of this particle in deep inelastic scattering.

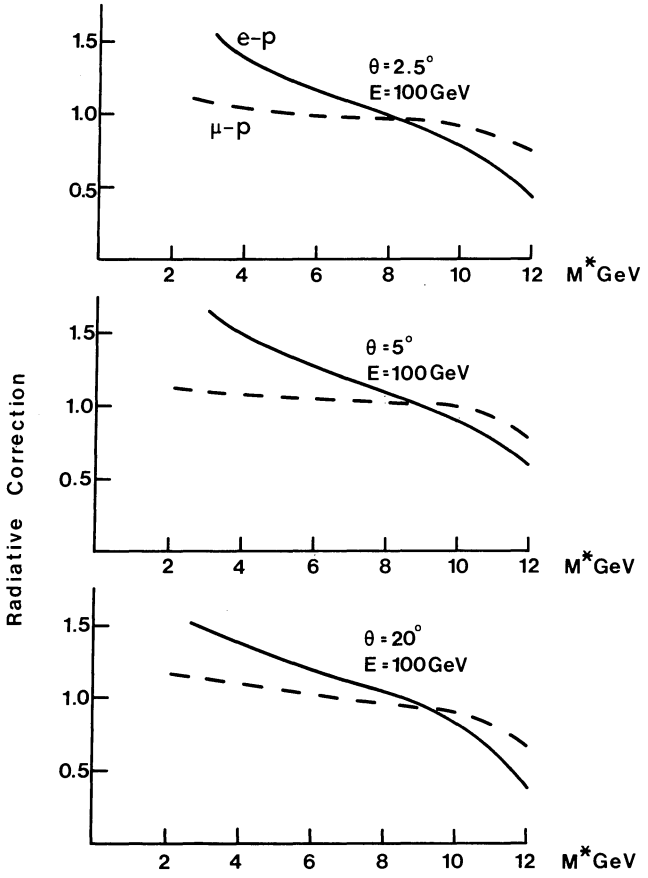

Fig. 6 The ratio $(d^2\sigma/d\Omega E')_{meas.}$ for e-p and μ-p scattering at a primary energy of 100 GeV (Ref. 13)

2.5 Lepton and photon physics in the West Area

An electron beam provides a method for producing real and virtual photon beams with which to make a detailed study of the electromagnetic interaction of γ-rays with nucleons or nuclear matter.

A real photon beam is produced by bremsstrahlung either in an amorphous target or in a crystal one. The last method, as is very well known, provides beams of almost monochromatic, linearly polarized photons.

Lepton scattering can be considered in terms of the cross-section for absorption of virtual photons. This cross-section can be examined over a large kinematical range by varying the virtual photon mass q^2 and energy ν. The virtual photons are polarized in longitudinal and transverse directions, and the ratio of these two polarizations (ε = longitudinal over transverse) is given by

$$\varepsilon = \left[1 + 2\,\mathrm{tg}^2\,\frac{\theta}{2}\left(1 + \frac{\nu^2}{q^2}\right)\right]^{-1} .$$

These beams, real and virtual photons, enable one to study inclusive and exclusive reactions. The use of polarized lepton beams on polarized targets enables one to unravel the various helicity amplitudes for off-mass-shell photon scattering. For example, the forward scattering of polarized muons provides a beam of almost real ($q^2 \to 0$) completely circularly polarized photons. If the target nucleons are polarized parallel and anti-parallel to the beam direction, then one has a means of checking the Drell-Hearn-Gerasimov sum rule[14].

Such a facility seems ideally suited to the West Area: in fact an electron beam of about 10^7 e/pulse at 80 GeV, from 200 GeV protons, has been designed[15].

The Omega spectrometer, together with the long spill of the proton machine, should allow a detailed study of exclusive reactions to be made. In the event of the SLAC recirculating program going forward, this electron-photon facility still maintains its importance as a means of exploring exclusive channels in inelastic scattering.

A muon beam to the West Area would have to be of low energy ($\gtrsim$ 20 GeV) because of the restriction in decay length[15]. With such a beam one could perform experiments on polarization effects in exclusive reactions, and marginally extend the present muon-deep inelastic scattering. We feel, however, that this beam could be exploited only in a limited way, while the electron-beam provides us with an electron-photon facility.

3. MUON-ELECTRON UNIVERSALITY AND THE SEARCH FOR HEAVY LEPTONS

In spite of the extensive similarity between the muon and the electron, these two particles differ in two fundamental respects: first the muon mass is about 200 times that of the electron mass; secondly, they have different internal quantum numbers (lepton numbers) which are separately conserved in all interactions. The special relationship between these two particles is summarized in the principle of 'muon-electron universality'. One can say that the muon and the electron behave in the same way in all interactions under the equivalence

$$\mu^-(\mu^+) \leftrightarrow e^-(e^+)$$

and

$$\nu_\mu(\bar{\nu}_\mu) \leftrightarrow \nu_e(\bar{\nu}_e) \ .$$

One aspect of this universality is the belief that both the muon and the electron are point-like (Dirac) particles. In saying this, one neglects some higher-order terms in quantum electrodynamics which lead to effects similar to those of a non-zero dimension for these fermions, but in any case one does not consider that these effects represent an intrinsic particle size. In other words, our belief in the point-like nature of the leptons is related to the fact that they do not interact strongly.

Among the tests of muon-electron universality one can mention: the equality of their electric charge [$e_\mu/e_e = 1 \pm (1 \times 10^{-13})$] [16]; the fact that the gyromagnetic ratio of the electron and the muon can be calculated exactly from quantum electrodynamics and the only differences are those attributed to their mass difference[17]; the equality of the cross-sections for charged lepton-proton elastic scattering[18]; the fact that all high-energy tests performed at colliding beams ($e^+e^- \to e^+e^-$, $e^+e^- \to \mu^+\mu^-$) agree with the predictions

of QED; the fact that the Bethe-Heitler processes [wide-angle electron (muon) bremsstrahlung, electron (muon) tridents, electron (muon) pair production] follow QED[17]; and, finally, the equality of the charged lepton-proton inelastic scattering cross-sections[19]. One of the advantages of this latter is that the test of muon-electron universality is extended to a larger kinematic region in which ν and q^2 can be varied independently ($\nu > q^2/2m_p$). Moreover, if a violation of this principle involves hadrons, it would be detected more readily in inelastic scattering where no restrictions are placed on the nature of the final hadronic state. Furthermore, inelastic scattering is more sensitive to lepton form factors at higher values of q^2, owing to the larger cross-section compared to that for elastic scattering.

The test carried out at electron-positron colliding beams consists of examining the process

$$e^+ + e^- \rightarrow \mu^\pm + \mu^\mp ,$$

and the results have shown that the muon behaves like a heavy electron in the integrated time-like range of q^2 from 2.56 to 4.0 $(\mathrm{GeV/c})^2$ [20a]. If this result is taken in conjunction with that from experiments on the process

$$e^+ + e^- \rightarrow e^\pm + e^\mp$$

which effectively explores the space-like region of four-momentum transfer [at present from -0.38 to -3.4 $(\mathrm{GeV/c})^2$] [20b], we see that the crossing symmetry of quantum electrodynamics is checked at the level of ±2%. This serves to illustrate the general point that many tests of μ-e equivalence are also searches for breakdown in quantum electrodynamics.

The continuation of these experiments with 3 GeV colliding beams at DESY and SPEAR will extend the time-like limit of the region in which μ-e universality is tested by a factor of 6 or so, while the lepton-proton scattering experiments at CERN Lab. II could similarly extend the limit in the space-like region. Thus we have the possibility of comparing these two leptons over a very large range of both space-like and time-like four-momentum transfer in an effort to find the hole in the principle of μ-e universality.

3.1 Lepton bremsstrahlung

The process

$$\ell + p \rightarrow \ell + p + \gamma \qquad \text{(see Fig. 7)}$$

should be studied at CERN Lab. II because it may reveal a breakdown of QED for either time-like or space-like lepton propagators (Figs. 7a and 7b, respectively).

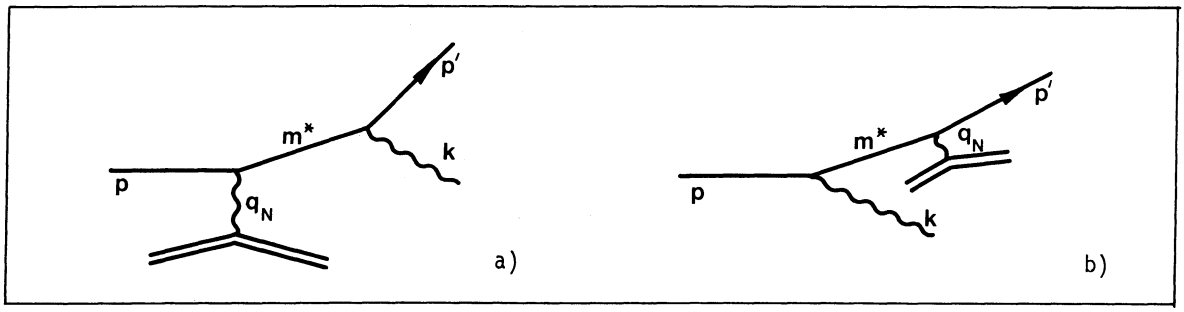

Fig. 7 Time-like (a) and space-like (b) virtual leptons in lepton bremsstrahlung

The wide-angle bremsstrahlung cross-section is roughly given by[21]

$$\sigma \sim \frac{1}{q_N^4}\left(\frac{1}{m^{*2} - m_\ell^2}\right)^2 ,$$

where q_N is the momentum transfer to the target nucleus. This momentum transfer has a minimum value given by

$$\left(q_N^2\right)_{min} = \left[\frac{m^{*2} - m_\ell^2}{2E_0}\right]^2$$

when the virtual lepton is collinear with the incident one in the time-like case, or with the outgoing one in the space-like case. This dependence on the incident energy means that the experimental rate obtainable at CERN Lab. II will be increased compared with that for experiments previously planned at around 10 GeV [17]. Typically, with a 100 GeV lepton beam the minimum value of $q_N^2 \sim 0.002$ $(GeV/c)^2$ for $m^* \sim 3$ GeV/c^2. It would be convenient to perform the experiment concurrently with the deep inelastic scattering. On the other hand, the effective rate depends upon the factor $Z^2\rho L/A$, where Z is the nuclear charge, A the atomic number, ρ the density, and L the thickness of the target. In order that the bremsstrahlung photons can emerge with high probability, the target thickness is limited (for example, one radiation length gives about 69% probability of emission without showering). Assuming the 100 GeV muon beam of Table 1, one can estimate the minimum cross-section to which the experiment would be sensitive. For one radiation length of carbon and 10 events per 10% bins in $\Delta m^*/m^*$, one can reach

$$\sigma_{min} \sim 10^{-36} \text{ cm}^2 ,$$

with 100 hours running.

Assuming a $(1/m^*)^4$ dependence of the cross-section, one could effectively explore up to virtual lepton masses of about 8 GeV/c^2 [22]. One should add that in such an experiment, background processes such as nuclear Compton effect, lepton-nucleon scattering, and inelastic bremsstrahlung require serious attention; and furthermore, that in order to perform this experiment at all with a muon beam the halo would have to be reduced well below the 20% figure given in the ECFA study report[9].

We would like to emphasize that lepton bremsstrahlung can clearly show the existence of heavy leptons of the type

$$\ell^* \rightarrow \ell + \gamma,$$

where the signal from this decay appears as a peak on the invariant mass spectrum.

3.2 Lepton tridents

The lepton production of lepton pairs in the Coulomb field of the nucleus is sensitive to a breakdown of QED in all possible channels: the lepton vertex (two real leptons); the lepton vertex (one real and one virtual lepton); the lepton propagator; and the photon propagator (see Fig. 8).

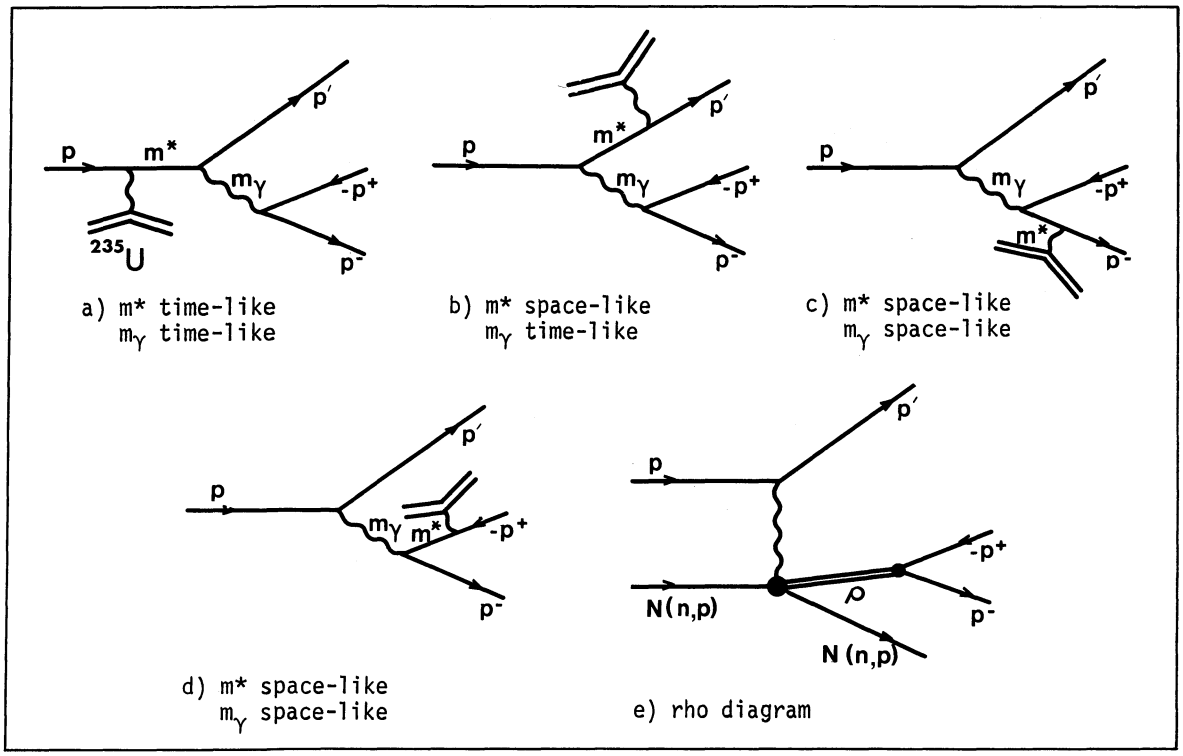

Fig. 8 Diagrams for lepton trident production on ^{235}U

In particular the muon trident experiment, which is a cheap type of muon colliding beam, provides a unique way of studying the muon-muon interaction at high energies. It is conceivable that an anomalous interaction of the muon could only appear in such a process. In other words, the muon could be coupled to the muon pair not only by exchange of a photon but also by the exchange of a heavy neutral boson.

Recently, Kessler and Coll[23] have computed comprehensively the muon trident differential cross-section for the process

$$\mu^- + {}^{235}U \rightarrow \mu^- + \mu^+\mu^- + \text{hadrons}$$

considering coherent and *all* incoherent types of scattering for the diagrams shown in Fig. 8. Figures 9 and 10 show the behaviour of the differential cross-section $d\sigma/dm_\gamma$ as function of the invariant mass of the muon pair (m_γ), for incident muon energies of 30 and 200 GeV, respectively. From a comparison of these two figures one sees that the contribution of the diagrams (e) and (c + d) is not strongly energy-dependent, while that of the diagrams (a + b) changes considerably from 30 to 200 GeV particularly at large m_γ where it dominates the cross-section. In the case of 200 GeV muons the cross-section decreases such that at m_γ = 12 GeV/c^2 it is 10^{-33} cm^2 while at 16 GeV/c^2 it is 10^{-34} cm^2.

The size of the cross-section encourages one to examine carefully the possibility of performing a trident experiment with 200 GeV muons. Any discrepancies at large invariant masses of the muon pair could be checked against an experiment on the process

$$e^- + {}^{235}U \rightarrow e^- + \mu^+\mu^- + \text{hadrons} .$$

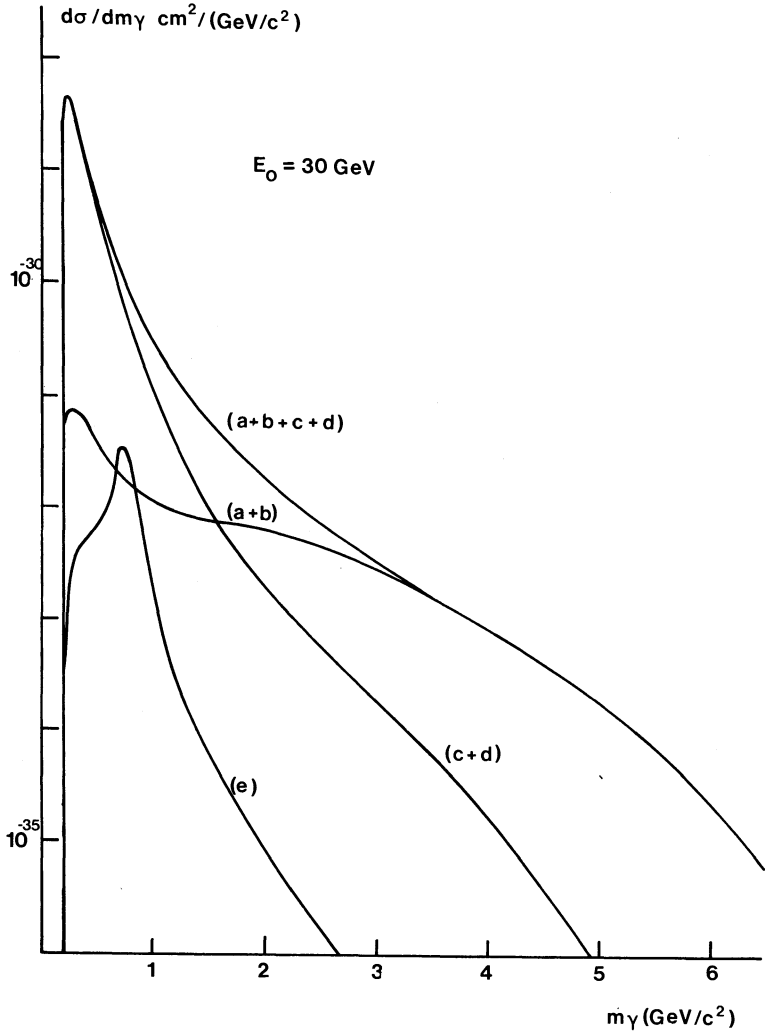

Fig. 9

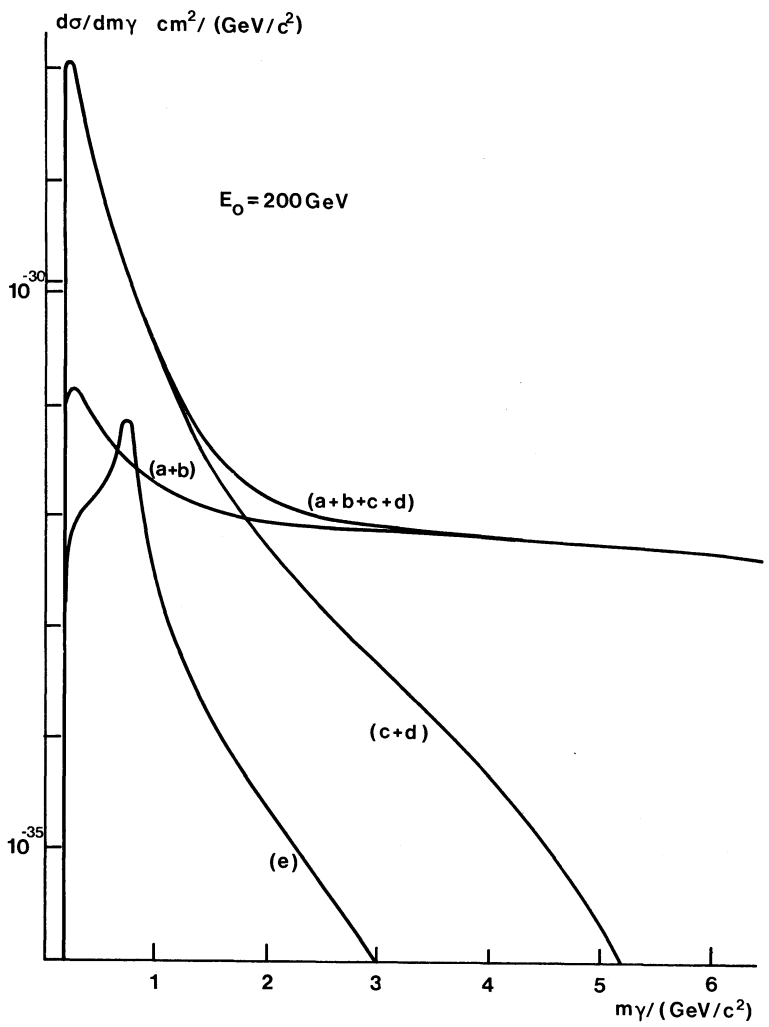

Fig. 10

Muon trident production cross-section as a function of the invariant mass of the muon pair for primary energies of 30 GeV (Fig. 9) and 200 GeV (Fig. 10). (The small letters attached to the curves indicate the relevant diagrams in Fig. 8.) (Ref. 23.)

3.3 Search for heavy leptons

One way out of the muon-electron puzzle is to avoid it and, in view of the large families of particles which exist in hadron physics, to ask instead if the charged lepton family is really restricted to just two members. There is no guarantee, of course, that this question will be any easier to answer than the original one.

In the realm of heavy leptons there are two principal possibilities:

a) Sequential leptons of which the electron and muon are the first two. Each member of the sequence has its own neutrino with which it shares a unique lepton number which is separately conserved in strong, electromagnetic, and weak interactions.

b) Excited leptons with the electron and muon as ground-state members. These excited leptons have the same lepton number as the electron or muon, and decay electromagnetically as

$$e^{*\pm} \to e^{\pm} + \gamma$$

and

$$\mu^{*\pm} \to \mu^{\pm} + \gamma \ .$$

Other speculations are possible[24], including the existence of either stable or very long-lived heavy leptons as suggested by Gerstein and collaborators[25].

It should be made clear at the outset that a high-energy lepton or photon beam is not necessarily the best way of producing heavy leptons. However, we start by considering two such possibilities.

3.3.1 Photon-nucleon collisions (Fig. 11)

Either real or virtual photons could provide a mechanism for heavy lepton production. In the case of point-like particles with unit charge, the photoproduction cross-section for pairs has been calculated most recently by Kim and Tsai[26]. In Fig. 12 the total cross-section for the following processes is shown.

a) Coherent production off the nucleus as a whole:

$$\gamma + \text{Nucleus} \to \ell^+\ell^- + \text{Nucleus} \ .$$

b) Quasi-elastic production off protons or neutrons in the nucleus:

$$\gamma + p,n \to \ell^+\ell^- + p,n \ .$$

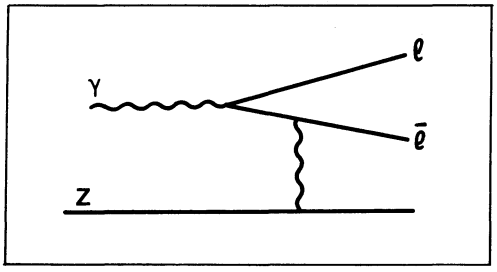

Fig. 11 Heavy lepton pair photoproduction off nuclei.

c) Inelastic production off protons or neutrons in the nucleus:

$$\gamma + p,n \to \ell^+\ell^- + \text{free nucleon} + \text{hadrons} \ .$$

This latter gives a negligible contribution.

The cross-section for the production of one lepton at an angle θ with momentum p, summed over all the allowed momenta and angles of the other lepton and over all hadronic final states, is given by

$$\frac{d^2\sigma}{d\Omega dp} = \frac{2\alpha^3}{\pi k}\left(\frac{E^2}{m_\ell^4}\right)\left[\frac{2x(x-1)+1}{(1+r)^2} + \frac{4x(1-x)r}{(1+r)^4}\right]\chi$$

where k is the photon energy, m_ℓ the lepton mass, E the lepton energy, $x = E/k$, $r = (E/m_\ell)^2\,\theta^2$, and χ is a function of the minimum four-momentum transfer to the hadronic vertex and of the form factor of that vertex. For small θ and $r \ll 1$ the cross-section is roughly proportional to $(1/m_\ell)^4$, which means that at forward angles the production of heavy leptons is suppressed compared to that of electrons and muons. At large angles with $\theta E \gtrsim m_\ell$, then $r \geq 1$ and the cross-section becomes independent of m_ℓ except for the term χ. Thus one can say that in this region all leptons are produced with roughly equal probability.

Owing to their relatively high masses, the heavy leptons will have short lifetimes and will have to be studied through their decay modes. A further difficulty is the fact that at high energies the total cross-section for the photoproduction of hadrons will be in the region of 10^4 to 10^8 times that for heavy lepton production.

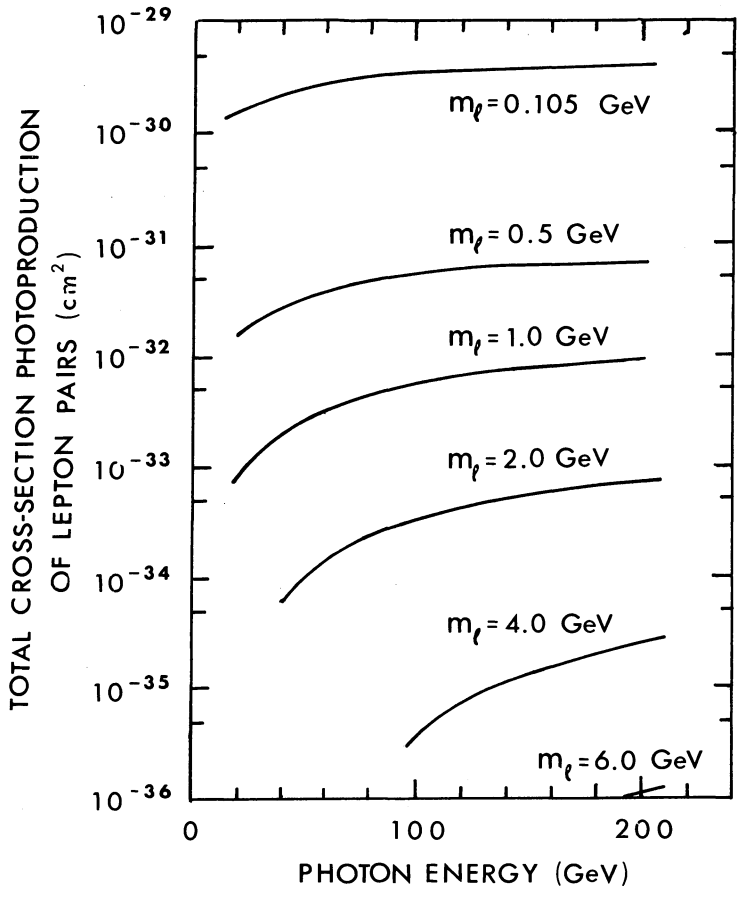

Fig. 12 Total cross-sections for photoproduction of heavy lepton pairs of various masses as a function of incident photon energy (Ref. 26)

3.3.2 Lepton-proton or lepton-nucleus collisions

In this method one searches for excited leptons produced in the reactions

$$e + p \rightarrow e^* + p$$

or

$$\mu + p \rightarrow \mu^* + p$$

with the subsequent decay mentioned earlier. The strength of this special interaction relative to the electromagnetic interaction is written as a dimensionless parameter λ, with the cross-section proportional to λ^2.

Past searches carried out at Orsay[27], DESY[28], and CEA[29] have found no excited leptons for masses up to 0.5 GeV/c^2.

We recall that the minimum four-momentum transfer to the proton is given by

$$(q^2)_{min} \sim \frac{m^{*4}}{(2E_0)^2}$$

and as $(q^2)_{min}$ increases, the form factors at the proton vertex lead to a rapid fall-off in sensitivity.

A variation of this method has been discussed above, and consists of looking for a peak in the invariant mass (m^*) distribution for lepton bremsstrahlung:

$$e,\mu + \text{nucleus} \rightarrow \underbrace{e,\mu + \gamma}_{m^*} + \text{nucleus} .$$

A further possibility is to search for heavy leptons in inelastic scattering, i.e.

$$e + p \rightarrow e^* + p$$

with $e^* \rightarrow e$ + other particles

or

$$e + p \rightarrow e^* + \text{hadrons}$$

with $e^* \rightarrow e$ + other particles .

Therefore a comparison of e-p and μ-p inelastic scattering could also be used as a search for heavy leptons, and this has been discussed at some length by Perl[24].

Let us now look briefly at some methods of searching for heavy leptons, as alternatives to those using high-energy photon or lepton beams at CERN Lab. II.

3.3.3 Electron-positron colliding beams

This facility provides for direct production via

$$e^+ + e^- \rightarrow \ell^+ + \ell^- .$$

Again under the assumption of point-like particles with unit charge, the cross-section is given by

$$\sigma = \frac{\pi\alpha^2}{2E^2}\beta\left(1 - \frac{\beta^2}{3}\right)$$

where E is the energy of the electron or positron and β the velocity of the heavy lepton $[\beta^2 = 1 - (m_\ell/E)^2]$.

One should note that production via the two-photon process[30]

$$e^+ + e^- \rightarrow e^+ + e^- + \ell^+ + \ell^-$$

could also become appreciable through the logarithmic dependence on the centre-of-mass energy of the cross-section, i.e.

$$\sigma \propto \frac{1}{m_\ell^2} \ln\left(\frac{E}{m_\ell}\right) \ln^2\left(\frac{E}{m_e}\right) .$$

However, this process is strongly peaked at forward angles and thus its contribution may be severely reduced by the experimental limitations.

Given that the colliding beams have sufficient energy, they seem to provide the best method for a heavy lepton search. The present results from Adone[31] have shown no heavy excited leptons with masses in the range 0.2 to 0.8 GeV/c^2. At SPEAR the initial maximum energy in each beam will be 2.5 GeV with a luminosity of 5×10^{31} (events/cm^2 sec). A later increase of the beam energy to 4 or 4.5 GeV will further extend the range of heavy lepton masses which are accessible to this device. For direct production of heavy leptons of mass 1.5 GeV/c^2, and taking into account all the experimental factors[24], the cross-section is given for $E >> m_\ell$ by

$$\sigma \sim 4 \times 10^{-2}\ \sigma(e^-e^+ \rightarrow \mu^-\mu^+) \sim \frac{8 \times 10^{-34}}{E^2}\ \text{cm}^2 .$$

Thus to get four events per hour a luminosity of about $(E^2) \times 10^{30}$ events/cm^2 sec is required.

The search for excited leptons with colliding beams is difficult, as there are backgrounds which can simulate the desired signal (e.g. $e^+e^- \rightarrow e^+e^-\gamma$; $e^+e^- \rightarrow e^+e^-e^+e^-$), and no other decay modes which can confirm the existence of the e^* or μ^*.

3.3.4 Proton-proton and proton-nucleus collisions (see Fig. 13)

The muon pair spectrum from the reaction

$$p + \text{Nucleus} \rightarrow \mu^+ + \mu^- + \text{hadrons}$$

has been measured by Christenson and collaborators[32]. Speculative theories[33] can be used to give a fit to these data and make predictions for electron, muon, and heavy lepton pair production at higher energies. Berman and collaborators[34] predict a total cross-section for the reaction

$$p + p \rightarrow \ell^+ + \ell^- \text{ hadrons}$$

by means of the Drell-Yan model[33]. One-parton-antiparton pair annihilates to form the heavy lepton pair (see Fig. 14). For energies sufficiently above the production threshold, the cross-section for this

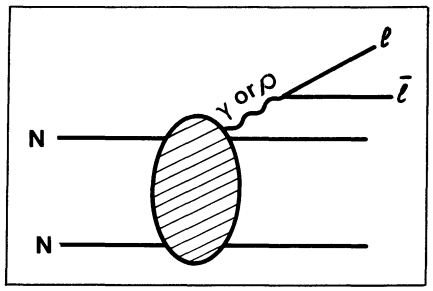

Fig. 13 Heavy lepton pair production via nucleon-nucleon collisions

process goes roughly like

$$\sigma \sim \frac{\alpha^2}{m_\ell^2} F ,$$

where α^2/m_ℓ^2 gives the cross-section for parton-antiparton into lepton-antilepton, and F is the probability that a parton in one proton and an antiparton in the other have the momentum that is necessary to create the heavy lepton pair. For a heavy lepton mass of about 10 GeV/c^2 one obtains a cross-section of about 10^{-34} F cm^2, and F is expected to be much less than unit (perhaps 10^{-2}-10^{-4}). For a luminosity in the ISR of, say, 10^{30} events per cm^2 sec, one would expect 0.4 F pairs per hour for heavy leptons with mass 10 GeV/c^2, and a luminosity of 10^{32}/cm^2 sec would make a search at the ISR well worth while. It seems that the ISR will either provide evidence for the existence of heavy leptons, or at least put limits on the cross-section which will give a guide as to where to look for them in the future. In this case, as for other low cross-section reactions, there is a possibility that improved luminosity at the ISR will reveal exciting new phenomena.

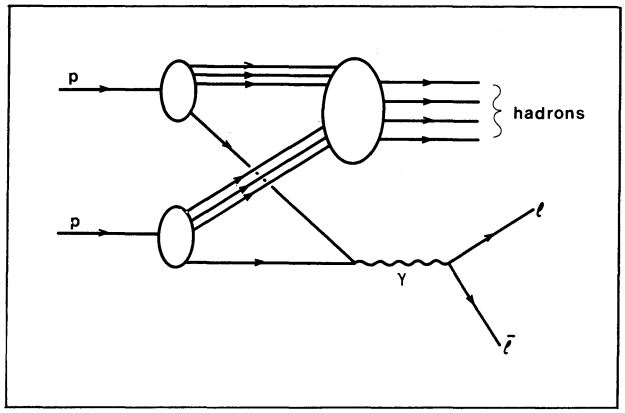

Fig. 14 Lepton pair production via parton-parton annihilation (Refs. 33 and 34).

Meanwhile, what of the CERN Lab. II PS? Let us just say that a beam of 10^{12} protons per sec on a 1 m hydrogen target would produce about 10^6 F heavy lepton pairs per hour for a mass of 10 GeV/c^2, if you know how to look for them.

4. CONCLUSIONS AND COMMENTS

i) The most important experiment to be planned at the CERN Lab. II with lepton beams is the deep inelastic lepton-proton scattering. One would like to see this experiment carried out with both electrons and muons. On the other hand, for reasons of intensity, radiative corrections, and the feeling that the muon is more likely to produce surprises, one would like to see the first experiment performed with muons. Such a beam obviously provides the possibility of also looking for polarization-dependent effects in the deep inelastic region. As a consequence of the rate required and the extensive kinematical region which can be explored, one would like to push most urgently for 400 GeV protons and to accelerate the construction of a muon beam in the North Area.

ii) Another important area to examine is the comparison of real and virtual photoproduction. This can be achieved with a combined electron beam and tagged photon facility. Such a facility, operating in the energy range 20 to 100 GeV, can be constructed in the West Area where the Omega spectrometer is available. We have preferred this to the alternative of studying polarization effects in exclusive reactions with a muon beam of around 20 GeV, on the assumption that the inclusive area will be covered by the SLAC single-arm experiment on a polarized electron beam.

iii) A third area which has to be considered is that of muon-electron universality, and this requires both muon and electron beams at higher energies (North Area). This

requirement is reinforced when one includes the necessity of high-energy photoproduction experiments.

Finally, we would like to add a few comments.

a) For the first time one can experiment with an extremely high value of the Lorentz factor (for $E_e \sim 200$ GeV, $\gamma_L \sim 400{,}000$). It would be surprising if Nature is so boring that it includes no phenomena with a high order dependence on γ_L.

b) It would also be surprising if, at these high energies, the extended life-times of unstable particles did not reveal further information. For example, a muon of 200 GeV will live for about 4 msec; then we will be in the same position with respect to observing it in the rest frame as would be a doctor who had a year in which to observe his patient rather than a mere four hours or so.

c) We hope that once experiments get under way at CERN Lab. II then all that we have discussed here will be made to look rather pedantic.

Acknowledgements

We would like to express our thanks to J. Drees, P. Kessler and D. Treille for helpful discussions and communication of unpublished results.

* * *

REFERENCES

1) J.D. Bjorken, Phys. Rev. 179, 1547 (1969).

2) E.D. Bloom, D.H. Coward, H. DeStaebler, J. Drees, G. Miller, L.W. Mo, R.E. Taylor, M. Breidenbach, J.I. Friedman, G.C. Hartmann and H.W. Kendall, Phys. Rev. Letters 23, 930 (1969).
M. Breidenbach, J.I. Friedman, H.W. Kendall, E.D. Bloom, D.H. Coward, H. DeStaebler, J. Drees, L.W. Mo and R.E. Taylor, Phys. Rev. Letters 23, 935 (1969). (For a recent review, see Ref. 5).

3) T.D. Lee, Physics Today, April 1972, p. 23.

4) J.D. Bjorken, Proc. Int. Symposium on Electron and Photon Interactions at High Energies, Ithaca, 1971 (Cornell University, Ithaca, 1972), p. 282.

5) H.W. Kendall, Proc. Int. Symposium on Electron and Photon Interactions at High Energies, Ithaca, 1971 (Cornell University, Ithaca, 1972), p. 248.

6) See, for example, T.F. Walsh and P. Zerwas, Report DESY 72/36, April 1972.

7) J.G. Rutherglen, Proc. 4th Int. Symposium on Electron and Photon Interactions at High Energies, Daresbury, 1969 (DNPL, Daresbury, 1969), p. 163.

8) J.F. Crawford, Z.G.T. Guiragossian, R. Hofstadter, E.B. Hughes, R.E. Rand, R.F. Schilling, M.R. Yearian, E.V. Hungerford III, G.S. Mutchler, G.C. Phillips and B.W. Mayes, NAL Proposal 164 (unpublished).

9) T.W. Aitken, R.W. Clifft and E. Gabathuler, CERN/ECFA/72/4 (1972), Vol. 1, p. 208.

10) Description and physics program of the proposed recirculating linear accelerator, prepared by the staff of the Stanford Linear Accelerator Center, Stanford University, SLAC 139 (Revised) February 1972.

11) Y.S. Tsai, SLAC-PUB-848, January 1971.
L.W. Mo and Y.S. Tsai, Rev. Mod. Phys. 41, 205 (1969).

12) J. Schwinger, Phys. Rev. 76, 760 (1949).

13) J. Drees and M. Leenen, CERN/ECFA/72/4 (1972), Vol. 1, p. 237.

14) S.B. Gerasimov, Yadernaya Fiz. 2, 598 (1965) [English Trans. Soviet J. Nuclear Phys. 2, 430 (1966)].
S.D. Drell and A.C. Hearn, Phys. Rev. Letters 16, 908 (1966).

15) ECFA -- 300 GeV Working group reports, CERN/ECFA/72/4 (1972), Vol. 1.

16) J. Bernstein, M. Ruderman and G. Feinberg, Phys. Rev. 132, 1227 (1963).

17) B.E. Lautrup, A. Peterman and E. de Rafael, Physics Reports, Vol. 3c, No. 4, May/June 1972.

18) L. Camilleri, J.H. Christenson, M. Kramer, L.M. Lederman, Y. Nagashima and T. Yamanouchi, Phys. Rev. Letters 23, 153 (1969).

19) T.J. Braunstein, W.L. Lakin, F. Martin, M.L. Perl, W.T. Toner and T.F. Zipf, Phys. Rev. D6, 106 (1972).

20) a) B. Borgia, F. Ceradini, M. Conversi, L. Paoluzi, R. Santonico, G. Barbiellini, M. Grilli, P. Spillantini, R. Visentin and F. Grianti, Nuovo Cimento Letters 3, 115 (1972).
b) B. Borgia, F. Ceradini, M. Conversi, L. Paoluzi, W. Scandale, G. Barbiellini, M. Grilli, P. Spillantini, R. Visentin and A. Mullachiè, Phys. Letters 35 B, 340 (1971).

21) L.M. Lederman and M.J. Tannenbaum, Advances in particle physics (Interscience, New York, 1968), Vol. 1, p. 1.

22) K.W. Chen, NAL Summer Study 4, 123 (1969).

23) P. Kessler, Private communication, to be published.

24) M.L. Perl, Paper presented at the Seminar on the μ-e problem, Moscow, September 1972 (SLAC-PUB-1062, July 1972).

25) S.S. Gerstein, L.S. Landsberg and V.N. Folomeshkin, Report IFVE 71-54, Serpukhov, 1971.

26) K.J. Kim and Y.S. Tsai, SLAC-PUB-1030 (1972).

27) C. Betourne, H. Nguyen Ngoc, J. Perez Y Jorba and J. Tran Thanh Van, Phys. Letters 17, 70 (1965).

28) H.J. Behrend, F.W. Brasse, J. Engler, E. Ganssauge, H. Hultschig, S. Galster, G. Hartwig and H. Schopper, Phys. Rev. Letters 15, 900 (1965).

29) R. Budnitz, J.R. Dunning, Jr., M. Goitein, N.F. Ramsey, J.K. Walker and R. Wilson, Phys. Rev. 141, 1313 (1966).
C.D. Boly, J.E. Elias, J.I. Friedman, G.C. Hartmann, H.W. Kendall, P.N. Kirk, M.R. Sogard, L.P. Van Speybroeck and J.K. de Pagter, Phys. Rev. 167, 1275 (1968).

30) M. Greco, Frascati Report LNF-71/1, January 1971.
S.J. Brodsky, T. Kinoshita and H. Terazawa, Phys. Rev. Letters 25, 972 (1970).

31) V. Alles-Borelli, M. Bernardini, D. Bollini, P.L. Brunini, T. Massam, L. Monari, F. Palmonari and A. Zichichi, Nuovo Cimento Letters 4, 1156 (1970).

32) J.H. Christenson, G.S. Hicks, L.M. Lederman, P.J. Limon, B.G. Pope and E. Zavattini, Phys. Rev. Letters 25, 1523 (1970).

33) S.D. Drell and T.M. Yan, Phys. Rev. Letters 25, 316 (1970).

34) S.M. Berman, J.D. Bjorken and J.B. Kogut, Phys. Rev. D4, 3388 (1971).

COMMENTS ON e, μ, AND PHOTON SESSIONS

G. Barbiellini
Laboratori Nazionali del CNEN, Frascati, Italy

J. Drees
Physikalisches Institut der Universität, Bonn, Germany

At the second ECFA Study Week on the 300 GeV CERN Accelerator, the results of the Working Party on μ, e, and γ beams were presented by two speakers: F.W. Brasse summarized and discussed the results on μ beams, and G. Barbiellini the results on e and γ beams.

As shown by Brasse, considerable progress has been made in designing a high intensity μ beam of small size. The following groups were involved in this work:

Aitken, Clifft, Gabathuler (Daresbury)
Behrend, Brasse, Gayler, May (DESY)
Treille, Vannucci (Orsay-CERN)
Jones, Lloyd (Rutherford-Oxford)

The groups of Daresbury and DESY concentrated on optimizing a μ beam; the two groups of Orsay-CERN and Rutherford-Oxford on a combined μ-ν beam. A few results of these studies can be summarized as follows[1]:

The muon channel should consist of three main parts. Behind the proton target it is useful to have a matching section for matching the acceptance of the decay channel (in solid angle and momentum) to the emittance at the target, and furthermore to allow the selection of a momentum band for the parent pions. In particular, this is important for the use of the polarization of the μ. The matching section is followed by the decay section. In order to avoid a considerable increase of the phase space of the beam due to π decay, and to keep the mean travelling angle of the π's (with respect to the beam axis) larger than the average decay angle of the μ (with respect to the direction of the π), one has to use a system of focusing elements. Calculations have been carried out for triplet systems as well as for FODO systems. From a cost point of view, the FODO system has to be the preferred one.

The last part of the μ beam line is the cleaning and analysing section. This part serves several important functions: absorption of the remaining hadrons; bending away from the ν beam and momentum selection of the μ; absorption and/or bending away the μ halo as far as possible. A method of reducing the halo is the use of a circular magnetic field in an iron absorber around the μ beam.

For a μ beam line of about 1 km in length incorporating a focusing system in the decay section, one can achieve an intensity of between 1.5 and 2.8 × 10^8 μ's per 3 × 10^{12} interacting protons when tuning the μ channel to half the energy of the primary protons. The beam size at the experimental target varies for different designs between 10 × 5 cm^2 (horizontal × vertical) and 15 × 15 cm^2.

Cost estimates have been made at Daresbury and at DESY. The Daresbury estimate is 9 MSF for a 100 GeV μ beam; the DESY estimate is 14.1 MSF for a 100 GeV beam and 23.8 MSF for a 200 GeV beam (400 GeV primary protons).

A μ beam of the proposed quality will make possible a rather broad physics programme. Figure 1 shows in the q^2-ν plane the total event rate per hour calculated for a bin of $\Delta q^2 = 1$ GeV^2 and $\Delta W = 1$ GeV, and for 10^8 μ/pulse of 200 GeV, using a 1 m H_2 target. In the region between W = 5 and W = 15 GeV one can measure up to q^2 larger than 50 GeV^2. As well as a measurement of the total inelastic structure functions νW_2 and W_1 (which by then may be done at NAL), some of the important experiments are the following:

- Deep inelastic scattering with detection of the hadronic final states in coincidence with the scattered μ. Inclusive as well as dominant exclusive reactions (ρ^0, $\pi^{\pm}$, $K^{\pm}$) could be studied.
- Scattering of polarized μ's. For example, for the scattering off a polarized target one can get information about two additional structure functions W_3 and W_4 and thus make a more specific test of models for deep inelastic scattering.
- Extrapolation to photoproduction (i.e. scattering at small q^2).
- Investigation of two-photon exchange effects by μ^+ and μ^- comparison and by elastic scattering off a polarized target.
- Comparison with e^- scattering at high q^2 (test on e-μ universality).
- Search for heavy (muonic) leptons.

CERN SPS being the only accelerator in Europe which can provide a charged lepton beam in the 100 GeV region, it is important to build a high-energy μ beam of good quality. It is only for the North Experimental Area that a μ beam with all required properties seems to be feasible; consequently the importance of an early development of this area was emphasized.

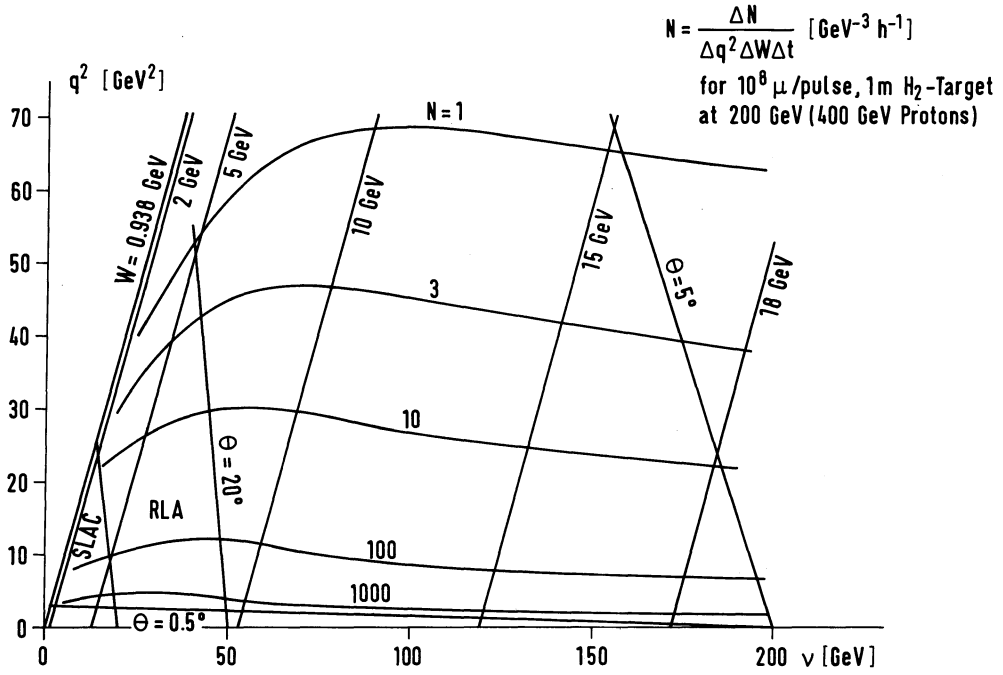

Fig. 1 Kinematics and total event rate per hour in the q^2-ν plane (as presented by Brasse)

During the discussion following Brasse's talk it turned out that a μ beam channel designed for 100 GeV can be transformed to 200 GeV by inserting additional magnets and quadrupoles. It was pointed out (Brianti and Wüster) that this beam might be the first beam in the North Area. Already with a few times 10^{11} interacting protons, one could get a beam of 10^7 μ/pulse, sufficient for inelastic scattering up to $q^2 \simeq 30$ GeV^2 at high W. Thus even if the intensity of the SPS is below its design value in the first time of operation, one could in principle make an early start with the μ physics.

Furthermore, the problems of a combined μ-ν facility were discussed. Winter and Allaby proposed to use the same protons for both a μ beam and a ν beam by using parents of positive charge for one beam and of negative charge for the other. It was also emphasized that both beams should be optimized separately. Any focusing in the decay channel has a negative effect on the ν beam.

The plans for an experimental apparatus are in a rather preliminary state. One possibility would be a design similar to that for the forward spectrometer of Hyams et al.[2] with additional identification for μ and π^0.

Proposals for building electron beams from
Ecole Polytechnique, Orsay,
University of Lancaster (Newton), and
University of Sheffield (Galbraith)

were presented by one of the Working Group secretaries (Barbiellini). Both proposals suggest a two-step production. The first target of light material produces π^0 from the proton beam. Gamma-rays from π^0 decay are converted in a second target with high radiation length/interaction length ratio. The collimation at a good focal point separates hadron particles from electrons, because of different angular production between electromagnetic and strong processes. Typical parameters of the two-step electron beams are: intensity, 10^7 electrons at 80 GeV for 3×10^{12} protons at 200 GeV; $\Delta p/p \simeq \pm 2\%$; purity $\simeq n_{\text{hadrons}}/n_{\text{electrons}} \simeq 10^{-3}$. For 400 GeV proton energy, the flux of electrons at 160 GeV increases. If higher purity is required for small $\Delta p/p$ beams, the synchrotron radiation loss in a magnetic chicane seems to be the best tool; for a higher $\Delta p/p$ beam with small angular divergence, the use of a DISC counter has been suggested.

The intensity of an electron beam at the SPS is adequate for building a tagged photon beam; in fact at the electron machine the intensity is reduced to this value in order to avoid accidental tagging coincidences.

A photon beam with γ-rays coming directly from π^0 decay is also feasible at proton machines. Another feature of a photon beam is that it is the only boson beam that can have a reasonable polarization. The coherent bremsstrahlung has been successfully used at lower energy for producing polarized photons. The feasibility of this method at the SPS energy has been studied by the Working Party.

The radiative correction in the electromagnetic phenomena plays an important role, and the handling of this correction has to be known and can be relevant to the choice of the lepton beam. A paper on this topic appears in Ref. 1 and was discussed in the Working Party Report. Lepton physics predicted for the future was represented by a review of the possible physics to be done with e-p colliding beams.

The discussion following Barbiellini's talk concentrated on two main points. The first concerned the utilization of the chicane for purifying the e beam. It was pointed out by Newton that for 80 GeV electron energy a chicane with 70 kG will cost about 1.5 MSF. However, for higher energy it gets cheaper. Roughly speaking it is suitable for energies > 100 GeV. Rubbia mentioned that from a physics point of view one would obviously prefer to start from 400 GeV protons to get an e beam of 160 GeV. However, this will cause two severe problems for the West Hall. First, the length of the West Hall limits a normal beam to $\leq$ 150 GeV; for an e beam the limit is even lower. Secondly, there are problems of μ shielding in the West Hall if one goes to 400 GeV. So this beam should be considered for the North Area. Picasso agreed with Rubbia that deep inelastic e scattering should be done with high energy in the North Area. However, the e beam in the West Hall is in any case good for photon physics, especially since at SLAC there is no Omega-like spectrometer, and also there is no long-spill beam in this energy region.

The impact of the electron deep inelastic results on the field of particle physics is clear from the growing number of proposals for constructing facilities that can extend the investigation from actual SLAC possibilities. Besides the present proposals for μ and e beams at the large proton accelerators (NAL, SPS), there are the following proposals for the near future: i) the Recirculating Linear Accelerator at Stanford (RLA); ii) the 40 GeV electron synchrotron at Cornell; iii) the DESY project for e-p collision at the DORIS storage ring.

If the e-p inelastic scattering results are correctly interpreted as effects due to the point-like constituent structure of the proton, the natural comparison among the proposals is the possibility of proving this hypothesis for shorter distances, i.e. higher momentum transfer than that done at SLAC. So the relevant quantities for judging the quality of the proposed beams are energy, intensity, and duty cycle.

In Table 1 several beams are compared.

Table 1

	Beam	E (GeV)	Flux (sec^{-1})	Duty cycle
SPS (400 GeV)	μ	200	$> 10^{7}$	$\sim 10\%$
	e	160	$> 10^{6}$	$\sim 10\%$
RLA	e	40	$> 10^{13}$	6×10^{-4}
	e	20	$> 10^{11}$	7%

In spite of the strong differences in the parameters among these beams, it is obvious that the existence of one of these facilities will not spoil the possibilities of the others.

For the SPS the μ beam is to be preferred from the point of view of energy and intensity. Also the problem of radiative correction is less severe. However, some experimental and technical problems (beam halo, beam length, and lepton detection) may be easier to solve with an electron beam which also offers the possibility of a tagged photon facility.

REFERENCES

1) For details see: CERN/ECFA/72/4 (1972), Vol. I, Chapter 6.

2) B.D. Hyams, W. Koch, E. Lorenz and U. Stierlin, CERN/ECFA/72/4 (1972), Vol. I, p. 342.

3) J. Drees and M. Leenen, 300 GeV Working Group, CERN/ECFA/72/4 (1972), Vol I, p. 237.

BACKGROUND PROCESSES IN HIGH-ENERGY PHOTON TAGGING SYSTEMS*)

T. Sloan
Dept. of Physics, University of Lancaster, England

1. INTRODUCTION

We have seen from the second ECFA Study Week held at Tirrenia that interesting physics can be obtained from photon and lepton scattering experiments. Tagged photon experiments are complementary to lepton scattering experiments for two reasons. The first is that they provide high statistics checks of extrapolations from the lepton experiments to $q^2 = 0$. The second is that they allow independent studies of the hadronic nature of the photon.

Tagging systems are used in photoproduction experiments for two reasons:

i) The photons produced by bremsstrahlung are not monochromatic. The tagging system allows the energy of each incident photon to be measured.

ii) The tagged photon is signalled electronically. The signal can be used as an absolute monitor of the number of incident photons and also in the trigger of counter experiments.

Figure 1 shows the tagging system proposed by Halliwell et al.[1] at NAL. An electron incident on the radiator emits a photon by bremsstrahlung. The photon energy is the difference between the incident and scattered electron energies. Scattered electron energies are measured from the pulse amplitudes in the lead-glass blocks T_1 to T_{11}.

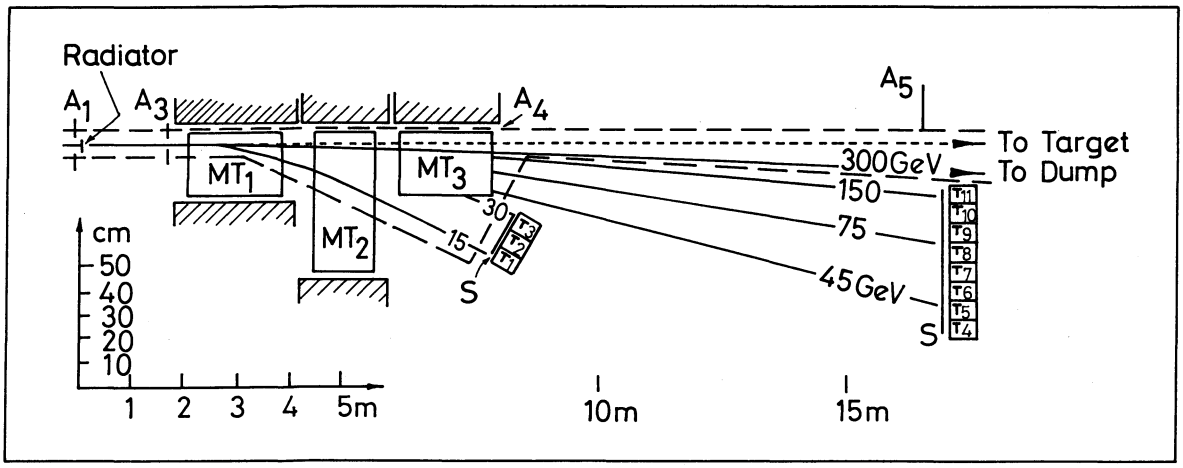

Fig. 1 Layout of the tagging system proposed by Halliwell et al. (Ref. 1) at NAL. MT_1 to MT_3 are bending magnets. T_1 to T_{11} are lead-glass shower counters. A_1 to A_5 are veto counters.

The resolution of the system shown in Fig. 1 is set by the accuracy with which the incident beam energy is defined and the accuracy of measurement of the scattered electron energy. Higher resolution than that of the tagging system mentioned in Ref. 1 could be

*) Contributed paper

achieved by using multiwire proportional chambers to detect and momentum-analyse the incident and scattered electrons.

2. BACKGROUND PROCESSES IN THE TAGGING SYSTEM

Two types of background process exist.

Type 1

Photons are produced in the beam line with charged particles in the wrong energy bin of the tagging system.

Type 2

Charged particles are scattered into the tagging system which have no associated photons along the beam line.

The following symbols will be used in calculations of these backgrounds:

E_I = the incident electron energy

E = recoil electron energy

ℓ_R = radiation length of the radiator = 6 g/cm^2 for lead

T = thickness of the radiator in radiation lengths

Z = the atomic number of the radiator = 82 for lead

A = the atomic weight of the radiator = 207 for lead

k_2 = the minimum tagged photon energy

k_1 = the maximum tagged photon energy

N = Avogadro's number = 6×10^{23}

α = fraction of the charged particles in the incident beam which are electrons (the beam is assumed to have a contamination of pions).

2.1 Type 1 backgrounds

2.1.1 Double bremsstrahlung

The largest contributor in this category is double bremsstrahlung, i.e. the electron undergoes more than one bremsstrahlung collision in the radiator. If one of the photons radiated has energy > δ (where 2δ is the bin width of the tagging system), the photon energy is wrongly measured. For reasonable thickness radiators (i.e. $\gtrsim 0.01\ \ell_R$) in a good resolution system, this background becomes significant.

The problem can be overcome by having a shower counter in the beam downstream from the experiment with energy threshold set at δ. An interacting γ which has a second photon in the beam is then vetoed. The singles rate in this detector should be manageable. For example, if δ = 100 MeV for 100 GeV incident electrons the singles rate will be $\sim$ 7 times the tagged photon rate which might typically be $\sim 10^5$ tags per pulse.

2.1.2 Bremsstrahlung followed by Compton electron scattering in the radiator

It is assumed that the photon scatters close to 0°, i.e. along the beam line.

A simple integration over the thickness of the radiator shows that the ratio of the probability of this process to single bremsstrahlung is $\sim 0.6 \times 10^{-3}\ t/(E_I - E)$. In this

calculation an approximation was made that the total Compton scattering cross-section at photon energy k is

$$\sim \frac{0.11 \times 10^{-26}}{k} \text{ cm}^2 .$$

This approximation is valid to ±50%.

This background ratio is $\lesssim 10^{-5}$ for a radiator of $< 0.1\ \ell_R$ thickness and 80 GeV incident electrons.

2.1.3 Electron-electron bremsstrahlung

From the cross-section given by Heitler[2], the ratio of this process to single nuclear bremsstrahlung is $\sim 1/Z$, i.e. $\sim 1.2\%$, and is independent of radiator thickness.

The screening corrections were assumed to be the same for atomic electrons and nuclei.

2.1.4 Photons produced by pion interactions in the radiator

A pion contamination of the electron beam will exist. An upper limit is calculated for this background, assuming that every pion interaction produces a photon along the beam and charged particles in the tagging system.

Therefore, the ratio of photons produced by π collisions to tagged photons from bremsstrahlung is at most:

$$\frac{1 - \alpha}{\alpha} \frac{N \ell_R \sigma}{A^{1/3} \log (k_2/k_1)} ,$$

where σ is the pion-nucleon total cross-section (~ 30 mb) and the pion-nucleus cross-section is assumed to be $\sigma A^{2/3}$. This ratio is then $\sim 2 \times 10^{-2} [(1 - \alpha)/\alpha]$.

If α is ~ 0.5, i.e. one pion for every electron, the background is $\lesssim 2\%$ for 80 GeV/c incident momentum.

Similarly, it can be shown that photoproduction reactions with the nuclei of the radiator produce a background ratio $\lesssim 10^{-3}$ for $0.1\ \ell_R$ radiator thickness.

2.1.5 Neutrons in the beam produced by pion interactions in the radiator

Estimates of this background can be made by assuming that the secondary particle spectra produced by pion interactions are the same as those produced by proton interactions. The Grote, Hagedorn, Ranft spectra[3] for secondary particle production on lead can then be used. The assumption was made that the beam will be collimated to a diameter of 2.5 cm at 30 m from the radiator. A simple calculation then shows that at 80 GeV/c incident momentum the ratio of neutrons to tagged photons is

$$\approx 3.3 \times 10^{-6} \frac{(1 - \alpha)}{\alpha} .$$

The asymptotic neutron cross-section is ~ 400 times the asymptotic photon cross-section. If neutron triggers are to be less than 1/100 of the photon triggers, this ratio must be $< 1/40000$. This condition is met if α is > 0.12, i.e. the beam must contain less than eight pions for every electron. Clearly this background will be small.

2.2 Type 2 backgrounds

2.2.1 Trident production

Tridents can be produced directly (by a virtual photon), i.e. $e^- + \text{nucleus} \to e^- + e^+ + e^- + \text{nucleus}$, or indirectly by a real bremsstrahlung photon which produces an e^+e^- pair in the radiator.

a) The direct process

The cross-sections have been calculated by Rossi[4] using the Weizacker-Williams method. This seems to be in reasonable agreement with experiment[5]. Integrating these cross-sections, we see that the probability per unit radiator thickness of obtaining direct tridents is

$$3 \times 10^{-4} \frac{dE}{E_I} \left\{ \frac{E_I}{E} \ln\left(\frac{E_I}{E}\right) - \frac{E_I}{E} + 1 \right\} + 7 \times 10^{-4} \frac{dE}{(E_I - E)} \ln\left(\frac{E_I}{E_I - E}\right) .$$

The probability of obtaining a recoil electron by bremsstrahlung per unit radiator thickness is

$$\frac{1}{\ell_R} \frac{dE}{E_I - E} .$$

Thus the ratio of direct tridents to recoil electrons from bremsstrahlung is

$$15.5 \times 10^{-4} \frac{(E_I - E)}{E_I} \left[\frac{E_I}{E} \log\left(\frac{E_I}{E}\right) - \frac{E_I}{E} + 1 \right] + 40 \times 10^{-4} \log \frac{E_I}{E - E_I} .$$

This background ratio is plotted in Fig. 2 for 80 GeV incident electrons on a lead radiator. The background is small but significant. It will be reduced considerably by vetoing the recoil positrons. Notice that this ratio is independent of radiator thickness.

b) Indirect trident production

This is calculated by integrating the probability of bremsstrahlung followed by pair production of the photon over the thickness of the radiator.

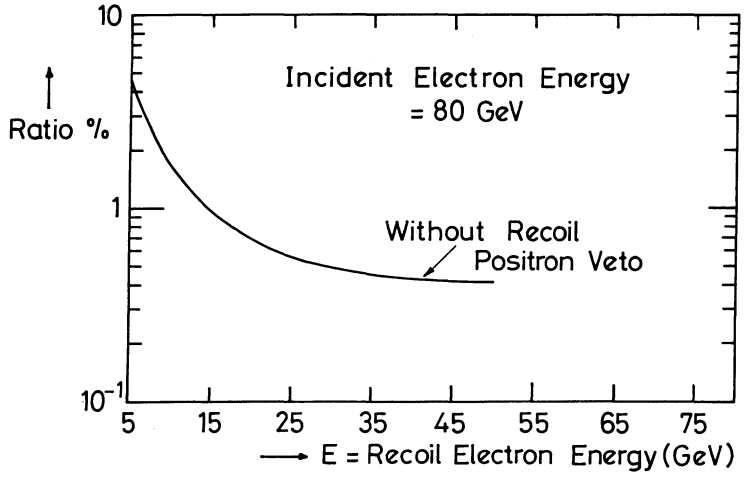

Fig. 2
Ratio (%) of recoil electrons produced by direct tridents to recoil electrons produced by bremsstrahlung versus recoil electron energy. The calculated curve is for 80 GeV incident electron energy. The ratio is independent of radiator thickness

The ratio of this process to that of recoil electrons from bremsstrahlung

$$\approx \frac{7}{18} T(E_I - E) \left(\frac{1}{E} - \frac{1}{E_I}\right).$$

It is assumed in deriving this ratio that the spectrum of electrons from pair production is flat, i.e. independent of the electron energy.

Figure 3 shows this ratio for E_I = 80 GeV. This background is large. The background can be reduced to insignificance by vetoing the recoil positrons. The ratio is plotted in Fig. 3 assuming that recoil positrons of energy > 0.2 GeV are vetoed. The curve was calculated by performing the integration to estimate the fraction of the events which give a recoil positron of energy < 200 MeV.

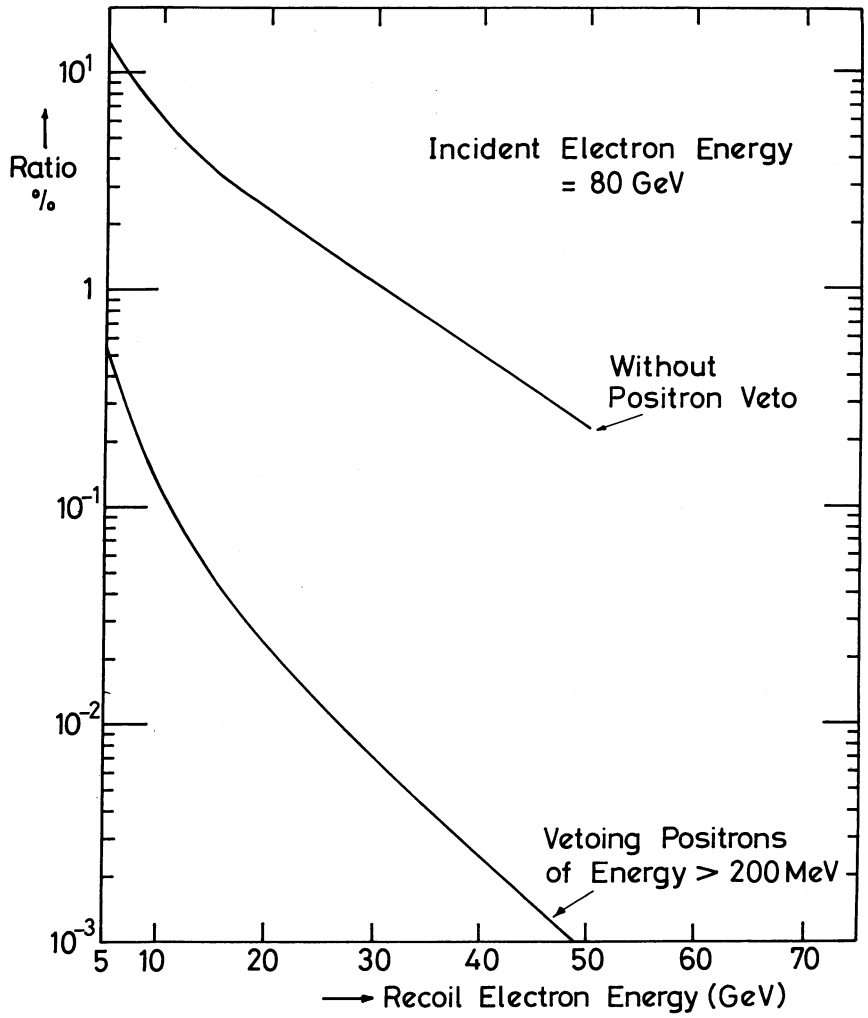

Fig. 3 Ratio (%) of recoil electrons produced by indirect tridents to recoil electrons produced by bremsstrahlung versus recoil electron energy. Also shown is the effect of vetoing positrons of energy > 200 MeV.
The curves are calculated for electrons of 80 GeV energy incident upon a radiator of thickness of 0.01 ℓ_R. The ratio varies linearly with radiator thickness.

2.2.2 Soft electron contamination of the beam

Collimation of the electron beam must be clean, as soft electrons consistute a type 2 background.

2.2.3 Electron-electron scattering

Using the cross-sections given by Heitler[2], this background ratio is estimated to be < 1% and independent of radiator thickness.

2.2.4 Compton scattering of low-energy bremsstrahlung photons

This background is insignificant. Using the approximation that the total Compton cross-section is $\sim 0.11 \times 10^{-26}\ k^{-1}\ cm^2$ for a photon of energy k, a simple integration shows that the ratio of recoil electrons from Compton scattering to recoil electrons from bremsstrahlung is $\lesssim 0.2 \times 10^{-3}\ T$.

This is calculated for 80 GeV incident electrons with tagged photons in the energy range 30-75 GeV.

3. MAXIMUM RADIATOR THICKNESS

One way of increasing the tagged photon flux will be to increase the radiator thickness. The only serious backgrounds which will contribute are from double bremsstrahlung and from indirect trident production.

The shower counter used to veto double bremsstrahlung will limit the tagged photon flux. Figure 4 shows the variation of the tagged photon flux with radiator thickness. This curve is computed by subtracting the calculated double bremsstrahlung rate from the single bremsstrahlung rate. Clearly one gains little by increasing the radiator thickness beyond 0.05 radiation lengths. The calculation is an approximation, neglecting effects in which > 2 bremsstrahlung photons are emitted.

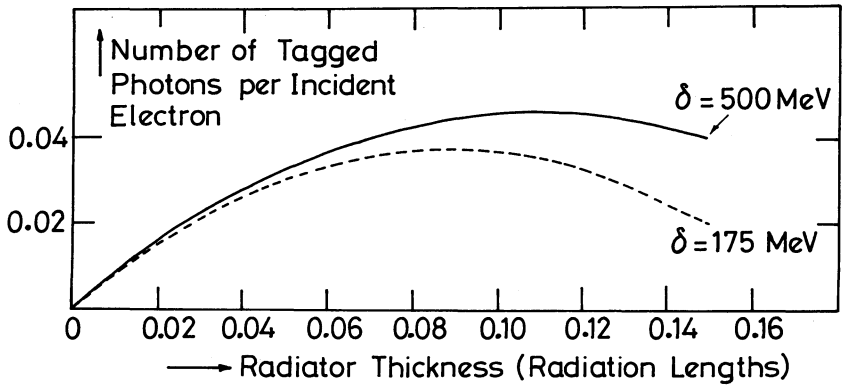

Fig. 4 Probability of obtaining a single tagged bremsstrahlung photon per incident electron versus radiator thickness. The parameter δ is the resolution assumed for the tagging system (half width). It is assumed that double bremsstrahlung collisions are vetoed.

At 0.05 ℓ_R radiator thickness the indirect trident ratio varies with recoil electron energy from 2.5% to 5×10^{-3}% if positrons of energy > 0.2 GeV are vetoed. These ratios are for tagged photons of 30-75 GeV energy with 80 GeV incident electrons. At higher energies this background would increase.

4. CONCLUSIONS

1) The background processes in high-energy photon tagging systems are small providing that recoil positrons of energy > 0.2 GeV are vetoed.

2) The contamination of pions in the electron beam can be as high as one pion per electron.

3) The maximum practicable radiator thickness is $\sim$ 0.05 radiation lengths of lead. A downstream shower counter must be used to veto double bremsstrahlung photons in order to avoid deterioration in the resolution of the system.

* * *

REFERENCES

1) C. Halliwell, P.J. Biggs, W. Busza, M. Chen, T. Nash, F. Murphy, G. Luxton and J.D. Prentice, Nuclear Instrum. Methods 102, 51 (1972).

2) W. Heitler, The quantum theory of radiation (3rd ed., Clarendon Press, Oxford, 1954).

3) H. Grote, R. Hagedorn and J. Ranft, Particle spectra (CERN, 1970).

4) B. Rossi, High-energy particles (Prentice-Hall, New York, 1952).

5) B. Grossetête, R. Tchapoutian, D.J. Drickey and D. Yount, Phys. Rev. 168, 1475 (1968).

SOME COMMENTS ON CHICANES AND ELECTRON BEAMS*)

D. Newton
Department of Physics, University of Lancaster, England

An electron beam contaminated with heavier particles may be purified by making use of the energy loss, due to synchrotron radiation, suffered by the electrons when the beam passes through a region of high magnetic field. Farley, Picasso and Bracci have shown that for a beam of energy E the mean loss in energy ΔE is

$$\frac{\Delta E}{E} = 6.4 \times 10^{-12} \cdot B^2 L \gamma ,$$

where B is the field in kilogauss, L the length in metres, and γ the relativistic factor. Owing to the quantum fluctuation in photon emission there is a spread in energy loss about the mean ΔE, and the standard deviation σ_E is given by

$$\frac{\sigma_E}{\Delta E} = \frac{1}{\sqrt{0.144 BL}} .$$

For a field of 7 Tesla and a length of several metres the standard deviation is of the order of 10% of the mean energy loss ΔE.

Farley, Picasso and Bracci have proposed the "chicane" configuration (+--+) for such a magnetic field region, and this results in no average deflection and essentially no displacement to the beam. A "chicane" may thus be inserted into a beam without affecting the beam optics. Another advantage of the "chicane" configuration is that the standard deviation of the deflection about the mean value zero is very small, less than 0.1 mrad for a case of interest to high-energy beams. Since the standard deviation on the (essentially zero) lateral displacement is also very small, of the order of 0.1 mm typically, this means that the increase in beam emittance is quite negligible for any realistic beam, e.g. 1 or 2 mrad x 2 or 3 mm, in each plane.

In use a chicane would probably be placed at a non-dispersive focus after momentum definition to $\delta p/p$ had taken place. This point would be chosen in order to keep the volume of very high field as small as possible. A later stage in the beam would be tuned to transmit the electrons of energy E - ΔE, but to stop or deflect-out the hadrons of energy E. The purity attainable for the electron beam would clearly depend on the relative magnitudes of ΔE and $\delta p/p$, also on the emittance of the beam in the plane of this later momentum analysis, and on the details of the technique used for stopping or deflecting-out the hadrons.

The cost of several metres of 70 kG dipole field, with 1972 prices for superconductor, would be in the region of 1 MSF.

---

*) Contributed paper

It is thought that the chicane is unlikely to be used in electron beams of less than 100 GeV at CERN SPS. Beams of lower energy will probably be used for physics which does not need the highest possible purity of the beam.

Drees and Hilger have proposed a device which compresses the momentum acceptance of the electron beam, for example from ±5% to ±1%. The end result would be a pure electron beam within a narrow momentum range, and with a relatively high intensity but with a larger beam emittance. Further details of this suggestion may be found in CERN/ECFA/72/4, Vol. I, Chapter 6, p. 234.

CHAPTER V

EXPERIMENTAL TECHNIQUES

Comments on BEBC Hadron Sessions

I. Butterworth *(Imp. College)* and R.T. Van de Walle *(Nijmegen)*

Comments on the Gargamelle Session

F. Jacquet *(Ecole Polytechnique)*

Comments on the Omega and Spectrometer Sessions

W. Beusch *(CERN)* and D.E. Fries *(Karlsruhe)*

Comments on New Facilities in Visual Devices

R.T. Van de Walle *(Nijmegen)*

Comments on Particle Identification Sessions

P.G. Murphy *(Manchester)* and J.P. Stroot *(IISN, Belgium)*

Kinematical Analysis at High Energies

W. Matt *(Munich)*

Considerations on the Design of a Vertex Detector for SPS Energies

A. Grant *(CERN)*

A Comparison of Properties of Rapid-Cycling Bubble Chambers and Streamer Chambers

E. Lillethun *(Bergen)*

COMMENTS ON BEBC HADRON SESSIONS

I. Butterworth
Imperial College, London, England

R.T. Van de Walle
Fysisch Lab., Nijmegen, The Netherlands

1. RF BEAM

Several speakers stressed again the absolute priority of the RF beam for hadron physics. To decide not to build such a beam would be equivalent to ruling out $K^{\pm}$ and π^{+} physics, since tagging is statistically unacceptable for this type of bubble chamber research. R. Wilson stated that NAL intended to provide an RF beam for the 15′ chamber, but that the first year of operation had been scheduled for neutrinos. They had held off an early definite decision in the hope of getting (X-band) superconducting cavities. Since, however, hadron physics might now form a larger part of the early programme than was originally foreseen, they would probably look into this matter again.

2. TRACK-SENSITIVE TARGET (TST)

Probably the most dominant feature of the bubble chamber discussion was the general enthusiasm for a TST rather than for a downstream (charged particle) spectrometer. The reasons were essentially those already presented in CERN/ECFA/72/4, Vol. I, Paper 2.3. In addition to permitting the identification of multineutral events, it did the same job of separating 1C-0C (slow neutral) events. It thus matched the general-purpose nature of the bubble chamber. Another possible bonus would be the increase in precision in the region of the vertex.

On the negative side was the consideration that the use of a TST would make necessary some reduction of beam density ($\lesssim$ 5 particles p.p.). However, in view of the fitted neutral events, the number of fitted events per frame would not be less, and they would present a less-biased view of high-energy interactions. Bowler pointed out that use of a TST as an alternative for a downstream spectrometer would lead to a worsening of the quality of the physics (i.e. larger errors on the effective masses)*). Of course, a spectrometer could always be added; in this sense a spectrometer is not in conflict of priority with the TST.

During this second study week, Leutz presented preliminary technical conclusions from a TST run just completed at RHEL by a CERN-Rutherford Collaboration. During this run more than half a million pictures were taken in the British 1.5 m chamber with a target immersed in a 77 mole % H_2-Ne mixture (radiation length = 40 cm). Several speakers expressed the hope that the present CERN-Rutherford Collaboration on TST development, which has been so successful, would be continued.

The considerable technical problems connected with developing a TST for BEBC were repeatedly stressed. Peyrou, for example, expressed his concern about the use of a TST

*) For the secondary momenta to be considered, the bare BEBC Δp's dominate over the corresponding $\Delta\theta$'s in the effective mass errors.

with bright field illumination, the much greater problems connected with operating a target in the horizontal plane (as opposed to the vertical plane in the successful RHEL experiment), the fundamental limitations due to the speed of sound in the H_2-Ne mixtures, etc. He felt that whether these problems are solvable or not could only be established by trial and error. His instincts told him that there would be disappointments. Even if all problems would be solved in time, he was certainly worried that the 1975 shut-down of BEBC would not be long enough to implement all the technical developments required. The bubble chamber community would probably have to accept reduced "conventional" BEBC running to pay for this development. Typically, a BEBC warm-up to change or repair a target could take some two months.

During the discussion it was also pointed out that in BEBC the analysis of TST pictures might give rise to additional problems (e.g. how to decide on associated γ's on the scanning table, etc.).

During his presentation of the case for a hadronic TST, Miller recalled the possibility of a veto-TST -- a TST terminated downstream by a lead plate. Such a veto-plate would reduce the background of 4C-fits due to (multi) neutrals, and increase the 4C-fits possibilities of BEBC both in purity and primary momentum range. Leutz suggested a specific veto-target made from a sandwich of multiple lead plates embedded in a plastic sheet. Butterworth and Grant pointed out that a reduction of the $\sim$ 15% impurity of 4C-fits at $\sim$ 100 GeV/c incident momentum did not justify the use of a veto-target, as it would also prevent the use of a downstream particle identifier, a device essential for most of the physics with BEBC. A viable TST should therefore reach to the chamber window.

A number of people expressed the hope that a target might be developed which would be a compromise between that best-suited to hadron physics and that best-suited to neutrino physics. Von Krogh (see CERN/ECFA/72/4, Vol. I, p. 173) presented calculations showing that from the physics point of view a target of $\sim$ 2 m^3 would be such a compromise; the number of fully reconstructed H_2 (or D_2) events would be comparable to the number expected in bare BEBC. The opinion of the BEBC and target constructors was, however, that the larger neutrino target with its increased hydrostatic pressure and hydrodynamic forces represented a much tougher technical problem than the thinner hadron target. From a technical point of view, therefore, the way to go was to construct and try the smaller hadron targets first.

3. PRIORITIES

Several speakers sketched their personal priorities and essentially agreed on the following priority sequences for hadron physics (RF beam assumed):

Level 1:
- MWPC's upstream for beam measurement;
- Particle identifier downstream.

Level 2:
- TST development
  (and purchase of neon).

Level 3:
- Downstream fast gamma detection.

A charged particle spectrometer was no longer considered as a general facility, in priority conflict with, say, a TST, but more as something that could be added downstream at any stage, when required by the physics of a specific experiment.

Peyrou stressed that in his opinion, apart from the particle identifier (which was relatively cheap), "neutrino items" such as neon and deuterium would have to come before TST development. He felt that not to buy deuterium in the hope that the neutrino TST would work (and therefore only smaller amounts of D_2 would be needed) would be very ill-advised.

3.1 Remarks

3.1.1 Particle identifier

In the discussion following Lehraus' presentation of a particle identifier based on relativistic rise of ionization, it was again stressed that good time resolution was not required for downstream detection of this type when used with bubble chambers. Particle densities per pulse were extremely low, and geometric information alone would be sufficient to unscramble the secondary particles. The good time resolution of a Čerenkov detector could be used but is not essential.

Beusch expressed his worries about an ionization detector as described by Lehraus; to maintain adequate performance of such a large assembly of counters (with analog read-out) was, in his opinion, a difficult project.

3.1.2 Downstream gamma detection

Miller, Bowler and others restressed the importance of the downstream fast gamma detector (see CERN/ECFA/72/4, Vol. I, p. 17). This is necessary in order to resolve 1C events with very fast neutrals, a task which neither a TST nor a charged particle spectrometer can handle. The fundamental limitation in this case comes from the Coulomb scattering errors on slow charged tracks. Fisher pointed out that this problem would also exist for any mutiparticle counter spectrometer experiment in the 100 GeV/c region using hydrogen targets of $\sim$ 1 cm.

4. MISCELLANEOUS

In discussing a one-arm versus a two-arm spectrometer, Fisher stated that, though his analysis of a two-arm spectrometer had been triggered by BEBC, he now no longer felt such a two-arm set-up would be appropriate to that chamber. It could, however, be relevant to some more specifically designed vertex detector. He furthermore stated that in his opinion even a one-arm spectrometer should have less priority than a TST.

In the discussion about the possibilities of bare BEBC, Badier stated that from the point of view of fit-physics, bare BEBC was just a 4C device; however, for a 4C-fit device as such, he felt there were more efficient and cheaper solutions than BEBC. An interesting additional question, raised but not really discussed, was the problem of the relevance of the non-4C physics. At 100 GeV/c the 4C-fits certainly only represent a small fraction of the final state; but do they not contain the largest fraction of the "exclusive" physics one needs to know?

It was recalled in the discussion that, if BEBC successfully double-pulsed as intended, a possible mode of operation was to alternate hadron and neutrino frames by having an RF spill and a neutrino spill on the same beam pulse. Reinhardt confirmed that the 2 m depth of focus of the cameras was satisfactory for either sort of physics.

Matt discussed how the inclusion of multiple scattering errors and track correlation could improve track measurement precision and hence reduce ambiguity problems. For example, it could reduce the 15% contamination of 4C-fits at 100 GeV/c to 7½%. The incident momentum up to which 1C-fits were reliable in bare BEBC would be correspondingly raised. Though clearly desirable, these improvements would not change any of the conclusions about support equipment for BEBC (see contribution by W. Matt, p. 211).

COMMENTS ON THE GARGAMELLE SESSION

F. Jacquet
Ecole polytechnique, Paris, France

During the discussion it appeared that the main argument for the transportation of Gargamelle is that of the neutrino physics programme.

The role of Gargamelle in the context of the full programme has been summarized as follows:

1) Gargamelle now exists and has provided one million pictures of good quality during the last year. Efficient apparatus for data analysis is functioning in many laboratories in Europe. Thus Gargamelle and its equipment will be ready to give rapid results when the SPS is ready to go into operation.

2) Gargamelle is a good instrument for neutrino physics. This has been proved by results given at the Batavia Conference on the comparison between ν and $\bar{\nu}$ total cross-sections, on neutral currents, and on hyperon production. At higher energies Gargamelle appears to be quite comparable to BEBC for some of the fields envisaged in neutrino physics (purely leptonic reactions, search for W bosons, neutral currents, deep inelastic scattering).

3) The neutrino bubble chamber physics programme in Europe is extremely long, but deserves the highest priority, using ν or $\bar{\nu}$ in hydrogen, deuterium, and heavy liquid (neon or freon). All these experiments are important and give complementary results. To use BEBC alone at, say, one million pictures per year with half of the SPS intensity would give a programme lasting six years. This time can be significantly reduced by moving Gargamelle behind BEBC.

COMMENTS ON THE OMEGA AND SPECTROMETER SESSIONS

W. Beusch
CERN, Geneva, Switzerland

D.E. Fries
Kernforschungszentrum, Karlsruhe, Germany

1. OMEGA

In his summary talk on the work of the Omega Working Group[1], J. Dowell indicated the present situation of Omega. Three groups have partially set up their triggers, and have taken a sample of data which will allow them to start their analysis. Multiprong events are clearly visible when the Plumbicon digitizings are played back. However, some adjustments have to be done to improve spark efficiency for such events. The coexistence of several counter groups around a single magnet spectrometer is a new feature in high-energy physics; the coexistence has been quite peaceful so far.

Asked for the order of priorities regarding the extensions to Omega, J. Dowell felt that Čerenkov counters for particle identification are essential. He personally would give next priority to γ detectors and add multiwire proportional chambers (MWPC) later. If one were to start with a 100 GeV/c beam, a downstream magnet would be required first. J. Steinberger recommended converting the Omega to MWPC before the start of the SPS.

J. Lefrançois asked if the effort of extending the capabilities of Omega to high energy should not rather be directed to equipment in the North Area. J. Dowell felt that the investment is modest in view of the large number of experiments that become possible with Omega.

A few questions were related to the usefulness of Omega at high energy. The Omega system has been optimized for 20 GeV physics. At 200 GeV only a small fraction of the field volume may actually be used. Moreover, is the Omega really a good detector for slow particles produced in target fragmentation? The detection efficiency for such particles (at present $\sim$ 50%) is a problem to be studied; a different geometry of the chambers around the target will be tried in the near future. One should also study a set-up with a solenoid magnet around the target, the target being upstream of the Omega magnet. K. Winter remarked that Omega may give too much dispersion to fast particles if considered as a 4π target fragmentation analyser (this is even more so for BEBC), to the extent that one may actually have to turn down the Omega field. W. Beusch thought that the large dimensions of the downstream equipment (Čerenkov, detector planes) needed to cope with this dispersion also have their advantages. In the case of multiparticle events, the dispersion separates the tracks spatially towards the exit of Omega, thus making pattern recognition and particle identification easier. Moreover, it may also be interesting to do experiments that do not follow the forward-backward fragmentation picture. Čerenkov counters are foreseen for particle detectors (rather than ionization detectors, as for BEBC) because this high time resolution is essential.

W. Beusch also felt that the question of charged lepton and photon physics in Omega has not been sufficiently discussed. J. Drees remarked that the physics of μ scattering at 20 GeV, as proposed by J.K. Bienlein[2], can be done much better with electrons at the recirculating linear accelerator (RLA) at SLAC. T. Sloan made the following comment on these points.

The Omega spectrometer can be used for tagged photon and electron experiments at 100 GeV. Electron experiments would require considerable modifications to Omega before it could accept an electron beam of 10^7 electrons/sec intensity.

Tagged photon experiments can be performed in Omega [3]. The spark chamber system would be the same as that for hadron physics. The trigger would require special design to avoid accepting triggers from pair production. Tagged photon experiments produce several interesting physics results. A well-rounded deep inelastic scattering program requires tagged photon experiments to compare with extrapolations to $q^2 = 0$ from muon or electron scattering experiments.

Measurements with tagged photons into Omega will produce much larger event rates than will similar experiments performed at linear accelerators such as SLAC. The reason for this is the very poor duty cycle of the linear accelerator. A good duty cycle with the RLA can only be obtained at energies below 20 GeV.

The practical difficulties of electron scattering experiments can be estimated from the experience gained in an experiment now being performed at DESY, using a streamer chamber. H. Meyer remarked that one of their difficulties was the large flux of soft (few MeV) γ-rays associated with the electron beam and produced also in the hydrogen target. These γ-rays produce low-energy electrons in the material of the detector. They move in tight spirals around the magnetic field lines. They might produce an unacceptable number of spurious sparks in spark chambers or overload the data acquisition system of MWPC.

Another unsolved question is the purity of an electron beam fed to Omega. The relative number of hadrons should be at the 10^{-6}-10^{-7} level. Identifying the electrons in the beam seems unpractical owing to the required high flux and the γ background produced in any material exposed to the electron beam. These questions are being studied further.

D. Treille made the following remarks.

1) Problem of the electron beam purity: At large momentum transfers ($q^2 > 1$ GeV^2) the requirement on beam purity may be less stringent than usually stated ($\pi/e \leq 10^{-7}$), since hadronic cross-sections have a steeper q^2 dependence than that of inelastic electron scattering. Identification of the electron and measurement of its energy in a Pb glass total absorption counter will give a large rejection factor ($\sim 10^2$) for hadronic events if also the electron momentum has been measured independently. This rejection can be done off line; it is uncertain how it would work on line (for triggering). Production of electrons with momentum $p_e \geq 1/2\ p_{inc}$ in hadronic events (from $\pi^0 \to \gamma\gamma$, $\gamma + Z \to e^+e^- + Z$, or π^0 Dalitz pairs) is very rare, however.

Identification of electrons in a beam contaminated by hadrons may not be excluded *a priori*, even in view of its obvious difficulty. One might tag electrons using their synchrotron radiation in a bending magnet of the beam line [4], or consider a differential Čerenkov counter.

2) Background associated with electron beams: 10^7 e/burst is an upper limit of the estimated beam intensity. It is difficult to estimate the probability of the various background reactions. Their effect may be inferred from a test with the present Omega set-up. One would only have to trigger the Omega chambers on incident electrons a few hundred times in order to observe the various background phenomena.

Sonderegger outlined that the experimental program of Omega at the SPS now comprises, in arbitrary order: very rare (exotic) reactions in the 8-15 GeV range with the RF beams; meson and baryon exchange with the RF beam in the 15-40 GeV range; exploratory work with the unseparated hadronic beam up to 80 GeV; and physics with the 80 GeV electron beam, the tagged photon beam and, finally, possibly a rather low-energy muon beam. Each of these fields probably means several different experiments, requiring at least one year altogether on the average. This program will be done on a hydrogen target, and most of it should then be repeated on a polarized target.

In total, such a program might therefore take 10-12 years -- which is not necessarily unreasonable.

If nevertheless one wanted to reduce the pressure on Omega, one might envisage shifting the program on rare reactions (elastic and inelastic scattering near 90°; exotic baryon exchange in K^--p and $\bar{p}$-p; exotic meson exchange; Ξ^* production) to a special 5-20 GeV/c beam equipped with a large acceptance spectrometer.

The beam should be short enough ($\sim$ 50 m) to yield as much as 5% K^- above 8 GeV/c at the experimental target (in a good PS beam the ratio K^-/π^- is, at best, three times smaller in the 6-12 GeV/c region). It could be derived from target T1 or T3 and bent towards the South, to the corner of the E3 hall, or possibly towards the North beyond the BEBC RF beam. The experiment would in both cases be located well outside the cone of high muon background from the production targets.

The spectrometer could have somewhat less resolution and acceptance than Omega, but should be equipped with fast detectors: if it could stand 10^7 particles per burst, the effective kaon flux of 500,000/burst would be equal or higher, up to 12 GeV/c and for a rather small primary proton intensity, as in the Omega RF beam with high proton flux (the latter should yield 500,000 K^- at 12 GeV/c, for 3×10^{11} interacting protons/burst; and an order of magnitude less at 8 GeV/c).

2. SPECTROMETERS

W. Koch gave a rapporteur's summary on the major contributions concerning proposed spectrometers for SPS physics.

All contributions but two[5,6], which were covered in the session, are contained in the Status Report (CERN/ECFA/72/4, Vol. I). Pointing out that most counter experiments on the SPS will make use of a spectrometer in one form or another, he suggested thinking about a modular system of equipment. Experimental equipment such as Čerenkov counters, magnets, etc., could be interchanged between experiments. It would be especially useful to have magnets with variable gap width.

In the discussion, J. Steinberger raised the question, What advantages does a large forward spectrometer of the MPI-CERN type have in comparison with the Omega detector?

W. Koch felt that both instruments cannot directly be compared: the Omega has large detection power around the target, and the forward spectrometer has good analysis power for fast particles. It is possible to use both instruments in conjunction, when the Omega is run with reduced field. On the other hand, although many reactions can actually be studied by both detection systems, one should pursue physical problems with more than one instrument, working rather in parallel than in series.

P. Spillantini and J. Steinberger made comments concerning future measurements at large four-momentum transfer t for which most spectrometers seem to be badly suited.

C. Damerell, when asked what precision on the beam momentum is required for the high resolution single-arm spectrometer, answered that beam resolution has to be matched to the spectrometer design.

M. Martin pointed out that many experiments can be done without using a large forward spectrometer, since total absorption hadron and photon counters provide good resolution at SPS energies. D. Fries wondered whether the hyperon spectrometer as proposed by J. Lefrançois and A. Wagner could not be equipped with a streamer chamber. A streamer chamber would be well suited as far as resolution, data rate, and 4π detection efficiency is concerned, in particular since it may be hard to disentangle the topology of the hyperon decays using wire chambers.

J. Lefrançois felt that as far as the rate of data taking is concerned, the streamer chamber compares unfavourably with proportional chambers.

* * *

REFERENCES

1) See CERN/ECFA/72/4 (1972), Vol. I, Chapter 8, Part A.

2) J.K. Bienlein, CERN/ECFA/72/4 (1972), Vol. I, p. 306.

3) T. Sloan, Experiments to study the interaction of high-energy γ-rays in the Omega system at energies $\sim$ 100 GeV, ECFA Working Group Report 72-8 (1972).

4) B. d'Almagne, Sychrotron radiation of high-energy electrons: Useful formulae and possible application, Orsay Report R.I.72-4 (1972).

5) J. Badier, Proposition de détecteur pour la physique à 100 GeV/c, private communication.

6) H.E. Stier, A spectrometer for inelastic e-p and μ-p scattering, CERN/ECFA/WG/72-163.

COMMENTS ON NEW FACILITIES IN VISUAL DEVICES

R.T. Van de Walle
Fysisch Lab., Nijmegen, The Netherlands

1. During the discussion on rapid-cycling bubble chambers it became clear that such a device requires substantially more complex beam facilities than was previously realized. Brianti and others pointed out that from the point of view of machine operation it is not possible to produce the beam structure required by a rapid-cycling bubble chamber (50 to 100 fast bursts per machine cycle, each 5-20 μsec long) using multiple fast ejection, as suggested in CERN/ECFA/72/4, Vol. I, p. 125 point (b). Such a beam structure has to be realized by 'chopping' either the slow extracted proton beam (before targeting) or the secondary beam itself (after separation).

   In the first case one could, for example, envisage a branch of the SEPB carrying, say, 30% of the total intensity ($I \sim 3 \times 10^{12}$ ppp; flat top ~ 0.7 sec), switching 50 times per machine cycle for a duration of approximately 5 μsec onto the separator target. In this mode the RF separator would have to operate at 50 cycles per second. For a momentum bite of $\Delta p/p \sim 0.3\%$, and even making some concessions to the quality of separation, such a set-up would be rather marginal in terms of K's per burst in the bubble chamber (a few K's per cycle). Increasing the momentum bite (and measuring the $p_{incident}$ externally) or longer RF pulses (i.e. 25 μsec instead of 5 μsec) would then be the only methods to improve on this mode of operation.

   In the second solution (i.e. switching after the separation) the switch would have to operate in phase with the separator 50 c.p.s.; the RF beam stopper would be placed after the switch in the beam line deviated towards the bubble chamber; and in between separator bursts, a non-deviated (unseparated) secondary beam would be available downstream. An advantage of this solution is that now the switching magnet has only to bend the secondary momentum (as opposed to the SEPB momentum in the first method). For K physics this solution is, of course, as marginal intensity-wise as the first one.

   An interesting improvement on the second solution could be the use of a superconducting d.c. separator, whose output is divided (by a switch) between the rapid-cycling chamber and a device such as, for example, Omega, which would be rather insensitive to the fact that, say, 50 × 200 μsec = 10 msec (or approx. 1.5%) of beam is 'eaten' away from a total spill of some 700 msec.

2. Van de Walle expressed the opinion that the use of the larger event rate possibilities of the streamer chamber as opposed to the rapid-cycling bubble chamber (beam intensities of $\sim 5 \times 10^6$/sec for the streamer chamber, compared with $\sim 10^3$/sec for the rapid-cycling bubble chamber) will in practice be very hard to exploit, because (as recent SLAC experience indicates) it is very difficult to achieve a trigger of the level required.

3. In the parallel session on "Special Topics on Instrumentation" Charpak presented a paper (related to 'new visual devices') on the state of the art in projection chambers. He was able to show that although still far from being a completely operational tool, the prototypes possess significantly improved properties compared with conventional streamer chambers in terms of isotropy and ionization information.

COMMENTS ON PARTICLE IDENTIFICATION SESSIONS

P.G. Murphy
Physics Department, University of Manchester, England
J.-P. Stroot
IISN, Belgium[*)]

Most of the efforts of this Working Group have already been reported in CERN/ECFA/72/4, Vol. I. Additional work was presented at Tirrenia on

- transition radiation;
- spot-focusing Čerenkov counters;
- multiwire proportional chamber optimization.

Further work has also been done on

- a total absorption spectrometer.

1. TRANSITION RADIATION

1.1 Particle identification by the observation of transition radiation in the X-ray region[**)]

These remarks are based on results obtained in an experiment performed at the Bevatron last December by the Hawaii-Maryland-Oxford Collaboration. A full report of this experiment is in the process of publication and is available as a preprint[1)].

1.1.1 Transition radiation

A review of transition radiation was given by Prünster[2)] at the first Tirrenia meeting; other useful references are papers by Garibyan[3)], the Brookhaven group[4)], and Ellsworth et al.[5)]. As a brief reminder, the main features that are important in determining the performance of a detector of transition radiation can be summarized as follows:

a) The yield is low, the probability of emission being $\sim \alpha$ per interface; therefore many interfaces are required.

b) For high γ ($= E/m \geq 1{,}000$) the radiation is mainly in the X-ray region (> 1 keV), and the typical angle of emission is $\sim 1/\gamma$. Thus the effect can be amplified by stacking many foils in front of the device used to detect the X-rays. The yield, per interface, is proportional to γ.

c) However, absorption of the X-rays in the foils constitutes a very serious loss. At the same time it is not possible to make the foils arbitrarily thin: interference between the radiation at the front and back surfaces of a single foil results in a yield proportional to t^2 for t (foil thickness) $< t_f$ [6)]. The compromise is a sandwich array:

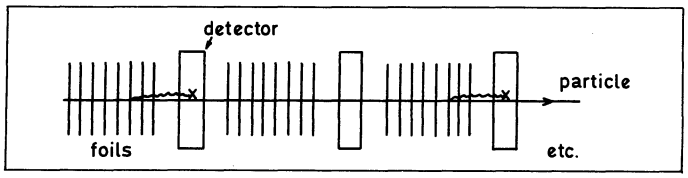

*) Visitor at CERN.

**) Paper contributed by J.H. Mulvey, Nuclear Physics Laboratory, Oxford University, England.

1.1.2 X-ray detection

A multiwire proportional chamber (MWPC) is in many ways a very good choice for a detector of the X-rays.

a) Most of the X-rays are in the 1-30 keV band, and a proportional chamber is efficient for those energies, especially if filled with a high-Z gas such as krypton or xenon.

b) An MWPC provides good spatial resolution, wide angular acceptance, and multiparticle capability, all important for a device which is to be placed downstream of a target to identify secondary products.

c) Because of the $1/\gamma$ emission angle, the transition radiation photons remain close to the parent particle trajectory, providing a "label"[7]; in the gas of a MWPC the ionization energy loss by a relativistic particle is relatively small, a few keV.

1.1.3 The Bevatron experiment

Details of this experiment are given in Ref. 1. An array of eleven modules, each consisting of a radiator followed by a MWPC 1.5 cm thick, was used. There were three types of radiator:

i) 100 foils, each of mylar 12 μ thick and spaced 0.75 mm apart in air;

ii) 100 foils of 4 μ mylar, spaced 1.5 mm;

ii) 2-inch slabs of styrofoam.

Runs were also made with single sheets of plastic of the same total thickness as the radiators, and also with no material present. These runs confirmed that the background from bremsstrahlung or δ-rays produced in the foil material was negligible.

The MWPC were operated with fillings of argon (93%) plus methane (7%), and also krypton (93%) plus methane (7%).

The pulse height was recorded from each MWPC, and data were taken with 3.0 GeV/c and 1.3 GeV/c electrons and pions.

Since the measured pulse height is proportional to the total of ionization energy loss plus any X-ray that might have been absorbed, the number of X-rays cannot be simply counted. However, by comparing the pulse-height distributions with and without radiators, the number detected can be estimated. Table 1 gives the lower limit to the number of detected X-rays under different conditions. (This limit is simply obtained by assuming not more than one X-ray detected per chamber per particle.)

The yields are small; to predict the use of such a device for identifying high-energy pions, one can consider the yield for 3 GeV/c e^- as being equivalent to that of 820 GeV/c pions.

The yield from 4 μ foils is lower than that for 12 μ foils; this is a consequence of the interference noted above.

Krypton is more efficient than argon because of the K-edge at $\sim$ 14 keV.

Figure 1 shows the distribution in the total pulse height (sum over eleven chambers) with krypton filling under three different conditions: (a) was obtained with 3 GeV/c pions; 3 GeV/c electrons without radiators gave distribution (b) (dotted) which is clearly shifted

Table 1

N_γ, lower limit to total number of X-rays detected in eleven chambers

Particle	Radiator	Gas	N_γ a)
3 GeV/c e^-	100, 12 μ	argon	3.6 ± 0.7
		krypton	5.0 ± 0.5
$\gamma \sim 6{,}000$	100, 4 μ	argon	2.0 ± 0.8
(pion 820 GeV/c)		krypton	2.6 ± 0.7
	2″ styrofoam	argon	1.4 ± 1
1.3 GeV/c e^-	100, 12 μ	argon	2.5 ± 0.8
$\gamma \sim 2{,}600$	100, 4 μ	argon	1.0 ± 1.0
(pion 350 GeV/c)			
3 GeV/c π^-	100, 12 μ	argon	0.3 ± 1
$\gamma \sim 21.6$			

a) The errors shown are conservative estimates of the uncertainty due to variations in chamber calibration between the runs being compared to obtain N_γ; statistical errors are much smaller.

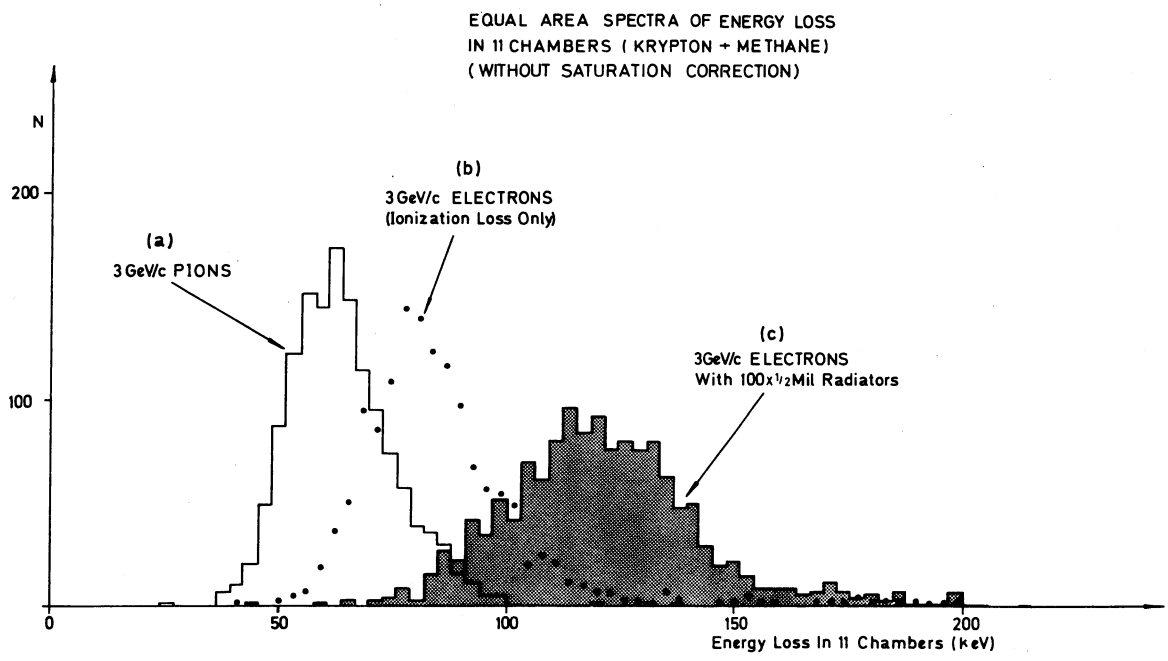

Fig. 1

to higher values by the relativistic rise[8,9]; the detection of transition radiation is clearly demonstrated by the displacement to still higher total pulse height of distribution (c) obtained when foils are placed in front of the chambers. Similar results have been obtained by the Brookhaven group[10,11].

1.1.4 Particle identification

Very crudely (c) is equivalent to the distribution which would be obtained with 820 GeV/c pions and (b) is an approximation to 820 GeV/c protons; the "separation" which would be obtained by applying a simple threshold is about 85% efficiency for counting pions and 15% for protons. This is not very good, but by using more chambers, more foils, xenon gas, etc., a similar system could be constructed which would achieve much better efficiencies at these high values of γ. Transition radiation has been proved effective in the separation of electrons and pions. But the problem which needs a solution is that of identifying a number of secondaries (hadrons) over a wide solid angle in a momentum range of, say, 10-400 GeV/c. In spite of many optimistic assertions in the literature, the detailed design of a device based on transition radiation and satisfying this need with adequate efficiency is still lacking[12]; it is unlikely that a system of the type I have described will be useful for particles with a $\gamma \leqslant 3{,}000$ (pion momentum $\leqslant$ 400 GeV/c).

Loss of transition radiation X-rays by absorption in the foils is a very serious effect; for example, in the experiment using 3 GeV/c electrons and one hundred 12 μ mylar foils per chamber, the number of X-rays produced (of energy $\geqslant$ 1 keV) is estimated to be about sixteen times greater than the number detected using krypton. To lower the losses by photoelectric absorption, material of lower Z must be used, and Bateman[13] has suggested the use of a deuterium or solid hydrogen foam; if this technique is feasible, and the cryogenic problem of maintaining the foam within a container providing large aperture and very thin windows can be solved, then certainly the prospect of using transition radiation for secondary particle identification down to lower γ would be significantly improved.

1.2 Counting techniques applied to transition radiation X-rays and the suppression of signals due to ionization losses*)

(summarized by rapporteurs)

Experimental results from an arrangement similar to that of Mulvey (Section 1.1 above) were reported. Three multiwire proportional chamber arrays were used both to reconstruct particle tracks and to detect transition radiation X-rays from 200 mylar foils, 0.035 mm thick, or 20 cm of polyethylene foam. 1 GeV electrons passed through the foils and the chambers. In each proportional chamber about 120 ion pairs were produced by the ionization effect of the high-energy particles. A typical transition radiation X-ray would liberate about 400 ionization electrons within a small volume, producing one large pulse, in contrast to the ionization signal which would appear as a succession of smaller pulses more spread out in time. By lowering the voltage below 3 kV the chambers could be made relatively insensitive to ionization signals without losing efficiency for X-ray detection. Figure 2 shows the results for a) the efficiency of detection of the ionization signal, and b) the efficiency for detection of transition radiation X-rays from 20 cm of polyethylene foam.

---

*) Paper contributed by S.J. Prünster, DESY, Hamburg, Germany.

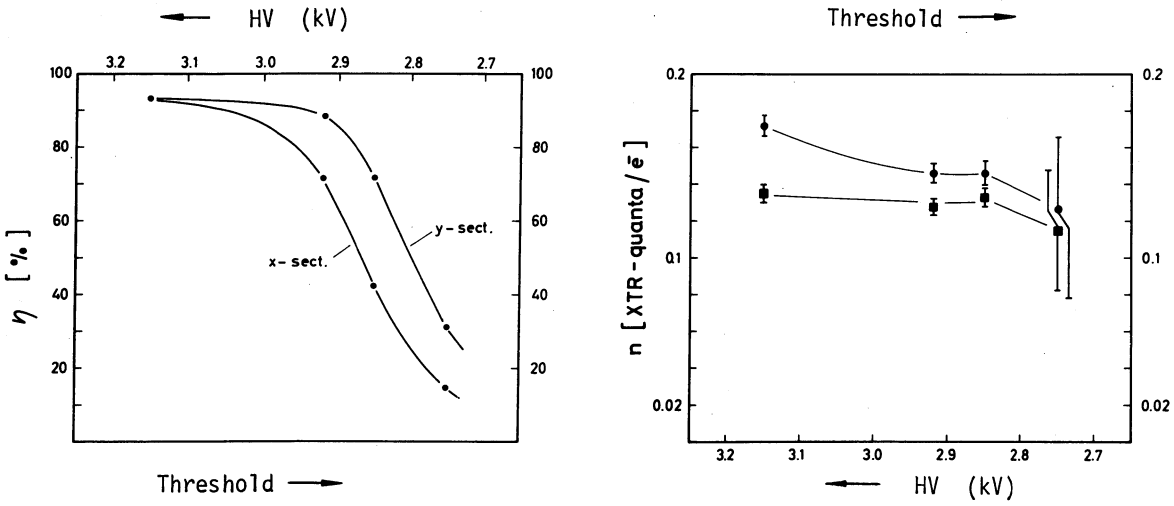

Fig. 2

Thus it should be possible to make a device predominantly sensitive to transition radiation, which would give improved discrimination between particle types.

2. SPOT-FOCUSING ČERENKOV COUNTERS

2.1 A spot-focusing Čerenkov counter for the detection of multiparticle events at high energies*)

(summarized by authors)

2.1.1 Introduction

Several attempts have been made**) to devise a Čerenkov counter which can accept a diverging beam of particles. These have been based on the principle, as illustrated in Fig. 3a, of using spherical optics in order to focus the Čerenkov light into a ring image.

The present report outlines an improvement in the design of such a counter for the case of detecting particles coming from a small volume in space, such as from a target. This detector uses conical or toroidal optics to focus the Čerenkov light of a particle with a given velocity β_0 (or $\gamma_0 = E/m$) into a small spot image. The concentration of the light yield simplifies the detection problems. For a particle with velocity $\beta \neq \beta_0$, a ring image is produced instead of a spot, the radius of the ring being related to the particle velocity. The position of the spot (or centre of the ring image) yields information on the angular coordinates of the particle.

The principle of the spot-focusing detector is illustrated in Fig. 3b in which the conical waves of the Čerenkov light are converted into plane waves, which can then be focused to a spot. The conversion of conical waves into plane waves is performed by introducing an optical path-difference proportional to the height of impact of the light-ray from the particle trajectory; such a path-difference is produced by using an axiconic lens or mirror.

---

*) Paper contributed by M. Benot, J.M. Howie, J. Litt and R. Meunier, CERN, Geneva, Switzerland.

**) A more detailed version of this report containing all relevant references is to be submitted for publication in Nuclear Instrum. Methods.

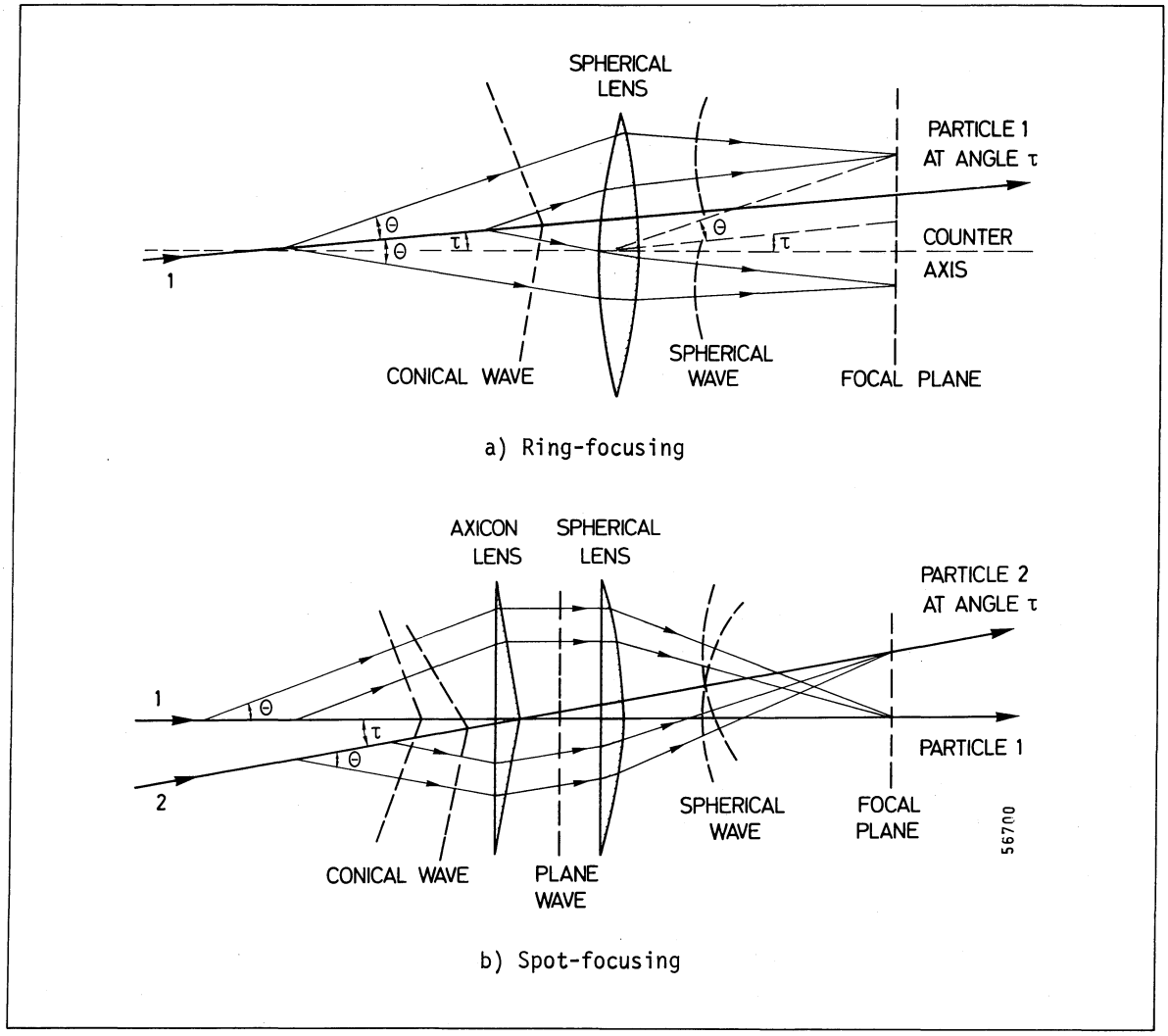

Fig. 3

One necessary condition for achieving spot focusing is that the trajectory of the particle must pass through the apex of the optical element; and in fact for multiparticle detection the apex must coincide with the position of the production target.

2.1.2 The spot-focusing detector

a) Optical configuration

The simplest configuration for a spot-focusing detector is shown in Fig. 4. In this case, the axicon is placed virtually at the target position using an inclined plane mirror. The target is located at the centre of curvature of a spherical mirror and the optics are thus free from large coma aberrations. The spot focus is formed at a virtual image in the focal plane F of the spherical mirror. A conventional transfer lens is used to produce the final real image in the plane of the electronic detection system. The magnification in the last stage is designed to match the required angular resolution to the detector size. Since this latter point is a rather well-known design problem, it will not be pursued further in this report.

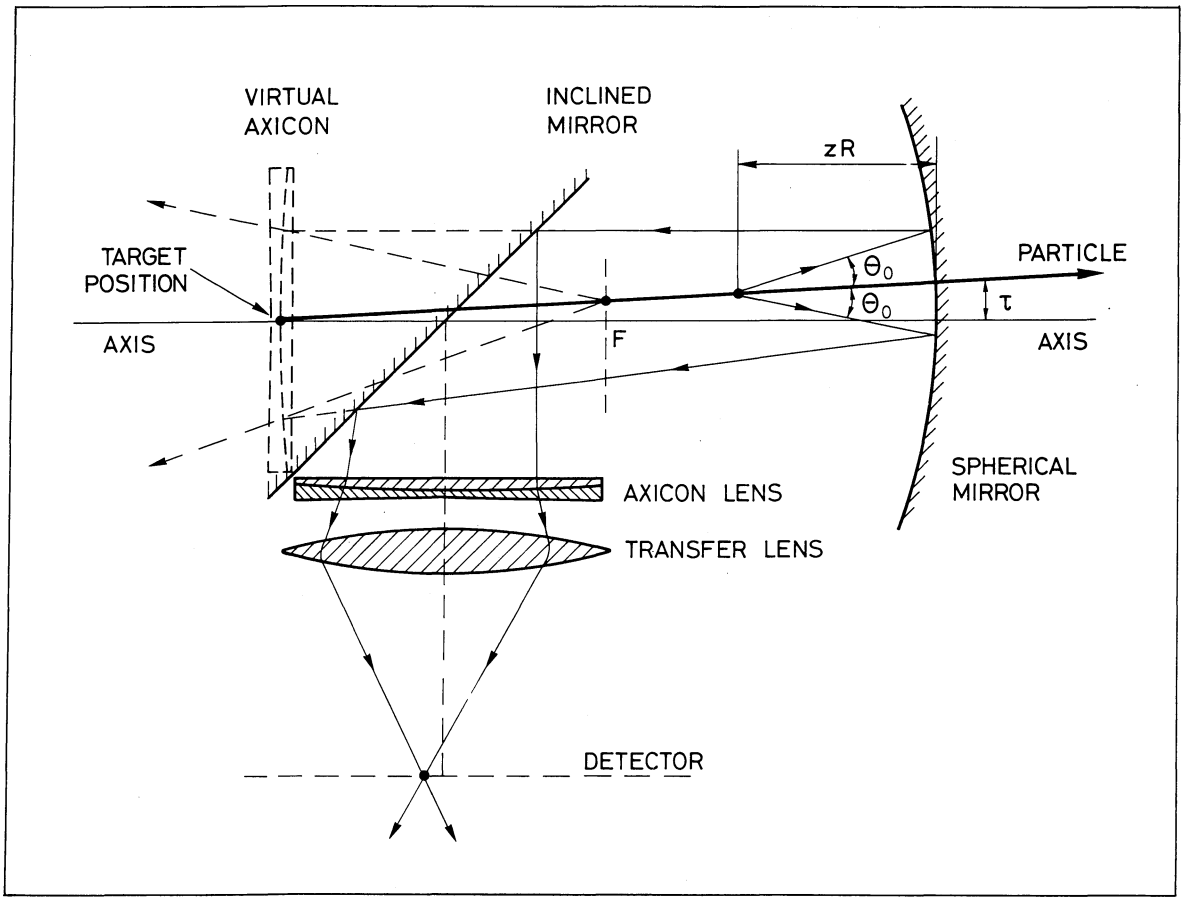

Fig. 4

b) The basic design parameters

A ray-tracing simulation has been performed for the spot-focusing counter based upon the configuration of Fig. 4 and having the following design parameters:

i) The gas pressure in the counter is set to produce spot-focused images for particles with $\beta_0 = 1$ (or $\gamma_0 = \infty$). Helium gas at 6 atm pressure is used, which corresponds to a Čerenkov angle $\theta_0 = 20$ mrad for particles with $\beta_0 = 1$.

ii) The radius of curvature R of the mirror is 10 m, and the length L of gas radiator is 8 m.

iii) The radius a of the cross-sectional area of the production target is nominally set at 1 mm, and the maximum divergence angle τ of detected particles is ±20 mrad.

iv) The axicon bends the rays of light to produce spot-focusing and, at the same time, corrects to first order the chromatic dispersion of the Čerenkov angle. In order to perform these two functions an axicon doublet has been assumed, with elements of sodium chloride and fused silica.

v) The detection of light is based upon the use of photomultipliers which, for each detected particle, produce a total output of about 30 photoelectrons from the photon wavelength interval 280-440 nm. (The detector coefficient A is assumed to be A = 100 cm^{-1}.)

c) Evaluation of the image

In Fig. 4, a particle is shown which is emitted from the centre of the production target with a velocity β_0 and which forms a spot image in the focal plane of the spherical mirror. One can consider the general case of a particle of velocity β which is produced at a distance a (radially) from the centre of the target and having a divergence angle τ and azimuthal angle ψ. Čerenkov light (at an angle θ) is emitted from a point along the particle trajectory at a distance zR from the mirror, where R is the radius of curvature of the mirror and z is a multiplicative factor restricted to having values between 0 and 0.8. If one selects a particular ray of light making an angle ω around the Čerenkov cone and traces this ray through the optical system, then

$$X = -r \sin \omega + \Delta \cos \omega + \frac{1}{2} R\tau \sin \psi \ ,$$

$$Y = r \cos \omega + \Delta \sin \omega + \frac{1}{2} R\tau \cos \psi \ ,$$

where Δ and r are defined by

$$\Delta = \frac{a\theta_0}{2\theta\ (1 - z)} \sin \omega$$

$$r = \frac{R}{2} |\theta - \theta_0| \approx \frac{R}{4\theta_0} \left| \frac{1}{\gamma^2} - \frac{1}{\gamma_0^2} \right| \ .$$

The shape of the image as described by the above equations is given in Fig. 5, from which one can conclude the following:

i) For a particle of velocity β_0 (or $\gamma = \gamma_0$) for which the counter is "tuned" and for an infinitely small target size (a = 0), the image is theoretically a point at S (if chromatism and high-order aberrations are neglected).

ii) A particle of any other velocity β, and when a = 0, will produce a ring image, denoted by "ρ" in Fig. 5, which is centred on the point S.

iii) The error due to the target size a transforms the expected ring image ρ into a fourth-order curve, which is shown as "ρ^*" in Fig. 5.

iv) Along the trajectory of the particle, each light-ray will correspond to a different value of z, and thus the final image in the focal plane will be made of points each belonging to a different curve ρ^*.

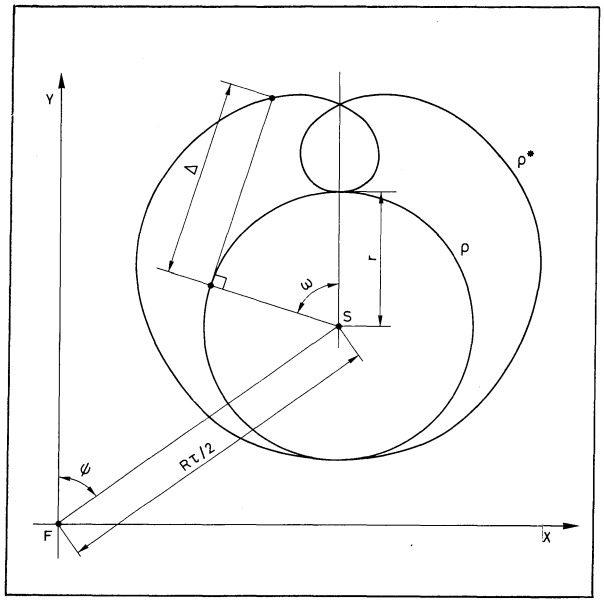

Fig. 5

Hence the evaluation of a spot-focusing detector must take into account the above properties of the image, together with a smearing of the pattern by effects such as the residual optical aberrations, multiple scattering, and photoelectron statistical fluctuations.

d) Optical aberrations

In the design of the axicon doublet one can choose the conical angles of the two elements in order to achieve spot-focusing and to minimize the residual chromatic aberrations in the final image. An optimization of the axicon doublet design has produced a ratio of the primary to the secondary (residual) chromatism of 5 : 1, and the final angular chromatism which remains in a spot image for a target radius of 1 mm is approximately $\Delta\theta_{chr} \approx 4 \times 10^{-2}$ mrad.

The coma aberration can be reduced below the level of $\Delta\theta_{coma} \approx 1 \times 10^{-2}$ mrad by slightly changing the angle which the first surface of the axicon doublet makes with the axis. The spherical aberration, which is already quite small, can be further reduced by introducing toroidal (instead of conical) lenses.

e) Multiple scattering

Multiple scattering in the target, entrance window, and gas radiator cause a spread of the image in the focal plane. An estimate of the size of the effect in the gas is given by the r.m.s. multiple scattering angle, which for 8 m of helium gas at 6 atm and for a 100 GeV/c particle corresponds to $\Delta\theta_{ms} \approx 5 \times 10^{-2}$ mrad. The multiple scattering in the production target, the thickness of which is determined by the requirements of a particular experiment, must also be taken into account.

2.1.3 Results of simulation and performance evaluation

The results from a simulation program have been studied for the detector design of Fig. 4 and having the basic parameters outlined in Section 2.1.2 (b). Figure 6 shows typical patterns formed in the image plane by randomly generated light-rays from a single particle trajectory.

It can be shown that the spot-focusing detector and differential Čerenkov counter have an equivalent phase-space acceptance. The main difference between these two detectors is

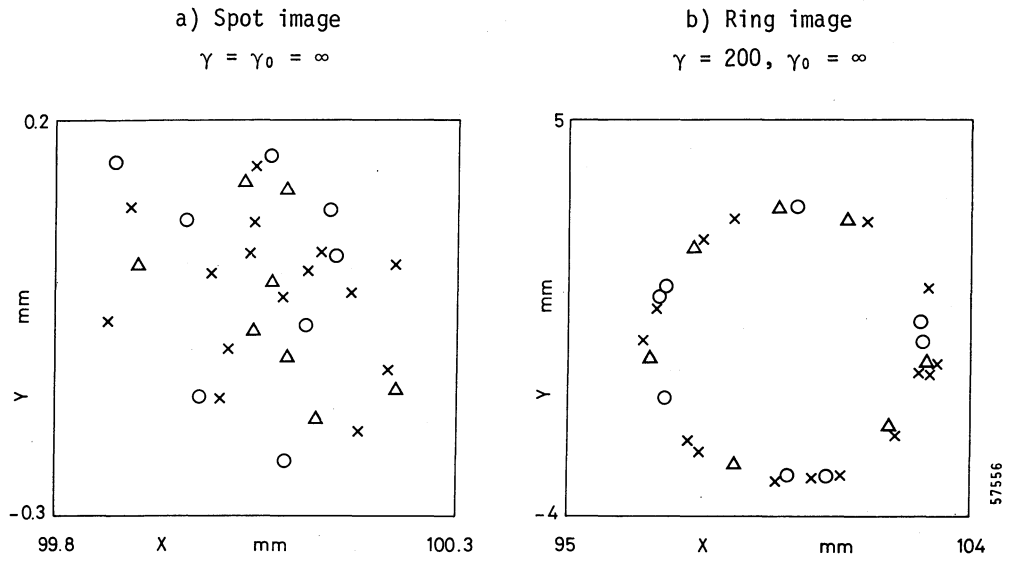

Fig. 6

that the differential counter is a single-channel device, whereas the spot-focusing counter can be multiplexed, and therefore can produce more information concerning a given high-energy interaction.

2.1.4 Conclusions

The preliminary design studies indicate the feasibility of the spot-focusing Čerenkov detector, provided that it is used together with a small-sized production target. For a target radius of about 1 mm, the detector can provide the angular coordinates of each particle track to within $\approx \pm 0.1$ mrad and the velocity to an accuracy $\Delta\beta \approx 2 \times 10^{-6}$. The counter is sensitive within a given design range of γ and for large angular acceptance values up to $\approx \pm 20$ mrad.

An instrument which can detect multiparticle (charged) events and provide the angular coordinates and velocity of each separate particle will be a useful complement to the position and sign-of-charge information from magnetic wire chamber systems. The spot-focusing detector is a novel application of the Čerenkov technique which might prove to have an important role in high-energy physics instrumentation.

This example has been chosen to illustrate the principle of the spot-focusing counter, and is suitable for the particular application of detecting forward-going particles from a high-energy interaction. In principle, this technique can have a wider application; for example, to the detection of large production angles, and for larger target sizes at the expense of obtaining a lower velocity resolution.

3. MULTIWIRE PROPORTIONAL CHAMBERS

3.1 Optimization of multiwire proportional chambers*)

(summarized by rapporteurs)

Results were presented for a method of improving the uniformity of the pulse-height information given by a multiwire proportional chamber. This was achieved by a simple arrangement allowing independent adjustment of the voltages on the individual wires. Uniformity of pulse height within a few per cent was obtained.

4. TOTAL ABSORPTION SPECTROMETERS

4.1 A total absorption spectrometer for energy measurements of high-energy particles**)

This report has been submitted to Nuclear Instruments and Methods. It describes the performance of a sandwich of iron and scintillator plates when used as a total absorption counter for the measurement of energies of neutrons or other strongly-interacting neutral particles. An energy resolution of ±11% was achieved at 24 GeV/c. The authors have recently estimated that the resolution should be better by a factor of 2 at 100 GeV/c.

---

*) Paper contributed by J. Renuart and G. Grégoire, University of Louvain, Belgium.

**) Paper contributed by J. Engler, W. Flanger, B. Gibbard, F. Mönnig, K. Runge and H. Schopper, CERN, Geneva, Switzerland and Institut für Experimentelle Kernphysik, Karlsruhe, Germany.

REFERENCES AND FOOTNOTES

1) F. Harris, T. Katsura, S. Parker, V.Z. Peterson, R.W. Ellsworth, G.B. Yodh, W.W.M. Allison, C.B. Brooks, J.H. Cobb and J.H. Mulvey, Oxford Nuclear Physics Preprint 57/72, submitted to Nuclear Instruments and Methods.

2) S. Prünster, CERN/ECFA/71-18.

3) G.M. Garibyan, Yerevan preprint EFI-TF-13 (1970). This article contains references to many other papers on transition radiation.

4) L. Yuan, C.L. Wang and S. Prünster, Phys. Rev. Letters 23, 496 (1969).
L. Yuan, C.L. Wang, H. Uto and S. Prünster, Phys. Rev. Letters 25, 1513 (1970).
L. Yuan, C.L. Wang, H. Uto and S. Prünster, Phys. Letters 31 B, 603 (1970).
H. Uto, L. Yuan, G. Dell and C.L. Wang, Nuclear Instrum. Methods 97, 389 (1971).

5) R.W. Ellsworth, J. MacFall, P.K. MacKeown and G.B. Yodh, Proc. 6th Inter-American Seminar on Cosmic Rays, La Paz, Bolivia, 1970 (Univ. S. Andrés, La Paz, 1970), Vol. 2, p. 344.

6) t_f [often called the "formation zone[3]"] is a function of γ, the energy and angle of emission of the X-ray, and the foil plasma frequency; for example, the value of t_f for emission of 10 keV photons at an angle $1/\gamma$ by a particle of γ = 6,000 entering mylar is $\sim$ 6 microns.

7) A long drift-length aided by magnetic bending has been used to separate the particle and photon trajectories spatially after the radiator stack. This geometry is not easy to use if a sandwich array, with more than one radiator stack, is needed for sufficient yield.

8) The magnitude of the relativistic rise obtained is 1.64 ± 0.14 in argon and 1.71 ± 0.13 in krypton. Both are about 10% lower than the values predicted by Sternheimer and Peierls (see Ref. 9).

9) R. Sternheimer and R.F. Peierls, Phys. Rev. B3, 3681 (1971).

10) C.L. Wang, G.F. Dell, H. Uto and L.C.L. Yuan, Phys. Rev. Letters 29, 814 (1972).

11) L. Yuan, Z. Dimčovski, H. Uto and G.F. Dell, CERN/ECFA/72/4 (1972), Vol. I, p. 359.

12) In a recent paper, Wang et al. (see Ref. 10) quote efficiencies of 65% for pions and 10% for kaons at 400 GeV in an arrangement in which magnetic deflection is used to separate spatially the transition radiation photons and particle trajectories. A great improvement in efficiency and rejection must be achieved to reach a useful level of performance; also the arrangement proposed would be most easily accommodated in primary beams where, although expensive, Čerenkov devices have far superior rejection characteristics. It has also been suggested (Ref. 11) that by the combination of relativistic rise and transition radiation -- as detected in a gas-filled MWPC -- it will be possible to separate "all particles in the 300 GeV region and above". However, the relativistic rise in a gas at atmospheric pressure reaches a plateau by $\gamma \sim 200$; thus this effect cannot contribute to the discrimination of particles of 300 GeV/c momentum or higher. Without a considerable improvement in technique there is a large gap between the upper limit in γ of usefulness of relativistic rise, and the lower limit to the effective use of transition radiation.

13) J.E. Bateman, Nuclear Instrum. Methods 103, 565 (1972); see also CERN/ECFA/72/4 (1972), Vol. I, p. 353.

KINEMATICAL ANALYSIS AT HIGH ENERGIES *)

W. Matt
Max-Planck-Institut für Physik und Astrophysik, Munich, Germany

1. INTER-TRACK CORRELATIONS

A single vertex event with n charged tracks can be described by the following parameters:

$1/p_i$, λ_i, ϕ_i the inverse momentum, dip, and azimuth angle for each track.

X_0, Y_0, Z_0 the coordinates of the vertex.

If all 3n + 3 parameters were fitted simultaneously in a geometry program, the resulting error matrix would contain inter-track correlations (i.e. the parameters $1/p_i$, λ_i, ϕ_i of track i are correlated with $1/p_j$, λ_j, ϕ_j of track j).

In the geometry programs generally used in bubble chamber physics, each track is fitted independently from the others. Thus for each track, $1/p_i$, λ_i, ϕ_i, Y_i, Z_i (X_i is held fixed) is fitted, giving in total 5n parameters. This means that 2n - 3 parameters are fitted unnecessarily, giving away valuable information contained in the measurements of bubble chamber pictures.

It has been shown[1] that without losing the computational advantage of fitting the tracks separately, the inter-track correlations can be retrieved later by eliminating the unnecessary parameters (i.e. imposing the constraint that all tracks have to go through one point, i.e. the vertex).

The question arises whether this additional information is really relevant for the kinematical analysis.

To answer this question, the reaction

$$K^+ + p \to K^+ + p + \pi^+ + \pi^- + \pi^0$$

was studied. The track length in BEBC was determined, and the errors on the track parameters were computed for the contribution of the measurement error and multiple scattering. For each Monte Carlo event, the probability was calculated that this event can be interpreted as

$$K^+ + p \to K^+ + p + \pi^+ + \pi^- ,$$

i.e. a 4C-fit.

It was found that using the inter-track correlations the number of wrongly interpreted events can be reduced by a factor of two compared to the standard procedure of forgetting the vertex parameters. Thus only about 3% of the π^0 events will fit to a 4C hypothesis, and this can be tolerated.

An improvement in the error on the missing-mass squared of 20-30% could be observed for events with a slow π^0.

---

*) Contributed paper

2. NEW ERROR FORMULAE

The formulae for computing the contribution of measurement error and multiple scattering to the errors of the track parameters were derived at a time when mass-dependent fitting was not used. For tracks losing a significant fraction of their energy within the chamber, multiple scattering near the end of the track (the measurement error can be neglected for these tracks) has less influence on the fitted momentum when the mass-dependent fit is used than in the case in which a helix fit is performed. Thus different error formulae for the fitted track parameters should be used; these are derived elsewhere[2].

According to the old formulae, the contribution of the momentum error to the error on the missing-mass squared (in the case of the neutral system being fast) is maximum for protons which are slow but do not stop in the bubble chamber[3]. For BEBC this corresponds to a momentum region of 0.7 to 1 GeV/c. In this critical region, the new error formulae decrease the error on the missing-mass squared by about a factor of two, thus allowing one to separate some 1C-fits from 0C-fits up to a momentum which is twice as high as that estimated so far.

3. TRACK SEGMENTATION

The improvement in momentum determination described above can only be reached when measurements go beyond the so-called "optimum length". With the standard mass-dependent fit, the multiple-scattering errors on the angles defining the initial direction might in this case become unacceptably large. This can be overcome by the parametrization method[2,4] (i.e. by dividing the track into segments) where the errors on track direction do not increase when measurements go heyond the old optimum length. Thus one can take full advantage of the improved momentum. By segmenting the track, a gain up to a factor of two in angular precision can be achieved compared with the standard mass-dependent fit over the whole track length. A chamber with a smaller measurement error helps to improve the determination of the starting direction even for tracks where multiple scattering dominates, since it allows one to use a smaller segment length.

A smaller error in track direction due to segmenting the track and a smaller error on the track momentum due to the new formula will reduce the error on missing-mass squared and increase the energy range where one can separate 1C-fits from 0C-fits. This will be 20-30 GeV/c in BEBC (ε = 300 μ) and 40-50 GeV/c in a small high-precision chamber (ε = 30 μ).

* * *

REFERENCES

1) W. Matt, CERN-ECFA Report WG/72-148 (1972).

2) W. Matt, CERN-ECFA Report WG/72-18 (1972).

3) W. Matt, CERN-ECFA Report WG/72-147 (1972).

4) P. Laurikainen, W.G. Moorhead and W. Matt, Nuclear Instrum. Methods 98, 349 (1972).

CONSIDERATIONS ON THE DESIGN OF A VERTEX DETECTOR FOR SPS ENERGIES*)

A. Grant
CERN, Geneva, Switzerland

A vertex detector is a device incorporating a target which has the capacity to measure the momenta and angles of one or more slow tracks with sufficient accuracy over a large fraction of 4π solid angle. The range of momentum of the detector has been taken as less than 2 GeV/c. Tracks of momenta greater than 2 GeV/c are assumed to be measured in a "forward spectrometer" of the Hyams-Koch type (CERN/ECFA/72/4, Vol. I, Section 8.8).

The complete apparatus, spectrometer and vertex device, should have the capacity to fully reconstruct all tracks of an interaction, in an unbiased way, at incident momenta greater than 100 GeV/c.

There are three possible ways in which a vertex detector can be used, each with different conditions of angle and momenta accuracy:

i) as a recoil spectrometer with no measurement of fast tracks;

ii) as part of a general device to measure all charged particles and fit neutrals from the kinematic constraints;

iii) as part of a general device to measure only charged particle reactions; neutrals, e.g. π^0's, are vetoed by anticoincidence with gamma detectors.

The purpose of this note is not to propose any particular hardware, but to consider in general terms the features any reasonable detector must have in order to satisfy the conditions of measurement accuracy. In particular, it is possible to show from considerations of error formula that the type of detector used puts strong constraints on the size and magnetic field of the whole apparatus.

It is clear that, in general, errors on momenta and angles of slow tracks are dominated by the multiple scattering contributions. This effect is ignored in the following sections. There can be no simple answer to the elimination of multiple scattering, only the careful design of the detector, target, and beam in such a way as to remove all unnecessary material.

1. VERTEX DETECTOR AS A RECOIL SPECTROMETER

It was found from the discussion on errors of a missing mass Δm_x^2 given in CERN/ECFA/72/4, Vol. I, p. 31 that the contribution to Δm_x^2 from the i^{th} measured track is

$$\Delta m_x^2 = 2(E_x\beta_i - p_x \cos\theta_i)\Delta p_i$$

$$\Delta m_x^2 = 2p_i p_x \sin\theta_i \, \Delta\theta_i \, .$$

For a missing-mass spectrometer the condition $\Delta m_x = 20$ MeV at $m_x = 2$ GeV and $p_x = 200$ GeV is reasonable. In Figs. 1 and 2 are shown the minimum required $\Delta p/p$ and $\Delta\theta$ errors calculated from the formulae above (for slow measured tracks). It can be seen that apart from the 'Jacobian peak' region, the 20 MeV error condition would require

$$\Delta q = \frac{\Delta p}{p^2} \leq 4 \times 10^{-4}$$

*) Contributed paper

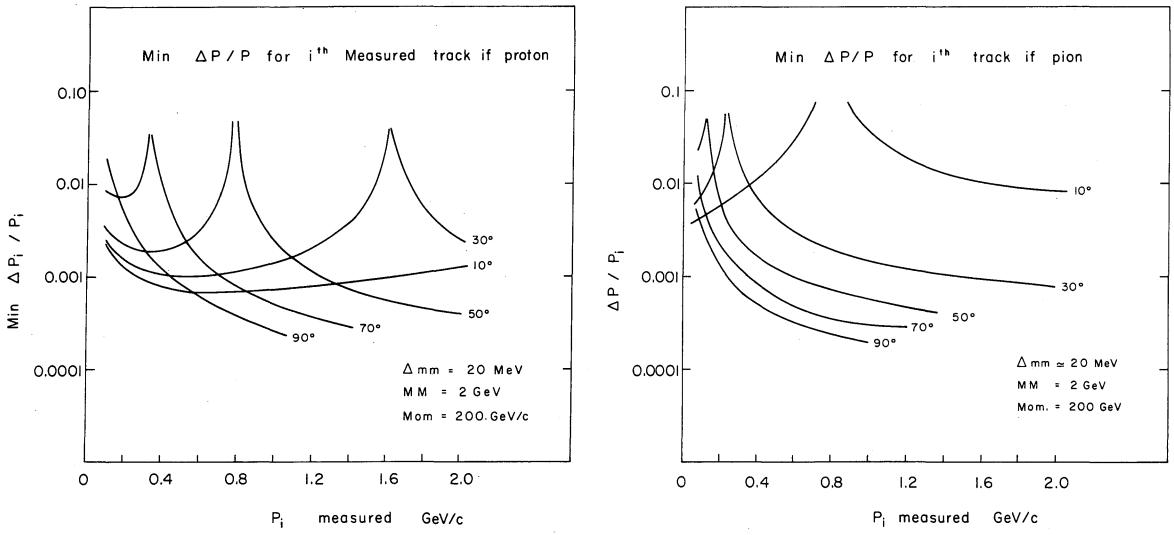

a) b)

Fig. 1

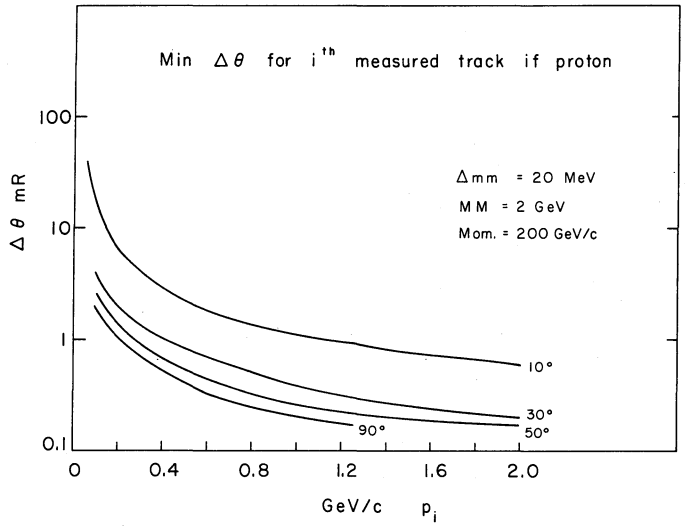

Fig. 2

and

$$\Delta\theta \lesssim 0.2 \text{ mrad} .$$

A general device with this accuracy seems unreasonable. However, work in the 'Jacobian peak' region where the recoil is against a single particle still seems possible.

2. VERTEX DETECTOR FOR ALL EVENTS

In this case the requirement is that all tracks are measured with sufficient accuracy such that single π^0's may be kinematically reconstructed. In particular, for slow measured tracks this implies

$$\Delta m_X = m_\pi \quad \text{at} \quad m_X = m_\pi \quad \text{at momenta of 100 GeV/c} ,$$

which gives

$$\Delta q = \frac{\Delta p}{p^2} \lesssim 10^{-3}$$

and

$$\Delta\theta \lesssim 5 \times 10^{-4} \quad \text{for } p > 0.5 \text{ GeV/c}$$
$$\Delta\theta \lesssim 10^{-3} \quad \text{for } p < 0.5 \text{ GeV/c} .$$

Tracks with momenta greater than 2 GeV/c are measured in a forward spectrometer.

In the following discussion, error formulae for $\Delta\theta$ for Δq have been used in the two cases.

i) Measured points in the field region:

$$\Delta\theta = \frac{\sqrt{96}}{\sqrt{N + 4.9}} \frac{\varepsilon}{L \cos\lambda}$$

$$\Delta q = \frac{\sqrt{720}}{\sqrt{N + 5}} \frac{\varepsilon}{L^2 \cos^2\lambda \ (0.3 B)}, \qquad q = \frac{1}{p} .$$

ii) Measured points outside the field region:

$$\Delta\theta = \frac{\sqrt{2}}{\sqrt{N}} \frac{\varepsilon}{L \cos\lambda}$$

$$\Delta q = \frac{2}{\sqrt{N}} \frac{\varepsilon}{L \cos^2\lambda \ 0.3 B\ell} .$$

N points measured with setting error ε in length L at field B tesla.

It may be seen from these error formulae that there is a significant loss in accuracy for the same N, ε, and L in the case where the measured points are inside the field region. In some cases this loss, due to the correlations between p and θ, can be recovered after full kinematic fitting.

From the conditions on Δm_x and the formulae above, some general conclusions can be drawn about the size and field of the detector required.

i) Points measured in the field region:

The important parameters are N, the number of points measured; B, the field; and ρ, the spacing of measured points:

$$\text{length of track} , \quad L = \rho N$$

$$\text{set } \cos\lambda = 1 .$$

Figure 3 shows a plot of N against B kG, the curves shown correspond to the limits set by

$$N\sqrt{N + 4.9} \gtrsim \frac{\sqrt{96}\ \varepsilon}{\rho\ B\theta} \tag{1}$$

$$N^2\sqrt{N + 5} \quad > \frac{\sqrt{720}\ \varepsilon}{\rho^2\ \Delta q\ 0.3\ B} \tag{2}$$

and

$$N \gtrsim 3$$

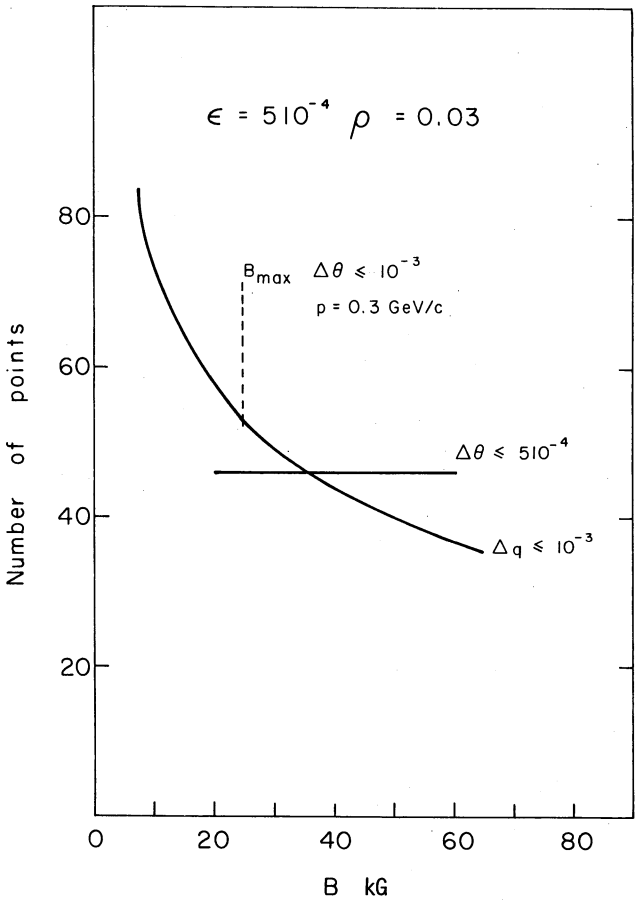
$\epsilon = 510^{-4}$ $\rho = 0.03$
B_{max} $\Delta\theta \leq 10^{-3}$
p = 0.3 GeV/c
$\Delta\theta \leq 510^{-4}$
$\Delta q \leq 10^{-3}$
Number of points
80
60
40
20
0
20
40
60
80
B kG

Fig. 3

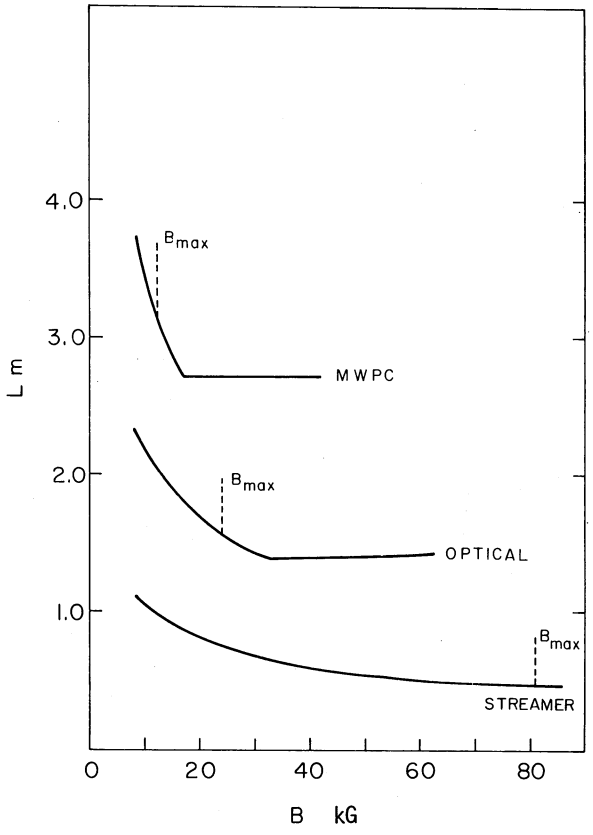
4.0
3.0
2.0
1.0
L m
B_{max}
MWPC
B_{max}
OPTICAL
B_{max}
STREAMER
0
20
40
60
80
B kG

Fig. 4

with

$$\varepsilon = 5 \times 10^{-4} , \quad \rho = 0.03$$

and

$$\Delta q \lesssim 10^{-3} , \quad \Delta\theta \lesssim 5 \times 10^{-4} .$$

Any viable detector must operate above the envelope of these curves.

A further condition may be added such that there is a maximum field possible to allow sufficient points to be measured on a slow spiraling track:

$$B \lesssim \frac{2\pi\, p}{0.9\, N\rho} .$$

This assumes that after $\phi > 60°$ and $< 120°$, measured points are bad owing to non-isotropy of detector. The effect of this constraint is shown in Fig. 3 as the line B_{max} at 2.4 tesla for p = 300 MeV/c and the angular error $\Delta\theta \leq 10^{-3}$.

Three examples of different kinds of chambers have been taken:

MWPC 2 mm wire spacing
one coordinate every 15 cm ε = 0.7 mm

Optical with Plumbicon
one coordinate every 3 cm ε = 0.5 mm

Streamer with film
one coordinate every 0.5 cm ε = 0.2 mm .

The comparison of these chambers is shown in Fig. 4, a plot of minimum required track length, L metres against magnetic field B in kG. Only in the case of the streamer chamber is the point density sufficiently high to allow the use of high magnetic fields:

MWPC	B_{max}	11.5 kG	L_{min}	3.3 m
Optical	B_{max}	24 kG	L_{min}	1.6 m
Streamer	B reasonable	35 kG	L_{min}	0.7 m .

The conclusion of this would be that only with a streamer chamber is it possible to obtain the required accuracy on Δp and $\Delta\theta$ consistent with a reasonable size of magnet.

ii) Measured points outside the field region:

As mentioned previously, there is a significant gain in accuracy obtained by decoupling the measurements of p and θ. This is the normal situation with, for example, single-arm spectrometers. However, to generalize a spectrometer of this type to cover a large fraction of 4π is clearly technically very difficult, and could only be possible, from the point of view of cost, if the angle measurements are made in a short distance. Figure 5 shows schematically a possible layout of the device. 'C' magnets are used to make sectors of a ring, leaving the target in a field-free region in the centre.

There are several other advantages of having a field-free region round the target:

- simpler pattern recognition and vertex reconstruction;
- greatly reduced computer time for reconstruction of tracks.

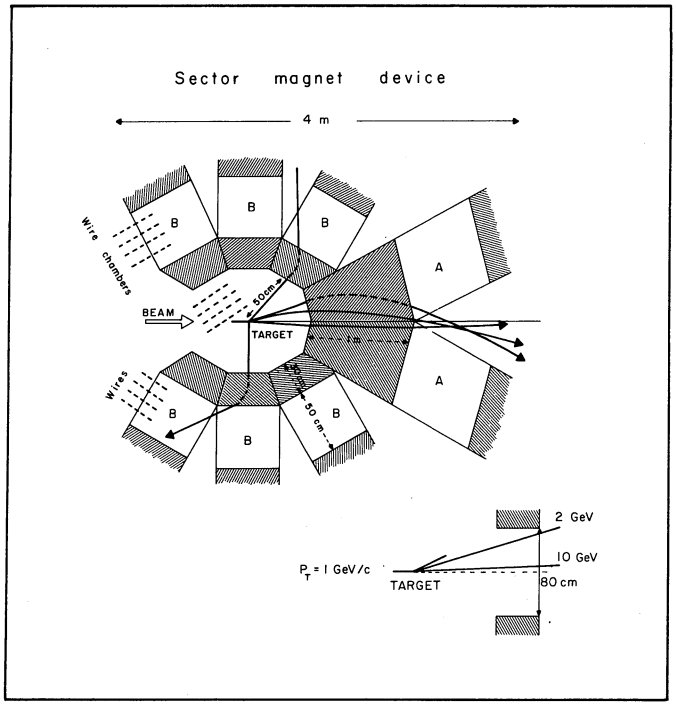

Fig. 5

As in the previous section, conditions can be placed on the dimensions and field of the device. The most obvious is that there is a maximum field for each of the sectors such that a slow track may be measured before and after the magnet. If the bending angle is $< 60°$ for a track of 300 MeV,

$$B\ell \lesssim \frac{\pi}{3} .$$

Using the conditions on Δq and $\Delta\theta$ as before and the error formula, (ii) gives:

$$\Delta\theta \lesssim 5 \times 10^{-4} , \quad \Delta q \lesssim 10^{-3}$$

$$B\ell = \frac{\sqrt{2}\,\Delta\theta}{0.3\,\Delta q} \lesssim \frac{\pi}{3}$$

$$\text{gives} \quad \Delta\theta \lesssim 2.2 \times 10^{-4} .$$

To satisfy this new condition on $\Delta\theta$ for each of the chamber types discussed before, with $B\ell_{max} = 1.1$ Tm:

MWPC	$\varepsilon = 0.7 \times 10^{-3}$	$\rho = 0.15$	$L = 1.47$ m
Optical	$\varepsilon = 0.5 \times 10^{-3}$	$\rho = 0.03$	$L = 0.71$ m
Streamer	$\varepsilon = 0.2 \times 10^{-3}$	$\rho = 0.005$	$L = 0.21$ m .

As before, only the streamer chamber gives, with the required accuracy, a magnet dimension which could be considered reasonable.

3. VERTEX DETECTOR FOR CHARGED PARTICLE REACTIONS

In this case the vertex detector is again assumed to be used with an accurate forward spectrometer which measures all tracks with momenta greater than 2 GeV/c. In addition, it is assumed that all fast π^0 events are removed by anticoincidence or are measured in angle

and energy by total absorption counters. Slow π^0 can be removed, by simple kinematic constraints, from the well-measured fast tracks. If these conditions are satisfied it would in principle be unnecessary to measure the momenta of up to three slow particles provided their angles and ionization were well measured.

This last case looks very attractive for a wide range of physics which can be studied in the only charged "4C" channels. The loss of slow π^0 events is more than compensated by the simplicity and lack of bias of any scheme with no magnetic field in the target region.

The fact that positive particle identification is necessary and is not obtainable from the kinematic constraints strongly favours the use of a streamer chamber as the vertex device.

4. CONCLUSION

The single point which comes out clearly from the above considerations on a vertex detector design is that the streamer chamber or the "crystal" projection chamber of Charpak have the required properties of low multiple scattering, high point density, and perhaps ionization measurements. It is unlikely that ultra-high magnetic fields $\sim$ 70 kG are required; the optimum seems to be in the 20-30 kG region. The question of the axis direction of the field used in a detector has not been discussed in this report, although an axial field, along the beam direction does have attractive features.

A COMPARISON OF PROPERTIES OF RAPID-CYCLING BUBBLE CHAMBERS AND STREAMER CHAMBERS*)

E. Lillethun
University of Bergen, Norway

At the panel discussion on results of the working parties, a request was submitted for a comparison of the use of streamer chambers and rapid-cycling bubble chambers in high-energy experiments. The answer showed that there are still some misunderstandings with respect to the possibilities of these types of chambers.

In the following I shall therefore try to clarify some relevant points.

The basis for the comparisons made below is mainly the data given in CERN/ECFA/72/4, Vol. I, paper 4.1: Rapid-Cycling Bubble Chambers by C.M. Fischer; and paper 4.2: The Use of a Streamer Chamber in High-Energy Experiments by H. Meyer. The comparison is by no means exhaustive.

1. SIZE

The rapid-cycling bubble chamber (RCBC) is inherently relatively small (linear dimensions 30-50 cm). At high energies it is therefore only of interest as a vertex chamber. A streamer chamber can be made larger and can be used not only as a vertex chamber but also as a detector in other parts of an experiment (e.g. a spectrometer).

The following comparison will mainly deal with the chambers used as vertex chambers.

2. TRIGGER POSSIBILITIES

An RCBC will go through the expansion cycle at a fixed rate (20-100 Hz depending on size). It cannot be triggered by an event selected by a trigger system. However, the recording of the picture of the event can be suppressed or performed according to such a trigger.

A streamer chamber can be triggered by a counter system that can provide the high voltage to the chamber within about 1 μsec.

Its memory time is of the order of a microsecond, but there are possibilities of "freezing" the event by a prepulsing of high voltage using a coarse, fast trigger, and then using a slow trigger (e.g. computer) to decide within milliseconds whether to record the event or not.

3. RECORDING SYSTEM

For the time being the events are photographed and the films scanned and measured in the usual way, either manually or by means of devices such as the HPD. However, much work is being done to introduce a digitized recording system using Plumbicon systems (see G. Amato and B. Powell, CERN/ECFA/72/4, Vol. I, Section 4.4).

---

*) Contributed paper

A successful solution of this problem is necessary before the repetition rate can be increased substantially beyond 10 Hz, since the film advance time is typically 0.1 sec.

It also seems that development work will make it feasible to use image intensifiers in the recording of streamer chambers. This could increase the measurement accuracy (smaller streamer size) and reduce the dead-time of the chambers.

4. BEAM REQUIREMENTS

The RCBC needs a pulsed beam giving a short burst at the rate of the chamber expansions (20-100 Hz). This results in a request for a beam-sharing system with, say, 50 bursts per sec. During a flat top of 1 sec, this could result in a "beam intensity" of 800-1000 particles per synchrotron cycle. The possibilities for the beam-sharing system needed have been discussed in the preceding paper by R.T. Van de Walle.

The streamer chamber requires a beam of steady rate. In order to have an average of less than 10 beam tracks per picture, the beam intensity should be kept to $(0.5\text{-}1) \times 10^7$ particles per second.

5. TARGET

The RCBC is of course in itself the target, with an active length of 20-40 cm of liquid hydrogen.

Liquid hydrogen targets in streamer chambers have been made in lengths from 4 to 40 cm with diameters from 10 mm upward. For special problems, hydrogen gas targets may also be used.

In the DESY chamber the separation of the liquid hydrogen from the chamber gas is made by 25 μ thick H-foil (beam windows of 12 μ), surrounded by a perspex foam, Rohacell, of 10 mm thickness (0.06 g/cm^2). For protons the momentum must be greater than about 140 MeV/c in order to penetrate this and be detected.

Only in a bubble chamber can the tracks be followed to the vertex itself. In the streamer chamber the vertex is reconstructed by extrapolation with an accuracy from 0.5 to 2 mm.

Clearly, for experiments where it is imperative to detect particles of the lowest momenta (e.g. the "spectator" recoil proton in deuterium experiments) and/or to measure the vertex point with great accuracy, the RCBC is preferable. Such experiments include those where the measurement of short decay lengths (e.g. of $\Sigma^{\pm}$, Λ^0, $\bar{\Lambda}^0$) are important.

6. MEASURING ACCURACY

The measuring accuracy in an RCBC is about 30 μ, while in a streamer chamber it is about 200 μ in space. Therefore at first sight it seems that the RCBC is much more accurate. But the smaller multiple scattering combined with the possibility for longer tracks in the streamer chamber results in very comparable accuracies for angle and momentum.

From the point of view of measuring accuracy, it is expected that special requirements of different experiments may in some cases favour one of the chamber types, and in other cases the other.

7. SOLID ANGLE

Both chamber types claim a useful solid angle of nearly 4π. In the case of a streamer chamber with the electric and magnetic fields parallel, there will be an unmeasurable cone with axis through the target and parallel to the fields with an opening angle of about 15° (in the DESY chamber the electric and magnetic fields are parallel, but this choice is only for convenience and is not a necessity). Poor measuring accuracy will of course continue beyond the 15° since these properties do not change abruptly.

No such region is specified for the RCBC, but there may be regions with poor stereoscopic measuring accuracy owing to the positioning of the cameras (this is also true for streamer chambers).

8. COST

The estimate for an RCBC is somewhere between 1 and 3 MSF. A reliable estimate for the cost of a streamer chamber is not available, but it should not exceed half a million Swiss francs, even for a chamber of relatively large size. The magnet costs are not included here, since they will depend very much on the dimensions chosen.

9. MEASURABLE CROSS-SECTIONS

From what has been said about target, beam requirements, and triggering, one can get an idea about the possibilities for measuring small cross-sections.

The high average multiplicity limits the average number of interactions per burst to less than one to make the RCBC picture easily analysable. The average number of events per machine cycle of 40-50 bursts will therefore be about one per millibarn.

The streamer chamber with a 10 cm target in a beam of 5×10^6 particles per machine cycle will see one event per machine cycle for a cross-section of about 5 μb.

It should be remembered that the streamer chamber has a dead-time of about 10-100 msec. If the trigger system is not made selective enough, a great deal of the useful beam intensity may be lost due to the dead-time imposed by the recording system.

To illustrate this in the extreme, imagine a trigger whose only requirement is that a beam particle has undergone a collision, i.e. corresponding to about 40 mb. Only about 40 beam particles will, on the average, go through the target before a collision happens; and with, say, 50 msec dead-time the experiment makes use of only about $20 \times 40 = 800$ particles in a machine cycle instead of the 5,000,000 available in the above-mentioned beam.

The high sensitivity of the streamer chamber set-up for events of low cross-section is therefore completely dependent on a trigger system that reduces the trigger rate to the order of one trigger per machine cycle.

10. CONCLUSIONS

From the above it should be clear that both rapid-cycling bubble chambers and streamer chambers will be useful in high-energy experiments.

The rapid-cycling bubble chamber has its greatest advantage when it comes to measuring particles of very low momenta close to the vertex and to measuring the vertex position with accuracy.

When an experiment is designed to give high statistical accuracy for events of low cross-section with a necessity for measuring close to the vertex, the streamer chamber is preferable because it can stand a collision rate in the target 10^3-10^4 times that in a bubble chamber. Still, by trigger selection, the number of events recorded will be about the same as in the rapid-cycling bubble chamber.

CHAPTER VI

GESSS REPORT

Studies for a European Superconducting Synchrotron

W. Heinz *(Karlsruhe)*

STUDIES FOR A EUROPEAN SUPERCONDUCTING SYNCHROTRON (A GESSS REPORT)

W. Heinz

Institut für Experimentelle Kernphysik, Kernforschungszentrum Karlsruhe, Germany

1. INTRODUCTION

The highest centre-of-mass energy ever obtained by a man-made accelerator is the energy of the CERN Intersecting Storage Rings (ISR), with beam momenta of 31.4 GeV/c in each ring equivalent to over 2000 GeV of a conventional accelerator beam striking a stationary target. The accelerator with the highest energy particles in the accelerated beam itself is now the American proton synchrotron at NAL, Batavia, which has reached 300 GeV and is expected to reach 400 GeV this year. An equally powerful machine will be the European proton synchrotron now under construction at CERN, Geneva, which is scheduled to reach the first beam at a 200 GeV level in 1976 and have full energy of 300 or 400 GeV two years later.

The conversion of any of these accelerators into a superconducting synchrotron would equip the high-energy physics community not only with a powerful research instrument but also with the biggest liquid-helium-temperature cryogenic plant. Together with plasma physics the requirements of high-energy physics have been and will continue to be a challenge to physicists and engineers to develop new technologies. A superconducting magnet system for high-energy accelerators or superconducting beam lines would give great impetus to the development of superconducting and cryogenic components. This might help to establish superconducting and cryogenic technology on a full industrial scale and possibly open new resources of support for fundamental research.

2. SUPERCONDUCTING HIGH-ENERGY ACCELERATORS

The energy available from accelerated beams has steadily increased from the several hundred keV of the first cascade of Cockroft and Walton in 1932, to the several hundred GeV of the Batavia synchrotron in 1972. Whenever the existing techniques reached their inherent limits, a new acceleration principle was invented. In a nuclear reaction the available energy is the centre-of-mass energy of the hitting particles, which at high energies is proportional to the square root of the peak energy of the particles in the accelerated beam. Total energy is available if two particles of equal but opposite momentum collide. Consequently the latest new principle now successfully in operation is the colliding beam technique where two particle beams circulating in opposite directions cross at definite collision points to enable head-on collisions of the particles in the two beams.

A survey of the development of the maximum energy of accelerators is given in Fig. 1. For storage rings the figure gives the equivalent laboratory energy which would be necessary to obtain equal centre-of-mass energy with a target at rest. In looking at this diagram one has to keep in mind that the usefulness of an accelerator is determined by a number of parameters. Energy is only one of them; other important ones are intensity, duty cycle, and the kind of available particles. So the development of accelerators goes into different directions, and a superconducting synchrotron may well be the next step.

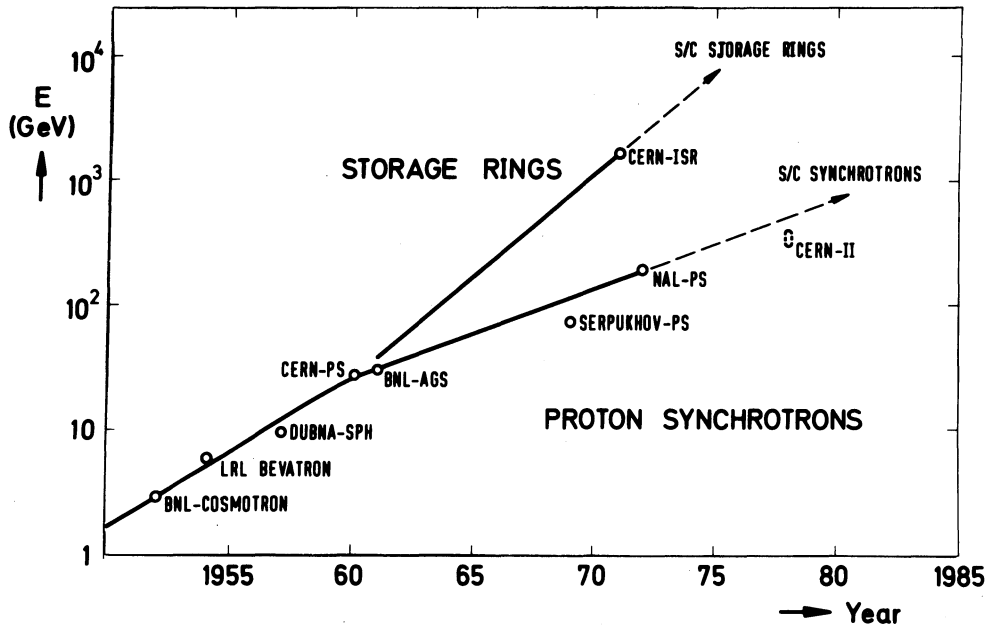

Fig. 1 Maximum energy of various accelerators versus data of first beam obtained

The magnets in a conventional synchrotron accelerator operate at a maximum field of 1.5 to 2 T. If these magnets could be replaced by superconducting magnets of 4 to 6 T, the energy of the accelerator could be increased by a factor of three or four. Pulsed superconducting magnets have been built in a number of laboratories since 1967. By 1971, model dipole magnets representative in many respects of those required for a superconducting synchrotron had been built and tested. In Europe this work was given great impetus by the decision to build the 300 GeV machine in Geneva. This machine will be built as a so-called missing magnet machine: half of the bending magnets will be left out in the first stage. The gaps can be filled with additional conventional iron magnets to give the "design" energy of 300 GeV. With the full set of bending magnets in position and powered to 1.8 T the energy will be 400 GeV. As energy of 1000 GeV could be reached by replacing the iron magnets by superconducting ones operating at a maximum field of 4.5 T [1,2]. The missing magnet scheme allows superconducting magnets to be installed during the completion of the accelerator if they are found technically feasible and economically reasonable. This can be done in several ways. After reaching 200 GeV (stage A) a set of superconducting magnets could be installed in the lattice rather than another set of conventional magnets. This "missing magnet solution" will give a final energy of 500 GeV with the superconducting bending magnets powered only. The iron quadrupoles are designed to focus an accelerated beam up to this energy, possibly with some additional correcting devices. In a later stage all the conventional magnets could be replaced by superconducting magnets to give 1000 GeV or more depending on the field level. The missing magnet solution requires the matching of the apertures and lattice to the existing part of the machine. It allows the use of all the facilities already in place: RF accelerating system, control system, part of the vacuum system, etc.

Another solution could be to place the superconducting magnets above the main ring magnet system in the same tunnel. The 200 GeV of stage A would be used as an injector into the

superconducting ring. This "separate ring solution" could be advantageous in several respects. Compared to the missing magnet solution there are less restrictions in the design of the cryogenic system and in choosing the lattice; the aperture is small because of the higher injection energy. But additional facilities for injection, acceleration, and control of the beam are needed.

Appropriate lattices for the missing magnet and separate ring solutions were found to be compatible with the lattice chosen for the conventional machine. At 200 GeV the beam may be transferred from the conventional to the superconducting ring on top, using the long and medium straight sections of stage A. Reasonable ejection schemes at a 1000 GeV level were found[2].

A variant of these solutions utilizes an extra tunnel to accommodate the superconducting ring, concentric to the first one but several metres away. This last solution would allow the maximum degree of freedom in designing the lattice for the superconducting synchrotron, and might in part compensate the extra cost. Another attractive feature of this solution is the minimum interference of running experiments during construction time. In separate ring solutions, distortion problems due to remanent fields are less severe because of the relatively high injection field.

In 1970 a group of three national laboratories (RHEL, Chilton, England; CEN, Saclay, France; IEKP, Karlsruhe, Germany) formed the GESSS Collaboration -- Group for European Superconducting Synchrotron Studies. The objective is the co-ordination of their work, directed towards pulsed superconducting magnets, and their application in future accelerators, especially in a possible completion of the European 300 GeV machine with superconducting magnets or a conversion of this machine to a fully superconducting one. This collaboration is closely linked to the CERN laboratories. Each of its laboratories co-operates with national industry. A number of working groups exist to cover special subjects.

3. SUPERCONDUCTING MAGNET DEVELOPMENT

3.1 Preliminary remark

The parameters of pulsed superconducting magnets are determined by the requirements of superconducting and low-temperature techniques and by those of the accelerator builders and users. The final choice of parameters will be a balance between physical, technological, and economical requirements. Dipole magnets built and under study have central fields ranging between 4 and 6 T, useful aperture diameters of 5 to 12 cm, and effective lengths of 0.4 to 3.0 m; ultimately the effective length will be 5 to 7 m depending on the lattice. Field rise-times reached are above 5 T/sec in dipoles, thus allowing a cycle time of several seconds. Dipoles have been tested with and without cold iron.

Superconducting d.c. magnets have been studied, built, and used since the discovery of "hard" superconductors in 1961. The biggest representatives of this type are the bubble chamber magnets built at Argonne and Geneva. Operation of a superconducting magnet in a pulsed mode was not possible until the development of low loss superconductors by the Rutherford laboratory in 1968; these are intrinsically stable multifilamentary composites of NbTi filaments embedded in a copper or cupro-nickel matrix.

Dynamic losses in the superconducting composite are mainly due to hysteresis in the superconductor itself, eddy current losses, and coupling effects. Other contributions (self-field losses, etc.) may be neglected[3]. The dynamic losses depend on the size and mutual coupling of the individual superconducting filaments in the composite and on the rate of change of the magnetic field. For example, in a dipole with a composite conductor of 10 μ filaments, the a.c. losses are about 11 W/m at a rise-time of 1.5 T/sec allowing for a 10 sec cycle with a flat top of 4 sec at 4.5 T.

Additional losses are due to eddy currents in the iron, to the heat leak of the cryostat, and losses down the current leads. The total loss of a dipole magnet system is expected to be between 10 and 20 W/m. Measurements are in agreement with calculations. The power consumption of the refrigerator at room temperature is 300 to 500 times this value. This has to be compared with the ohmic losses of conventional pulsed iron magnets, e.g. 5.7 kW/m in the case of the 400 GeV CERN SPS. This means that a superconducting synchrotron has roughly the same losses as a conventional one but with a considerable gain in energy.

3.2 Conductor development

The key to the reliable performance of a pulsed superconducting magnet is the development and use of a suitable composite conductor. Superconducting magnets will be operated at currents of several thousand amperes to restrict the inductance of the coil and charging voltages to reasonable levels, so the use of braids or cables is required. The conductor parameters should be optimized with respect to its mechanical, thermal, and electrical performance in the final magnet. Some vital items are: intact filaments of constant thickness, an appropriate ratio of copper to superconductor, low a.c. losses, and a good insulation between filaments and strands. Alternating current loss behaviour of superconducting composites is reasonably well understood[3,4]. Degradation and training effects are under study in several laboratories.

Current superconducting wires for use in pulsed magnets are based on NbTi with a critical temperature of 9.5 K and a critical field of about 12 T. The critical current density at 5 T is about 2×10^5 A/cm^2. Superconductors with higher critical parameters are known and may well be used in the future. Materials of particular interest are Nb_3Sn and V_3Ga. They show high critical current densities at high fields. One of their attractive features is high critical temperature: Nb_3Sn - 18.25 K, V_3Ga - 15 K, thus allowing higher operation temperatures at reduced cooling costs. Because of their brittleness they are difficult to produce in the form of multifilament wires. Encouraging results have, however, been obtained at Brookhaven[5].

Type II superconductors such as NbTi are dissipative in a changing field. The generated heat can make the superconductor normally conducting. This has to be prevented by stabilization of the conductor. From d.c. applications the principle of "static stabilization" is well known: the heat generated in the superconductor has to be removed to its surroundings faster than it is generated. This is achieved by cladding the superconductor with copper (e.g. in big bubble chamber coils). In a.c. applications this copper would cause additional losses and hamper stable operation. In this case dynamic stabilization can be achieved by limiting the rate of energy release in the superconductor to become commensurate with the thermal diffusivity of the composite. Some copper is required because

of its thermal properties, but the ratio of copper to superconductor can be as low as about 1:1. The heat release is limited by very thin filaments of superconductor down to several microns, by twisting these filaments with a pitch of several millimetres and by embedding the superconducting filaments in a matrix with highly resistive barriers. Niobium titanium multifilament wires now available from several firms have typical filament diameters of down to 5 μ, strand diameters between 0.2 and 1 mm, with several hundred to several thousand filaments in a single strand. These filaments are embedded in a pure copper or copper/cupro-nickel matrix. Cupro-nickel provides the resistive barriers to interfilament current flow; copper is included to provide stable operation. The superconducting wire is twisted with a pitch of typically 0.2 to 1 cm.

The required number of strands for delivering the design current is woven into braids or fully transposed cables and finally compacted to the correct cross-section used in the coil. Braids or cables are now available from different firms with currents of several thousand amperes at 5 T. They have about 10 to 30 strands, which are combined by twisting and full transposition. Twisting of strands without full transposition can cause self-field effects, leading to a non-uniform current distribution, conductor degradation, and additional losses. A non-uniform current distribution, even a negative current in the central strand, has indeed been observed[6]. A fully transposed cable or braid has a low filling factor and a large nubmer of cross-over points between strands, which may cause strand or filament breakage when compacted to desired dimensions. These dimensions have to be maintained during and after the winding procedure to get the required field homogeneity in the useful aperture of the final dipole ($\Delta B/B$ less than 10^{-3}). This can best be achieved by using a highly compacted braid or cable where single strands are fixed by some means.

A first possibility could be the return to a single strand conductor. This development is under way at Rutherford laboratory and IMI, Birmingham, England. At a field of 5 T, a single 5 μ filament of NbTi will only carry about 30 mA. A total of 10^5 filaments have to be connected in parallel to get a typical current of 3000 A. There are limits in the number of filaments in the composite owing to filament coupling effects which will limit the ultimate size of composites in pulsed magnets. The present limit with a three-component conductor seems to be about 20,000 [7] owing to losses in the matrix. If these losses can be reduced by a more effective and sophisticated arrangement of filaments and resistive barriers, the upper limit can be expected to be as high as 10^5 filaments of 5 μ diameter. A 1 mm diameter composite conductor containing 13,255 NbTi filaments, 5 μ thick, in a copper and cupro-nickel matrix, was manufactured by IMI. It carries 470 A at 5 T [1].

Another way to maintain cable shape during coil manufacturing is to fix the single strands by soldering with a high resistivity solder. One of the Karlsruhe dipoles has been built with such a cable, another one is under construction. The advantage of such an approach is a performance predictable from short sample values with respect to the maximum attainable field and the field quality, because of tight mechanical tolerances of the conductor. The drawback is the relatively high heat release in pulsed operation, thus introducing a lower limit for the maximum rate of change of the magnetic field. Soldered cables could well be used with long cycle times (above 10 sec).

The Brookhaven group[8] has developed a promising metal composite and a metallurgical processing by decoupling single strands in the braid or cable. Finally, organic insulated

strands and cables are developed by industry. They are highly compacted (above 0.7 filling factor) and mechanically stable during winding.

It is important to design superconducting magnets in such a way that their performance is predictable and reproducible in many specimens. Improved prediction of performance leads to reduced safety margins for reliable operation and a more economic design. So a lot of quality tests of the conductor and of potted and unpotted test coils were taken in all GESSS laboratories to study the effects of training and degradation.

An example for short sample measurements of individual multifilament NbTi wires down to 4 μ filament diameter is shown in Fig. 2. From U-I curves measured, a resistivity ρ is determined and plotted against current density J in a logarithmic scale showing slope and take-off

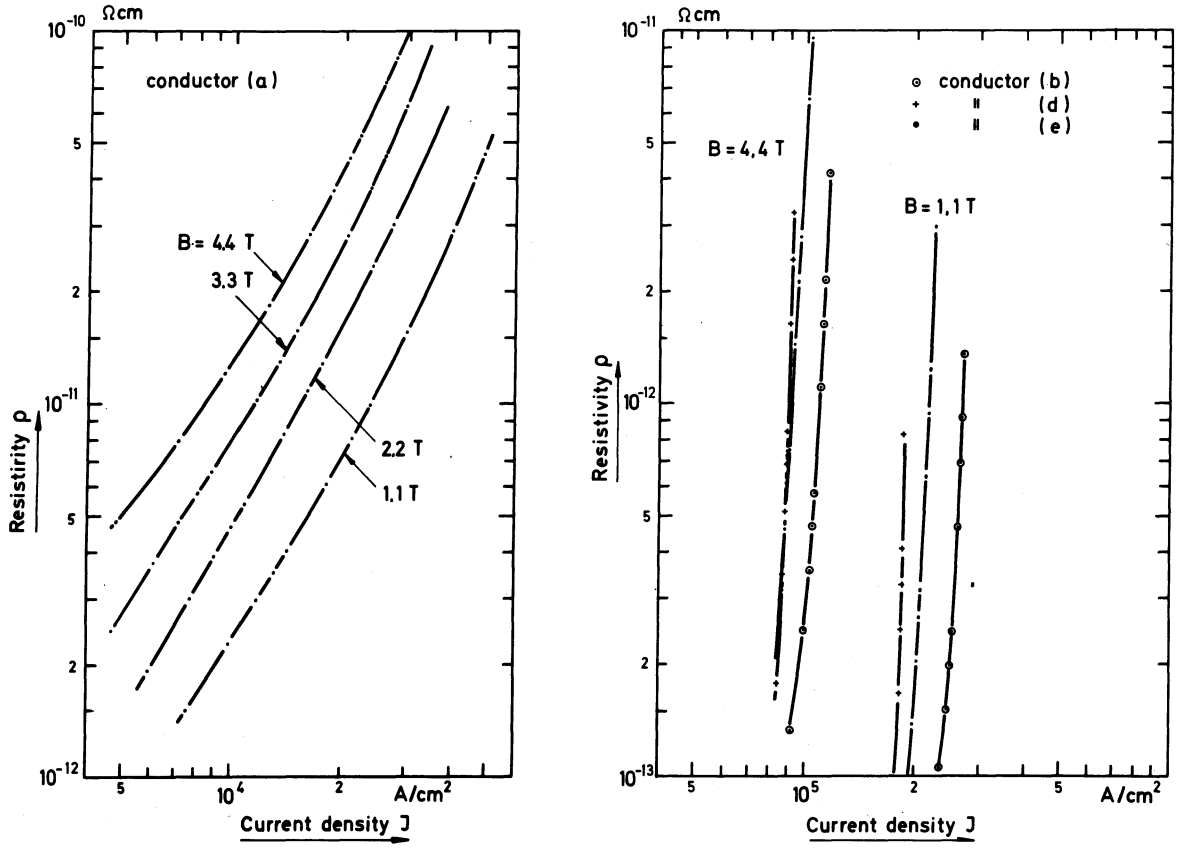

Conductor	Diameter		Number of filaments	Cu : Sc ratio
	Wire (mm)	Filament (μm)		
(a)	0.4	10	300	3.8 : 1
(b)	0.4	24	130	1.2 : 1
(c)	0.28	10	361	1.25: 1
(d)	0.38	8.5	1000	1 : 1
(e)	0.2	7.5	400	1 : 1

Fig. 2 Short sample characteristics: Resistivity versus current density for some selected conductors

currents. The curve shown in the left part was obtained from a conductor which was known to contain many broken filaments. Obviously the slope of these curves is a sensitive measure of the integrity of filaments.

3.3 Coil structure and magnet design

Synchrotron magnets are pulsed dipoles and quadrupoles of high field quality. In classical magnets, field accuracy is guaranteed by the correct shape of the iron surface and the reproducible performance of the normal conducting field coils. Superconducting magnets go to fields where iron saturates. The iron surface can no longer act as an equipotential plane and can therefore no longer be used to shape the field properly during the whole cycle. A superconducting coil has to produce the required field distribution by an appropriate distribution of the currents in the coil.

There are two idealized theoretical coil cross-sections which would produce a uniform dipole field: the intersecting-ellipses configuration with a homogeneous distribution of current outside their overlapping parts, and a distribution with concentric boundaries and therefore circular aperture with a cosine variation of current density. Practical designs approximate these configurations in various ways. Different ways are used in the three GESSS laboratories: concentric layers at RHEL (Fig. 3a), shaped blocks of horizontal layers at CEN (Fig. 3b), and spaced sectors wound of several layers at IEKP (Fig. 3c). The correct position of conductors is determined by computer calculations. The thickness of layers, their azimuthal position and extension, and the space between layers for impregnation and heat drains or cooling channels give enough degrees of freedom to get rid of or minimize the contributions of higher-order multipoles. From this point of view, all designs are equally well suited to give the required field accuracy. So design concepts are determined by engineering approaches.

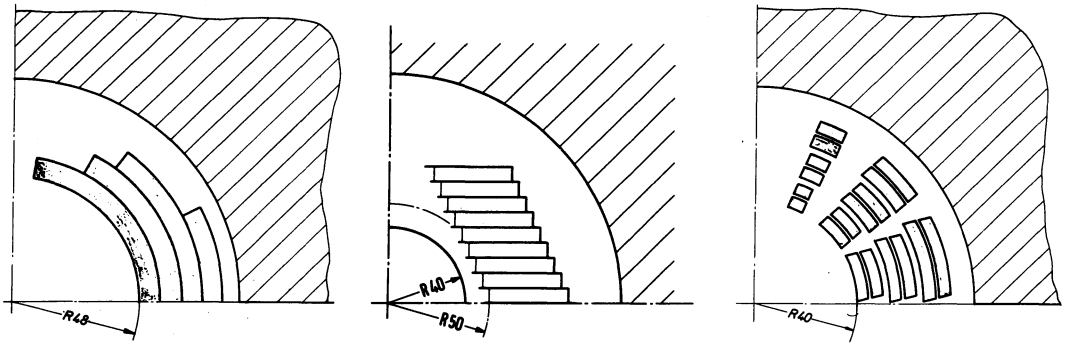

a) Concentric layers (RHEL)

b) Shaped block of parallel layers (RHEL)

c) Spaced sectors with three double layers (IEKP)

Fig. 3 Conductor configurations

The coils will be surrounded by an iron shield in the form of a laminated steel cylinder. It will reduce stray fields and stored energy by enhancing the central dipole field without enhancing the current. To maintain the field accuracy during the whole cycle, iron saturation has to be avoided or carefully controlled. The iron shield will be an integral part of the design, and will act as part of the magnet structure to withstand electromagnetic forces during operation and keep the coils in their correct position.

The conductor has to be fixed and stay in place during cycling. Conductor movement would not only introduce field distortions but cause additional heat release. Therefore the winding is potted in a suitable material, mostly epoxy resins, and bandaged and supported by a glass-fibre or stainless-steel structure.

A rather compact coil package will result, preventing free access of the cooling medium to the conductor if no precautions are taken. The heat generated in a coil package has to be carried away through the coil and transferred to the helium. Cooling channels or heat drains have to be provided in order to prevent local overheating. The maximum thickness of a coil package, a layer or double layer, is limited by the allowable temperature rise within the layer.

Little experience has been gained so far in tackling the problem of differential thermal contraction of different parts of the dipole (coil, coil bandages, iron shell, cryostat, etc.). It is particularly important to maintain the symmetry of the magnet and thus avoid harmful coupling terms in the field. Components could be matched thermally and prestressed during assembly, which might partly compensate for differential contraction.

3.4 Superconducting pulsed dipoles completed and under construction

This report will present the current status of the development, and in particular the progress obtained since the GESSS report[1] at the spring ECFA meeting in Geneva. Several completed magnets were presented at that time, among them an iron core magnet DT (IEKP) and an air core magnet AC3 (RHEL).

The dipole DT [9] is a 0.4 m long dipole (Fig. 4) wound from a 10 strand cable with a central copper strand, the cable being InSn-soldered to ensure mechanical rigidity. The iron yoke is of the window-frame type with a rectangular window. It is laminated and hyperbolically shaped towards the ends in order to linearize field decrease. It is immersed in liquid helium. The coil is an unpotted flat race-track coil with cooling channels between every two layers.

During the first period of operation the magnet has been tested for almost 10,000 cycles with triangular pulses down to 2 sec pulse duration. At a slow field rise of about 0.1 T/sec, a central field of 4.5 T and a peak field of 5.2 T on the

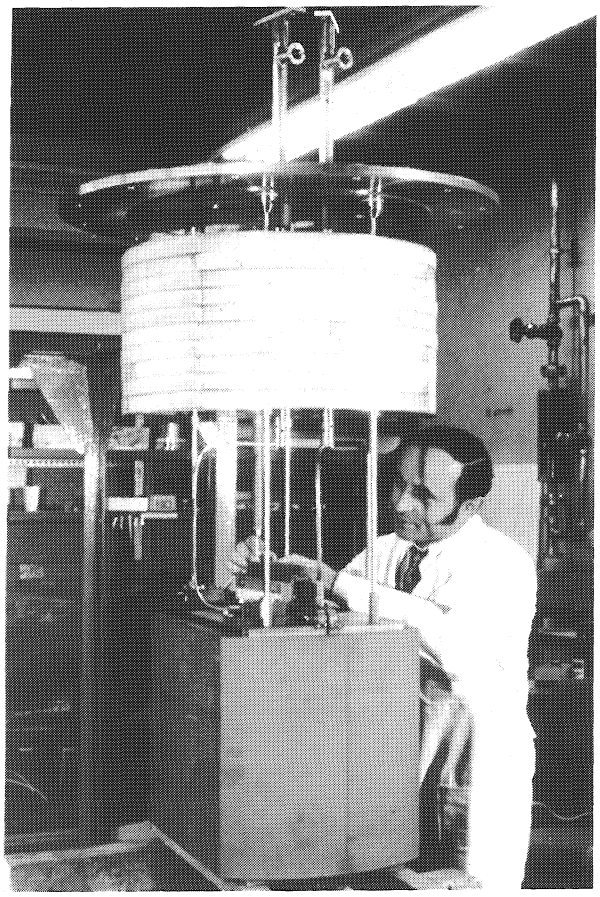

Fig. 4
DT dipole magnet (IEKP)

winding surface were obtained. This corresponds to short sample values; neither training nor degradation were observed. Degradation occurred at faster rise (Table 1). The peak field values given represent the maximum fields attainable during half an hour pulsing ("permanent pulse mode"). They are considerably reduced with decreasing rise-times. This is most likely because of the high losses of the low resistivity solder of the cable and the eddy currents in the copper strand and iron sheets. The losses per cycle are approximately proportional to the frequency and the square of the field.

Table 1

Losses in dipole DT at peak field

Rise-time (sec)	Peak central field ("Permanent pulse mode") (T)	Losses (J/cycle)
45	4.5	< 8
31	3.5	14
5	3.2	130
2.5	3.0	107
1	2.4	90

In the same iron yoke a high purity aluminium coil (resistivity ratio 9200) has been tested. A peak field of more than 4 T was reached with a power consumption of 60 to 70 W at helium temperature when triangular pulses of 3 to 10 sec/pulse duration were applied.

AC3 is a magnet of approximately the right size and shape for a synchrotron operating at realistic values of field, current, and rise-time[10]. It is 0.4 m long without an iron yoke and has a circular aperture of 10 cm diameter. In a first version, a central field of 4 T was reached at 5200 A. In a second version two additional pancake coils reducing the aperture to 7.5 cm diameter were used to give a central field of 4.6 T at a current of 4500 A. Like DT, it is operated vertically. A schematic drawing of the coil geometry is given in Fig. 5. The ends are bent up vertically to give minimum field disturbance. Cooling is provided by laminated copper heat drains placed between layers. The dipole is vacuum impregnated with a semiflexible resin which has good crack resistance at low temperature. The fully assembled magnet is shown in Fig. 6.

Measured a.c. losses are in good agreement with calculations. At a rise-time of 3 sec considered for a superconduction version of the European synchrotron, the decrease of quench current is negligible compared to d.c. operation. At 0.25 sec rise-time, the quench current is decreased by about 25%.

In the meantime the successor of AC3 has been successfully tested. AC4 has two double layers per pole[6] and uses a 25 strand cable of 2035-filament superconducting wire rated at 5400 A. The coil aperture is 9 cm in diameter. AC4 has a split iron yoke with laminated iron of 0.5 mm thickness. Each pancake coil is separately vacuum-impregnated with a filled epoxy resin. The dipole is operated horizontally. Cooling channels between each layer of

windings are used instead of the heat drains in AC3. They allow vertical passage of the helium from below the coil by natural convection. Figure 7 shows the dipole fully assembled. During the first run it was pulsed to over 4.5 T, corresponding to a current of 5300 A with 2 sec rise-time, and a few per cent less with 1 sec rise-time. All losses are as predicted. Field measurements are under way. A field uniformity of 4×10^{-4} over a "good field" region of 6 cm diameter is expected.

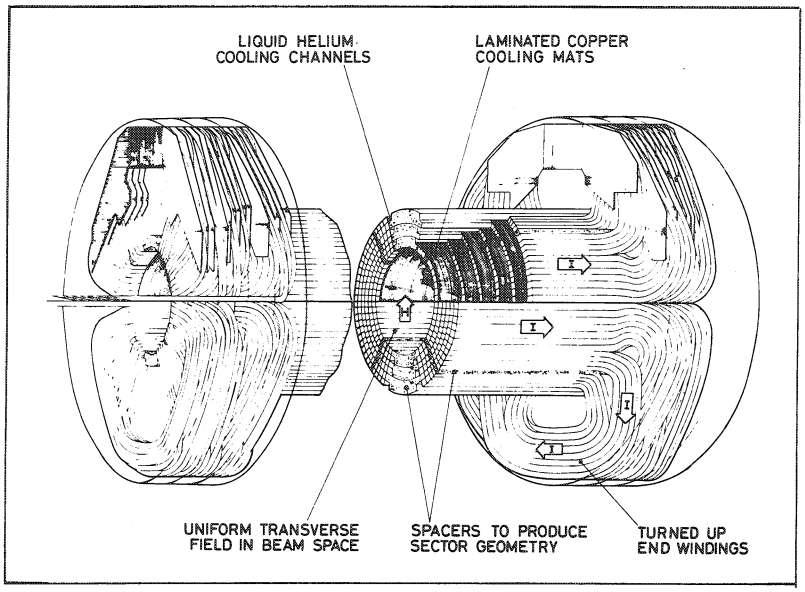

Fig. 5
Schematic view of coil geometry of dipole AC3 (RHEL)

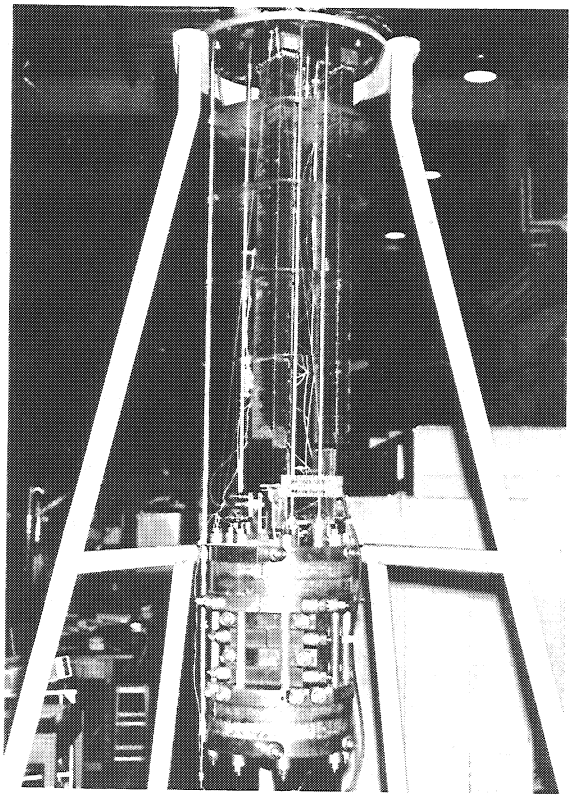

Fig. 6 AC3 fully assembled

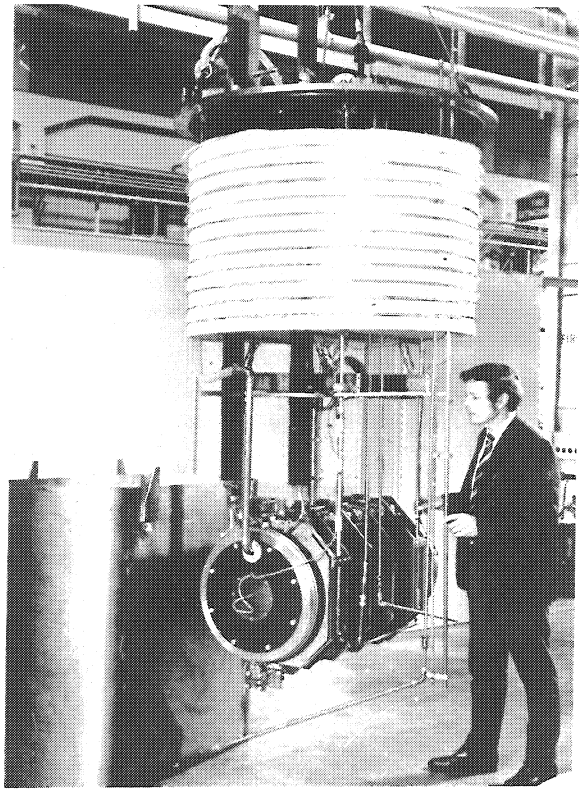

Fig. 7 AC4 fully assembled

The next dipole to be built at RHEL (AC5) will be based on the design of AC4. It will be about 1.5 m long with a specified pulsed field of 4.5 T and field rise-time of 3 sec. The conductor has yet to be finally selected. Completion of AC5 is expected in mid 1973.

GESSS laboratories try to cover all the relevant parameters for the final design of a prototype synchrotron dipole to be used in the big European machine. The experience with different physical and engineering parameters and techniques in these laboratories is complementary. So MOBY[11], the dipole magnet under construction at CEN-Saclay, is the highest field pulsed magnet at present considered in the GESSS laboratories, being designed for a central field of 6 T.

MOBY has a coil aperture diameter of 10 cm and a magnetic length of 0.5 m. It is designed for a rise-time of 5 sec and an operating current of 1500 A. The coil is a block of a parallelogram shape with layers of conductors parallel to the horizontal plane. A circular iron shielding is provided very close to the coil. The coil is totally epoxy-impregnated and is cooled by means of copper heat drains. Figure 8 shows the coil and iron shielding configuration. The type of winding is unique. It makes use of a technique of going a constant turn perimeter per layer (Fig. 9) and produces a stable mechanical location of turns without any stretching forces. It is possible to build a whole pole with only one piece of conductor. The influence of this configuration on the end fields has to be measured. Some experience with this winding technique has been gained from two d.c. quadrupoles (OGA) built formerly.

The conductor is a 24-strand compacted braid. The braid was chosen to get the desired rectangular cross-section. Many broken strands and filaments due to the braiding and compaction procedure were observed. This was also found at other places.

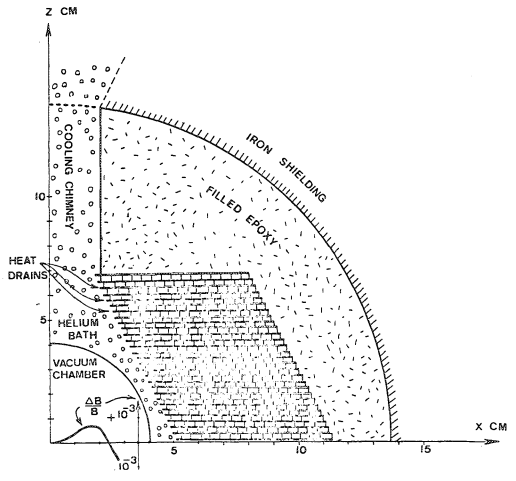

Fig. 8 Coil and iron shielding configuration of MOBY (CEN)

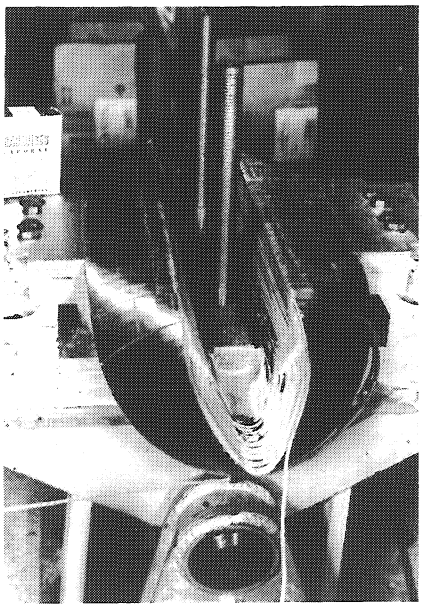

Fig. 9 Completed brass model showing winding technique of MOBY

A difficult problem with this design is the positioning of the coil inside the shielding because of the different thermal contractions of the coil and iron shield. All the coil support is from the outside; the inner part serves for cooling only. The helium circulation on the inner coil surface where the heat drains protrude is made by natural convection in chimneys through the stacking.

The winding of MOBY is in progress, the iron shielding is completed. The main parts of the cryostat are also completed (see Fig. 17). Low-temperature tests are in progress, and the first test runs are planned for the end of this year.

Another magnet based largely on MOBY design is ALEC. It is of greater aperture (11 cm) and length (1.5 m) than MOBY, but with slightly reduced central field (5.5 T). Winding, impregnating, and cooling techniques are the same as those used with MOBY. An attempt has been made to design both magnets as close as possible to an engineering version. Industry will be involved in the construction to ease technology transfer to the manufacturer.

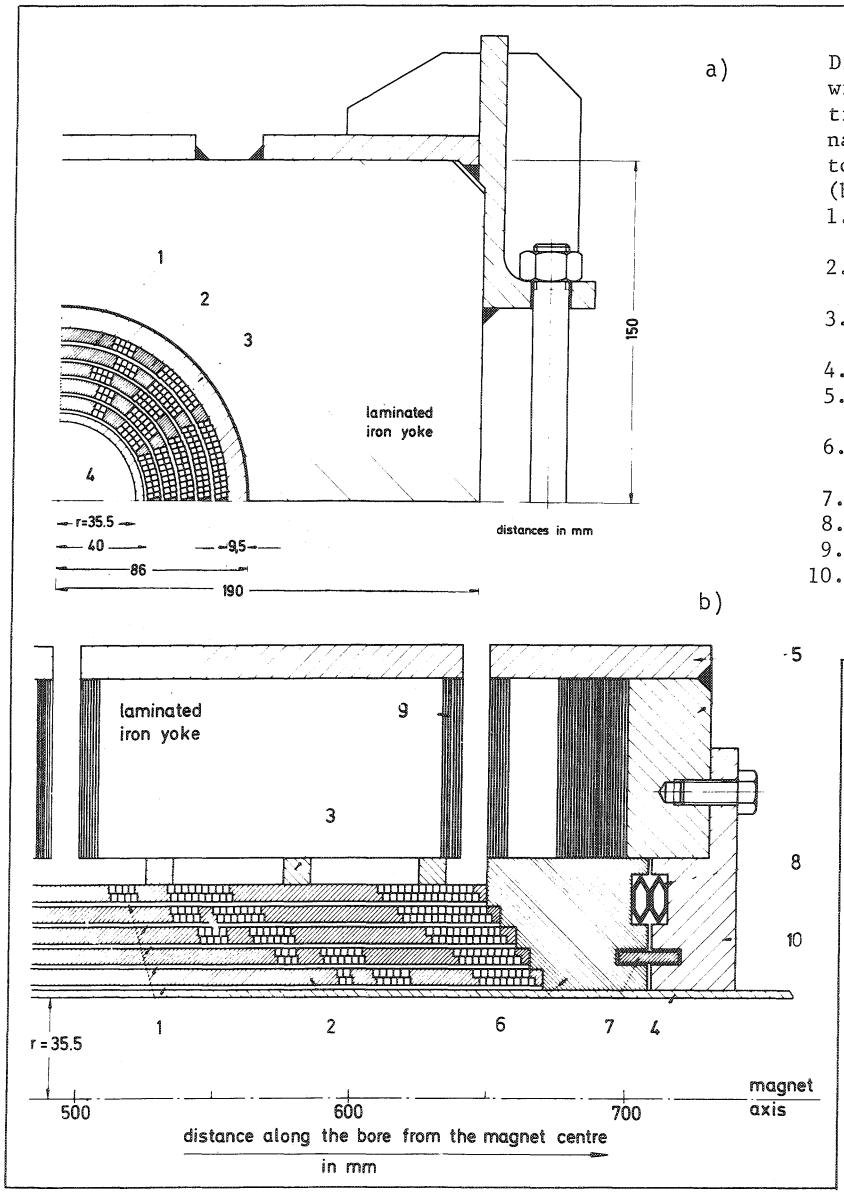

Dipole D2a cross-section with conductor configuration (left) and longitudinal section with conductor end configuration (below):

1. Cooling channels, 1.5 mm in width.
2. Spacers, glass-fibre reinforced epoxy.
3. Support rings, stainless steel.
4. Tube, stainless steel.
5. Yoke top and end plate, stainless steel.
6. Sleeve, glass-fibre reinforced epoxy.
7. Guide pin.
8. Belleville springs.
9. Cooling hole.
10. Front panel, stainless steel.

Fig. 10
Dipole D2a (IEKP)

a) Radial cross-section

b) Axial section of the end region

The design philosophy for a superconducting magnet depends on a lot of parameters. The Karlsruhe programme is designed for a set of longer magnets of 4.5 T central field with a small circular aperture of 8 cm in diameter.

Dipole D2 of 1.5 m length will actually exist in two versions with different conductors: D2a, which is at present being wound, employs a soldered rectangular cable, while D2b will be wound from a flat cable with fully organic insulated strands. Dipole D3 will be based on the design of D2b but with a length of 3 m. For all magnets a modified cos θ current distribution is chosen because of its symmetry (Fig. 10a) which is relevant to the problems associated with differential thermal contraction during cool-down. As the field will be uniform, independently of the position of the iron shell, two approaches for D2 are under investigation. The first one, with an inner diameter of the iron shell of 17.2 cm, becomes saturated as the magnet goes to high induction; the other one, with an inner diameter of 21.6 cm, remains unsaturated throughout the cycle. The coils for D2a and D2b may be used in either the iron shell or with no iron at all.

The number of layers chosen depends on the cable or braid which is available. We have decided to use fully transposed cables (no central strands) instead of braids, because cross-over points are eliminated as potential shorts and higher packing factors are obtained (∿ 70% versus 50%). Like a braid, a fully transposed cable gives good cooling conditions in an impregnated coil because all strands are periodically carried to the coil surface to allow contact with the liquid helium. While a braid can easily be compacted to a rectangular shape, this is difficult with a fully transposed cable. If the strands are soldered, however, the cable may be shaped as required. The drawback is that the high losses in a metal-insulated cable allow only reduced rise-times.

For D2a, a superconducting soldered cable with 2.1 × 2.6 mm cross-section was chosen. It is wrapped with a terylene-glass braid insulation 0.2 mm thick. A current of 2000 A at 5 T and 4.2 K is guaranteed by the manufacturer (IMI).

The peak field at the conductor surface is designed to be only a few per cent above the central field. Owing to the losses in the solder, the shortest rise-times will be between 10 and 20 sec. The cable has to be wound into double layers because of the winding technique. They will be mounted together to form a magnet pole. Since the number of double layers does not essentially influence the field accuracy, from this point of view a low number is desirable in order to simplify winding and impregnation of the individual double layers. On the other hand, ease of shaping the three-dimensional ends limits the height of the flat cable. This leads to a design with two or three double layers for D2b as shown in Fig. 11. Double layers are separately vacuum-impregnated and mounted on a glass-fibre coil structure with spaces for the coolant between each of them.

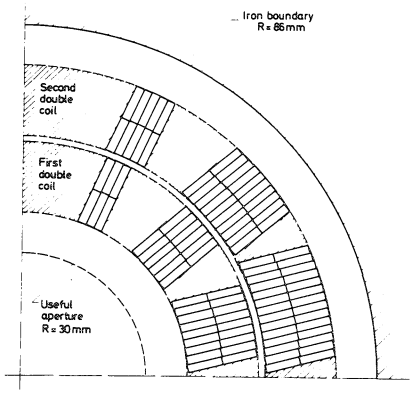

Fig. 11 Cross-sections of a two-double-layer dipole using a flat cable:

B_0 = 4.5 T
I = 3190 A
N = 95 turns/pole

The end regions of the coil were designed very carefully in order to avoid a variation of $\int B\,dl$ over the coil aperture and field enhancement at the coil ends. In contrast to conventional iron magnets, the latter effect has to be considered because the current-carrying capacity of a superconductor decreases with increasing local field. By lengthening the inner layers and shortening the outer ones, a negligible field enhancement in the ends is achieved. Figure 10b shows the end region of D2a, which also gives constant integrated field within 0.1% and no substantial eddy currents in the iron.

The iron yoke of the final version D3 will be chosen according to the results obtained with the saturated and unsaturated iron yokes of D2. The effects of iron saturation on a.c. losses, peak field, and field uniformity will be measured. The expected field as a function of current for a saturated, unsaturated, and no-iron shell is shown in Fig. 12, together with the critical current characteristics at different operating temperatures and the iron enhancement factor of the field. The iron is laminated and coated with a 10 μ phosphate layer.

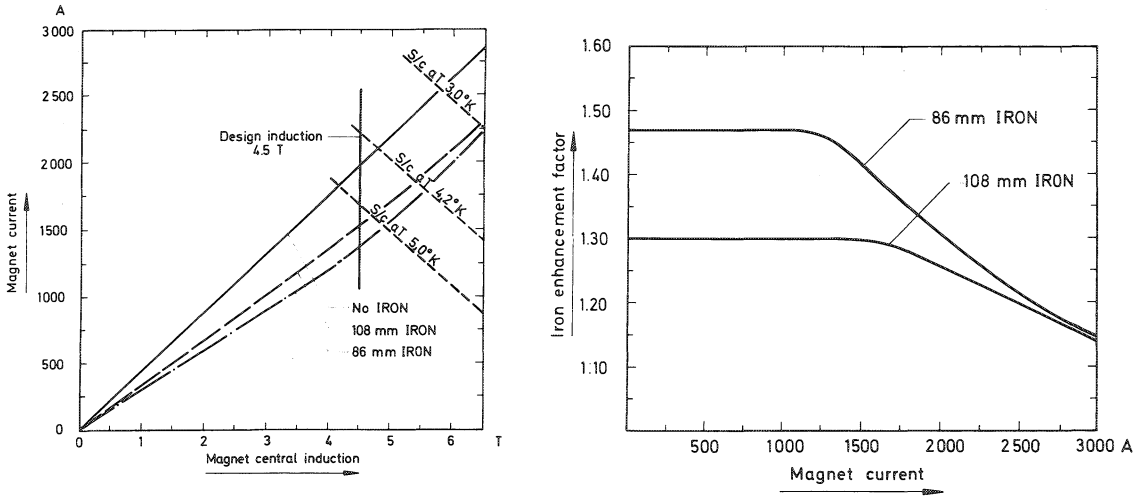

a) Dipole D2a operating current versus central induction and short sample characteristics of the cable used

b) Field enhancement factor for saturated (86 mm) and unsaturated (108 mm) iron version

Fig. 12

Magnetic forces will be supported by stainless-steel rings. Liquid helium will flow between the coil and the iron and through the cooling channels between each of the double layers which allow natural convection cooling through holes drilled into the top and bottom of the iron shell. The cooling channels will also permit forced cooling in axial direction.

The coils of D2a are at present being wound. Figure 13 shows a trial coil winding of a double layer pancake of this dipole. Completion is expected in January 1973. An axiometric view of the magnet is given in Fig. 14.

3.5 Low-temperature properties of materials

The current density in a superconducting composite is more than an order of magnitude higher than in normal conducting material; the fields applied are 2 to 4 times higher. Thus the forces on the conductor are increased by one or two orders of magnitude compared

Fig. 13
Trial coil winding of D2a (IEKP). Over-all view and detail

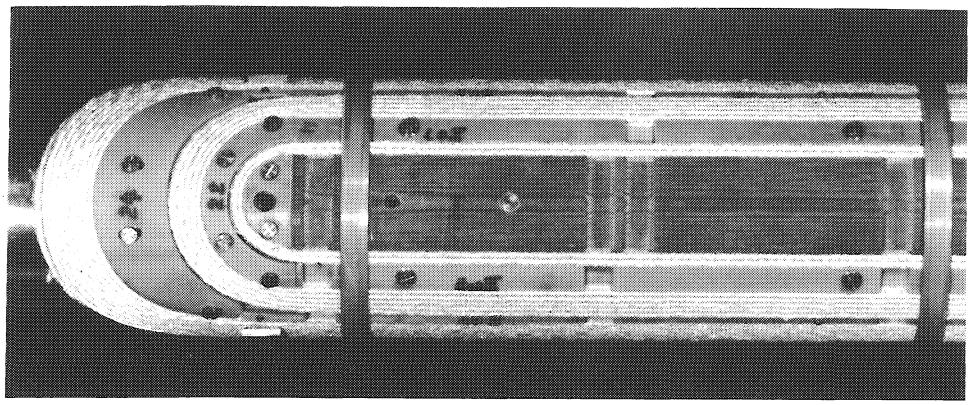

to room-temperature magnets. Although the material strength is increased at low temperatures, the gain is not nearly sufficient to compensate the increased strain by Lorentz forces. The development of heat at low temperatures owing to eddy currents in metallic structure material has to be avoided as far as possible because of the bad over-all efficiency of a refrigerator. Therefore non-metallic materials, e.g. glass-fibre or epoxy resins are widely used.

No comprehensive data on the low-temperature mechanical, thermal, and electrical properties are available for the materials of interest. Extensive test programmes have been started in different GESSS laboratories. The main interest is directed to understanding the behaviour of the epoxy resins used to impregnate the coils. Degradation effects observed in most of the coils and magnets already built are partly due to the misbehaviour of the impregnation material. Mechanical release of energy within the coil may raise the temperature locally and thus initiate degradation. Frictional energy can be generated by

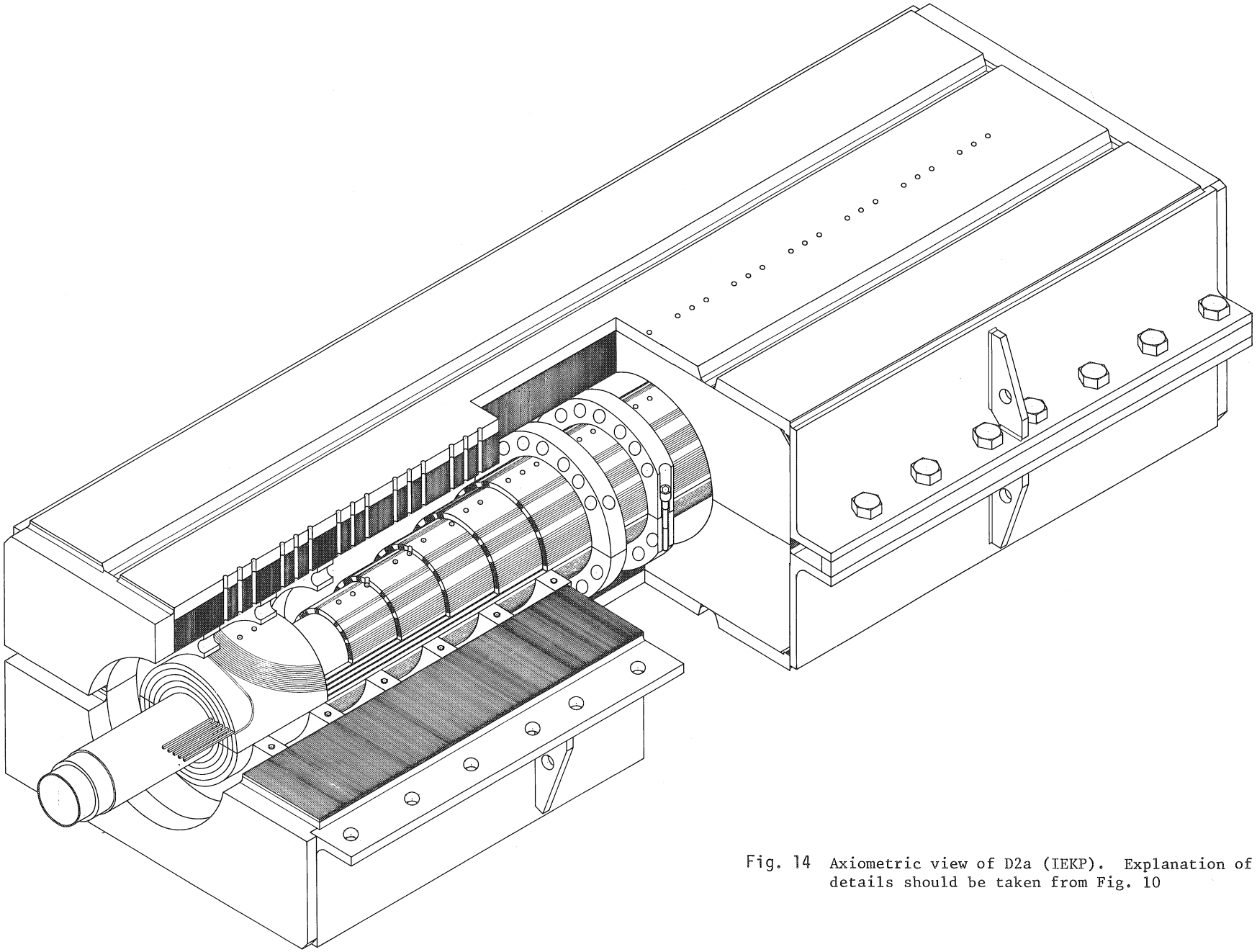

Fig. 14 Axiometric view of D2a (IEKP). Explanation of details should be taken from Fig. 10

conductor movement; mechanical strain energy can be stored during fabrication and cool-down due to differential thermal contraction, and subsequently released when the magnet is pulsed. This is especially dangerous if it happens in the impregnated coil near the conductor itself, as would be the case with a badly matched impregnation material. Otherwise, a reasonably well-matched impregnant should ensure satisfactory coil performance at nearly critical current.

The objective in selecting the epoxy resin should be twofold: minimum differential thermal contraction between conductor and resin to avoid cracks during cool-down, and minimum irreversible deformation and crack energy per unit volume to reduce temperature rise in case of a crack. The force developed by differential thermal contraction is proportional to the product of Young's modulus E(T) and relative thermal contraction $\Delta L/L(T)$, which has to be minimized. Unfilled or filled resins, and resins which are flexible or rigid at room temperature can be chosen, since they behave in a similar manner when cooled down. Flexible resins have smaller Young's moduli but the contraction is greater; rigid resins have a contrary behaviour (Fig. 15).

The filler increases Young's modulus approximately as much as it decreases thermal contraction. The higher curing temperature of rigid resins gives an additional contraction and therefore enhanced forces. Thus flexible and filled epoxy resins with relatively low curing temperatures seem to be favourable.

Investigations of the influence of fillers and different epoxies on crack energy are under way.

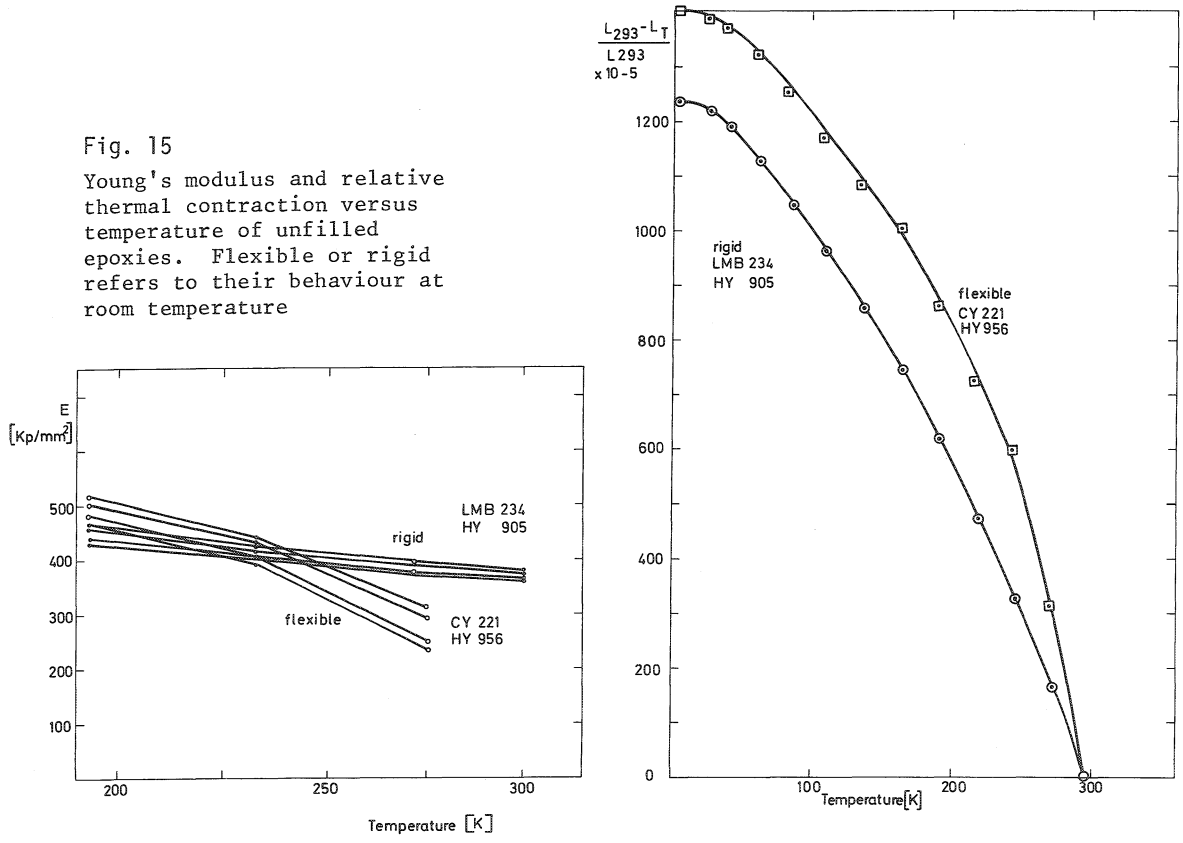

Fig. 15
Young's modulus and relative thermal contraction versus temperature of unfilled epoxies. Flexible or rigid refers to their behaviour at room temperature

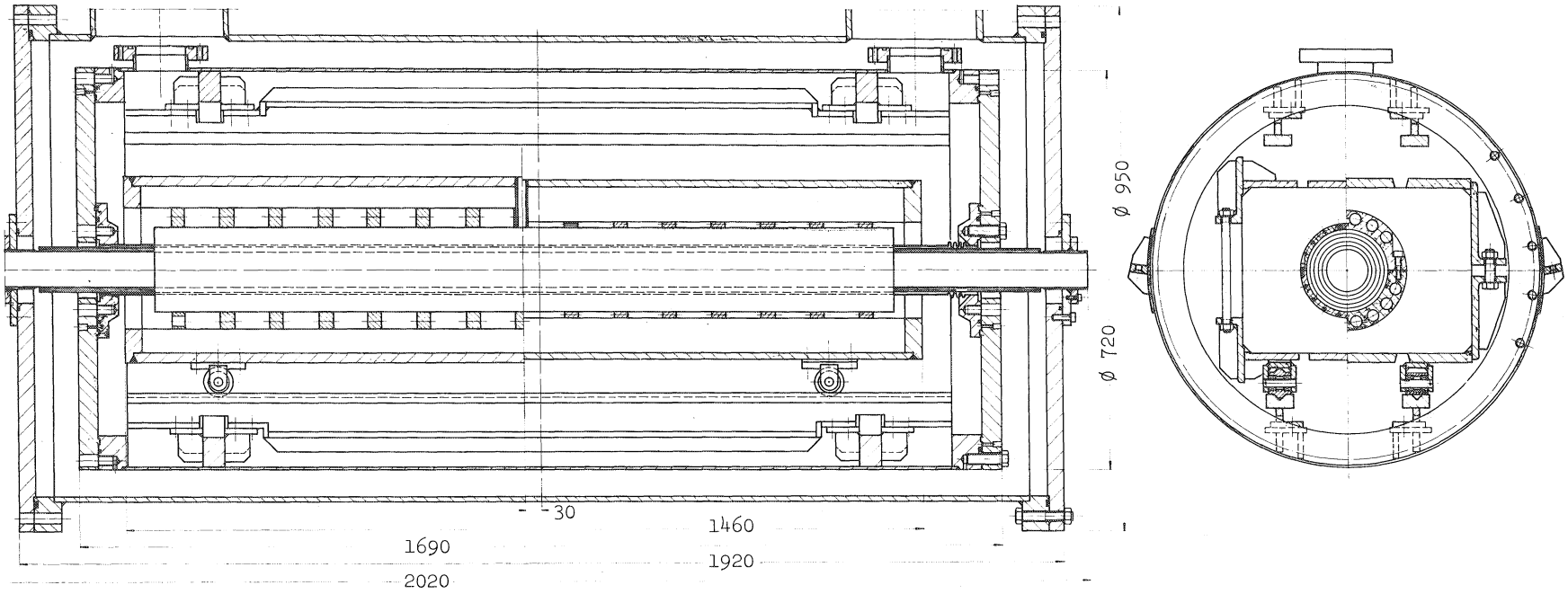

Fig. 16 Axial and radial views of cryostat for D2 (IEKP)

4. MAGNET POWER SUPPLIES

Stored energy and field rise-time determine the size of the power supply. Stored energy can be minimized by minimizing the magnet aperture, and this on the other hand depends on the requirement of an effective injection and ejection. A high injection energy (separate ring on top of the conventional injecting machine) and an effective ejection scheme (high β insertions) may limit total stored energy to less than 500 MJ. Three types of power supplies may be considered: a motor-generator set as used in most big machines; a static power supply, where power is directly drawn off the electric grid, as is used at NAL, Batavia; and a superconducting energy storage system as proposed by Smith[12]. The first two may be well adapted to a 1000 GeV superconducting version of the CERN machine.

5. MAGNET CRYOSTAT AND REFRIGERATION SYSTEM

5.1 Cryostat

The superconducting magnet is put into a cryostat and maintained at helium temperature. It has to give a rigid support to the magnet with a total weight of several tons (1 to 1.5 t/m), and on the other hand to minimize the flow of heat to the helium vessel to reduce static heat losses. Heat leaks will occur by radiation, and by thermal conduction down the support system, the supply necks, and electric leads. By superinsulation the heat input can be reduced to between 0.3 and 1 W/m^2 and by an additional nitrogen shield by another factor of 3 to 4. Heat input down the electrical leads is about 10 W/1000 A of current per pair. Therefore, magnets and cryostats will be interconnected at low-temperature level. A design chosen for D2 is shown in Fig. 16. Parts of the cryostat for MOBY are shown in Fig. 17.

The cryostat of a prototype dipole should be an integral part of the magnet design, possibly even including helium transfer lines. Several magnets may be contained in one cryostat, up to half a period in the separate ring solution (Fig. 18).

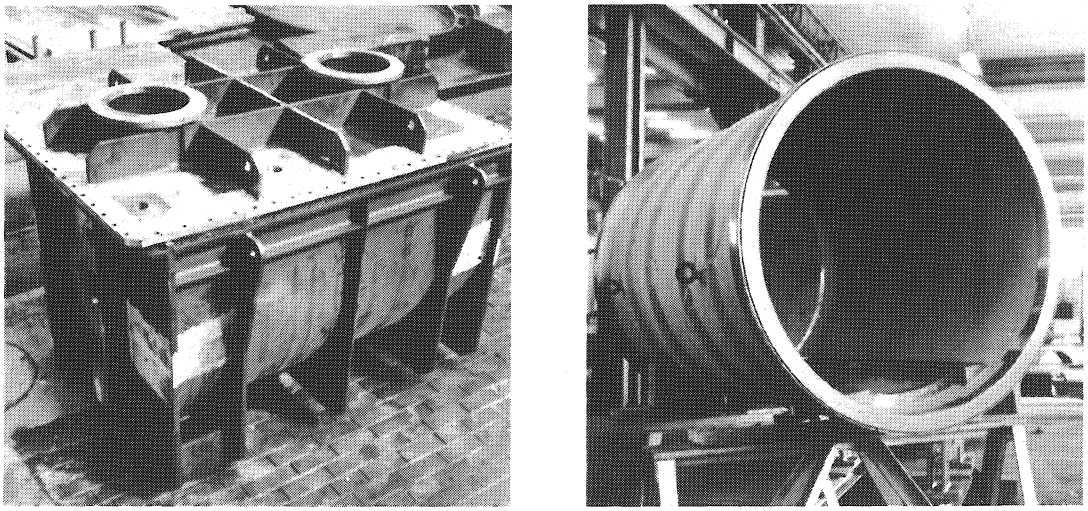

a) Vacuum tank b) Helium tank

Fig. 17 Cryostat for MOBY (CEN)

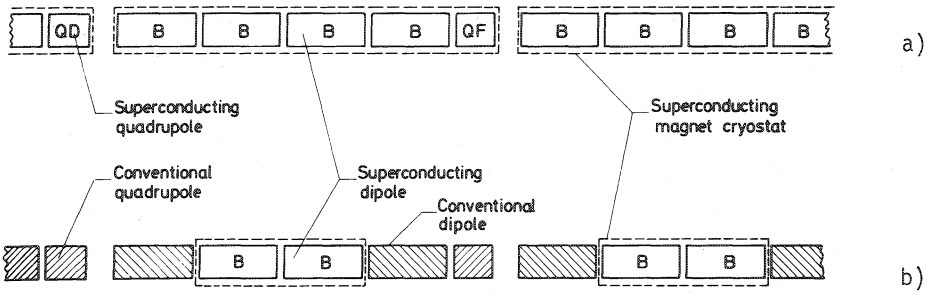

Fig. 18 Possible arrangements of cryostats
a) in a separate ring solution, and
b) in a missing magnet solution

5.2 Refrigeration system

Estimates have been made of the total heat load of a 1000 GeV synchrotron at helium temperature. Including dynamic losses in the superconductor, losses in the iron shield caused by hysteresis, and static heat losses of the magnet cryostat and in distribution pipes, a total of between 10 and 20 W/m is obtained. The heat load at the refrigerator is thus 50 to 100 kW at liquid-helium temperature. Large accelerators are subdivided into superperiods, e.g. six in the case of the 300 GeV accelerator. The same might apply to the refrigeration system.

A preliminary design study was completed[13]. It was found advantageous to subdivide the system and operate it economically at the average energy loss rate, storing refrigeration during low-loss time intervals. Interconnecting all the refrigerators by a common supply ring might offer a high degree of redundancy in case of a fault. A common compressor or six compressors interconnected by supply lines could be used.

Serious consideration has to be given to the operating temperature of the cryosystem. Current superconducting wires for use in pulsed magnets are made of NbTi composites with a critical temperature of 9.5 K. Its critical current density at 4.2 K is about 2×10^5 A/cm^2 at 5 T and changes rapidly with temperature: about 35% per degree K. Thus a lot of superconducting material can be saved by lowering the temperature in the coil, but more refrigeration has to be used. Over-all economics seem to favour operating temperatures below 4.2 K. Parameters of the refrigerator are going to be worked out by the cryogenic subgroup of GESSS. A technical and economical study by national industries will be based on these data.

6. OUTLOOK AND SUMMARY

The development of superconducting pulsed magnets has made rapid progress in both Europe and the United States. A lot of dipoles have been finished. Test results gives confidence that most of the physical and engineering problems are reasonably well understood. We are now at the stage of investigating fully engineered preprototype synchrotron

magnets which cover most of the relevant parameters for a full-scale prototype: apertures ranging from 8 to 11 cm, central fields from 4 to 6 T, and lengths of magnets between 0.5 m and 3 m. Different winding configurations, impregnation techniques, and cooling measures are applied in different laboratories. The conductors used include braids and cables, soldered and fully insulated versions with current-carrying capacities ranging between 1000 and 6000 A at 5 T. Field rise-times are as low as 1 sec without significant degradation.

One of the most important features of the magnet development is the conductor available. Magnet design and development reflect the development of the conductor and will continue to do so. If, in the future, superconducting materials with higher current densities and higher critical parameters will become available in the form of appropriate conductors, improved design parameters will be used. The higher current densities will allow more compact coil designs with smaller amounts of superconducting material. Higher magnet operation temperatures, e.g. typically 10 K rather than 4 K, will greatly reduce refrigeration requirements. The higher critical magnetic fields of these superconductors could point a way to even higher energy accelerators.

After having completed the dipoles now under consideration by the end of 1973, enough information should be available to make it possible to select parameters for a pre-production prototype synchrotron magnet to be manufactured by or in close co-operation with industry. Different dipole magnets then available should be assembled to a series of magnets operated simultaneously, thus simulating a magnet system in a closed refrigeration loop.

The work of GESSS will be relevant to all types of pulsed magnets (dipoles, quadrupoles, etc.) as considered in various laboratories. It will be equally relevant to d.c. operated magnet rings and d.c. beam-handling elements which are counterparts of their pulsed equivalents.

Acknowledgements

The author is grateful for many discussions with colleagues of the GESSS Collaboration. Especially the exchange of latest results and relevant photographs is greatly appreciated. He thanks F. Arendt for his critical reading of the manuscript.

* * *

REFERENCES

1) GESSS Collaboration, Towards a European Superconducting Synchrotron, GESSS-1, May 1972.

2) F. Arendt, M.A. Green, M.R. Harold, N.M. King, J.R. Maidment, G. Neyret, J. Parain, C.W. Planner and G.H. Rees, Proc. 8th Int. Conf. on High-Energy Accelerators, Geneva, 1971 (CERN, Geneva, 1971), p. 171.

3) G. Ries and H. Brechna, KFK Rep. 1372 (1972).

4) P.F. Smith, J.D. Lewin, C.R. Walters, M.N. Wilson and A.H. Spurway, RHEL preprint RPP/A-73 (1969) (unpublished); J. Phys. D3, 1517 (1970).

5) M. Suenaga and W.B. Sampson, Appl. Phys. Letters 18, 584 (1971); 20, 443 (1973); and BNL-16415 (1972).

6) P.F. Smith, Proc. 8th Int. Conf. on High-Energy Accelerators, Geneva, 1971 (CERN, Geneva, 1971), p. 35.

7) M.N. Wilson, RHEL preprint RPP/A89 (1972).

8) A.D. McInturff, Proc. Applied Superconductivity Conf., Annapolis, Md, 1972 (to be published).

9) P. Turowski et al., Karlsruhe (to be published).

10) D.B. Thomas, Proc. 8th Int. Conf. on High-Energy Accelerators, Geneva, 1971 (CERN, Geneva, 1971), p. 190.
M.N. Wilson, Proc. Applied Superconductivity Conf., Annapolis, Md, 1972 (to be published).

11) A. Berruyer et al., Proc. 4th Int. Conf. on Magnet Technology, Upton, NY, 1972 (to be published).

12) P.F. Smith, Proc. 8th Int. Conf. on High-Energy Accelerators, Geneva, 1971 (CERN, Geneva, 1971), p. 213.

13) J.W. Dean, RHEL Memorandum, RHEL/M/A22 (1971).

CHAPTER VII

COLLIDING BEAMS

COLLIDING BEAM DEVICES

K. Johnsen,
CERN, Geneva, Switzerland

In this talk I shall concentrate mainly on p-p devices. However, some attention will also be paid to e-p, whereas I consider e-e outside the framework of my talk.

1. SPECULATIONS ON p-p DEVICES

As proven by the experience at the CERN Intersecting Storage Rings (ISR) together with studies at several laboratories in the world, it seems feasible to build colliding beam p-p devices up to the highest accelerator energies existing or under construction. Furthermore, the BNL study of the intersecting storage accelerators (ISA) has also shown that it may be possible to make p-p devices that are independent of an accelerator capable of injecting at the highest energy of the colliding beam device. Modest tests of this have been made recently at the ISR, where we have injected and stacked at 26 GeV and then retrapped and accelerated to 31.4 GeV in each ring.

1.1 Luminosity

Luminosity has been in the past, and will continue to be in the future, the main problem in colliding beam devices. The ISA study talks about luminosities of 10^{34} cm^{-2} sec^{-1} -- a considerably higher luminosity than we have achieved at the ISR. (We are at present at 1-1.5 $\times$ 10^{30} cm^{-2} sec^{-1}.) Therefore we have recently taken a fresh look at this problem. In particular, E. Keil has tried to optimize storage ring parameters with respect to luminosity, taking into account the experience gained over the last two years on the ISR and results from other studies, especially some recent thinking on beam-beam electromagnetic interaction. Further details of this can be found in a CERN report written by Keil (CERN/ISR-TH/72-33). Keil's optimization results can be summed up as follows:

i) The resulting luminosity of an optimized machine is roughly proportional to the assumed achievable stacked current.

ii) Luminosity is proportional to the energy for which one designs.

iii) Very little is gained in making low-β sections with $\beta_{min} < \sim 1$ m, and he found it appropriate to assume $\beta \approx 3$ m in some numerical examples.

Table 1 shows some numerical examples taken from Keil's report. In all examples it is assumed that the tolerable beam-beam Q-shift (detuning of the betatron oscillation frequency) is 0.01, i.e. a factor 2.5 lower than what is tolerable in e-e machines. However, there is no radiation damping in proton machines, and there is some theoretical evidence that even the figure 0.01 is optimistic. It should be mentioned that the Q-shift does not come only from the crossing but is a result of the interaction between the beams also after they have separated; in fact, in these examples, up to ±15 m away from the crossing point, i.e. 30 m altogether. The assumed beam emittance is about the same as that observed in machines such as the CPS and the AGS. Furthermore, we have assumed in the examples about 15 A maximum of circulating current. It will be remembered that we have reached a maximum circulating beam current of a little more than 12 A in the ISR, but that we are, in fact, limited to well

Table 1

Numerical examples of optimized intersection regions

Beam-beam limit ΔQ	0.01		
Normalized emittance (μrad · m)	30π		
Maximum current (A)	14.4		
Amplitude function at X (m)	3		
Length of interaction region (m)	30		
Length of beam crossings (m)	0.67		
Energy (GeV)	30	100	300
Crossing angle (mrad)	5.1	2.8	1.6
r.m.s. beam width at X (mm)	0.9	0.5	0.3
Luminosity 10^{33} cm^{-2} sec^{-1}	0.3	1.1	3.4

below 10 A for safe operation during physics runs. The figure of 15 A may nevertheless turn out to be a little pessimistic in this optimization procedure. (The ISA study also assumed 15 A, which facilitates comparison.) The main results of the optimization calculations come in the last line of the table.

Allowing for uncertainties it is more appropriate to quote ranges of luminosity, and this is done in the summary (Table 2).

From this it could be concluded that there is a feeling of optimism about the possibility of reaching the 10^{33} cm^{-2} sec^{-1} range for future p-p devices of 100 to 300 GeV in each ring. The reason why we do not dare to quote figures quite as high as in the ISA study is that we feel that they have been a little too optimistic (or at least they were some months ago) about the beam-beam electromagnetic interaction, neglecting long-range forces and perhaps assuming too high a value of the permissible Q-shift.

Table 2

Summary (allowing for uncertainties)

E (GeV)	L (cm^{-2} sec^{-1})
30	3×10^{31} - 3×10^{32}
100	10^{32} - 10^{33}
300	3×10^{32} - 3×10^{33}

1.2 Examples of possible approaches to higher energy p-p devices in Europe

Several approaches are possible, and they are listed below in the sequence of ambitiousness involved.

1.2.1 Conversion of the ISR

If we can make 5 to 7 tesla superconducting magnets, we may reach 100-150 GeV in a converted ISR. There should then be room for straight sections of the order of 50 m long, and the luminosity should come out in the range 10^{32} to 10^{33} cm^{-2} sec^{-1} (cf. Table 2). The ISR is very nicely placed for taking beams from the SPS (as seen from Fig. 1), which is of course a great advantage, perhaps the main advantage, of this solution, together with the fact that the technical installations and much civil engineering exist, which would make the cost of such a project considerably lower than that of a completely new and separate project. However, the disadvantages should also be listed. The main one is the limitation in energy, and this would be even more serious if we could not hope for 7 tesla in the future. The other obvious disadvantage is that we are limited to about 50 m long straight sections. Finally, although existing civil engineering and other technical advantages make such a conversion economically advantageous, the corresponding restriction in the flexibility of the design must be listed as a disadvantage. Nevertheless, the cost may be such a determining factor that this project may become very attractive compared with other ones.

A variant of this project would be to inject into the converted ISR directly from the CPS and accelerate as proposed for the ISA. It is doubtful whether this variant can compete with the first one.

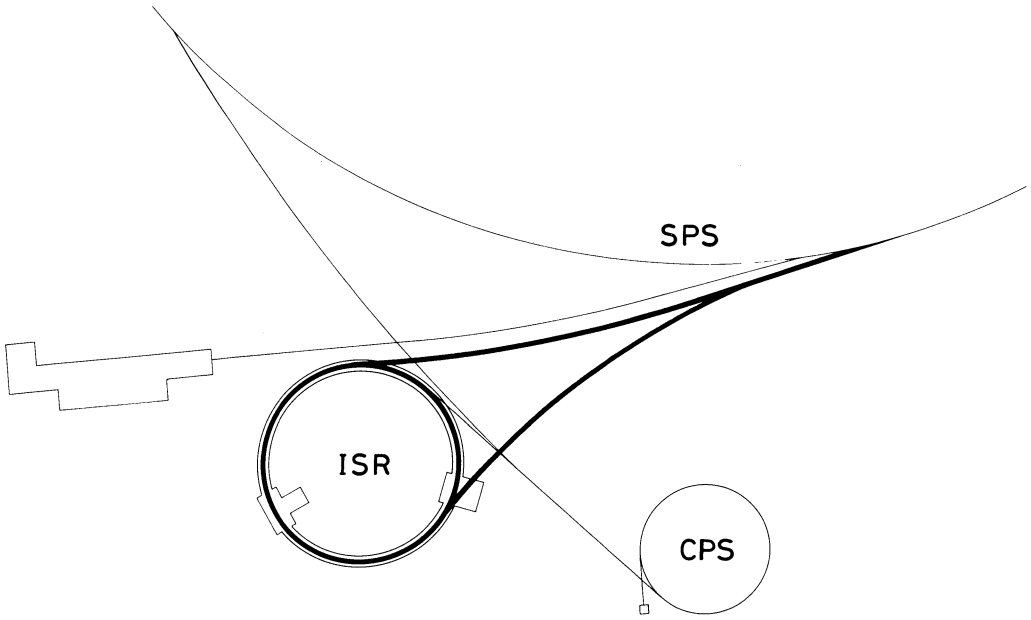

Fig. 1 Possible beam transfer from SPS to modified ISR

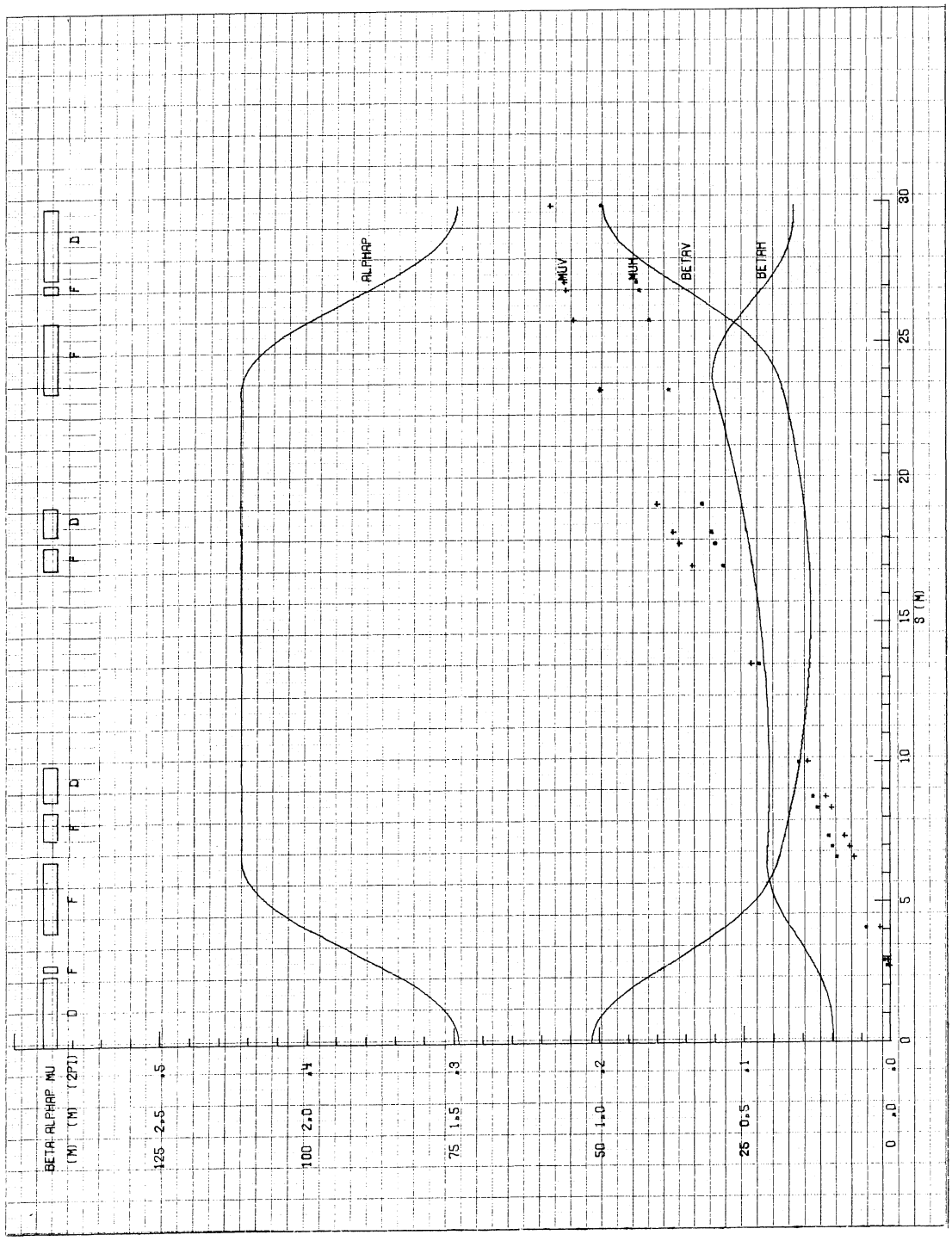

Fig. 2 Present interaction region of the ISR

1.2.2 Separate storage rings for 400 GeV

The next possibility is the obvious one of making separate storage rings for, say, 400 GeV with the SPS as injector. This kind of project might have conventional or superconducting magnets, depending on which solution is the cheapest.

The main advantages are that higher energy can be reached than in the converted ISR, and correspondingly higher luminosity, there is complete freedom in geometrical design, for instance in long straight sections, and we do not have to depend on superconductivity.

The main disadvantage is that it is a new and very large project, more costly and ambitious even than the SPS at present being constructed.

1.2.3 Separate set of accelerating storage rings with the SPS as injector

The most ambitious project would be to make accelerating storage rings with the SPS as injector. This could then go to, say, 1000 GeV in each ring and would be the ISA on a larger scale. For this, superconducting magnets would be essential. The project would be very ambitious and costly, but very interesting indeed for future high-energy physics.

1.3 Plans for higher luminosity in the present ISR

As you will have noticed, there are certain things that I have talked about that are essential for the future; in particular, superconducting magnets that satisfy storage ring requirements with respect to field strength, field accuracy, reliability, etc., and devices for beam manipulations such as low-β sections, etc. The potentialities of some of these things can be tested on the present ISR at the same time as they serve the purpose of bringing the ISR's luminosity nearer to the optimum as presented in Table 3. (We may never reach optimum since the ISR was not designed along an optimization process of the kind we can now think about.) We have therefore started working on plans for superconducting low-β sections in one of the ISR intersections.

Figure 2 shows the amplitude functions in a long straight section of the present ISR. By inserting six superconducting quadrupole lenses, we believe that we can modify the amplitude functions as illustrated in Fig. 3, where also the position of the lenses is indicated. If we can thus reach $\beta \simeq 0.6$ m we should gain a factor of 5 in luminosity. At present we are between 1 and 1.5×10^{30} cm^{-2} sec^{-1}. We have good hope in the future of reaching 15 A by pumping very hard on the vacuum system, and therefore without low-β sections we should be able to come near to 4×10^{30} cm^{-2} sec^{-1}. Consequently, with low-β sections 2×10^{31} cm^{-2} $\times$ sec^{-1} should be within reach. This would mean that this "old-fashioned" machine would start approaching the lower bracket of the optimized parameters of Table 2. To get higher up in that bracket we would certainly have to attack the crossing angle as well, in which case we might not be able to work with such a low β, owing to beam-beam interaction. (For further details on the low-β insertion for the ISR, cf. CERN/ISR-MA/72-45 by B. Autin, in press.)

2. ELECTRON-PROTON DEVICES

Electron-proton devices were already mentioned back in 1961 when intersecting storage rings were first discussed at international conferences, and these were pressed for somewhat harder by Goldzahl and Michaelis in 1966. This kind of device has recently entered into the discussion much more strongly, mainly initiated by Stanford and Berkeley, resulting in the so-called positron-electron-proton (PEP) study.

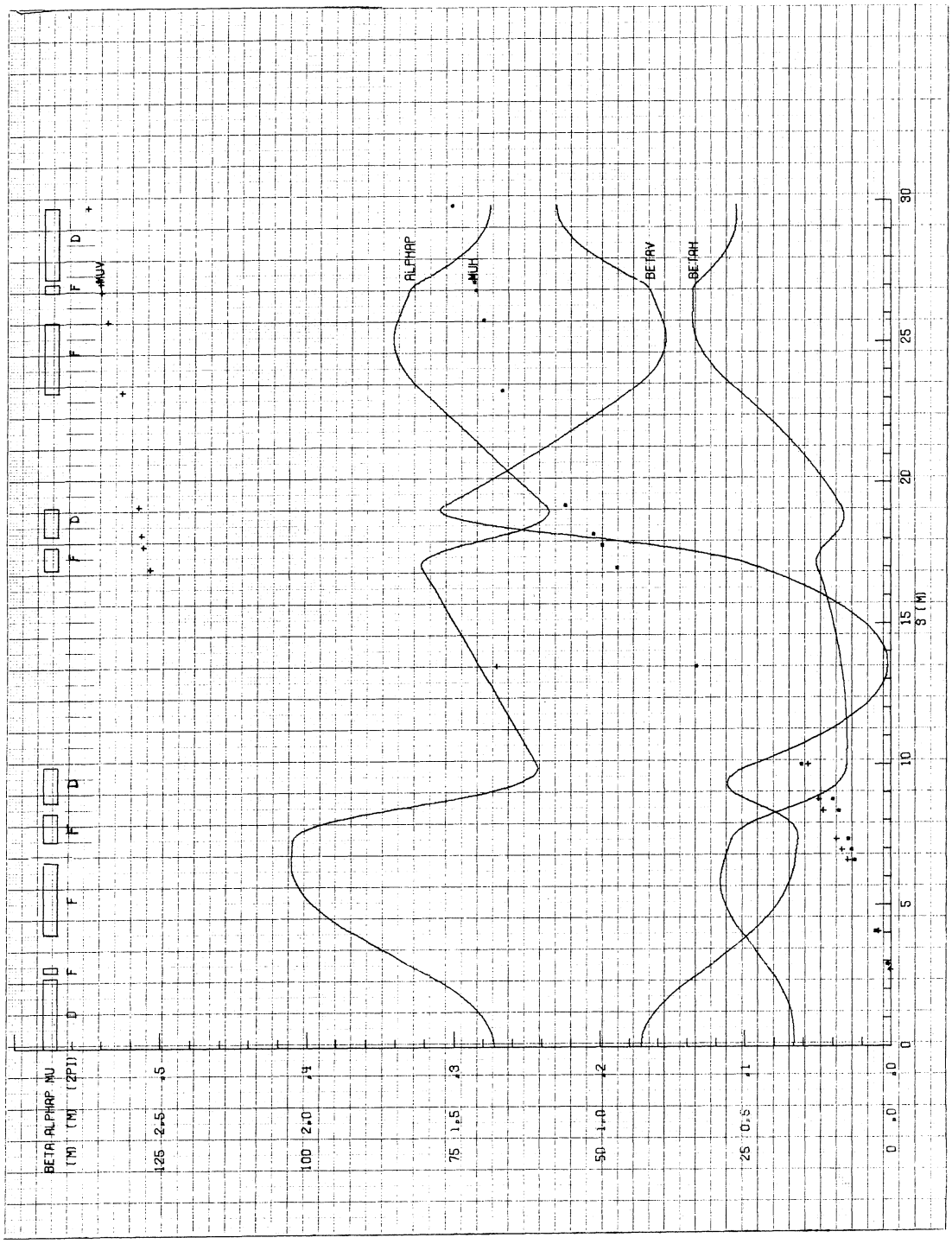

Fig. 3 An interaction region with low β_V insertion

In Europe similar discussions have taken place at Frascati and at DESY, as well as at CERN. Physics considerations seem to lead to the requirement of a minimum luminosity around 10^{32} cm^{-2} sec^{-1} in order to make this interesting at all. To achieve this, the PEP study has gone to the extreme of squeezing beams in all possible directions -- both the transverse dimensions and the longitudinal dimensions, by low β and extremely tight bunching. Thus they arrive at moderate average currents. They are still a little below 10^{32} cm^{-2} sec^{-1} in spite of rather optimistic machine parameters.

At CERN we have tried a few examples, spanning a large spectrum of possibilities, in particular with respect to circulating currents. We have not yet been able to develop a general optimization of the kind that I have illustrated for p-p; therefore the numbers may still be off optimum.

Table 3 illustrates some of the parameters arrived at, and difficulties encountered. For comparison, some PEP parameters are listed. It should be noted that since the electron beam can be squeezed more than the proton beam, the dominant factor is the geometry for the proton beam, but the intensity for the electron beam.

Montague has recently proposed putting a bending field on the interaction region (cf. CERN/ISR-DI/72-44, in press). This has the advantage of reducing the fraction of the electromagnetic interaction contributed by the regions outside the collision volume. This concept is incorporated in the examples in Table 3. (Such a bending field on the interaction regions might also be of interest for p-p storage rings.)

Table 3

Some examples of possible (impossible?) e-p devices

	PEP		SPS by-pass or equivalent		ISR conversion		Separate rings with protons from SPS	
Luminosity (cm^{-2} sec^{-1})	0.6×10^{32}		10^{32}		10^{32}		10^{32}	
E_{cm} (GeV)	65		90		70		118	
Particles	p	e	p	e	p	e	p	e
E (GeV)	70	15	400	5	150	8.2	300	11.6
$\bar{R}$ (m)	300	300	1100	55	150	150	480	480
$\bar{I}$ (A)	0.06	0.08	0.07	1.35	1-5	0.9	1-5	0.32
$\hat{I}$ (A)	$\sim$ 500	2400	12	> 230	1-5		1-5	
No. of bunches	1	1	200	10	0		0	
β_{min} (m)	0.25	0.2	1	0.1	0.4	0.2	0.4	0.2
RF power (MW)		5.3		3.5		5		4.5

As already mentioned, further optimization is needed. Nevertheless, the examples show that it is not easy to reach the desirable luminosity. The required electron currents, for instance, are well above those so far achieved in electron machines. It would appear that there may be one or two orders of magnitude difference between the luminosities achievable in e-p devices as compared with p-p devices.

3. CONCLUDING REMARKS

Both for e-p and p-p the existing installations which we have here in Europe make a very good start indeed. The choice between e-p and p-p may be a difficult one. It would seem realistic to assume, in future discussions about these two possibilities, that the luminosity of e-p will be considerably lower than luminosity for p-p. Also it would seem that these two kinds of devices are so different that it will be very difficult to cover both in one device, although it is easy to prove the opposite when you try to prove it on paper. Later conversion programs are, of course, not excluded -- the devices are similar enough for that. Furthermore, for both categories of devices there is a wide choice (mainly governed by economy) of projects on which to embark, according to the degree of ambition. However, we are far from any final designs yet, and there are many problems to be studied concerning beam behaviour, beam manipulations, the superconductivity used in devices such as these, and also with respect to the very important point of interrelation between the machine and the experimentation. On the other hand, Europe at present has her hands rather full with the program to which she is already committed; so there ought to be time for a proper study before embarking on the construction of new devices. Realistically, one cannot hope to start construction earlier than 6 to 10 years from now. On the other hand, the years pass quickly and there is much to do during those years.

THE DESY ELECTRON-PROTON COLLIDING BEAM PROJECT *)

A. Febel, H. Gerke, M. Tigner, H. Wiedemann and B.H. Wiik
Deutsches Elektronen-Synchrotron DESY, Hamburg, Germany

Colliding electron-proton rings make it possible to study the electromagnetic and the weak interactions at extremely high energies. For example, as compared to the secondary lepton beams at NAL and CERN SPS, the available kinematical regions expressed in q^2 (mass squared of the virtual photon) and w^2 (mass squared of the final hadron system) can be extended by more than an order of magnitude in both variables. A detailed discussion of the potential physics to be done with these devices can be found in a recent SLAC-LBL report[1]. However, in order to be able to exploit this rich physics program, luminosities of the order of 10^{32} cm^{-2} sec^{-1} will be needed. Although such high luminosities might be possible, it is difficult to predict with great confidence that they can be achieved. It is therefore important to be able to study questions such as, for example, the tolerable tune shift for protons due to beam-beam interaction, or the maximum longitudinal phase-space density for protons experimentally, before constructing a large device.

DESY is in the fortunate position that the electron-positron (electron) storage ring DORIS, now nearing completion, consists of two independent rings with vertical crossing. With some modifications to the RF system, protons can be injected[2] into one of the rings and various questions related to e-p rings can be studied experimentally. However, this device will not only be a valuable tool for accelerator studies, but with a luminosity between 10^{30} and 10^{31} cm^{-2} sec^{-1} and centre-of-mass energies of 7 GeV (later 9 GeV) we can also study inelastic electron-proton scattering. Figure 1 shows the kinematical region which will be available for these experiments.

The storage ring will in particular be well suited for electroproduction experiments with complicated final states. This is because it is possible to construct a detector which covers a large fraction of 4π and has a large momentum acceptance. In Fig. 2 the rates are shown for 3.5 GeV electrons colliding with 3.5 GeV protons. It is clear that detailed studies can be made up to q^2 of about 10 $(GeV/c)^2$.

Protons will be injected from a 3 MeV Van de Graaf into a booster synchrotron. In the booster the protons are accelerated up to 1 (GeV/c) and then transferred to the storage ring. The booster can deliver about 5×10^{10} protons per pulse to the ring; this value is about a factor of two below the space-charge limit at injection. The space-charge limit of DORIS is at about 4×10^{13} protons at 1 GeV/c. This corresponds to a maximum of 800 injection pulses. Therefore, in order to minimize the cost, we have chosen a slow repetition rate of 2 pulses/sec for the booster, corresponding to a maximum filling time of 7 min. The synchrotron optics were chosen so that the transition energy is well about the end-point energy. Since this is also the case in DORIS, the protons will never have to go through transition and therefore will suffer no losses in phase-space density due to this effect. After filling the ring, the protons will be slowly accelerated up to the end-energy and the RF turned off. After a short time protons will be continuously distributed around the ring.

---

*) Contributed paper

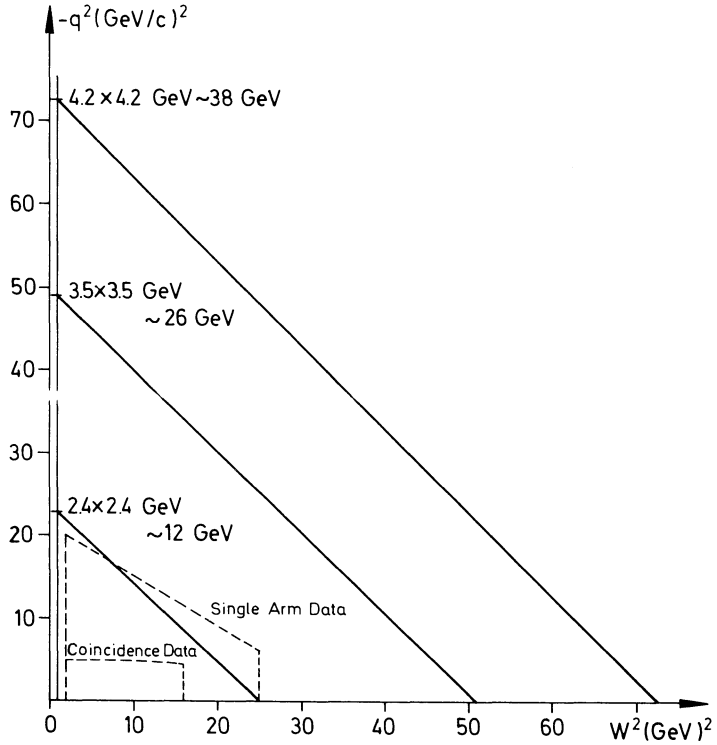
$-q^2(GeV/c)^2$
4.2×4.2 GeV~38 GeV
3.5×3.5 GeV
~26 GeV
2.4×2.4 GeV
~12 GeV
Single Arm Data
Coincidence Data
70
60
50
40
30
20
10
0
10
20
30
40
50
60
$W^2(GeV)^2$

Fig. 1

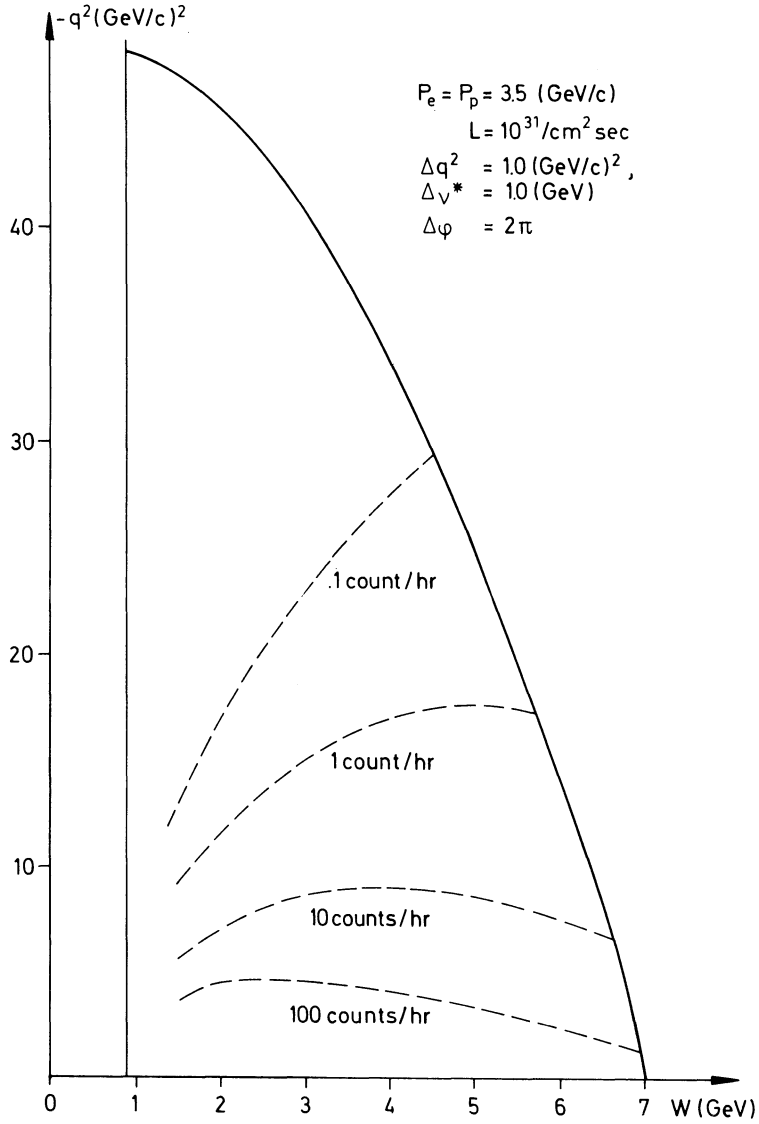
$-q^2(GeV/c)^2$
$P_e = P_p = 3.5$ (GeV/c)
$L = 10^{31}/cm^2$ sec
$\Delta q^2 = 1.0$ (GeV/c)^2,
$\Delta_V^* = 1.0$ (GeV)
$\Delta\varphi = 2\pi$
.1 count/hr
1 count/hr
10 counts/hr
100 counts/hr
40
30
20
10
0
1
2
3
4
5
6
7
W (GeV)

Fig. 2

In this mode of operation the invariant phase-space density is roughly $10^{22}/m^3$, which is of the same order as the phase-space densities at present achieved[3] at the CERN PS below transition. The tune shift of the electrons due to the beam-beam interaction is of the order of 0.0048 at 3.5 GeV/c. This is to be compared with 0.025, the limit commonly accepted for this instability. The computed tune shift for the protons is about two orders of magnitude below this limit.

This is the mode of operation planned for physics experiments. Of course we also have the option of collecting the protons into very tight bunches with very high phase-space densities and very large tune shifts in order to study the questions mentioned earlier.

The construction of the proton synchrotron will start in 1973, and the project should be completed by 1976.

* * *

REFERENCES

1) SLAC-LBL Collaboration, Particle physics with positron-electron-proton colliding beams, SLAC-146, LBL-750, UC-34 (1972).

2) H. Gerke, H. Wiedemann, B.H. Wiik and G. Wolf, DESY H-72/22 (1972).
H. Wiedemann and B.H. Wiik, DESY F-35-72/3 (1972).

3) O. Barbalat, CERN MPS-DL-Note 71-16 (1971).

LIST OF DOCUMENTS RECEIVED BY THE ECFA WORKING GROUP FROM JULY UNTIL NOVEMBER 1972

Ref.	Date	Title	Authors
72-144	August 9	A magnetized iron filter for high-energy neutrino experiments	R. Hartman/H. Leutz
72-145	June 23	Background processes to the bremsstrahlung of photons by electrons which can affect a photon tagging system at CERN SPS energies	T. Sloan
72-146	July 17	Further background processes in high-energy tagging system	T. Sloan
72-147		Usefulness of the new error formulae at high energies	W. Matt
72-148		Kinematic analysis at high energies using inter-track correlations	W. Matt
72-150	Sept. 8	A spot-focusing Čerenkov counter for the detection of multiparticle events at high energies	J. Litt
72-151	Sept. 8	Study of $\bar{K}p$ events producing V^0's at high energy in BEBC	B. Tallini
72-152	Sept. 8	Ideal fluxes and the use of conventional and non-conventional horns at the 300 GeV accelerator	A. Pullia
72-153	Sept. 8	The experimental identification of individual particles by the observation of transition radiation in the X-ray region	J.H. Mulvey et al.
72-154	Sept. 1	Research proposals submitted to NAL and the current status of the proposals	
72-154	Sept. 1	List of approval experiments - NAL	
72-156	Sept. 1	Approved experiments at NAL displayed by category of physics coverage	
72-159	August 19	A total absorption spectrometer for energy measurements of high-energy particles	J. Engler et al.
72-160	Sept. 20	Possible utilization of the West Hall	J.V. Allaby
72-161	July 24	Hadron cascade calculations of angular distribution of integrated secondary particle fluxes from external targets and description of program FLUKU	J. Ranft and J.T. Routti
72-162	August	Thermodynamic inclusive single-particle spectra and particle production ratios at the ISR	J. Ranft
72-163	Sept.	A spectrometer for inelastic e-p and μ-p scattering	H.E. Stier
72-164	Oct.	A high quality electron-photon beam for NAL	Z.G.T. Guiragossian and R.E. Rand

Any of the documents listed above may be obtained directly from the authors upon request.